

Die approbierte Originalversion dieser
Dissertation ist in der Hauptbibliothek der
Technischen Universität Wien aufgestellt und
zugänglich.
<http://www.ub.tuwien.ac.at>



The approved original version of this thesis is
available at the main library of the Vienna
University of Technology.
<http://www.ub.tuwien.ac.at/eng>



DISSERTATION

Hydrogen Production by Steam Reforming of Hydrocarbons from Biomass Gasification Modeling and Experimental Study

Ausgeführt zum Zwecke der Erlangung des akademischen Grades eines Doktors der technischen
Wissenschaften unter der Leitung von

Dipl. –Ing. Dr. Reinhard Rauch
Univ. Prof. Dipl. –Ing. Dr. Hermann Hofbauer

Institut für Verfahrenstechnik, Umwelttechnik und Technische Biowissenschaften der
Technischen Universität Wien,(E166)

Fakultät für Maschinenwesen und Betriebswissenschaften

von

Dip. - Ing. Parham Sadooghi, MSc

Matr. Nr. 1027588
Lobenhauergasse 40-42/30,1170,Wien,

Wien, am 27. November 2013

.....
Parham Sadooghi

To My Lovely Mom

and

To the Soul of My Great Father

**“Try not to become a man of success
but rather try to become a man of value”**

Albert Einstein

ACKNOWLEDGEMENTS

This Dissertation is the result of my three years work done at the Institute of Chemical Engineering in Vienna University of Technology and I am very grateful for the possibility to work on this topic as my doctoral Thesis.

First of all I would like to thank and express my deepest gratitude to my major supervisor Dr. Reinhard Rauch. Thank you for all the good ideas, advices, and for your deep knowledge and interest in this subject. I sincerely appreciate all I have learned from you, not only scientific parts but also your patience, motivation and continuous positive attitude all the way throughout the project.

I would like to thank head of the Chemical Engineering Institute and my supervisor, Professor Hermann Hofbauer, for accepting me as one of his doctoral students and giving me this chance to be part of the ongoing projects in the department. Thank you for all the notes that I received from you in meetings and discussions during the past three years.

I would like to take this opportunity and thank Professor Friedl and Professor Puncochar for being a part of my Dissertation committee.

My special thanks also go to all my friends and staff members at Vienna University of Technology for the good time that we had together and for providing me an enjoyable atmosphere during my research work.

Last but not least, I would like to acknowledge the financial support of the Austrian Climate and Energy Fund since this work was carried out under the Projects "distributed SNG" and "BioH₂-4industries". Moreover, I would like to express my thanks to the team members of Bioenergy 2020+ for delivering the experimental data of the pilot scale reformer.

List of publications

- 1. Sadooghi, P. and Rauch, R. , Mathematical modeling of sulfur deactivation effects on steam reforming of producer gas produced by biomass gasification, Fuel Processing Technology, 110, 46-52,2013**
- 2. Sadooghi, P. and Rauch R. (2013) Pseudo heterogeneous modeling of catalytic methane steam reforming process in a fixed bed reactor, Journal of Natural Gas Science and Technology, 11, 46-51, 2013**
- 3. Sadooghi, P. and Rauch R., Hydrogen production by catalytic steam reforming of methane mixture with propylene, Energy Journal, Submitted for publication.**
- 4. Sadooghi, P. and Rauch R., Sulfur effects on hydrogen production by steam reforming of methane from biomass gasification, COMSOL Multiphysics Conference, Milan, Italy, October 2012**

Abstract

Hydrogen and synthesis gas are the most important energy carriers in the sustainable energy supply system of the future and play a key role in production of many chemical and petrochemicals in oil and energy industries. Steam reforming of light hydrocarbons, like methane, ethylene and propylene, produced from biomass gasification, is proven to have many advantages and environmental benefits. It is an efficient and economical option in industry and the most common process for hydrogen production.

Steam reforming process converts light hydrocarbons from biomass into hydrogen and carbon monoxide at high temperatures in the presence of a nickel or noble metal based catalysts. The process uses fixed bed reactors, filled with catalyst particles in order to increase the reactive surface area between the flow phases and improve the efficiency of the reactions. Due to the strongly endothermic nature of the process, a large amount of heat is supplied to the reactor and therefore the tube wall and the catalyst particles are exposed to significant axial and radial temperature gradients. In developing such reactors, the knowledge of the temperature profile within the reactor is important for designing and optimizing the catalysts structure and the reactor geometry to achieve the best performance. However, due to insufficient room for a thermocouple or to potential interference with local fluid dynamics, temperature measurement within the reactor becomes difficult. Therefore, to evaluate not only the local temperature profiles but the whole reactor performance in terms of conversion and selectivity, accurate descriptive and predictive models are necessary.

A steady state experimental and theoretical model is developed to investigate the performance of the catalytic steam reforming tubular reactor. A packed bed reactor consisting of cylindrical catalyst particles is simulated numerically to investigate the reforming chemistry and evaluate the diffusional resistances. The mathematical modeling and solutions consist of both pseudo-heterogeneous model and a pseudo-homogeneous model. Pseudo-homogeneous reactor models do not distinguish between the gas and solid phases in the fixed bed reactor. Averaged properties are used and the temperature,

pressure and concentrations are equal inside the catalyst and in the gas phase. Heterogeneous models distinguish between the fluid phase and the solid phase to correctly account for the heat transfer in the reactor. Reaction kinetics, reaction rates, effectiveness factors and partial differential equations including mass transfer and energy balance equations are studied in detail. This thesis includes the extensive review of the already published research papers in this field to find empirically correlations for packed bed reactors, suitable for different cases. Wide varieties of correlations are used to calculate effectiveness factors, dispersion and diffusion coefficients according to the type and shape of the catalysts.

Hydrogen sulfide is known to deactivate nickel based steam reforming catalysts by chemisorptions on the metal surface. The metal sulfur bond is so strong and even at extremely low gas phase concentrations of hydrogen sulfide the catalytic activity is substantially reduced. Using conventional sulfur cleaning has a negative effect on process efficiency and steam reforming has to be run without cleaning the gas prior to the reactor. This thesis aim is to describe and model sulfur deactivation effects and steam reforming process in a combined kinetic equation. All chemical reactions are mathematically solved and modeled by the state of the art, COMSOL Multiphysics 4.3 software, which represents a powerful and general class of finite element methods and techniques for approximate solution of partial differential equations. Choosing similar operating conditions in terms of inlet composition and temperature as in experiments allows a direct comparison between experimental and modeling results to validate and see how well the simulation predicts the experimental results.

The result of the modeling shows temperature and pressure distribution, and gas composition along the reactor and predicts accurate results when the inlet and process conditions are changed. They are also able to find the optimum characteristics and geometry dimensions for a steam reformer used for a specific process. The effect of varying operating parameters like steam to carbon molar ratio, temperature, gas composition, space velocity, different amount of sulfur on the hydrocarbon conversion, hydrogen yield and reforming efficiency are investigated carefully.

Contents

1. Introduction.....	1
1.1. Energy.....	1
1.2. Renewable energy.....	3
1.2.1. Biomass as an energy source.....	5
1.2.2. Biofuels fuel.....	6
1.2.3. Hydrogen.....	10
1.3. Biomass conversion.....	11
1.3.1. Gasification and producer gas.....	13
1.3.2. Steam reforming and synthesis gas.....	15
2. COMSOL Multiphysics Software.....	19
2.1. Introduction.....	19
2.2. Organize & customize.....	21
2.3. Chemical reaction engineering module.....	22
3. Technology of steam reforming.....	26
3.1. Introduction.....	26
3.2. Steam reforming of light hydrocarbons.....	27
3.2.1. Methane.....	27
3.2.1.1. Chemistry.....	27
3.2.1.2 Thermodynamics.....	29
3.2.1.3. Kinetics and reaction rates expressions	31
3.2.2. Ethane and propane.....	34
3.2.2.1. Chemistry, thermodynamics and kinetics.....	35
3.2.3. Ethylene and propylene.....	37

3.3. Catalytic fixed bed reactors.....	41
3.3.1. Role of catalyst.....	44
4. Modeling of steam reforming reactors.....	47
4.1. Introduction.....	47
4.1.1. History of steam reforming process.....	48
4.2. Modeling	50
4.2.1. Pseudo-homogeneous models.....	50
4.2.1.1. Boundary and initial conditions.....	53
4.2.2. Pseudo-heterogeneous models.....	53
4.2.2.1 Fluid phase.....	54
4.2.2.2 Solid phase.....	55
4.2.2.3. Boundary and initial conditions.....	57
4.3. Effectiveness factors.....	57
5. Experimental correlations for packed bed reactors	60
5.1. Introduction.....	60
5.2. Radial effective dispersion coefficient.....	60
5.3. Radial heat transport parameters.....	63
5.3.1. Radial Effective thermal conductivity.....	64
5.3.2. Wall heat transfer coefficient.....	66
5.3.3. Component diffusion coefficient.....	67
5.4. Catalyst parameters.....	68
5.4.1 Mass transfer coefficient of the catalyst.....	68
5.4.2 Convection heat transfer coefficient.....	68
5.4.3 Conductive heat transfer coefficient.....	69
5.5. Thermodynamic of the gas mixture.....	69
5.5.1. Density.....	69

5.5.2. Thermal conductivity.....	69
5.5.3. Specific heat capacity.....	70
5.5.4 Viscosity.....	71
5.5.5 Porosity or void fraction.....	73
5.5.6. Partial pressure.....	73
6. Sulfur poisoning and carbon formation.....	74
6.1. Introduction.....	74
6.2. Sulfur poisoning of reforming reactions.....	74
6.2.1. Chemisorption of hydrogen sulfide.....	75
6.2.2. Chemisorption equilibrium.....	78
6.2.3. Impact of sulfur on reforming reactions.....	80
6.3. Carbon formation.....	82
7. Experimental and modeling results.....	87
7.1. Materials and reaction kinetics apparatus.....	87
7.2. Experimental procedure.....	89
7.3 Comparison of experimental and modeling results.....	90
7.3.1. Steam to carbon ratio effects.....	91
7.3.2. Sulfur effects.....	97
7.3.3. Temperature effects.....	102
7.3.4. Space velocity effects.....	109
7.4. Modeling and experimental results from Güssing	116
Conclusion.....	130
Outlook and future work.....	134
Nomenclature.....	137
References.....	145
Appendices.....	156

1. Introduction

1.1 Energy

Energy matters and it is essential to life because human civilization and the use of energy are connected. Energy is a fundamental enabler of economy and it means that energy is necessary to continue economic development and growth. Revolutionary changes in energy cost and effectiveness, from animal and food to coal, oil, petroleum, and nuclear technologies have been deeply shaped throughout history and societal evolution worldwide. The advancement of civilization and technology was made possibly by the ability of the early humans to draw on energy flowing through the environment and convert it to forms that they can use. They harnessed the power of fire and utilized sunlight, water, and the wind energies for other mechanical needs such as sailing ships and water wheels, without the use of the advanced technologies. By generating heat and light and transferring it to mechanical and later to electrical energy, societies were able to shift into industrial societies. Fuel wood was the most significant energy source in most of the civilizations until the 1850 and advent of industrial revolution. The intense energy requirements for the massive industrial production of coke, iron, steel and powering locomotives, steamboats and other machinery, led to the discovery of coal. Coal ended the long dominance of fuel wood as the main energy source about 1850, only itself to be surpassed in 1951 in United States by petroleum and then natural gas a few years later, [Energy information agency, 2003].

Discovery of these hydrocarbons based fossil fuels, led to significant growth in production, population and wealth and fossil fuel secured its place as the main energy source for 20th century. Although coal, oil, and natural gas are the world's most important

energy sources, their dominance does not extend to all corners of the globe. Fossil fuels need many thousands of years to form and their resources are limited. A huge amount of fossil fuel reservoirs are already consumed and due to the increasing exploitation of their reservoirs, future extraction will be more and more difficult, technically challenging and therefore, much more expensive than today. It has been argued that, for standard of living to increase, the consumption of energy must also increase. Growing populations and developments ensure a rising demand for the energy in the future.

Studies predict that by 2050 the energy demand will increase by a factor of 2.3 to 4 compared to 1990 and will intensify the problems of today already high energy consumption and rapid depletion of fossil energy resources, Figure 1.1.

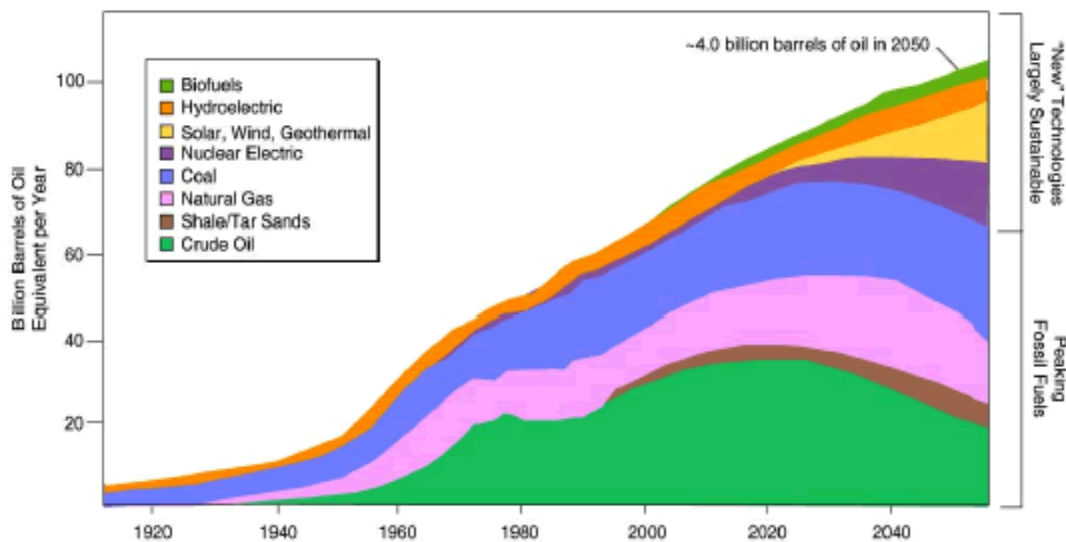


Figure 1.1 History of the world energy consumption and world energy demand in 2050 [American association of petroleum geologists report, 2011]

On the other hand, since 1960s climate change and air quality have become major and often controversial issues in many countries. Prominent among these issues is the green house effect, in which the gradually increasing atmospheric concentration of carbon dioxide, which is caused mainly by burning fossil fuels, methane and nitrous oxide are believed to cause significant ambient temperature increases. Other issue is ozone layer destruction due to interaction of hydrocarbons, carbon monoxide and nitrogen oxide

emissions primarily from motor vehicles which can cause cancers and acid rain which is caused by sulfur oxide emissions from the combustion of sulfur containing fossil fuels. Considering limited number of today's technologies will survive the 21st century due to very limited reserves of conventional energy carriers and to avoid the worst impact of climate change, are sufficient reasons for the society to act quickly and transform its energy system to one that is renewable, sustainable and results in zero emission of carbon dioxide, Figure 1.2.

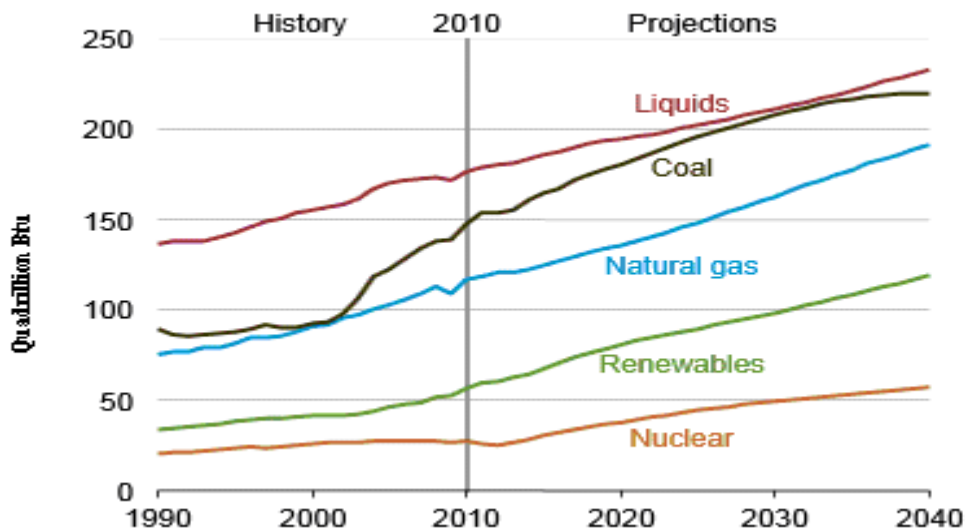


Figure 1.2 World energy consumption by fuel type since 1990 and projections towards 2040 [World energy outlook, 2013]

1.2 Renewable Energy

The threat of catastrophic climate change, limited resources and rising prices for conventional energy, are putting renewable energy sources at the center of public interests. In addition, competitive renewable resources could reduce the risk of nuclear energy use and avoid major increases in the production, transportation and storage of nuclear materials. Renewable energy comes from sources that are easily replenished, from solar and photovoltaic energy to wind power, hydropower, geothermal energy, biomass and biofuel. Sun is by far the most significant source of renewable energy. This

abundant source of energy can be utilized directly by solar thermal or photovoltaic systems.

During the past twenty years outstanding progress has been made in the technology used to convert wind energy to electricity. Many wind turbines have been integrated into existing utility grids and are routinely operated in conjunction with conventional sources. Geothermal energy which has been used to generate electricity and heat is a wide spread resource found through out the world. Estimates show that if the existing resources are exploited, twelve billions tones of oil equivalent energy could be generated within the next ten to twenty years. Hydro power including wave and tidal power is a derived energy from kinetics energy of flowing water and energy contained in the ocean supplies the vast majority of renewable energy resources and electricity. Biomass would be widely used and grown sustainably and converted efficiently to electricity, liquid and gaseous fuels like methanol, ethanol, methane and hydrogen using modern technologies.

The prospects are good that these energy carriers can be produced from biomass at competitive costs under a wide range of circumstances. Moreover the large scale utilization of biomass for energy can provide a basis for rural development and employment in many countries. All of these renewable energy resources can be found almost everywhere and provide not only environmental benefits but also because the size of the most renewable energy equipments is small, renewable energy technologies can advance faster than conventional technology. While large conventional energy facilities require extensive construction in the field, where labor is costly and productivity gains difficult to achieve, most renewable energy equipment can be constructed in factory where it is easier to apply modern manufacturing techniques and therefore meet much of the growing energy demands at prices lower than those usually forecast for conventional energy.

By 2050, renewable sources of energy could account for the three-fifths of the world electricity market and two –fifths of the market for fuels used directly. As mentioned, electricity could be provided by various combinations of renewable power sources cost effectively in most regions, without the need for new electrical storage technologies and

would be fed to large electrical grids and marketed by electric utilities. Electricity and hydrogen play a major role as an energy carrier in energy system of the future and harnessing of renewable energy sources offer a promise of future free of danger of global warming, nuclear energy problems and energy crisis. This is why renewable energy will dominate the energy technology of the 21st century. Figure 1.3 shows world energy consumption by different resources in 2011.

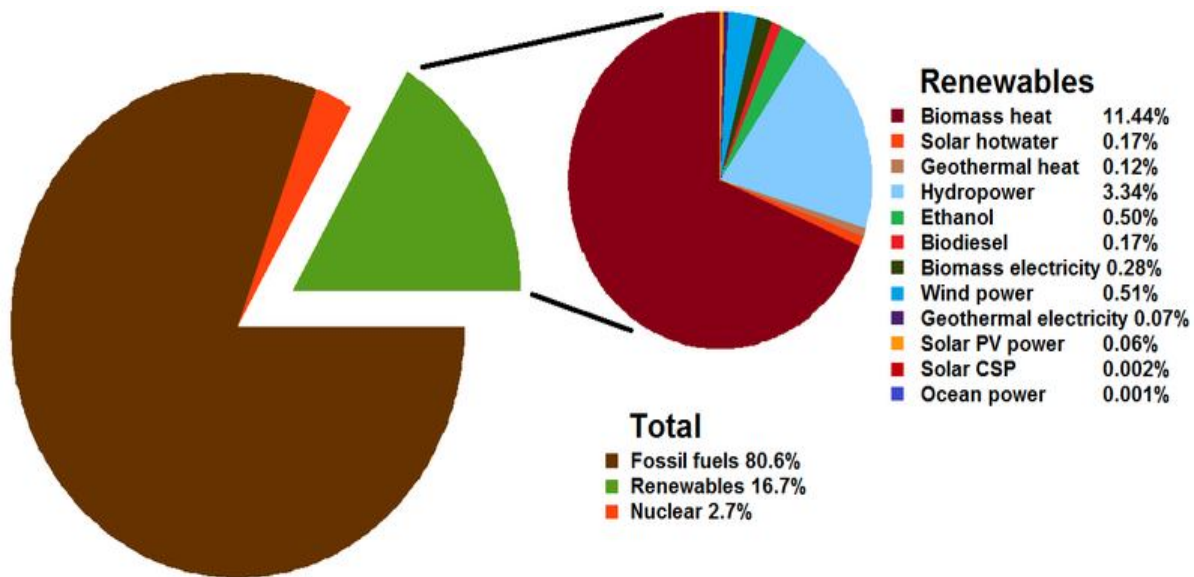


Figure 1.3 Total world energy consumption by source [World energy outlook, 2012]

1.2.1 Biomass as an Energy Source

Biomass can be utilized for the production of heat, steam, power, electricity and can be converted by thermal or biological routes into a range of useful energy carriers such as synthesis gas and liquid fuels. The term biomass is used to describe any material of recent biological origin and includes plant materials such as trees, grasses and agricultural crops, as well as animal manure and municipal sewage. As a raw material, biomass is a nearly universal feedstock due to its domestic availability and renewability. Indeed, until the wide spread utilization of crude oil as an energy source in the 19th century, biomass supplied the majority of the world's energy needs. In one sense, the situation has now come full circle: decreasing petroleum reserves coupled with increasing global energy

demand and concern over the environmental effects of fossil fuel combustion have brought about a resurgence of interest in the utilization of biomass as an energy source [Hodge, 2010].

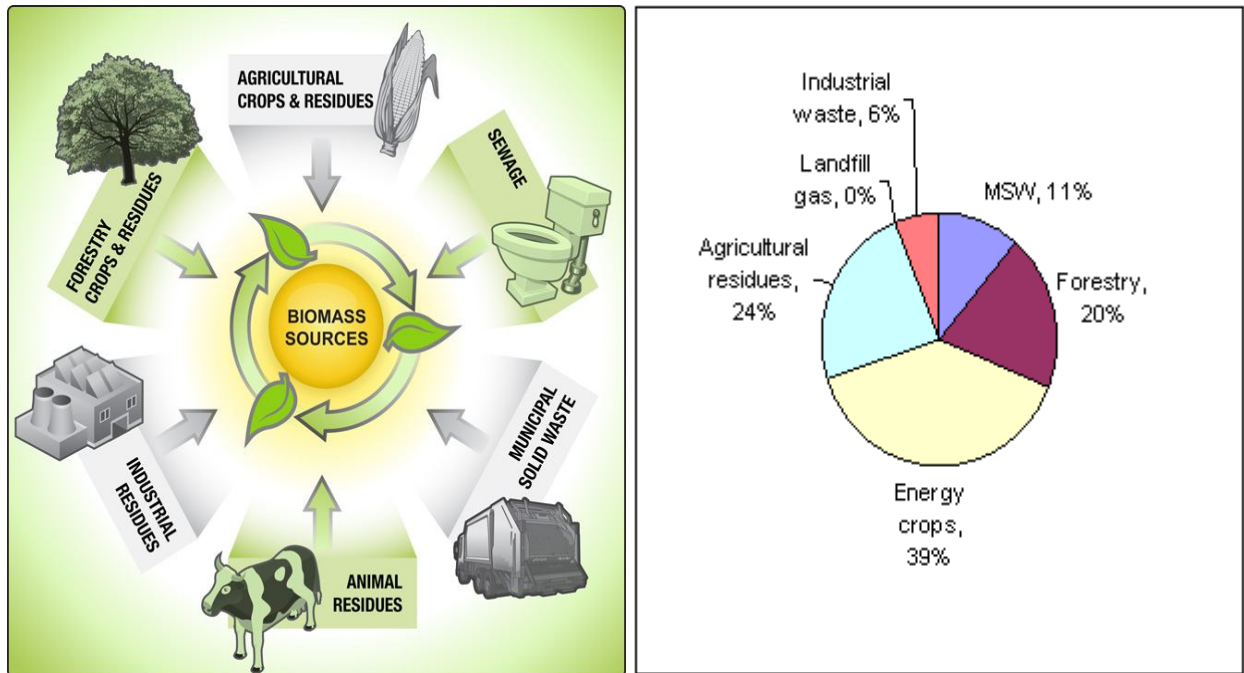


Figure 1.4 Biomass resources and projected distribution in EU in 2030 [Jorgensen et al., 2003]

Biomass has traditionally supplied a large fraction of the energy needs in many developing countries and the production of biomass as an energy source has many benefits. Biomass is a wide spread resource, the utilization of which can diversify the fuel supply and in turn lead to an energy supply that is more convenient. It can be utilized not only as an energy source in its raw state by combustion with fossil fuels for electricity generation but also it can be converted to liquid fuels. Substituting fossil fuels with bio-fuels is a long term solution to rising demand for clean transportation fuels and lead to a reduction in greenhouse gases, principally carbon dioxide. The increased agricultural activity associated with the production of energy corps can generate employment in rural areas and result in increased farm income, thereby, reversing the trend of rural depopulation prevalent in many countries [Khanal et al. 2011].

1.2.2 Biofuels

Biofuels are transportation fuels derived from agriculture, forestry and other type of biomass sources. Owing to their high energy density and ease of shipping and distribution, liquid fuels are far more versatile than solid fuels and are utilized in a wider range of applications. In addition world demand for clean liquid transportation fuels grows, and the production capacity of traditional petroleum reservoirs decreasing, resulting in upward pressure on the global price of petroleum. Coupling this with increasing uncertainty of supply, many national programs encouraging domestic production have arisen, typically focused on the use of domestic biomass resources to meet demand for biofuels. Cereals, grains, sugar crops and other starches are fermented to produce alcohol, (usually ethanol) which can be used either as blending component in gasoline as motor fuel in pure form or as gasoline additives.

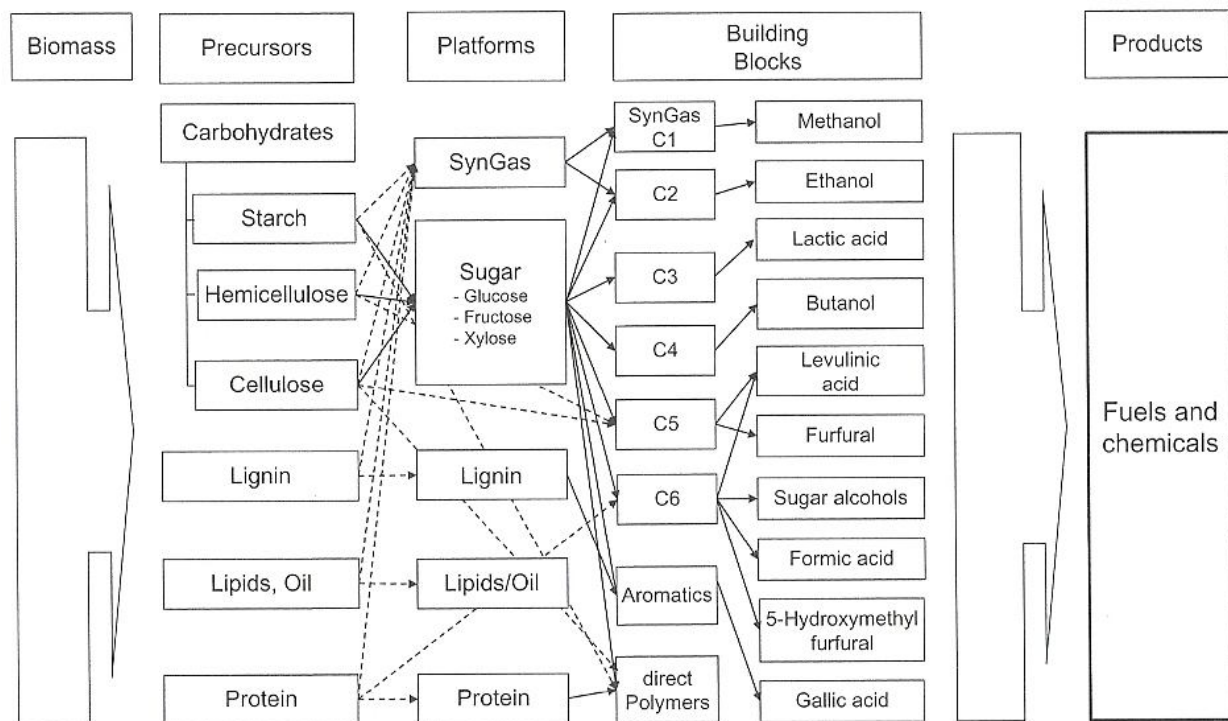


Figure 1.5 Model of bio-based product flowchart for biomass feedstock bio-refinery [Crocker, 2011]

Oil seed crops like rapeseed, soybean, and sunflower can be converted in liquid fuels which can either be blended with conventional diesel fuel or used as pure biodiesel. Cellulosic materials including grasses, trees and various waste products from wood processing facilities and municipal solid waste can also be converted to alcohol and biofuels.

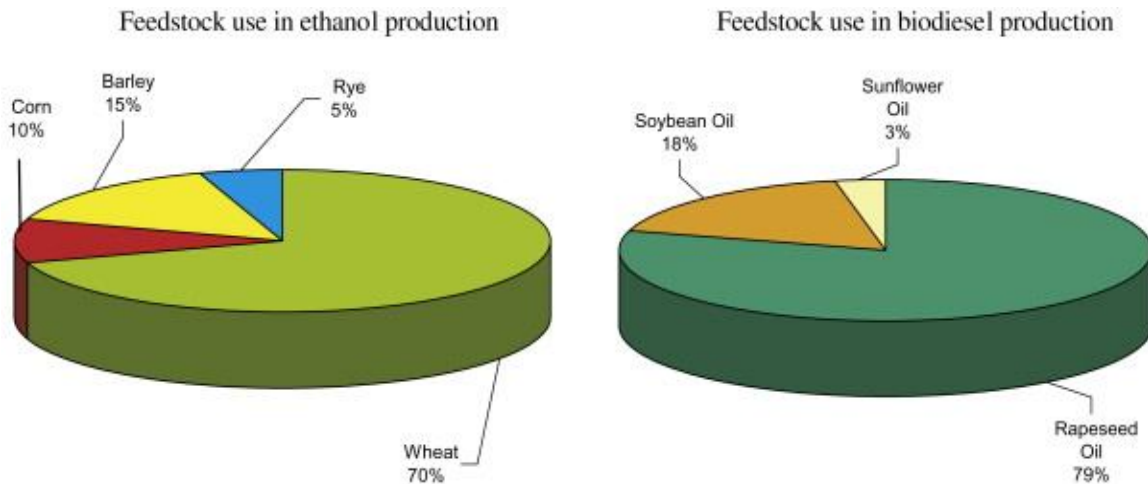


Figure 1.6(a) Worldwide resources for ethanol and biodiesel production [Ajanovic, 2011]

There are compelling reasons to find ways of converting biomass to biofuels. In the energy field, increasing the efficiency of energy, utilization and producing liquids, gaseous fuels and electricity have generated a need to convert the conventional fuels such as coal, fossil fuels and biomass to biofuels. The low density of biomass compare to fossil fuels and high water content of biomass makes shipping costs prohibitive in many cases, yet most subsequent refining processes required centralized facilities, where large scale operations greatly improved process efficiencies and economics. Owing to their high energy density and ease of shipping, transport and distribution, liquid fuels are far more versatile than solid fuels and consequently are utilized in a far wider range of applications.

Demand for biofuels can be attributed primarily to transportation uses including automotive, marine bunker, and aviation fuels. They are also utilized in a wide range of

applications including domestic heating, electricity generation and potentially as hydrogen carrier. Transportation demand for biofuels is unique, in that demand is relatively unaffected by increase in price [Mench, 2008]. Furthermore, some energy users, such those employing diesel and jet engines, require fuel processing high energy density, which current batteries can not achieve [Briggs, 2009]. As shown in Figure 1.2, worldwide liquid fuels represent the most heavily utilized source of energy.

Ethanol provides a major part of liquid fuel requirement and its production accounts for around 90% of bio-fuels in the world. For years Brazil was the biggest world producer of biofuels for the production of ethanol from sugar cane. Ethanol production has increased significantly since 2000 due to increased ethanol production in other countries and since 2006 has made the United States number one in biofuels.

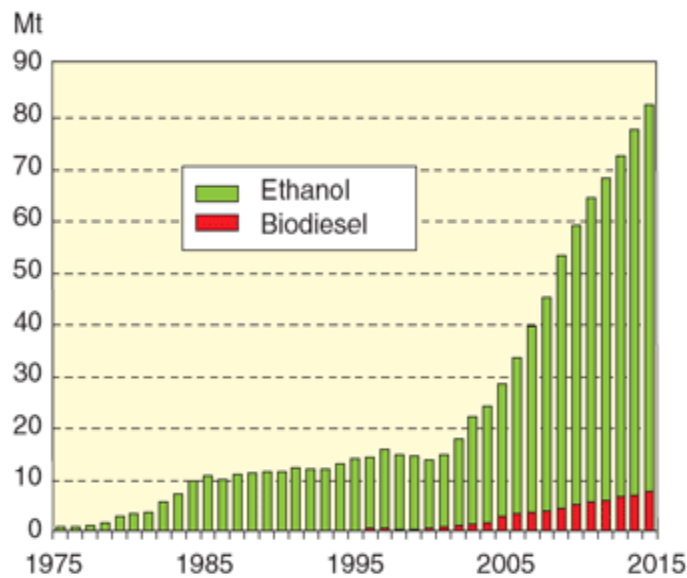


Figure 1.6(b) Worldwide biodiesel and ethanol production and projection until 2015 [Licht et al., 2009]

The bio fuels production including biodiesel, ethanol, other alcohol fuels and bio oils has grown substantially within the last decade. World production of bio-fuels was 1.5 million barrel/day in 2008 [Nelson, 2011] and it is expected to accelerate over the next several decades, Figure 1.6(a,b).

1.2.3 Hydrogen

Hydrogen play a key role in energy supply system of the future and it is used as a means to solve the problems caused by fossil fuels [Momirlan et al., 2005]. Hydrogen consumption is expected to increase dramatically in near future as it is used as a fuel for fuel cells, in chemical industries and in petroleum refineries to process heavier feedstock's and produces different fuels. The idea sounds quite reasonable: Hydrogen is one of the most abundant elements in the universe, and some vehicle manufacturers have demonstrated that hydrogen can be used directly in combustion engines like jets, turbines; four and two strokes and diesels and fuel cell powered cars have also been constructed.

Although, most of the electricity is produced by burning fossil fuels like coal, natural gas, and petroleum, hydrogen can be converted in a fuel cell to electricity plus some heat and water via the electrochemical combination with oxygen. The only byproduct is water whereas burning of fossil fuels produces carbon dioxide and a variety of pollutants, which enhance the global warming problem. In contrast to electricity which is difficult to store in large quantities, hydrogen is a storable gas. It can be used not only as an energy storage medium, as a gas in large depleted natural gas fields, in hydrogen absorbing alloys, as a cryogenic liquid or in activated carbon materials and carbon nanostructures, but also in the form of conventional fuels such as methanol which some regard as a superior fuel to carry hydrogen. Hydrogen can fulfill the indispensable storage function of smoothing the daily and seasonal fluctuations of solar power and other intermittent energy sources. As a gas, hydrogen can transport energy over long distances, in pipelines like electricity and sometimes more efficiently. As a chemical fuel, hydrogen can be used in a much wider range of energy applications than electricity. It can also be used as a chemical raw material and is seen as a promising future fuel for different industries like aviation. However, due to its high reactivity hydrogen in nature is nearly always combined with other elements on the earth like oxygen, (water), and it has to be produced from other resources.

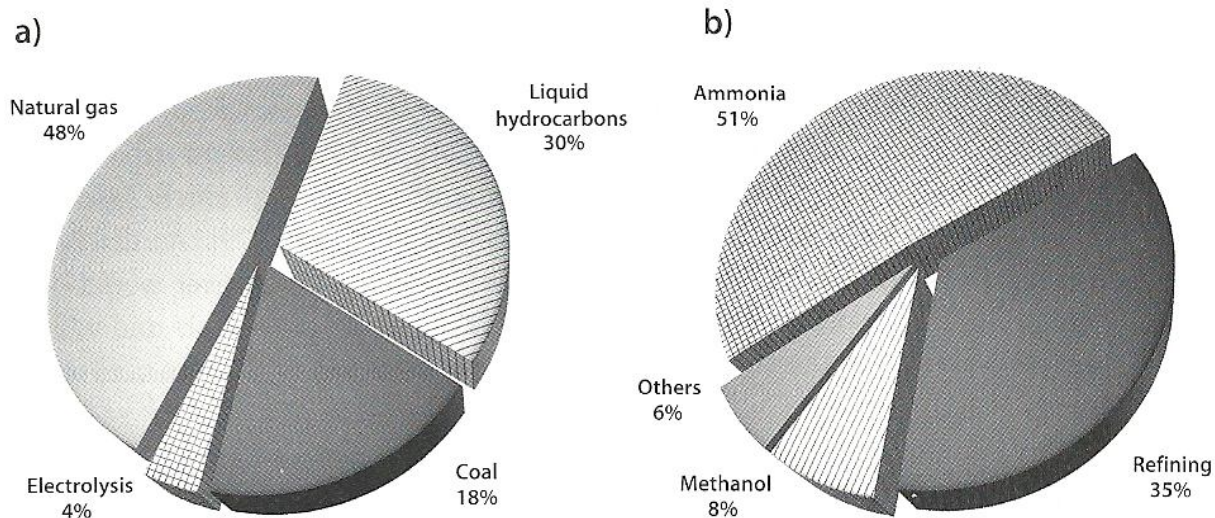


Figure 1.7 (a) Source of hydrogen production in the world, total production about 50 million tones, (b) The main hydrogen consuming sectors in the world [Olaf et al., 2006]

Therefore, hydrogen is not an alternative fuel but an energy carrier. Hydrogen can be generated from many primary sources. Today, hydrogen is extracted mostly from fossil fuels but it is present in water and thereby in every living organism. It is also present in hydrocarbons like methane, in organic compounds and in several other natural as well as artificial compounds. In future hydrogen will be made from clean water and clean solar energy and from biomass. As discussed earlier; biomass can be used for the production of bio-fuels such as ethanol, methanol and biodiesel. Biomass can also be converted into hydrogen by gasification or pyrolysis coupled with steam reforming process.

1.3 Biomass Conversion

Biomass includes a large variety of materials generated by photosynthesis. Plants capture solar energy and use it to convert carbon dioxide and water to sugars $(CH_2O)_x$:



The sugars thus produced are stored in Lignocellulose which is composed of three major constituents: cellulose, hemicellulose and lignin. Biomass is typically composed of 65-85 wt% sugar polymers principally cellulose and hemicellulose with another 10-25 wt%

corresponding to lignin. Other biomass components, that are generally present in minor amounts, include triglycerides, sterols, alkaloids, resin and waxes often referred to as lipids and fatty acids. In general, routes for the conversion of biomass to liquid fuels can be classified into two main types: those based on thermo-chemical processes and those utilizing biological means. Thermo-chemical processes use heat, frequently in combination with heterogeneous catalysts to break biomass down into smaller constituent units, which are then further processed into useful molecules. Biological processes, in contrast, are typically based on the use of enzymatic catalysts under mild conditions like fermentation of sugars to ethanol [Crocker, 2011].

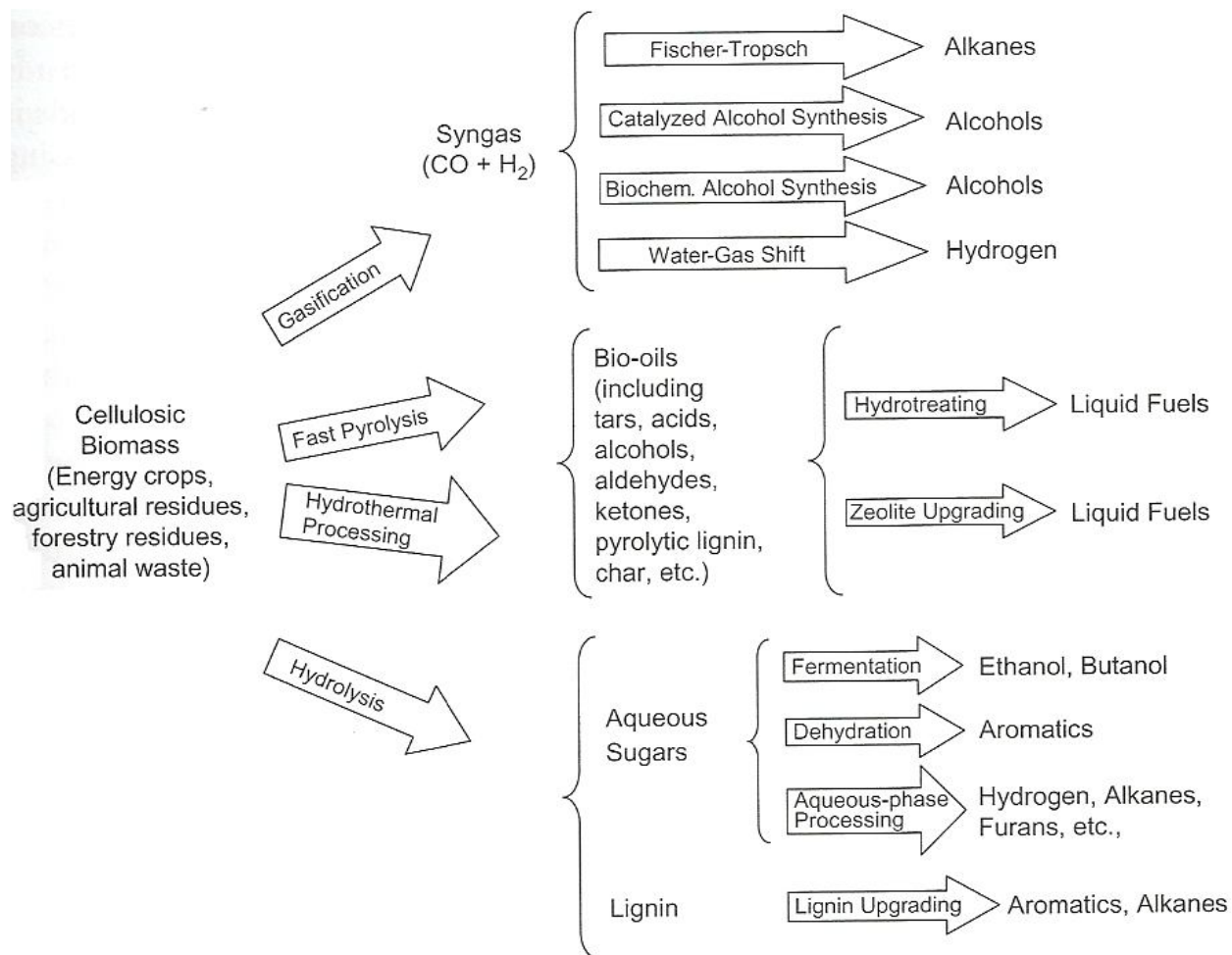


Figure 1.8(a) Summary of pathways of cellulosic biomass conversion to liquid fuels [Crocker, 2011]

Figure 1.8(a) show a range of pathways through which biomass can be converted to fuels. In general, sugar polymers such as cellulose and starches can be readily broken down to

their constituent monomers by hydrolysis, preparatory to conversion to ethanol, or other chemicals. A number of routes exist for the conversion of fatty acids to liquid fuels and chemicals as shown in Figure 1.8(b). In the case of lignocellulosic biomass, gasification, direct thermo-chemical conversion and hydrolysis are the main three approaches [Huber et al., 2006]. In the first of these, biomass is gasified to produce synthesis gas (syngas), which after treatment to remove tars and other impurities, can be catalytically converted to hydrocarbons via the Fischer-Tropsch synthesis or to alcohols. Other options include syngas conversion to ethanol using certain types of anaerobic bacteria or treatment with water gas shift catalysts to generate additional hydrogen from the water and carbon monoxide present in the synthesis gas.

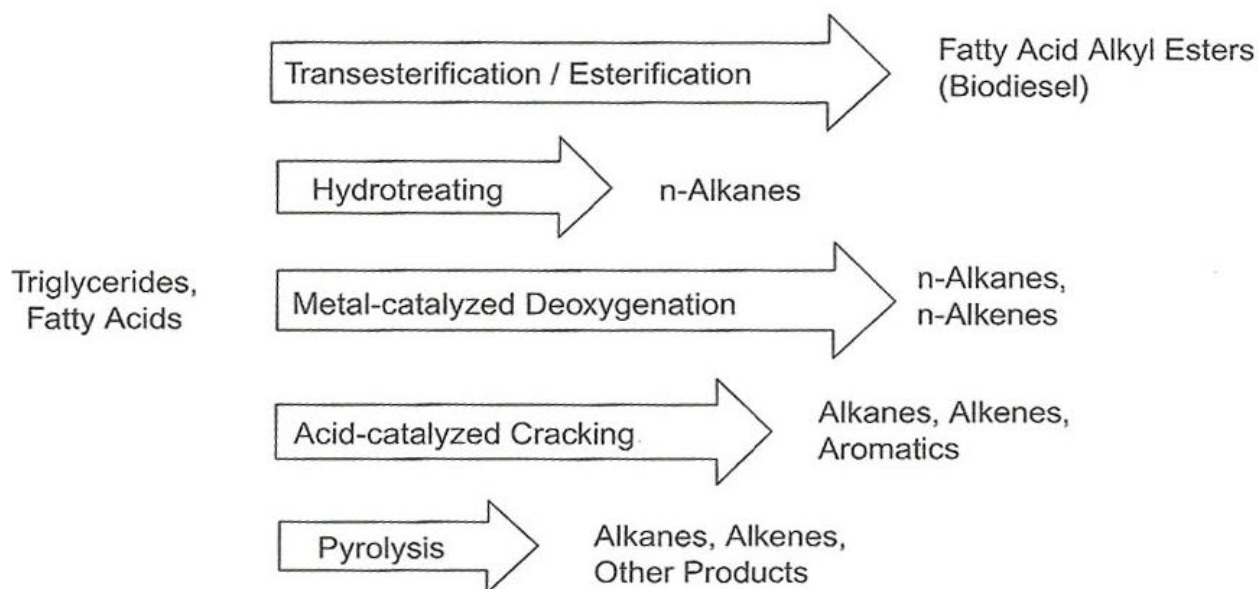


Figure 1.8(b) Summary of pathways of fatty acid biomass conversion to liquid fuels [Crocker, 2011]

1.3.1 Gasification and Producer Gas

Gasification is defined as thermal conversion of organic material to combustible gases under reducing conditions with oxygen added in sub-stoichiometric amounts compared with the amount needed for complete combustion to carbon dioxide and water.

Gasification is a well established technology and is seen as a key pathway toward hydrogen when starting from coal or biomass. It is considered one of the most efficient ways of converting the energy embedded in biomass, and it is becoming one of the best alternatives for the use of waste solids. The widespread availability of biomass has been widely recognized, and has its potential to supply much larger amounts of useful energy with fewer environmental impacts than fossil fuels. Wood, energy crops, and waste from the pulp and paper industry are examples of biomass, which can be gasified at high temperatures. Gasification includes the technologies of pyrolysis, partial oxidation and hydrogenation [Higman et al., 2003 and Basu, 2010]. Gasification has a wide range of applications as shown schematically in Figure 1.9. Gasifiers use direct oxygen for exothermic oxidation reactions to provide the energy necessary for gasification or by pyrolysis through the addition of sensible heat in the absence of oxygen. In both cases water in the form of steam may be added to promote additional production of hydrogen via the water gas shift reaction.

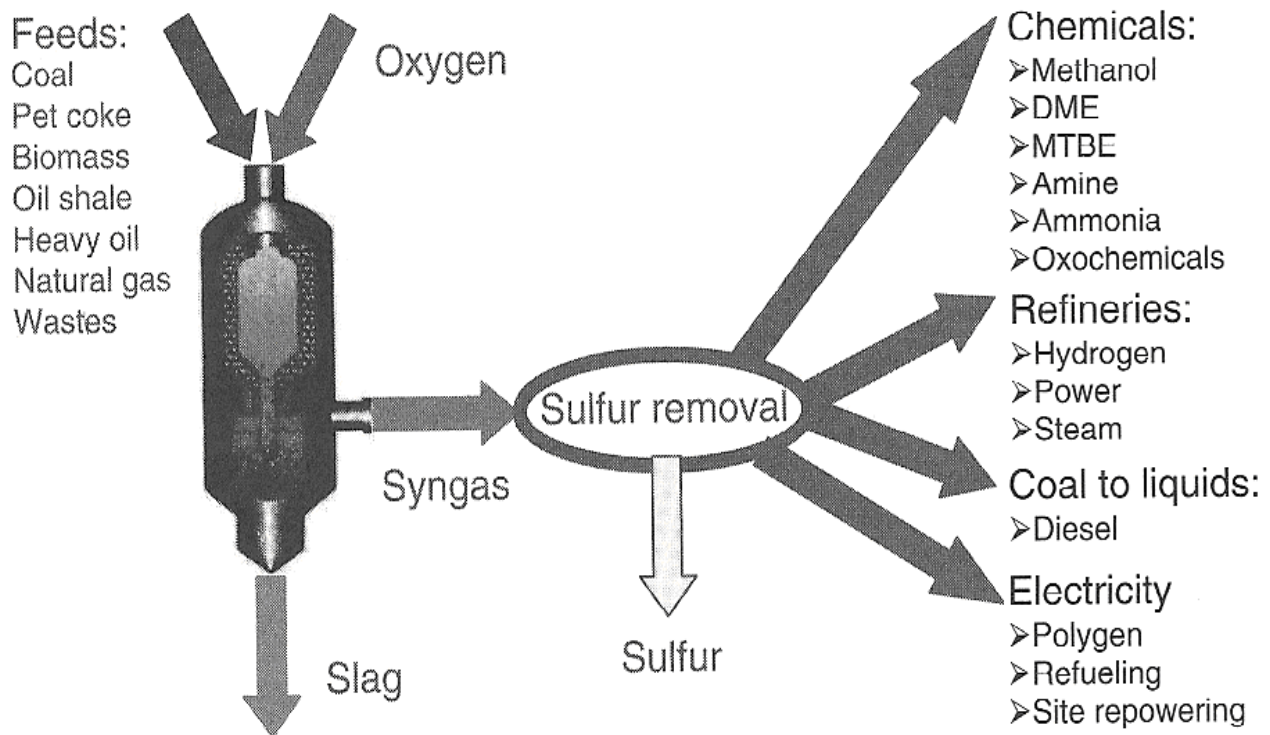


Figure 1.9 Application of gasification [Brown, 2011]

The technology is applicable to any hydrocarbon feedstock including natural gas, biomass and heavy refinery residues. Through gasification of biomass, a heterogeneous solid material is converted to producer gas, a gaseous fuel intermediate of consistent quality that can be processed and be used reliably for heating, industrial processes applications, electricity generation and liquid fuel production. Producer gas refers to the low heating value gas mixture of gaseous, liquid, and solid compounds. The gaseous products are mainly hydrogen, carbon monoxide, and carbon dioxide, methane, and other low hydrocarbons. Liquid products are water and an organic fraction, often called tar and consisting of higher hydrocarbons. The solid char residue contains mainly carbon and some inorganic components, which are present in the biomass. Nitrogen and sulfur, on the other hand, which also are incorporated in the biomass structure, are released into the product gas during gasification as ammonia and hydrogen sulfide, [Koningen et al., 1998]. To prevent downstream tar condensation, the product gas from a biomass gasifier can be led through a catalytic cracking unit, in which the tar compounds are converted easily in the presence of steam:



After removal of impurities, producer gas is usually steam reformed in a catalytic steam reformer to produce synthesis gas (syngas), a gas mixture of predominantly carbon monoxide and hydrogen, which is widely used for synthesis of fuels and chemicals.

1.3.2 Steam Reforming and Synthesis Gas

Synthesis gas and hydrogen are important building blocks in oil and energy industries and serve as feed stocks for production of wide variety of chemicals. Synthesis gas can be used as feedstock to the Fischer–Tropsch process for liquid hydrocarbons production [Rostrup-Nielsen, 2002, 2004, 2005, Ferreira, 2005 and Fonseca et al., 2005], methanol and olefins synthesis [Deluga et al., 2004 and Liu et al., 2005], ammonia production

[Dybkjaer, 1995], hydrodesulphurization, hydro-cracking [Rostrup-Nielsen, 1995 and Choudhary et al., 2000], fuel cell systems [Mcintoch et al., 2004 and Brown 2011], methanol production or in a gas turbine to produce electricity.

Figure 1.10 shows different processes for production of hydrogen from various carbon-containing feedstock. The most studied technology for hydrogen production is reforming of natural gas or producer gas, produced by biomass gasification, [Rostrup-Nielsen, 1984, 1995, 2002]. Reforming occurs when a hydrocarbon or alcohol fuel and steam or oxygen is passed through a catalyst bed under optimum operating conditions.

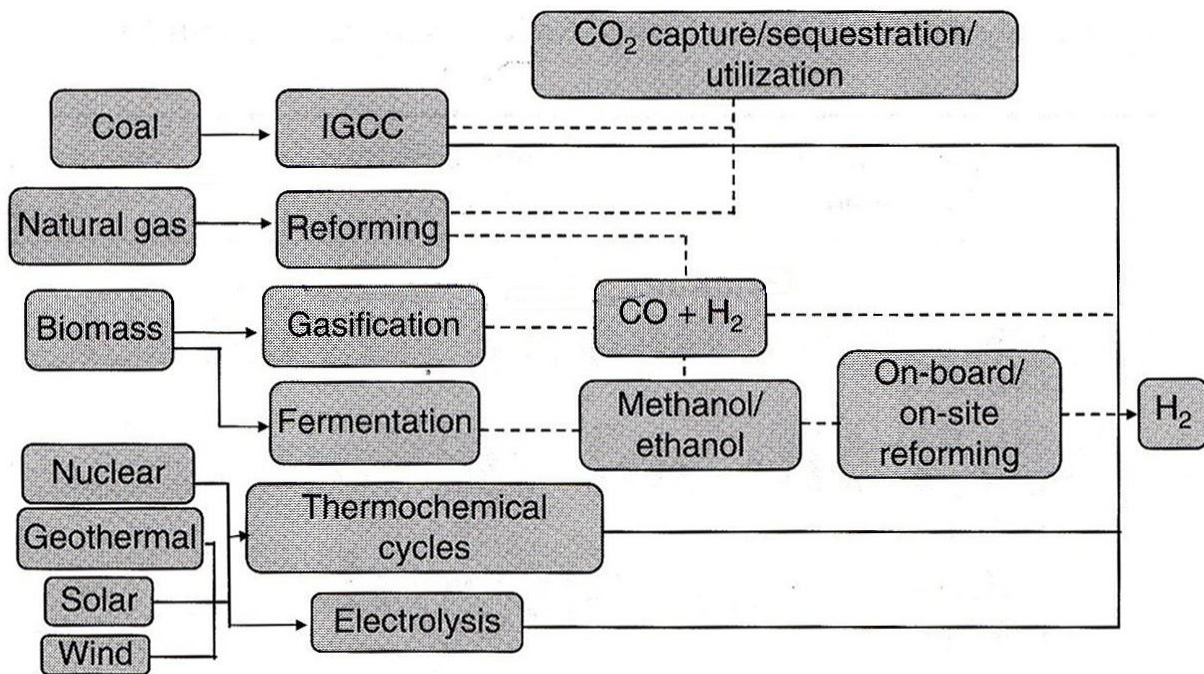


Figure 1.10 Technological options for the production of hydrogen from various carbon-containing feedstock [Liu et al., 2010]

Depending upon whether steam, oxygen or a mixture of steam or oxygen is used, the reforming technology is termed, steam reforming, partial oxidation and auto-thermal reforming, respectively. Reforming of natural gas with carbon dioxide, also known as dry reforming has also been reported in recent years. The choice of technology depends on the scale of operation and also the desired product stoichiometry [Rostrup-Nielsen,

2011]. Among the reforming technologies, steam reforming is the preferred process today for hydrogen and synthesis gas production because it offers relatively a higher steam to carbon ratio since a part of hydrogen comes from water. The hydrogen to carbon monoxide ratio can be varied over a wide range as shown in Figure 1.11, as the reforming reactions are coupled with the water gas shift reaction, [Rostrup-Nielsen, 2002]. Catalytic steam reforming (CSR), involves the extraction of hydrogen molecules from hydrocarbon or alcohol fuel and water over a base or noble metal supported catalyst.

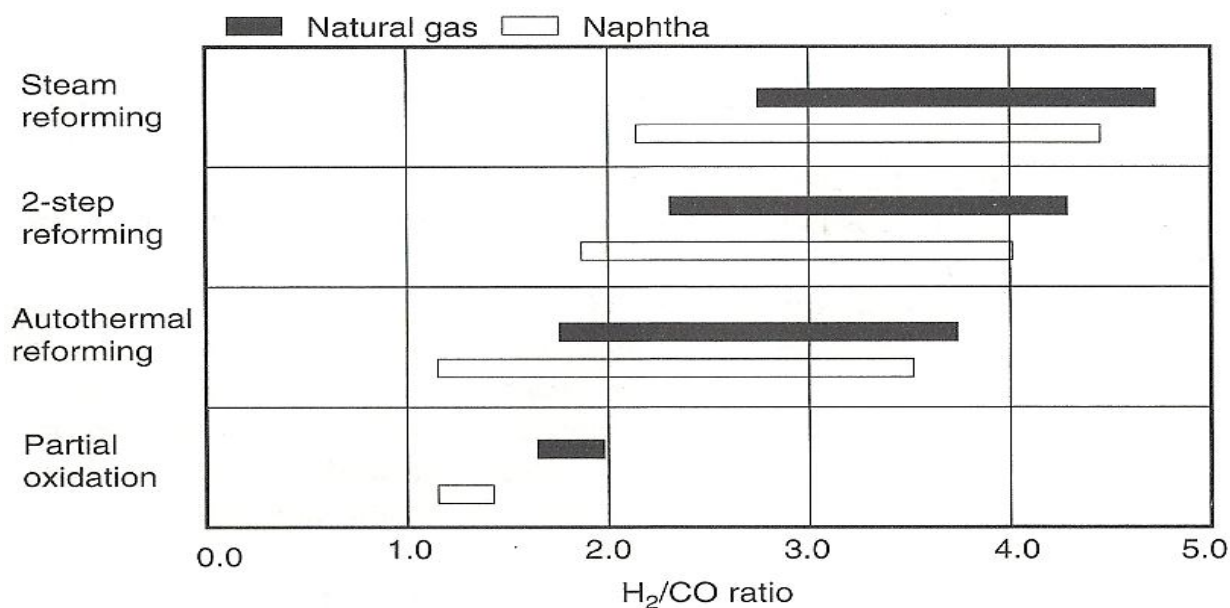


Figure 1.11 Possible hydrogen to carbon monoxide ratios, obtained from various synthesis gas production processes [Rostrup-Nielsen, 2002]

Steam reforming of hydrocarbon fuels, especially steam reforming of natural gas containing methane, is a well developed technology and practiced commercially for large scale hydrogen production [Matsumara et al., 2004 and Ross, 2005]. Knowledge gained from natural gas reforming is applied to the reforming of higher hydrocarbons, alcohols and biofuels for the manufacture of hydrogen or synthesis gas depending on the end use. Hydrogen sulfide is known to deactivate nickel based steam reforming catalysts by chemisorption on the metal surface. Numerous studies of this phenomenon have revealed that the metal-sulfur bond is so strong that catalytic activity is substantially reduced, even

at extremely low (ppm levels) gas phase concentrations of hydrogen sulfide. To fully exploit the activity of the catalyst, it would be necessary to remove the hydrogen sulfide before the steam-reforming reactor. Using conventional sulfur cleaning, which is run at ambient temperatures, requires the product gas to be initially cooled down and then reheated after sulfur removal. To circumvent this procedure, which has a negative effect on process efficiency; steam reforming has to be run without cleaning the gas prior to the reactor [Rostrup Nielsen, 1984, Strohm et al., 2006, Lakhapatri et al., 2009 and Hansen et al., 2010]. Carbon formation is also a phenomenon that can not be tolerated in steam reforming and therefore requires particular attention [Rostrup-Nielsen, 1984, 1991, Ruan et al., 1992, Froment, 2001 and Seheasted, 2006]. It leads in the first place to catalyst deactivation, thus causing hot spots that weaken the reactor tube. In this study the chemistry, thermodynamics, catalysts, kinetics, reaction mechanisms, and technology developments in the catalytic steam reforming of hydrocarbons are discussed in detail and experimental and numerical results are presented and compared.

2. COMSOL Multiphysics Software

2.1 Introduction

Computer simulation has become an essential part of science and engineering. Digital analysis of components, in particular, is important when developing new products or optimizing designs. Today a broad spectrum of options for simulations is available. Researchers use everything from basic programming languages to various high level packages implementing advanced methods. Each of the techniques has its own unique attributes to make the results more reliable. A computer simulation environment is simply a translation of real world physical laws into their virtual form. It would be ideal then, to have a simulation environment that included the possibility to add any physical effect to the model. That is what COMSOL is all about. COMSOL Multiphysics is an engineering, design, and finite element analysis software environment for the modeling and simulation of any physics-based system which is able to handle complex geometries and boundary conditions [Tabatabaian, 2014]. The COMSOL Multiphysics simulation software environment facilitates all steps in the modeling process, defining, solving, and then visualizing the results. The approach starts and model is created by predefined physics interfaces for different applications ranging from fluid flow and transport phenomena, heat transfer, chemical reaction, electromagnetic field theory, and solid mechanics as the basic fibers of the software. Then, in an elegant and flexible user interface, the software can weave these fibers together in a self-consistent way to solve the particular simulation needs. COMSOL is a flexible platform that allows users to model all relevant physical aspects of their designs. Advanced users can go deeper and develop customized solutions, applicable to unique circumstances. Certain characteristics of COMSOL become apparent

with use. Material properties, source terms and boundary conditions can all be arbitrary functions of the dependent variables. Since all material properties are functions of temperature, any model can be conceivably coupled to thermal interface. Moreover, COMSOL allows including heat generation from any other physics into a thermal model. COMSOL has also the ability to import data from other programs like Matlab [Schijndel, 2008].

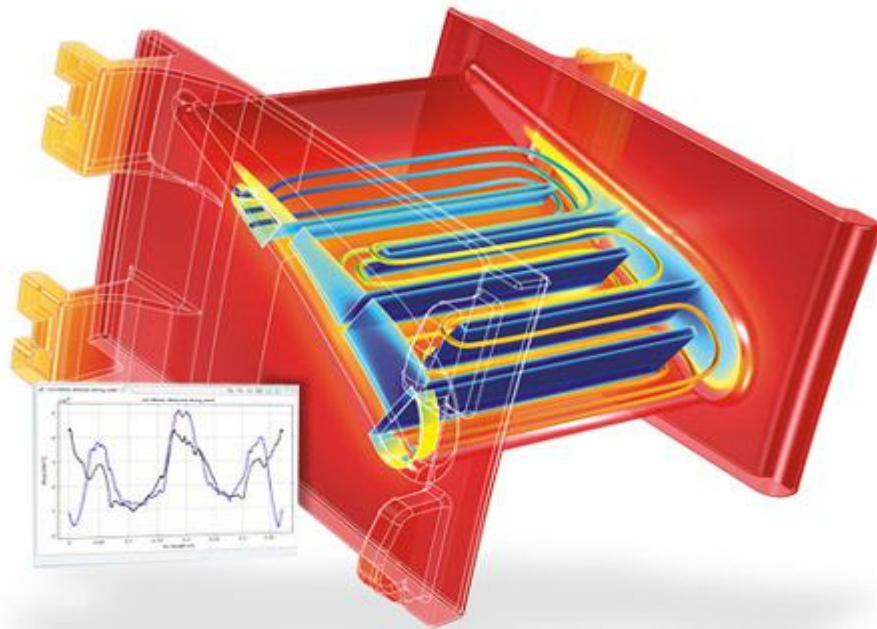


Figure 2.1 Thermal stress: a stator blade in the turbine stage of a jet engine is heated by the combustion gases. Shown is the temperature distribution throughout the blade, as well as the stresses in both welds [www.comsol.com]

Predefined multiphysics application templates solve many common problem types and different physics interfaces can be easily chosen. Different types of partial differential equations can be specified and interdependencies can be defined. Another noticeable characteristic of COMSOL platform is adaptability. As the modeling needs change, so does the software. It is also possible to include another physical effect or new formula to a geometry which is already modeled. Using advanced tools like parameterized

geometry, interactive meshing and custom solver sequences, it is possible to quickly adapt the model to a new requirement.

2.2 Organize & Customize

The COMSOL Desktop helps to organize the simulation by presenting a clear overview of the model at any point. It uses functional form, structure, and aesthetics as the means to achieve simplicity for modeling complex realities. For instance, task-specific tools appear on the Desktop, showing only the currently possible and necessary actions. They remove uncertainty from model building and bring order to the simulations.

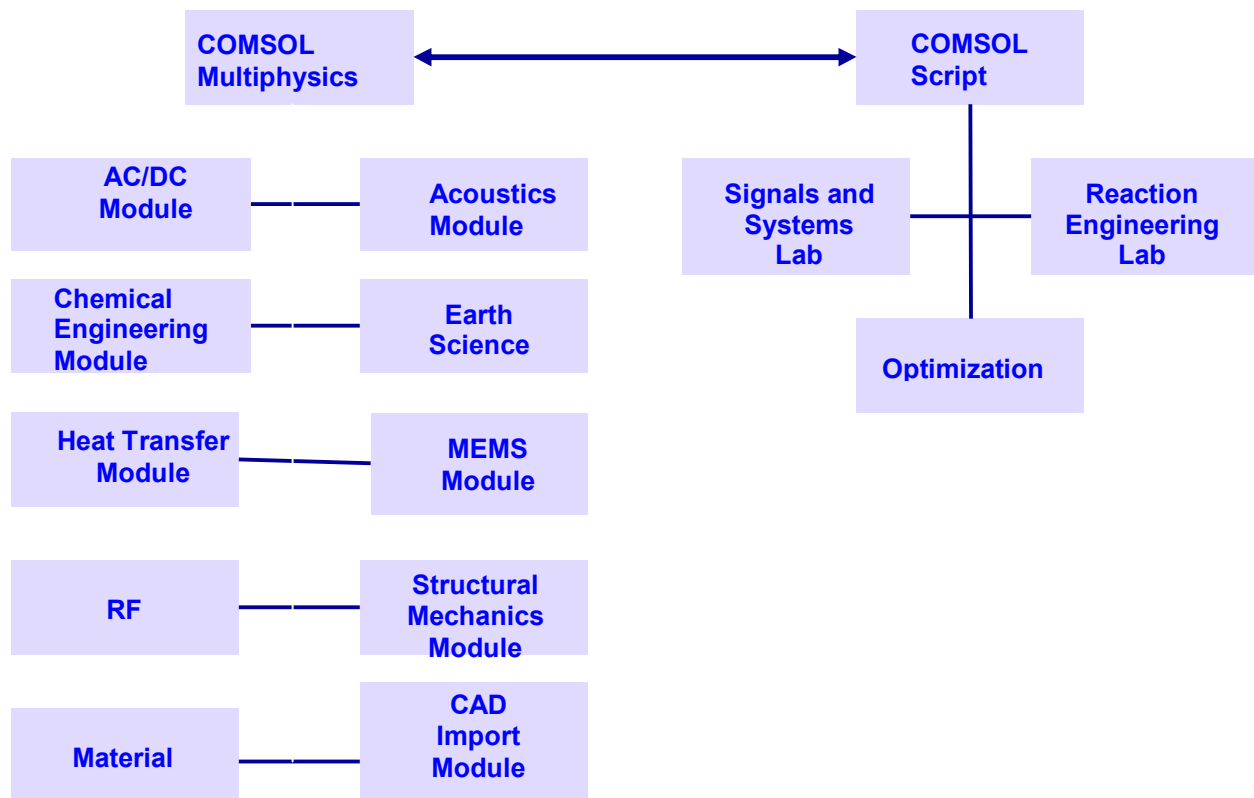


Figure 2.2 Product line of COMSOL Multiphysics 4.3 [www.comsol.com]

The Desktop is made up of several windows, which may or may not be displayed depending on the need. These windows include the Model Builder, Settings, Graphics, Messages, Progress, Help, and others. It is possible to easily customize the layout of these

windows on the Desktop to suit the particular work habits. All windows can be positioned and sized in any way. They can be detached from the Desktop and moved back and forth between computer displays. These settings can be saved as preferences for the next time when COMSOL Multiphysics is opened.

2.3 Chemical Reaction Engineering Module

Computer simulations is a well established area within chemical engineering development, allowing engineers and researchers to optimize process efficiency and explore new designs, while at the same time reducing costly experimental trials. A description combining several laws of physics as well as chemical reaction kinetics is often required to produce accurate simulations of real world applications.

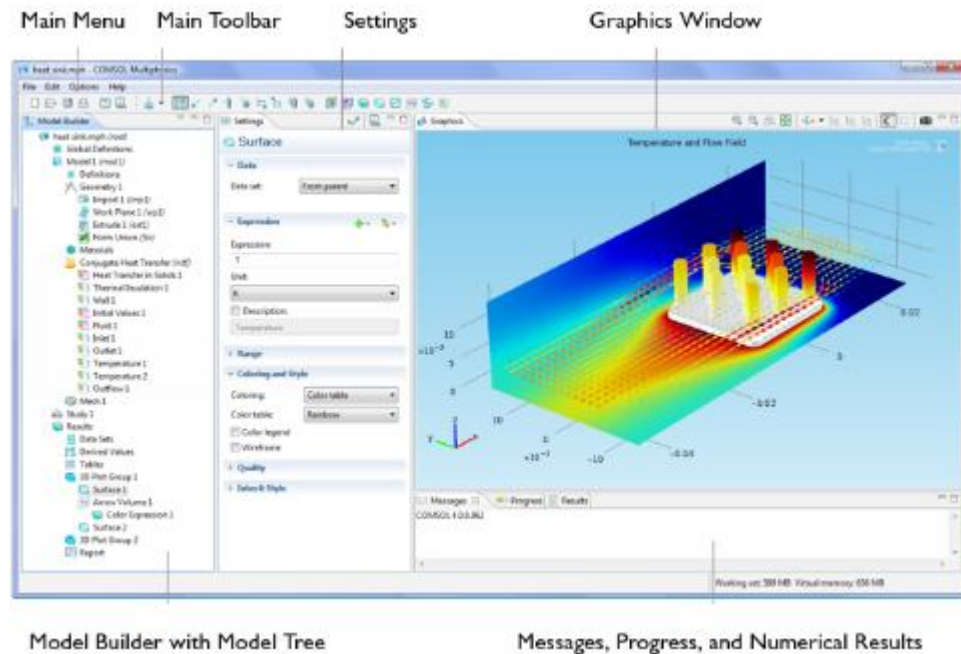


Figure 2.3 Graphical screen of COMSOL Multiphysics [www.comsol.com]

The combination of experimental work with theoretical analyses in computer models has shown to accelerate understanding as well as decrease development costs for new processes. The Chemical Reaction Engineering Module is an optional package that

extends the COMSOL Multiphysics modeling environment with customized user interfaces and functionality optimized for the analysis of mass transport and other transport phenomena coupled to chemical reactions for the modeling of reactors, filtration and separation units, separation and mixing processes, corrosion, chromatography, electrophoresis and other equipments common in the chemical and similar industries.

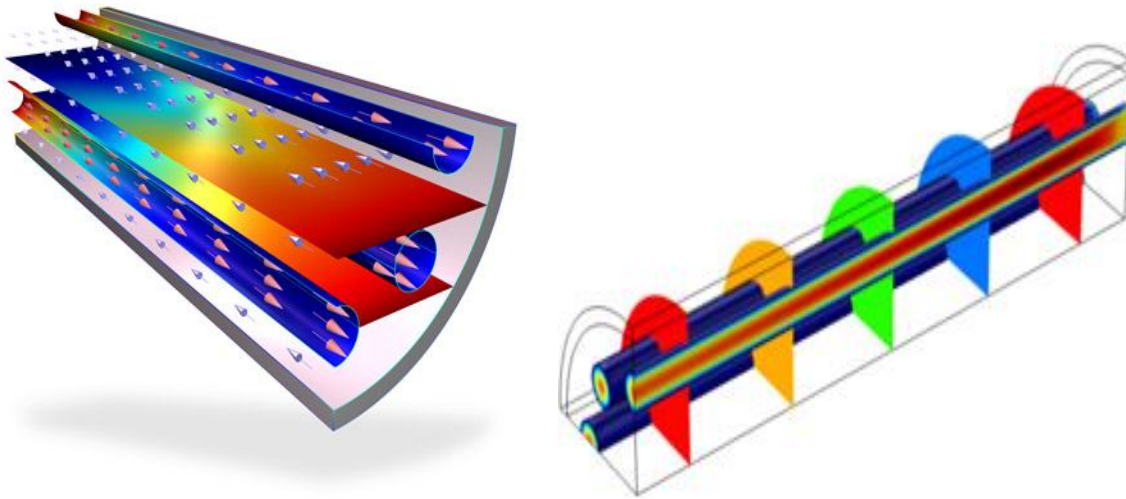


Figure 2.4 In power generators, a steam reformer unit typically produces the hydrogen needed for different purposes. The reformation chemistry occurs in a porous catalytic bed where energy is supplied through heating tubes to drive the endothermic reaction system [www.comsol.com]

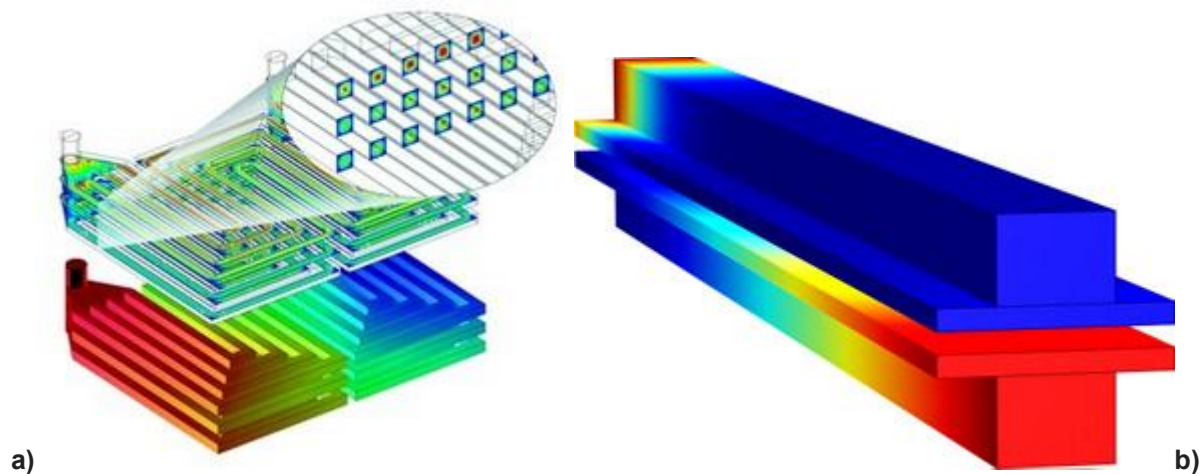


Figure 2.5 Fuel Cells, (a) The pressure distribution and velocity field in the channels of a fuel cell stack (b) Oxygen and fuel concentration distribution in the channels and the gas diffusion electrodes [www.comsol.com]

In addition to its application in traditional chemical industries, it is a popular tool for investigating clean technology processes and applications such as catalytic monoliths and reactive filters, micro laboratories in biotechnology, and in the development of sensors and equipment in analytical chemistry. It is specifically designed to easily couple fluid flow and mass and energy transfer to chemical reaction kinetics. Firstly, the Chemical Reaction Engineering Module uses reaction engineering formulas to create models of reacting systems. It can then solve the material and energy balances for such systems, including the reaction kinetics, where the composition and temperature vary with time, space, or both [Pryor, 2009].

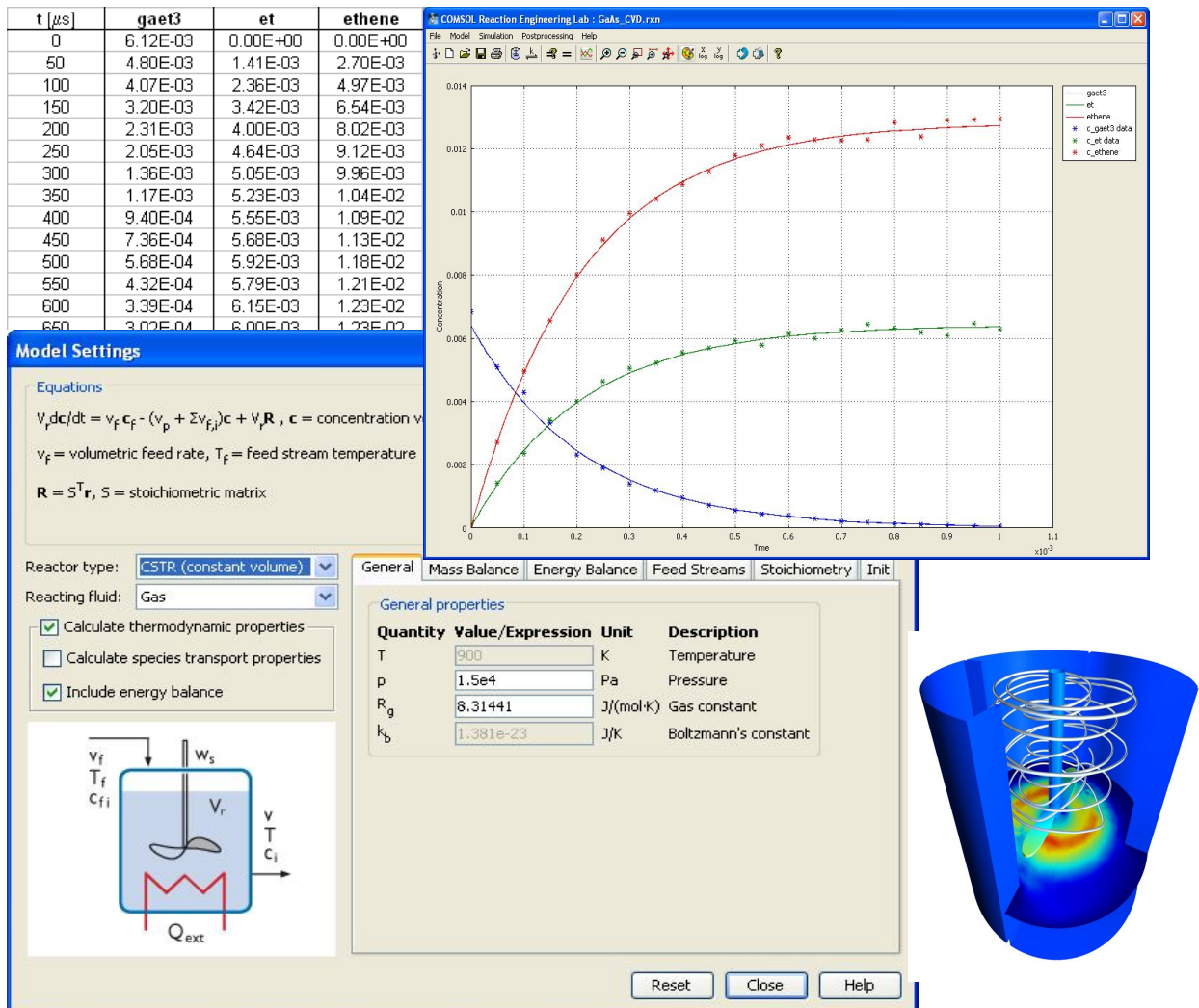


Figure 2.6 Calibrate the model according to experimental data [www.comsol.com]

The Chemical Reaction Engineering Module allows us to model the chemical reactions, calibrate the reaction model with experimental data, optimize the chemical processes in ideal reactors and explore the design in detailed reactor geometries. This allows for the inclusion of arbitrary expressions, functions, and source terms in the material property, transport, and reaction kinetic equations. Users also have access to a variety of thermodynamic and physical property data. Once a model of a product or a process is ready, it's possible to improve upon it. The optimization module can be used throughout the COMSOL Multiphysics product. It is a general interface for computing optimal solutions to engineering problems. Model inputs such as part shapes, material properties, or material distribution, can be treated as design variables, and any model output can be an objective function. The Optimization module computes the analytic sensitivities of the objective function to the design variables, considers any constraints imposed upon the problem, and uses a gradient-based optimization technique to find optimal designs.

3. Technology of Steam Reforming

3.1 Introduction

The use of hydrogen rich gas produced from coal and containing about 50% hydrogen with the rest mostly Methane and carbon dioxide, for lightening and heating began in early 1800s [Zittel et al., 1996]. The steam reforming reaction was introduced to the industry in the 19th century and included reactions of hydrocarbons and steam over calcium oxide and a cyclic process using nickel. The classical Haber Bosch process in 1917 was developed based on the reaction of steam with coke. Laboratory studies on the reforming reaction were published in the 1920s showing that product gases close to thermodynamic equilibrium were obtained over nickel catalysts. Fischer and Tropsch observed no significant differences when steam was replaced by carbon dioxide [Alzarmora et al., 1981 and Song, 2006]. The first patent on a tubular reformer using supported nicked catalysts was obtained by BASF in 1912 [Pichler et al., 1965] and the first industrial reformer was started in Baton Rouge in 1930. The reforming reaction took place over a catalyst in vertical tubes in parallel rows in a radiant fired furnace. Later, progress in production, design and use of more stable catalysts, led to the operation of steam reformers at more economic steam to carbon ratios. It enhanced the resistant to poisons without excessive carbon formation. The industrial breakthrough of steam reforming technology came in 1962, when ICI succeeded in stating two tubular reformers operating at high pressure (15bar) and using naphtha feedstock [Bridger, 1972]. The introduction of high pressure reforming meant that the energy consumption of the ammonia synthesis could be decreased significantly and as a result, a number of natural gas based ammonia plants were built [Rostrup Nielsen, 2008]. The first reformer

designed by Topsoe was started in 1965 followed by a hydrogen plant in 1966 operating at 42 bar [Rostrup Nielsen, 1975, 2002]. The Topsoe reforming technology was pioneered in full-size mono-tube pilot plant during 1960s, running on naphtha and since then steam reforming process became the preferred technology for synthesis gas for hydrogen and other petrochemicals production [Froment et. al., 2011]. Discovery of new solid catalysts and their application to steam reforming technology significantly improved the efficiency of the process. Catalytic steam reforming (CSR) involves the extraction of hydrogen molecules from a hydrocarbon or alcohol fuel and water over a base or noble metal supported catalysts and widely employed to produce hydrogen rich gas from various gaseous and liquid hydrocarbons fuels. Research in this area is still being pursued actively and knowledge from natural gas reforming containing methane is applied to reforming of higher hydrocarbons, alcohols and biofuels.

3.2 Steam Reforming of Light Hydrocarbons

3.2.1 Methane

3.2.1.1 Chemistry

Methane is an odorless and colorless gas and it is the principal constituent of the natural gas and producer gas from biomass feedstock. Methane from gasified biomass is most difficult to convert and has to be steam-reformed over a nickel or noble metal based catalyst at temperatures up to 1000 °C to increase the hydrogen and carbon monoxide yield. The gas exiting the reformer is cooled to about 350 °C and then subjected to the water gas shift reaction (WGS), in a high temperature shift converter. However, steam methane reforming is not just one reaction as indicated in equation 3.1 but involves contributions from several different catalyzed reactions such as water gas shift reaction (WGS), reverse water gas shift reaction (RWGS), carbon and methane decomposition reactions as described in equations 3.2-3.6 [Rostrup- Nielsen, 2011]:



The steps involved in steam methane reforming process for the production of pure hydrogen can be divided into feed pretreatment, steam reforming, carbon monoxide shift conversion and hydrogen purification. Pretreatment consists of desulfurization, which usually consists of a hydrogenator for the conversion of sulfur containing species into hydrogen sulfide followed by a zinc oxide bed for hydrogen sulfide scrubbing. After desulfurization, gas is fed into a reformer reactor, where it reacts with steam through reactions represented by equations (3.1-3.6). The reformer is composed of several reactor tubes filled with reforming catalysts and kept in furnace that provide heat necessary for the endothermic reaction and operated in high temperatures up to 1000 °C and pressure above 20 atmosphere [Rostrup-Nielsen et al., 2002 and Aparico et al., 2005]. Since the reaction produces an increase in the net number of product molecules, additional compression of the products would be necessary if the reaction were run at pressure smaller than 20 atm. Although the stoichiometry for equation 3.1 suggests that only one mole of steam is required for one mole of methane, the reaction in practice is being performed using high steam to carbon (S/C) ratio, typically in the range of (2.5-3.5) in order to reduce the risk of carbon formation and deposition on the catalyst surface and reformer wall [Froment, 2001]. In most of the industrial processes, the gas exiting the steam reformer is further processed for the industrial production of pure hydrogen or other chemicals. It is also used in Fischer-Tropsch process in order to produce wide variety of liquid and transportation fuels.

3.2.1.2 Thermodynamics

As shown in Equation (3.1 and 3.3), steam methane reforming reaction is highly endothermic; therefore, the reaction requires high temperatures to obtain high hydrogen productivity. Also, because reforming is accompanied by a volume expansion, it is favored by low pressure. On the other hand equation (3.2) is a water gas shift (WGS) reaction that is slightly exothermic and favors a low temperature condition while unaffected by changes in pressure. The changes in enthalpy and Gibbs free energy can be calculated; along with the corresponding equilibrium constants. The reaction requires certain temperatures to achieve sufficient activity Figure 3.1 shows the variation of Gibbs free energy as a function of temperature in the form of Ellingham type diagram for three representative reactions during steam methane reforming process: steam methane reforming, methane decomposition and carbon gasification [Rostrup Nielsen, 1984].

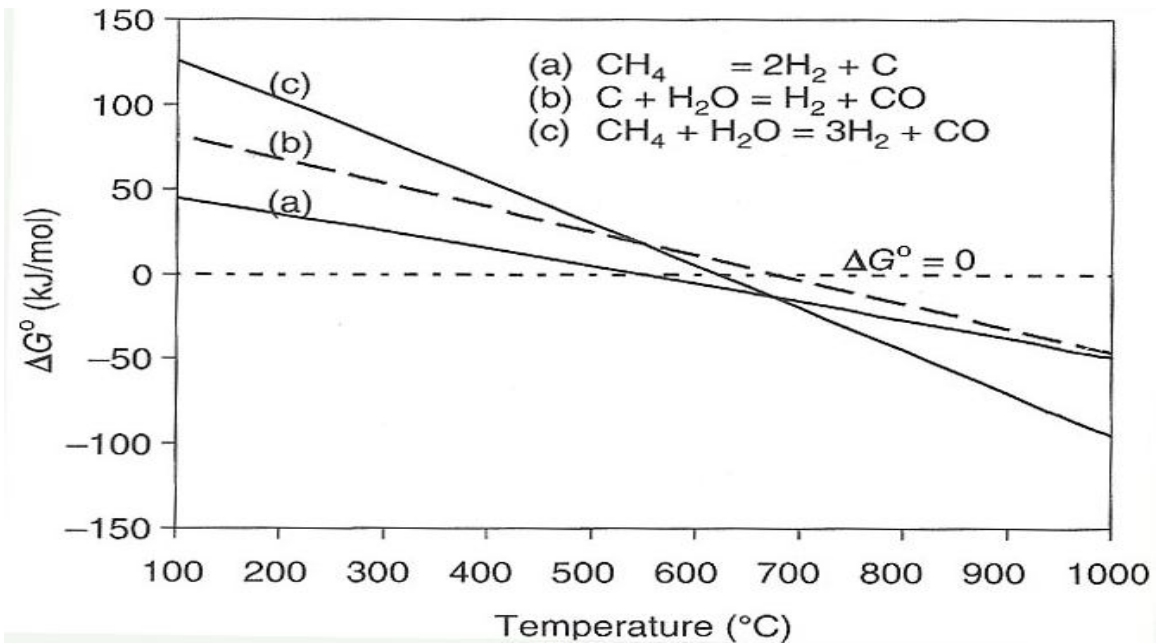


Figure 3.1 Variation of Gibbs free energy as a function of temperature [Rostrup-Nielsen et al., 2002]

ΔG declines as temperature increases for all three reactions, again reflecting the endothermic nature of these reactions. It can be seen that methane decomposition, (line a)

which leads to coke deposition, occurs at low temperature, around 500°C [Trimm et al., 2001]. However, carbon gasification reaction (line b) and the steam methane reforming (line c) require fairly high temperatures, (>700°C) to move forward.

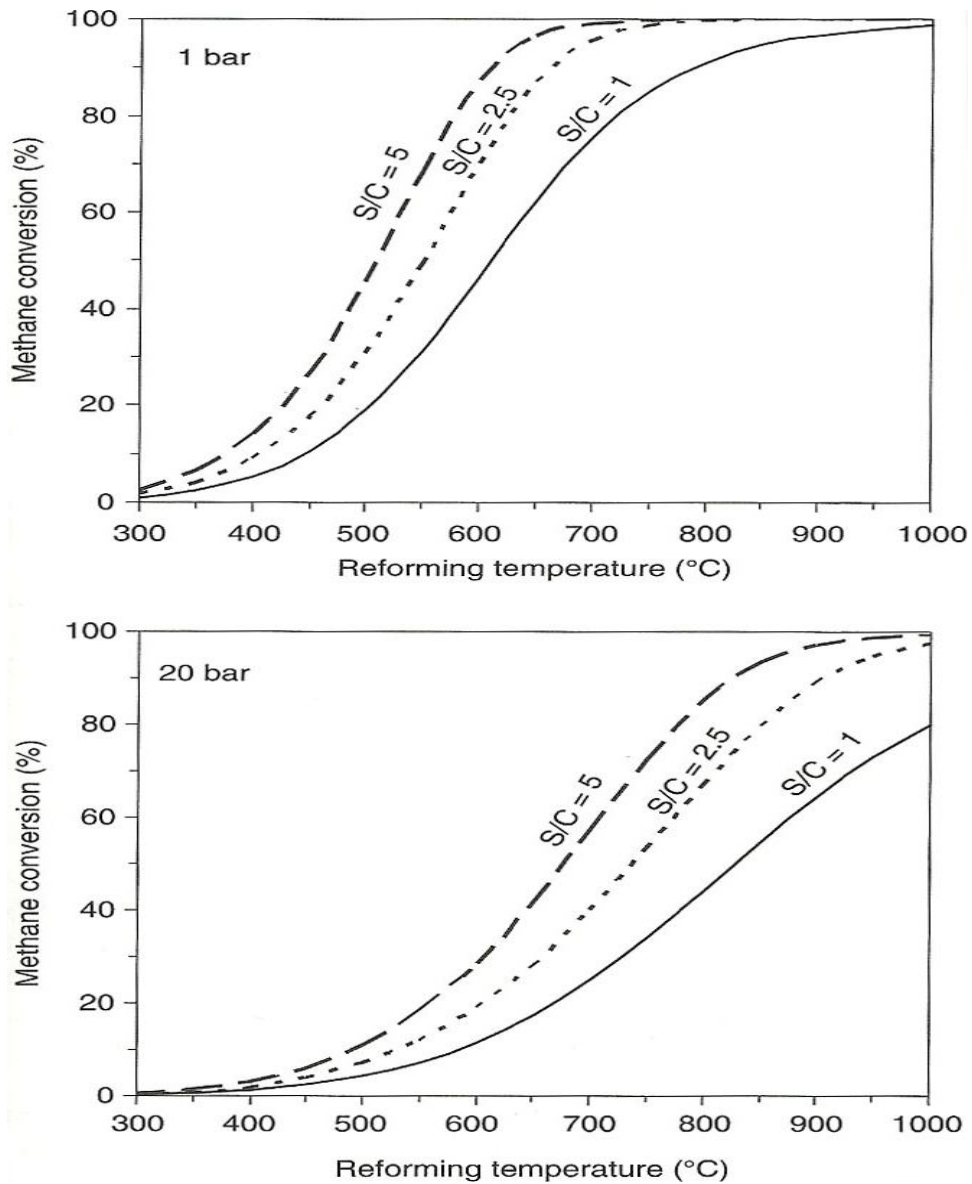


Figure 3.2 Equilibrium methane conversions at different temperatures, steam to carbon ratios and pressures obtained by thermodynamic calculations [Rostrup-Nielsen et al. 2002]

This makes heat transfer a critical reactor design component. It also shows the specific thermal requirements for material used for reactor manufacture. The equilibrium methane

conversions with increasing temperature calculated at different steam to carbon ratios and pressure between 1 and 20 bar are shown in Figure 3.2. The methane conversion increases with higher steam to carbon ratios and decreases with increasing pressure. A complete conversion of methane could be achieved at around 700°C at 1 bar pressure and the steam to carbon ratio of above 2.5, while a temperature above 900 °C would be required to achieve the complete methane conversion at 20 bar pressure. Presence of excess steam can suppress carbon deposition and avoid plant shut down caused by catalyst deactivation [Barthamolew, 1982, Trimm, 1997, and Snoeck et al., 1997a, 1997b]. Therefore, although stoichiometrically only steam to carbon ratios of one is needed for the steam methane reforming reaction, a 2.5-3.5 ratio is commonly used in practical applications. This requires an additional amount of energy to produce the steam [Rostrup-Nielsen 2002].

3.2.1.3 Kinetics and Reaction Rates Expressions

Many studies have been performed to investigate the kinetics of steam reforming, and while there is general agreement on first order kinetics with respect to methane, the reported activation energies span a wide range of values. This might be explained by experimental inaccuracies due to transport restrictions in the sense of diffusion and heat transfer restrictions in catalytic beds [Twigg, 1989]. A variety of kinetic models or rate expressions have been reported. The reaction mechanism of steam methane reforming is dependent on the catalysts, primarily on the active metal, the nature of the support and operation conditions. An extensive study of the intrinsic kinetics of the reforming and water gas shift reactions on a nickel based catalyst supported on alumina was performed by Xu and Froment [Xu et al., 1989a]. They developed a model, based on a Langmuir-Hinshelwood reaction mechanism, which includes as many as 13 reaction steps. The reaction rate of each reaction depends on the rate coefficients of the reactions, which incorporate temperature dependence, adsorption enthalpies, reaction activation energies, and entropies. It is also a function of partial pressure of each species, equilibrium

constants and adsorption constants [Hou et al., 2001, Rostrup-Nielsen 2002 and Gokon et al., 2009]. All of these parameters included in reaction rate expressions can be calculated experimentally according to different types of catalysts used in the experiments. The rate equations of the steam reforming reactions (3.1-3.3) can be written as:

$$r_j = k_j f_j(p, K_j) / Z^2(p, K_i) \quad j = 1, 2, 3 \quad i = CH_4, H_2O, CO_2, H_2, CO \quad (3-7)$$

Where k_j denotes the rate coefficient of reaction j , which incorporate temperature dependence, adsorption enthalpies, reaction activation energies, and entropies. f_j is a complex function of the partial pressures and equilibrium constants. Z is a function of partial pressures and the adsorption constants. The rate equations for the stoichiometric steam methane reforming reactions to synthesis gas and water gas shift reaction (3.1-3.3) are written as [Xu et al., 1989a]:

$$r_1 = \frac{\frac{k_1}{p_{H_2}^{2.5}} \left[p_{CH_4} p_{H_2O} - \frac{p_{H_2}^3 p_{CO}}{K_1} \right]}{DEN^2} \quad (3-8)$$

$$r_2 = \frac{\frac{k_2}{p_{H_2}} \left[p_{CO} p_{H_2O} - \frac{p_{H_2} p_{CO_2}}{K_2} \right]}{DEN^2} \quad (3-9)$$

$$r_3 = \frac{\frac{k_3}{p_{H_2}^{3.5}} \left[p_{CH_4} p_{H_2O}^2 - \frac{p_{H_2}^4 p_{CO_2}}{K_3} \right]}{DEN^2} \quad (3-10)$$

$$DEN = 1 + K_{CH_4} p_{CH_4} + K_{CO} p_{CO} + K_{H_2} p_{H_2} + \frac{K_{H_2O} p_{H_2O}}{p_{H_2}} \quad (3-11)$$

The temperature dependence of rate coefficients (k_1, k_2, k_3), adsorption coefficients of the gases, ($K_{CH_4}, K_{CO}, K_{H_2}, K_{H_2O}$) and equilibrium constants with temperature are described by an Arrhenius type function [Xu et al., 1989a]:

$$k_j = k_{j,0} \exp(-E/R_g T) \quad j = 1,2,3 \quad (3-12a)$$

$$k_1 = 4.22 \times 10^{15} \exp(-240100/R_g T) \quad (3-12b)$$

$$k_2 = 1.96 \times 10^6 \exp(-67130/R_g T) \quad (3-12c)$$

$$k_3 = 1.02 \times 10^{15} \exp(-243900/R_g T) \quad (3-12d)$$

To obtain the adsorption coefficient for each gas, the Arrhenius type function is used:

$$K_i = k_{i,0} \exp(-\Delta H_i/R_g T) \quad i = CH_4, H_2O, CO_2, H_2, CO \quad (3-13a)$$

$$K_{CH_4} = 6.65 \times 10^{-4} \exp(38280/R_g T) \quad (3-13b)$$

$$K_{H_2O} = 1.77 \times 10^5 \exp(-88680/R_g T) \quad (3-13c)$$

$$K_{H_2} = 6.12 \times 10^{-9} \exp(82900/R_g T) \quad (5-13d)$$

$$K_{CO} = 8.23 \times 10^{-5} \exp(70650/R_g T) \quad (5-13e)$$

The equilibrium constants for reactions 3.1-3.3 were calculated using the standard Gibbs energy of each reaction at the corresponding temperature.

$$K_1 = \frac{p_{H_2}^3 p_{CO}}{p_{CH_4} p_{H_2O}} = \exp(30.42 - 27106/T) \quad (3-14a)$$

$$K_2 = \frac{p_{H_2} p_{CO_2}}{p_{CO} p_{H_2O}} = \exp(-3.798 + 4160/T) \quad (3-14b)$$

$$K_3 = K_1 * K_2 = \frac{p_{H_2}^4 p_{CO_2}}{p_{CH_4} p_{H_2O}^2} = \exp(34.218 - 31266/T) \quad (3-14c)$$

The kinetic expressions were combined with conservation equations to give the reaction rates of each component:

$$r_{CH_4} = -(r_1 + r_3) \quad (3-15a)$$

$$r_{H_2O} = -(r_1 + r_2 + 2r_3) \quad (3-15b)$$

$$r_{H_2} = (3r_1 + r_2 + 4r_3) \quad (3-15c)$$

$$r_{CO} = (r_1 - r_2) \quad (3-15d)$$

$$r_{CO_2} = (r_2 + r_3) \quad (3-15e)$$

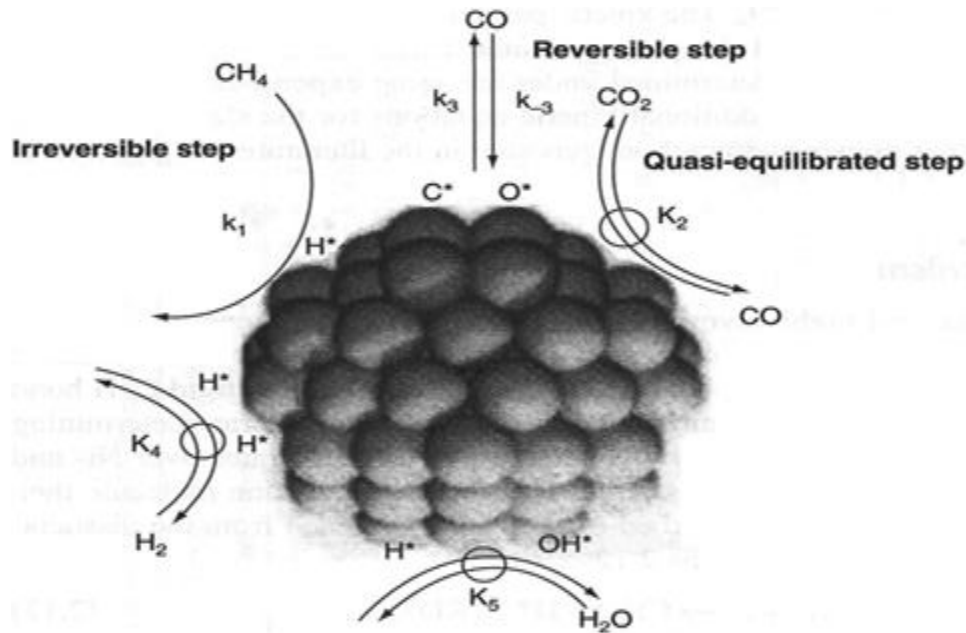


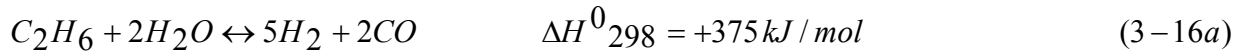
Figure 3.3 Sequence of elementary steps involved in the steam methane reforming and water gas shift reaction over nickel based catalysts [Wei et al., 2004]

3.2.2 Ethane and Propane

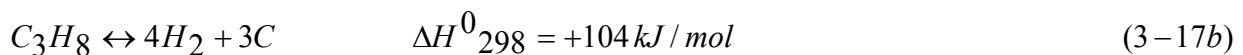
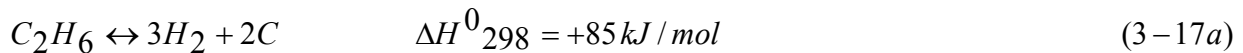
While natural gas reforming is the primary process for the industrial production of hydrogen, the reforming of other gaseous hydrocarbons such as ethane and propane, has been also explored for the production of hydrogen. The reforming of propane received particular attention in recent years because it is the primary constituent of liquefied petroleum gas (LPG) which is available commercially and can be easily transported and stored on site [Ogden et al., 1999 and Trimm et al., 2001]. Chemistry, thermodynamics and kinetics of steam reforming of ethane and propane are briefly discussed in this section.

3.2.2.1 Chemistry, Thermodynamics and Kinetics

Steam reforming reactions of ethane and propane are presented by equations (3.16a) and (3.16b) [Rostrup –Nielsen, 1984]:



Steam reforming of ethane and propane are endothermic and the endothermicity increases with increasing carbon number. These reactions are generally carried out in wide temperature range between 300 and 900 °C over a nickel or noble metal based supported catalyst. Under the reaction operating conditions other reactions such as cracking into carbon and hydrogen, cracking into methane can also occur [Rostrup –Nielsen, 1984]:



Similar to steam methane reforming process, the steam reforming of higher hydrocarbons in practice is also performed at higher steam to carbon ratios, typically between 1.5 and 3.5 in order to reduce the risk of carbon deposition. The nickel based catalysts known for steam reforming of natural gas is also active for steam reforming of $C_2 - C_4$ hydrocarbons. These reaction rates of the reactions are greatly attenuated in industrial tubular reactors by mass transfer resistance within the catalyst pellet and, to a lesser degree, by heat transfer resistance from the bulk fluid to the catalyst pellet surface. As with any intrinsic rate relationships, these rate expressions must be used in conjunction with a reactor model that accounts for these resistances for the model to be useful in assessing reformer performance and predicting the process as independent conditions are manipulated. The rate expression for steam reforming of higher hydrocarbons is written as [Rostrup –Nielsen, 1984]:

$$r_i = \frac{k_j * p_{C_nH_m} / p_{H_2}^{(m-n)/2}}{\left(1 + \frac{n * k_j}{K_j * K_{H_2O}} * \frac{p_{C_nH_m}}{p_{H_2}} * p_{H_2}^{(1-\frac{m-n}{2})} * K_{H_2O} * \frac{p_{H_2O}}{p_{H_2}} + \sqrt{K_{H_2} * p_{H_2}}\right)^2} \quad (3-18)$$

Each rate constant, (k_j, K_j) is a function of temperature and has its own pre-Arrhenius factor, as well as an activation energy (for k_j), and heat of adsorption (for K_j). The same K_{H_2} and K_{H_2O} is used for each reaction. These two are functions of temperature, with their Arrhenius factors and heats of adsorption. k_j and K_j values for each reforming reaction for hydrocarbons higher than methane are derived from rate data reported in the literature [Adris, 1996 and Rostrup-Nielsen, 1984], and validated with reformer outlet compositions measured in industrial furnaces. Each reaction also has an effectiveness factor associated with it. For higher hydrocarbons, equation (3.18) is expressed as follow,[Rostrup –Nielsen,1984]:

$$r_i = k_j * \exp\left(-\frac{E}{R_g T}\right) * (p_{C_n H_m})^a * (p_{C_n H_m})^b * (p_{H_2})^c \quad \text{mole}/(\text{kg cat} \cdot \text{s}) \quad (3-19)$$

For a nickel based catalyst the following expression was obtained for a steam reforming of Ethane and Propane [Rostrup–Nielsen, 1984]:

$$r_{C_2H_6} = 2.2 * 10^5 \exp\left(-\frac{9100}{T}\right) * (p_{C_2H_6})^{0.54} * (p_{H_2O})^{-0.33} * (p_{H_2})^{0.2} \text{mole}/(\text{kg cat} \cdot \text{s}) \quad (3-20)$$

$$r_{C_3H_8} = \frac{1.35 * 10^{14} \exp\left(-\frac{22.78}{T}\right) * (p_{C_3H_8})^{0.93} * (p_{H_2O})^{-0.53}}{1 + 52.48(p_{H_2})^{0.86}} \quad \text{mole}/(\text{kg cat} \cdot \text{s}) \quad (3-21)$$

The reaction order with respect to steam decreases with increasing temperature from 0.6 at 700 (K) to 0.2 at 900 (K). Kinetic parameters for the steam reforming of gaseous light hydrocarbons over various supported catalysts are presented in Table 3.1.

Hydrocarbon	Catalyst	Temperature Range (°C)	Pressure (MPa)	Order with Respect to		Activation Energy (kJ/mol)
				Hydrocarbon	Steam	
CH ₄	Ni/MgO	350–400	0.1	0.96	–0.17	60
C ₂ H ₆	Ni/MgO	450–550	0.1	0.60	–0.40	76
C ₂ H ₆	Ni/MgO	300–350	0.1	0.95	–0.46	81
C ₃ H ₈	Ni/α-Al ₂ O ₃	500–640	0.1	0.75	+0.60	67
C ₃ H ₈	Ni/MgO	300–350	0.1	0.93	–0.53	45
C ₄ H ₁₀	Ni/γ-Al ₂ O ₃	425–475	3.0	0.00	1.00	54
C ₄ H ₁₀	Ni/SiO ₂	400–450	0.1	0.00	1.00	–
C ₄ H ₁₀	Pt–Ni/ δ-Al ₂ O ₃	330–395	0.1	1.20	–0.18	81

Table 3.1 Kinetic parameters for steam reforming of gaseous light hydrocarbons, over various supported catalysts [Trimm, 2001]

3.2.3 Ethylene and Propylene

Ethylene and propylene can be steam reformed at high temperatures to produce hydrogen and synthesis gas. Steam reforming of alcohols such as methanol and ethanol is generally

considered as promising process for generating hydrogen especially for on-board fuel cell applications due to their easy availability, ability to transport, and reaction simplicity [Gencieu, 2002]. Both have high hydrogen to carbon ratio and they could be synthesized from renewable sources such as biomass [Deluga et al., 2004]. Unlike hydrocarbon fuels, methanol and ethanol are free from sulfur and this avoids additional sulfur removal step in the fuel processing. Alcohols can be reformed at lower temperatures of around 300 °C and this makes the fuel processing relatively simple and less complicated. Steam reforming is performed over Cu based catalysts or noble metals based supported catalysts in the temperature range between 200 and 300 °C at atmospheric pressure. Steam to carbon ratio is usually set between 1 and 2.

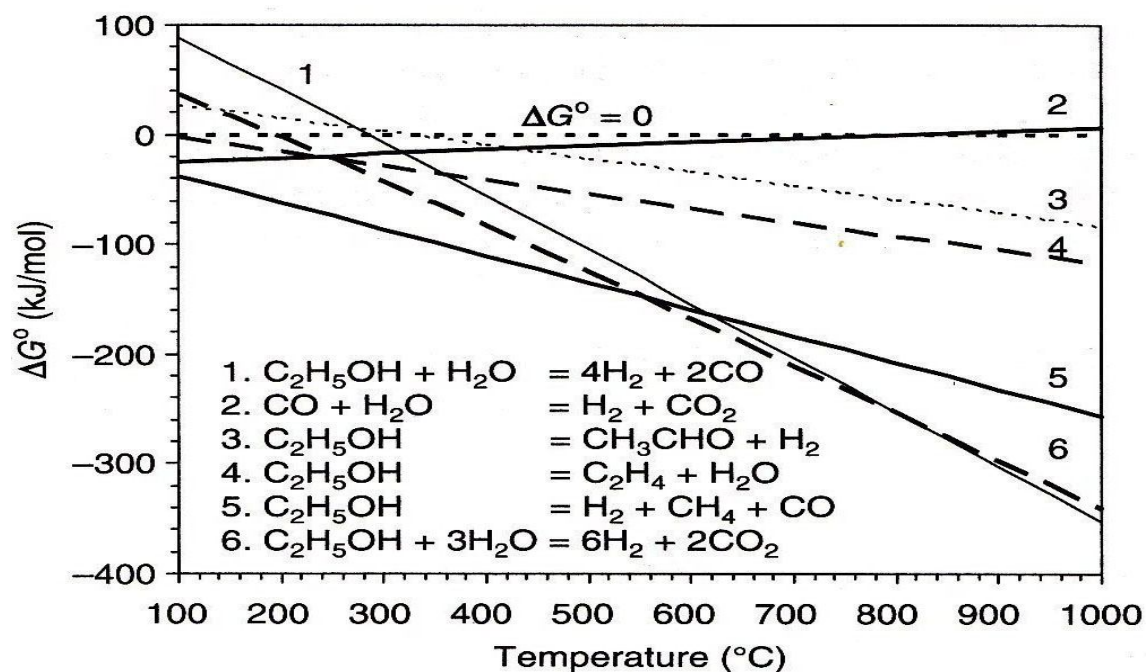


Figure 3.4 Free energy changes in the steam reforming, decomposition, dehydrogenation and dehydration of ethanol [Velu et al., 2007]

Higher steam to carbon ratios could favor the water gas shift reaction (WGS) which can reduce carbon monoxide concentration in the product stream and can also help in avoiding carbon formation on the catalyst surface. The reaction is highly endothermic and requires external heat supply. The process is highly efficient as hydrogen is coming

from both alcohol and water. Several other competing reactions such as dehydration to ethylene can also occur during steam reforming process at low temperatures. The variation of free energy values with respect to temperature for steam reforming of ethanol and accompanying reactions are shown in Figure 3.4. The values for steam reforming reactions to produce synthesis gas, (line 1) and hydrogen and carbon monoxide (line 6) become more negative above 200 °C, implying that these reactions are thermodynamically more favorable with increasing temperature. The free energy changes for the other reactions such as steam reforming of ethylene which could be formed as intermediates during the steam reforming of ethanol are shown in Figure 3.5.

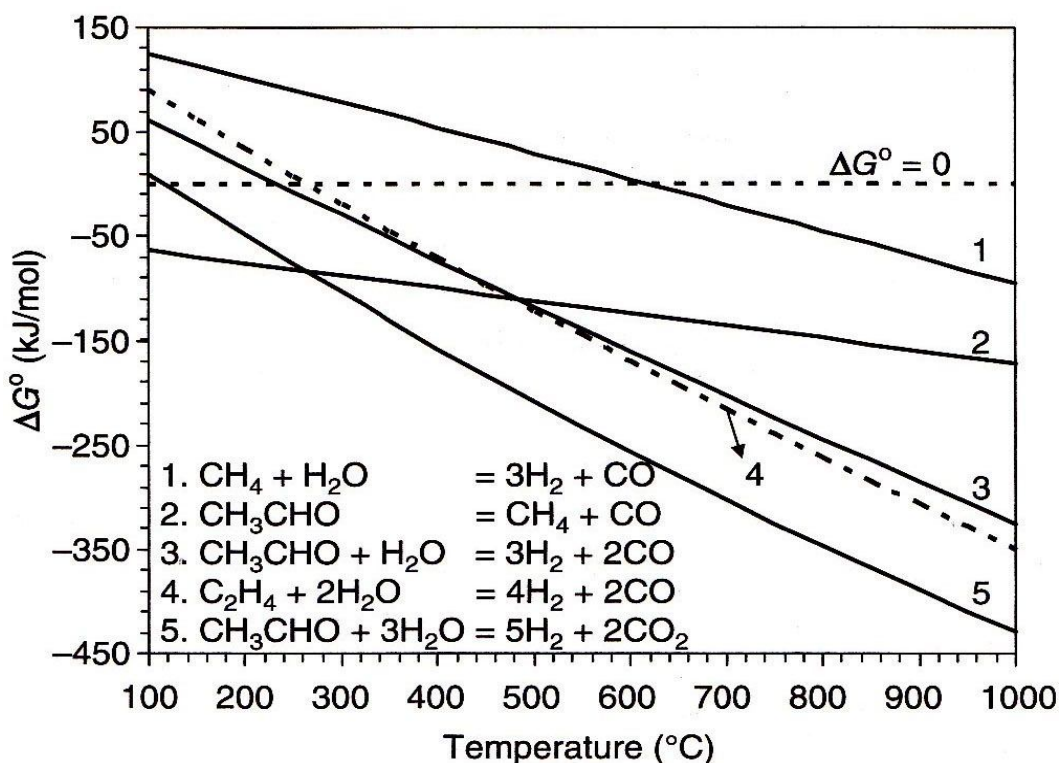


Figure 3.5 Free energy changes in the steam reforming of acetaldehyde, ethylene, and methane [Velu et al. 2007]

Side products like ethylene are steam reformed at high temperatures to produce synthesis gas. As can be seen a temperature of above 250 °C is required for steam reforming of

ethylene, (line 4). The reaction rate of ethanol steam reforming reaction is written as [Therdthianwong et al., 2001]:

$$r_{Ethanol} = 77.8 * (P_{Ethanol})^{2.52} * (P_{H_2O})^7 \quad (3-22)$$

Akande employed a power law model and expressed the rate equation in an exponential type function [Akande, 2005]:

$$r_{Ethanol} = k_j * \exp \left(-\frac{E}{R_g T} \right) * C_{Ethanol}^a \quad (3-23)$$

Where k_i is the rate constant of the reaction, E is the activation energy and T is the absolute temperature. The kinetic rates of steam reforming of ethanol over various supported catalysts are listed in Table 3.2.

Catalyst	Temperature (°C)	Rate Constant	Order w.r.t. Ethanol	Energy of Activation (E = kJ/mol)
Ni/Al ₂ O ₃	400	77.8 kmol/kg _{cat} /s/atm ^{9.52}	2.52	NA
Ni/Y ₂ O ₃	250–350	2.95 × 10 ⁻³ m ³ /kg _{cat} /s	1	7.04
Ni/Al ₂ O ₃	250–350	2.32 × 10 ⁻³ m ³ /kg _{cat} /s	1	16.88
Ni/La ₂ O ₃	250–350	19.1 × 10 ⁻³ m ³ /kg _{cat} /s	1	1.87
Ni/Al ₂ O ₃	320–520	NA	0.43	4.41
Cu-plated Raney nickel	250–300	NA	1	149

Table 3.2 Kinetic data of the steam reforming of ethanol over various supported nickel catalysts [Velu et al. 2007]

Intrinsic reaction rate relationships have been derived for steam reforming of ethylene and propylene based on Langmuir-Hinshelwood adsorption and reaction mechanisms. Regarding propylene reforming reaction, intrinsic kinetic expressions reported by Figueiredo and Trimm are adopted [Figueiredo et al., 1978]:

$$r_{C_3H_6} = 2.81 * 10^{-2} \frac{P_{C_3H_6}}{1 + 0.09 P_{C_3H_6}} * \exp(-8000/T) \quad \text{mole}/(\text{kg}_{cat} \cdot \text{s}) \quad (3.24)$$

As mentioned, kinetics expressions for steam reforming of other hydrocarbons are presented in Table 3.1.

3.3 Catalytic Fixed-bed Reactors

In chemical engineering processes, fixed bed reactors are very widely used, particularly for solid-catalyzed reactions in which the packing serves as the catalyst. Fixed bed reactors are preferred because of their simpler technology and ease of operation. As shown in Table 3.3, the major part of the catalytic processes of today's chemical and petroleum refining industries is carried out in fixed bed reactors [Froment, 2011]. In the fixed bed reactors, reactions take place on the catalyst particles (pellets) which are placed inside the reactor tubes either randomly or structurally [Agar, 1999]. The feed is given from one end of the reactor and products are taken from the other end of it. As shown in Figure 3.6, according to the energetic nature of the reaction, the heat is either supplied to the tube wall or taken out. In order to model a packed bed reactor, transport phenomena occurring in the bulk fluid, in the pellet, and at their interfaces must be considered utilizing the appropriate reaction rate expressions. In the design of these devices, fluid dynamics plays an important role, since the transport of chemical species, mixing or contacting catalytic surfaces is entirely described by the fluid dynamical conservation laws. The contacting of the solid by the gas tends to be quite uniform, and long contact times are possible. Fixed bed reactors are more difficult to control because of the process being distributed, nonlinear and sensitivity towards disturbances [Froment, 1972, 1974, Finalyson et al., 1981, Smith et al., 1982 and Folger, 2011]. Multi-tubular packed bed reactors composed of several vertical tubes with low tube to particle diameter ratios are especially selected for strongly endothermic reactions like steam reforming reactions. Steam reforming reactions take place in a catalytic fixed bed reactor filled with nickel or noble metal based catalysts particles. Due to the high heat input through the reformer tube wall and the endothermic reforming reactions, the catalyst tubes are exposed to

significant axial and radial temperature gradients [Rostrup-Nielsen, 1975 and Rostrup-Nielsen et al., 1988], therefore, packed beds have low diameter to height ratio to ensure efficient heat transport in radial direction. Scale up must often be done using many small diameter tubes in parallel rather than a single, large diameter bed. When the ratio of tube to particle diameter is low, the presence of the wall causes changes in bed structure, flow patterns, transport rates and the amount of catalyst per unit volume. In particular, the particles close to the wall will behave differently to those inside the bed. The velocity profile is quite complex in fixed bed reactors. When measured at a small distance from the surface of the packing, velocities are found to be approximately uniform except near the tube wall. Random packing gives more void space and thus higher velocities near the wall. Also, the large particle sizes needed to minimize pressure drop lead to diffusional resistances within the catalyst particles.

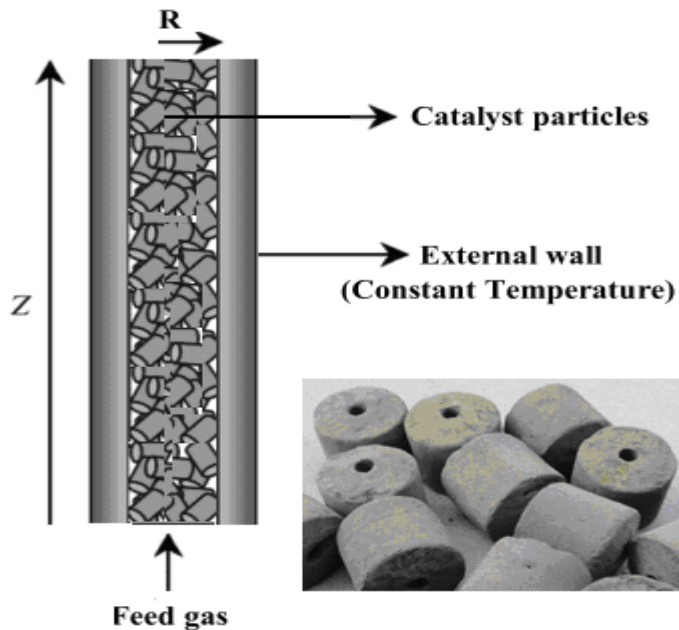


Figure 3.6 Schemes of the reformer tube, commercial and equivalent catalyst particles. Low diameter to height ratio ensures efficient heat transport in radial direction.

If catalyst deactivation is rapid, the fixed bed geometry may cause problems in regeneration. The tubes are heated by radiation from furnaces or by electrical heating bends. Effective heat transport to the reactor tubes and further into the centre of the catalytic fixed bed is a very important aspect during design and operation of steam

reformers. The challenge is to develop a better understanding of the interactions between flow patterns, species pellet diffusion, and the changes in catalyst activity due to the temperature fields near the wall region for modeling and design of these systems. The number of tubes in one unit is decided by the maximum feasible tube length. It would be economical to rather have a few long tubes than many short tubes but there is a limit of tube length determined by the risk of tube bending and by the pressure drop in the fixed beds. The maximum tube diameter is decided by the ability for efficient radial heat transport in the packed bed and the minimum tube diameter is restricted to the practical possibility for catalyst loading.

Basic chemical industry	Petrochemical industry	Petroleum refining
Steam reforming	Ethylene oxide	Catalytic reforming
CO conversion	Vinylacetate	Isomerization
Ammonia synthesis	Maleic anhydride	Polymerization
Sulfuric acid synthesis	Phthalic anhydride	Hydrocracking
Methanol synthesis	Styrene	Hydrodesulphurization

Table 3.3 Main chemical and petrochemical processes using packed bed reactors

In order to model a packed bed reactor, transport phenomena occurring in the bulk fluid, in the pellet, and at their interfaces must be considered utilizing the appropriate reaction rate expressions. According to the early classification [Froment et al. 2011], packed bed reactor models can be grouped in two categories; the pseudo-homogeneous and the heterogeneous models. Pseudo-homogeneous model consider the bed as a single phase, and lump the gas and solid phases together in the reactor modeling mass and energy balance equations. For very rapid reactions with important heat effects, it may be necessary to distinguish between conditions in the fluid and on the catalyst surface or even inside the catalyst. In case of heterogeneous models, gas and solid phases are modeled as separate mass balance and energy balance equations by considering interfacial gradients of temperature and concentration. In other words, in the pseudo-homogeneous model, the temperature inside the particles is not important, and the concentration and temperature in the internal field are the same as those in the external

field by which the reaction rate is obtained. However, in the heterogeneous model, transport processes play a finite role and the equations for the internal field have to be solved in order to obtain the reaction rate [Rostrup –Nielsen, 1988, Quinta et al., 2009 and Kvamsdal et al., 1999]. One of the important pseudo-homogeneous modeling applications on the methane steam reforming reactions is performed by Xu and Froment [Xu et al., 1989b]. They investigate the diffusional limitations of the intrinsic rate expressions and made a reactor simulation. There are also other results available comparing a pseudo-homogeneous and a heterogeneous two-dimensional models [De Wasch et al., 1972, Wijngaarden et al., 1989, Borkling et al., 1992, De Groothe et al., 1995, Froment, 2000, Piña et al., 2001 and Cao et al., 2005].

3.3.1 Role of Catalyst

In all reactors the desired conversion takes place on the catalyst and the role of the catalyst in all processes is to achieve equilibrium conversion as far as possible and maintain low pressure drop and in tubular and convective reformers to keep low tube metal temperatures. The catalyst should be mechanically stable under all process conditions. Breakdown of the catalyst pellets may cause partial or total blockage of the tube [Rostrup-Nielsen, 1984]. The catalyst must have sufficient activity, resistance to carbon formation and mechanical strength and are dedicated to serve in high temperature and high pressure conditions to meet the requirements for the reformer operation. Side reactions such as carbon formation are eliminated by use of proper catalyst type, controlled catalyst bed inlet temperature and a given steam to carbon molar ratio depending to the type of the feed. The particle size plays an important role for steam reforming catalyst activity. Smaller particles will provide a larger surface for reaction and hence improved catalyst activity. The catalysts can also be modified by basic metal oxides to be more carbon resistant. On the other hand, the shape of the catalyst pellet should be optimized to achieve maximum activity with minimum increase in pressure drop. The pressure drop depends strongly on the void fraction of the packed bed and

decreases with increasing particle size. The space velocity is used to determine the necessary catalyst volume for a given amount of feed but this parameter gives no information about pressure drop, heat transfer or carbon formation, so advanced models are necessary to evaluate a design. The catalyst ensures equal distribution of flow across the catalyst bed to protect the local overheating of the reactor tube leading to the shorter life of the reactor [Rostrup-Nielsen, 1988]. The activity of a catalyst is related to the surface area. The higher the active surface area of the catalyst, the greater the number of product molecules produced per unit time. Therefore, much of the art and science of catalyst preparation deals with high surface area materials (typically $100\text{--}400\text{ m}^2/\text{g}$). These are prepared in such a way that they are often crystalline with well-defined microstructures and behave as active components of the catalyst system in spite of their accepted name, supports. The (transition) metal atoms are then deposited in the micropores, and the sample is subsequently heated and reduced to produce small metal particles. Although the nickel surface area is generally increased with higher loadings, the dispersion or utilization of the nickel tends to decrease with increasing nickel content. Hence, the activity will not increase any further. In order to fulfill all the catalyst requirements in industrial practice, steam reforming of light hydrocarbons is performed over nickel or noble metal based catalysts. Nickel has been the favored active metal because of its sufficient activity and low cost compare to noble metals. Nickel is typically supported on alumina a refractory and highly stable material. The typical Al_2O_3 support for steam reforming catalysts is acidic and favors hydrocarbon cracking and polymerization. These catalysts are shaped into an optimal form, often in the form of multichannel wheels or cylindrical shape with one or more internal holes, as seen in Figure 3.6, in order to have a better heat and mass transfer and to minimize the pressure drop under the industrial operating conditions [Richardson et al., 1999 and Armor, 1999]. The nickel based catalysts suffer from catalyst deactivation by coke formation and sintering of metallic nickel active phase. Research has been undergoing to address these issues employing different approaches, including catalyst preparation and support

materials [Trimm, 1977, 1997, Sehested, 2001 and 2006]. Another major type of steam reforming catalysts is based on noble metals. The serious coking problem with nickel is caused by the formation, diffusion and dissolution of carbon in the metal [Rostrup-Nielsen, 2004]. However, carbon does not dissolve in noble metals yielding much less coking in those systems. Ru, Rh, Pd, Ir, and Pt were examined for their reforming performance. Ru and Rh displayed high reforming activity, stability and low carbon formation rates [Rostrup –Nielsen, 1984, Ridler et al., 1989 and Twigg, 1989]. However, the cost and availability of noble metals limit their application [Rostrup-Nielsen, 2002 and Nurunnabi et al., 2006].

4. Modeling of Steam Reforming Reactors

4.1 Introduction

Although the steam reforming process may appear straightforward from an overall consideration, in reality it is a complex coupling of catalysis, heat and mass transfer and mechanical design. The progress in steam reforming technology has resulted in less costly plants, in parts because of better materials for reformer tubes, better control of carbon limits, and better catalysts and process concepts with high feedstock flexibility. This progress has been accompanied by a better understanding of the reaction mechanism, the mechanism of carbon formation and sulfur poisoning, and the reasons for tube failure. Reactor modeling is an essential step in a scale up of new steam reforming reactor. Modeling of steam reformers has always been a challenge to chemical engineers and fixed bed modeling is one of the first applications widely used for steam reforming [Aris, 1969 and Elnashaie, 1992]. Recently, process modeling and simulation have attracted more attention because it can provide valuable data for design and optimization of commercial reactors. Process modeling result can also significantly improve the efficiency of steam reformer design and development and economic analysis, which is important for the success of steam reforming industry operation. Commercial processes for steam reforming use tubular reactors packed with supported nickel or noble metal based catalysts to improve the efficiency of the process. In the conventional reactors, strong endothermic reactions occur at high temperatures and conversion rate is high. In these conditions the reaction becomes diffusion controlled and as it is mentioned earlier, a suitable catalyst structure design play an important role in obtaining high activity and stability.

4.1.1 History of Steam Reforming Process

Numerous studies have focused on the kinetics of methane steam reforming therefore methane steam reforming kinetics in a conventional fixed bed reactor has been well described, especially on Ni catalysts [Bridger, 1980, Rostrup-Nielsen et al., 1988, Xu et al., 1989a, Aparicio, 1997, Luna et al., 1997, Craciun et al., 1998, Hou et al., 2001 and Kvamsdal et al., 2006]. Currently, the most accurate kinetics to represent the reforming reactions, particularly the Langmuir–Hinshelwood (Houghen–Watson) type expressions is reported by Xu and Froment [Xu et al., 1989a]. The mathematical model consists of a set of coupled ordinary or partial differential equations which can be solved with a standard numerical technique along the length of the reactor. A key concern is however that many kinetics and transport correlations have also been developed for the conventional models. Scale up requires a critical evaluation of all transport correlations, before they can be applied in numerical models. Conventional modeling of the catalyst side distinguishes the significance of the catalyst particle itself for the reactor performance and how heat transfer is taken into consideration. A given reactor can be modeled in different ways which are grouped in two broad categories: pseudo-homogeneous and heterogeneous models [Froment 1972, 1974]. Several comprehensive reviews have been written about steam reforming of hydrocarbons [Ridler, 1989, Liu et al., 2010 and Rostrup–Nielsen et al., 2011] and different types of catalytic reactors have been suggested. In addition, different methods have been used to address and simulate the steady state and non steady state operation of catalytic steam reformers [Yu et al., 2001, Robbins et al., 2003, Zafir et al., 2003 and Kolios et al., 2004]. One of the most important pseudo-homogeneous modeling applications on methane steam reforming reactions was carried out by Xu and Froment [Xu et al., 1989b]. They calculated diffusional limitations of the intrinsic rate expressions previously obtained by them [Xu et al., 1989a] and made a reactor simulation. They measured the pore size distribution of the steam reforming catalyst and calculated the effective diffusivity. A modified collocation method was used to obtain parallel pressure profiles of the reacting

components in the catalyst pellet. The simulation results were discussed in detail with an industrial steam reformer. A two-dimensional pseudo-homogeneous dispersion model was used to simulate a steam reformer by Kvamsdal et al. [Kvamsdal et al., 2006], considering the kinetic model given by Xu and Froment [Xu et al., 1989a] with additionally coke formation. The heat transferred to the reactor tube was calculated by axially varying overall heat transfer coefficient multiplied with a temperature change.

A heterogeneous model including coupled chemical reactions and diffusional limitations in catalyst pellet was derived by Salmi and Warna [Salmi et al., 1991], for fixed bed reactors. Froment [Froment, 2000] generated a model for the conceptual design of new reactor configurations and given its fundamental kinetics basis, for the development of more performing catalysts considering the steam and carbon dioxide reforming of natural gas. Pedernera et al. [Pedernera et al., 2003], analyzed the steady state operation of large scale primary reformers by means of a two dimensional heterogeneous model. The model accounts for the strong diffusion limitations in the catalyst particle at each axial and radial reactor position. The kinetic model reported by Xu and Froment [Xu et al., 1989a] was adapted, and therefore, to evaluate diffusional resistances the particle mass balances were numerically solved. The reforming unit which had cylindrical catalyst particles with cylindrical holes was studied by such a simplification that the complex geometry of the catalyst particles was represented by an equivalent annular model. As being a heterogeneous model, the governing equations for the bulk and the catalyst particle were generated for this system. For the catalyst particle, the effective diffusivities were calculated using expressions given by Xu and Froment [Xu et al., 1989a]. A two dimensional heterogeneous model, which accounts for transport in solid and fluid phases with axial and radial dispersions, was considered by Machac et al. [Machac et al., 2006] for studying heat and mass transport in a catalytic bed reactor where exothermic carbon monoxide oxidation reaction takes place. In the model for mass and energy balances, partial differential equations were considered in the fluid phase, and ordinary differential equations were used in the solid phase. Quinta et al. [Quinta et al., 2009], solved a heterogeneous two dimensional model to simulate a methane steam reformer with large-

pore catalysts, considering the strong internal mass transfer restrictions rigorously. In spite of this, the reforming reactions were represented by a first order single reaction; therefore, the diffusion reaction equation has a simple analytical solution. Cao et al. [Cao, et al., 2005] mathematically described and experimentally demonstrated the micro-structured catalysts used for steam methane reforming reaction in microchannel reactors. Two types of structures were evaluated in microchannel reactors and simulated with the developed heterogeneous reactor model. The modeling technique described in the paper provides a convenient way to evaluate variables in designing more efficient catalysts for steam methane reforming process. More recently Dybkjaer et al. and Liu et al. [Dybkjaer et al., 1995 and Liu et al., 2011] provide a general overview of synthesis gas technologies as well as in depth analysis of steam reforming process, provide a comprehensive introduction to this complex field, complete review of the works done in last decades and give a detailed analysis of the catalyst and process problems. They tackle crucial aspects in light of the new directions in the energy industry, in particular how to integrate fuel processing into contemporary systems. It comprehensively covers hydrogen and synthesis gas production and steam reforming process from its fundamentals to practical applications.

4.2 Modeling

4.2.1 Pseudo-Homogeneous Models

The model, used in most of the studies, is the pseudo-homogeneous model, which considers transport by plug flow in the reactor. Pseudo-homogeneous reactor models do not distinguish between the gas and solid phases in the fixed bed. The temperature pressure and concentrations are equal inside the catalyst or in the gas phase but rather involve averaged properties for both phases. The reaction rates are effective rates and calculated from bulk concentrations and temperatures. The reaction rates include effectiveness factors to compensate for the concentration differences between the gas and

internal in the particles [Kvamsdal et al., 2006]. The void fraction in a cross section of the bed varies from the wall to the central axis and concentration and temperature gradients occur in axial and radial direction, [Delmas et al., 1988 and Papageorgio et al., 1995]. The Navier Stokes equations for the momentum of the fluid in axial and radial directions are written as [Ergun, 1952]:

$$\rho_f \left(u_z \frac{\partial u_z}{\partial z} + u_r \frac{\partial u_z}{\partial r} \right) - \mu_f \left[\frac{\partial^2 u_z}{\partial z^2} + \frac{1}{r} \frac{\partial}{\partial r} \left(r \frac{\partial u_z}{\partial r} \right) \right] + \frac{\partial p}{\partial z} + \phi u_z = 0 \quad (4-1)$$

$$\rho_f \left(u_z \frac{\partial u_r}{\partial z} + u_r \frac{\partial u_r}{\partial r} \right) - \mu_f \left[\frac{\partial^2 u_r}{\partial z^2} + \frac{\partial}{\partial r} \left(\frac{1}{r} \frac{\partial}{\partial r} (r u_r) \right) \right] + \frac{\partial p}{\partial r} + \phi u_r = 0 \quad (4-2)$$

Where ϕ is given by the correlation of Ergun [Ergun, 1952]:

$$\phi = 150 \frac{(1-\varepsilon)^2}{\varepsilon^3 d_p^2} \mu_f + 1.75 \frac{(1-\varepsilon)}{\varepsilon^3 d_p} \rho_f |u| \quad (4-3)$$

Where, ε is the porosity of the packed bed.

The continuity equations for each gas component and the energy equation need to be added to the equations above. The continuity equation for the key reacting component i , and the energy equation can be written as follow in terms of concentration, single reaction and steady state [Froment et al., 2010]:

$$D_{er} \left(\frac{\partial^2 C_i}{\partial r^2} + \frac{1}{r} \frac{\partial C_i}{\partial r} \right) - u_z \frac{\partial C_i}{\partial z} - u_r \frac{\partial C_i}{\partial r} + \rho_b (1-\varepsilon) r_i = 0 \quad (4-4)$$

$$\frac{1}{r} \frac{\partial}{\partial r} \left(r \lambda_{er} \frac{\partial T}{\partial r} \right) + \frac{\partial}{\partial z} \left(\lambda_{er} \frac{\partial T}{\partial z} \right) - \rho_f C_P \left(u_z \frac{\partial T}{\partial z} + u_r \frac{\partial T}{\partial r} \right) + \rho_b (1-\varepsilon) \sum_j (-\Delta H_j) \eta_j r_j = 0 \quad (4-5)$$

The effective diffusion in radial direction describes the contribution arising from the transport in the fluid and corresponds to the mixing.

D_{er} represents this parameter based upon the superficial flow velocity. Similarly, λ_{er} shows the radial thermal conductivity. The conservation equations can be expressed in terms of partial pressures, p_i , after introducing the ideal gas law and assuming no radial change in total pressure. The axial dispersion is neglected as it is negligible compared to the axial convective transport at the operating Reynolds number in steam reformers, ($10^3 - 10^4$). The axial variations of the partial pressures are calculated as follow:

$$\frac{\partial p_i}{\partial z} = -\frac{p_i}{u_z} \frac{\partial u_z}{\partial z} + \frac{p_i}{T} \frac{\partial T}{\partial z} - \frac{R_g T}{u_z} \sum_j \varepsilon v_{ij} \eta_j r_j + \frac{1}{u_z} \left(\frac{\partial D_{er}}{\partial r} \frac{\partial p_i}{\partial r} + D_{er} \frac{\partial^2 p_i}{\partial r^2} - \frac{D_{er}}{T} \frac{\partial T}{\partial r} \frac{\partial p_i}{\partial r} + \frac{D_{er}}{r} \frac{\partial p_i}{\partial r} \right) \quad (4-6)$$

The boundary conditions at the center line of the reactor and at the wall are written as follow:

$$\frac{\partial p_i}{\partial r} = 0 \quad \text{at } r=0 \text{ and } r=R \quad (4-7a)$$

$$p_i = x_{i,in} p \quad \text{at } z=0 \quad (4-7b)$$

The sum of the balance equations for all the components, gives the total mass balance of the reactor in the form of the axial velocity:

$$\frac{\partial u_z}{\partial z} = \frac{u_z}{T} \frac{\partial T}{\partial z} - \frac{u_z}{p} \frac{\partial p}{\partial z} - \frac{R_g T}{p} \sum_j v_{ij} \eta_j r_j \quad (4-8)$$

The energy equation in the reactor is written as follow:

$$\frac{\partial T}{\partial z} = \frac{I}{\rho_f C_P u_z} \left(\lambda_{er} \left(\frac{1}{r} \frac{\partial T}{\partial r} + \frac{\partial^2 T}{\partial r^2} \right) + \rho_b (1-\varepsilon) \sum_j (-\Delta H_j) \eta_j r_j \right) \quad (4-9)$$

Where p_i is the partial pressure of the component, u_z is velocity along the reactor, η_j is the effectiveness factor, r_j is the reaction rate of the reaction j , D_{er} is diffusion coefficient, ρ_b is bulk density, λ_{er} is thermal conductivity coefficient and ε is porosity of the packed bed.

4.2.1.1 Boundary and Initial Conditions

The following general boundary and initial conditions are applied to the reformer [Froment et al., 2011]:

$$\begin{array}{l} \text{at } z = 0 \\ 0 \leq r \leq R \end{array} \rightarrow \begin{array}{l} C = C_0 \\ T = T_0 \end{array} \quad (4-10)$$

$$\begin{array}{l} \text{at } r = 0 \\ r = R \end{array} \rightarrow \frac{\partial C_i}{\partial r} = 0 \quad (4-11)$$

$$\text{at } p_i \rightarrow \frac{\partial T}{\partial r} = 0 \quad (4-12)$$

$$\text{at } r = R \rightarrow \frac{\partial T}{\partial r} = -\frac{h_w}{\lambda_{er}}(T_R - T_w) \quad (4-13)$$

Where h_w is the wall heat transfer coefficient. No distinction is made between the fluid and solid phase. The effect of the bed void fraction and, therefore, of the flow velocity profile is accounted for also in D_{er} and λ_{er} .

4.2.2 Pseudo-Heterogeneous Models

The Pseudo-heterogeneous model considers transport by plug flow again, but distinguishes between conditions in the fluid and in the solid (catalyst) phase. For very rapid reactions with important heat effects, it may be necessary to distinguish between conditions in the fluid and on the catalyst surface or even the conditions inside the catalyst [Froment et al., 2011, Wesenberg et al., 2001 and Pedernera et al., 2003].

Heterogeneous models distinguish between the fluid phase and the solid phase to correctly account for the heat transfer in the steam reformer reactor [De Wash et al., 1972, Pina et al., 2001 and Wesenberg et al., 2006]. This model consists of separate conservation equations for fluid and catalyst. Intra and external gradients are included and kinetics rate expressions are intrinsic multiplied by catalyst effectiveness factors. These considerations lead to the following mathematical model. The mathematical formulation is divided in two sections and is written for fluid and solid phase.

4.2.2.1 Fluid Phase

The fluid phase modeling equations is written as [De Wash et al., 1972]:

$$u_z \left(\frac{\partial C_i}{\partial z} + u_r \frac{\partial C_i}{\partial r} \right) = \frac{1}{r} \frac{\partial}{\partial r} \left(r D_{er} \frac{\partial C_i}{\partial r} \right) + k_g a_v (C_S^S - C_i) \quad (4-14a)$$

$$\rho_f C_P \left(u_z \frac{\partial T_f}{\partial z} + u_r \frac{\partial T_f}{\partial r} \right) = \frac{1}{r} \frac{\partial}{\partial r} \left(r \lambda_f \frac{\partial T_f}{\partial r} \right) + h_f a_v (T_S^S - T_f) \quad (4-14b)$$

Where, a_v is the specific surface area of the catalyst bulk per reactor volume.

In term of partial pressure and ideal gas assumption the above equations are written as follow. No radial change in pressure is assumed:

$$\frac{\partial p_i}{\partial z} = - \frac{p_i}{u_z} \frac{\partial u_z}{\partial z} + \frac{p_i}{T} \frac{\partial T}{\partial z} - \frac{k_g a_v}{u_z} (p_i - p_i^S) + \frac{1}{u_z} \left(\frac{\partial D_{er}}{\partial r} \frac{\partial p_i}{\partial r} + D_{er} \frac{\partial^2 p_i}{\partial r^2} - \frac{D_{er}}{T} \frac{\partial T}{\partial r} \frac{\partial p_i}{\partial r} + \frac{D_{er}}{r} \frac{\partial p_i}{\partial r} \right) \quad (4-15)$$

The boundary conditions at the center line of the reactor and at the wall are written as follow:

$$\frac{\partial p_i}{\partial r} = 0 \quad \text{at} \quad r = 0 \quad \text{and} \quad r = R \quad (4-16a)$$

$$p_i = x_{i,in}P \quad \text{at } z = 0 \quad (4-16b)$$

The sum of the balance equations for all the components, gives the total mass balance of the reactor in the form of the axial velocity:

$$\frac{\partial u_z}{\partial z} = \frac{u_z}{T} \frac{\partial T}{\partial z} - \frac{u_z}{p} \frac{\partial p}{\partial z} - \frac{a_v}{p} \sum_i k_g (p_i - p_i^S) \quad (4-17a)$$

The initial velocity at the inlet of the reactor is calculated from the molar input flow and considering cross section area of the reactor and inlet pressure and temperature:

$$u_{z,0} = \frac{R_g n T_0}{p_0 A} \quad (4-17b)$$

The energy transport in axial direction is dominated by the transport from axial convection, and thus axial conduction is neglected. With no radial convection, the only energy transport mechanism in radial direction is the effective conduction. The energy equation is simplified by assuming constant effective radial thermal conductivity:

$$\frac{\partial T}{\partial z} = \frac{I}{\rho_f C_P u_z} (\lambda_{er} (\frac{1}{r} \frac{\partial T}{\partial r} + \frac{\partial^2 T}{\partial r^2}) - h_f a_v (T - T_f^S)) \quad (4-18)$$

h_f is convection heat transfer coefficient at the catalyst surface, and a_v is the rate of surface area of the bulk catalyst to the reactor volume. The initial temperature at the inlet is a constant temperature.

4.2.2.2 Solid (Catalyst) Phase

When the resistance to mass and heat transfer inside the pellet is important, the rate of reaction is not uniform throughout the particle. The solid phase modeling equations is written as [De Wash et al., 1972 and Froment et al. 2011]:

$$k_g a_v (C_S^S - C_i) = \rho_c (1 - \varepsilon) r_i \quad (4-19a)$$

$$h_f a_v (T_S^S - T_f) = \frac{1}{r} \frac{\partial}{\partial r} (r \lambda_{er} \frac{\partial T_S}{\partial r}) + \rho_c (1 - \varepsilon) \sum_j (\eta_j (-\Delta H_j) r_j) \quad (4-19b)$$

The steady state diffusion mass transport balance equation for formation of components in a particle in cylindrical coordinates in term of partial pressures is written as [De Wash et al., 1972 and Froment et al., 2011]:

$$D_{er,i} \frac{\partial}{\partial y} (C_{tot} \frac{\partial x_{p,i}}{\partial y}) = -\rho_c \sum_j v_{ij} r_j \quad (4-20a)$$

$D_{er,i}$ is the effective diffusivity for each component within the catalyst pellet and it is a function of diffusivity, porosity, tortuosity and Knudsen diffusivity. It is calculated by [Rostrup-Nielsen, 1984]:

$$D_{er,i} = \frac{\varepsilon_p}{\tau_p} \frac{1}{\frac{1}{D_{m,i}} + \frac{1}{D_k}} \quad (4-20b)$$

ε_p is pellet porosity and τ_p is the pellet tortuosity factor . At operating pressures which is typical for steam reformers, it is shown that the Knudsen diffusivity is negligible [Rostrup-Nielsen, 1984]. The mass balance equation is solved for the active layer of the catalyst layer which is a fraction of the catalyst radius. The differential equation describing heat transport in a cylindrical catalyst is written as [Froment et al., 2011]:

$$\lambda_c \left(\frac{\partial T^2}{\partial r^2} + \frac{1}{r} \frac{\partial T}{\partial r} \right) = -\sum_j \rho_c (\eta_j (-\Delta H_j) r_j) \quad (4-21)$$

Where, λ_c is the catalyst thermal conductivity and assumed constant.

4.2.2.3 Boundary and Initial Conditions

The following general boundary and initial conditions are applied to the reformer, [Froment et al., 2011]:

$$\begin{array}{l} \text{at } z = 0 \\ 0 \leq r \leq R \end{array} \rightarrow \begin{array}{l} C_i = C_0 \\ T_f = T_s = T_0 \end{array} \quad (4-22)$$

$$\text{at } r = 0 \rightarrow \frac{\partial C_i}{\partial r} = \frac{\partial C_s}{\partial r} = 0 \quad (4-23)$$

$$\text{at } r = 0 \rightarrow \frac{\partial T_f}{\partial r} = \frac{\partial T_s}{\partial r} = 0 \quad (4-24)$$

$$\begin{array}{l} \text{at } r = R \\ T_f = T_s = T_w \end{array} \rightarrow \begin{array}{l} \frac{\partial C_i}{\partial r} = \frac{\partial C_s}{\partial r} = 0 \\ T_f = T_s = T_w \end{array} \quad (4-25)$$

$$\text{at } r = r_p \rightarrow C_i = C_i^S \quad (4-26)$$

$$\text{at } r = r_p \rightarrow T = T^S \quad (4-27)$$

Where C_i^S, T^S indicate the conditions at the surface of the catalyst. The above equations have to be solved simultaneously with the Reynolds averaged Navier Stokes equations and the Ergun equation given in previous sections to account for the radial void profile and generate both axial and radial flow velocity components. In these equations it is assumed that the heat transfer through the fluid and solid phase occur in parallel [Dixon et al., 1979, 1984, Delgado et al., 2006, Wesenberg et al., 2006].

4.3 Effectiveness Factors

Heterogeneous equations are of second order and highly nonlinear. That means, iterative solution procedure has to be necessary in each computational node. In order to consider the intra particle gradients, the effectiveness factors were introduced. The effectiveness

factors of the reactions are defined as the real reaction rates relative to the reaction rates for a completely active catalyst with temperature and partial pressures equal to those at the pellet surface. In the classical sense, an effectiveness factor is a factor that multiplies the reaction rate at the particle surface conditions to yield the rate that is actually experienced when the conditions inside the particle are different. For simple rate expressions and particle geometries, such as spherical and cylindrical, analytical solutions are available. In this case, the effectiveness factors are proportional to the particle diameter. For the catalyst particles with holes it is shown that the effectiveness factors varied linearly with surface to volume ratio and significant variations depending on kinetics and operating temperatures are found, [Rostrup-Nielsen, 2002]. The effectiveness factors are calculated by, [Froment et. al. 2011]:

$$\eta_j = \frac{\text{Rate of reaction with diffusion}}{\text{Rate of reaction with surface conditions}} \quad (4-28a)$$

$$\eta_j = \frac{\int_0^R r_j dv}{V_p r_j^s} \quad (4-28b)$$

The steam reforming catalysts have a variety of shapes, but for all only a thin layer close to the external surface is active. Therefore, planar geometry can be assumed. Then, the volume of the active part of the catalyst is:

$$V_p = a_v X r_p \quad (4-29)$$

Where, X is the radius of the active part of the catalyst. The effectiveness factor for this system can be written as:

$$\eta_j = \frac{a_v}{(1-\varepsilon)r_j^s} \int_0^{XR_p} r_j dx \quad (4-30)$$

Since the molecular diffusivity and thermal conductivity of the pellet catalyst are low, there is a resistant to heat transfer in the catalyst pellet and according to the literature effectiveness factors of the steam reformers are less than 0.5 [Rostrup-Nielsen, 2011]. Momentum equation which shows the pressure distribution in the packed bed reactor was described by the Tallmadge who proposed an extension of Ergun's equation under higher Reynolds numbers [Ergun, 1952, Tallmadge, 1970 and Froment et. al., 2011]:

$$\frac{dp}{dz} = -\frac{f\rho f_z^u}{d_p} \quad (4-31a)$$

The friction factor is written as [Froment et al. ,2011]:

$$f = \frac{(1-\varepsilon)}{\varepsilon^3} \left[1.75 + \frac{150(1-\varepsilon)}{\text{Re}_p} \right] \quad (4-31b)$$

For hollow cylinders and rings the equivalent particle diameter is calculated as:

$$d_p = 6 \frac{V(\text{Cylinder})}{S(\text{External Cylinder})} E^m \quad (4-31c)$$

$$E = \frac{V(\text{Particle}) * S(\text{External Cylinder})}{S(\text{Particle}) * V(\text{External Cylinder})} \quad (4-31d)$$

$$m = \frac{d_o/d_i}{\left(\frac{d_o}{d_i}\right)^{0.4} + 0.01\left(\varepsilon \frac{d_o}{d_i}\right)^{0.75}} \quad (4-31e)$$

Where, d_o and d_i are the external and internal diameters of the hollow cylinder respectively.

5. Experimental Correlations for Packed bed Reactors

5.1 Introduction

In order to model a reactor correctly, it is necessary to estimate the heat and mass transfer coefficients exactly. Empirical correlations for describing heat and mass transfer in packed bed reactors have been studied theoretically and experimentally for long time, [Dixon et al., 1979]. A great number of researchers have contributed to the knowledge of the heat and mass transfer mechanisms and how these can be transferred to empirical correlations. The estimated parameters from these correlations have wide range of variety because of the various different type of catalysts used, and different experimental methods and assumptions regarding the dependencies of the correlations. These dependencies are the geometry and shape of the tube and pellets, the physical properties of the fluid and the fluid velocity. These variations in correlations will be discussed in this section. The values or expressions estimated are based on the information in the literature or on assumptions that are usually used for this type of reactor.

5.2 Radial Effective Dispersion Coefficient

Dispersion plays an important role in reactant and product transport in packed bed reactors. Dispersion in packed beds depends on length of the reactor, viscosity and density of the fluid, ratio of reactor to particle diameter, particle shape and size distribution, effect of fluid velocity and effect of temperature. When a fluid is flowing through a bed of inert particles, one observes the dispersion of the fluid in consequence of the combined effects of molecular diffusion and convection in the spaces between

particles. Generally, the dispersion coefficient in longitudinal direction is superior to the dispersion coefficient in radial direction by a factor of 5, for values of Reynolds number larger than 10. For low values of the Reynolds number ($Re < 1$), the two dispersion coefficients are approximately the same and equal to molecular diffusion coefficient [Rase, 1990 and Delgado, 2006]. The flow in a packed bed reactor also deviates from the ideal pattern because of radial variations in flow velocity and mixing effects due to the turbulence and the presence of the packing. The flux due to this mechanism is described by Fick's law equation for mass transfer or Fourier's law for heat transfer by conduction. The proportional constants are effective diffusivities and conductivities. At Reynolds numbers of $10^3 - 10^4$, as usually seen in steam reformers [Rostrup-Nielsen et al., 1988], the axial dispersion is negligible compared to the axial convection. Therefore, only the radial dispersion coefficients exist. The volumetric molar flux caused by dispersion is modelled by Fick's law and the effective radial dispersion coefficient of the packed bed, is calculated as follow [Smith et al., 1982]:

$$N_i = \frac{1}{r} \frac{\partial}{\partial r} (E_{er} r C_{tot} \frac{\partial x_i}{\partial r}) \quad (5-1)$$

Where, N_i is total molar flux, and x_i is mole fraction of each component.

Depending on the shape of the catalyst and due to wide range of experimental and theoretical results there are many correlations available for dispersion coefficient in fixed bed reactors. For design purposes, dispersion coefficient is usually expressed in the form of Peclet number for dispersion and pellet diameter. One commonly used correlation is suggested by Froment et al. [Froment et al., 1987]:

$$Pe_E = \frac{10}{\varepsilon} (1 + 19.4 (\frac{d_p}{d_t})^2) \quad 10 < Re < 1000 \quad (5-2)$$

Where Peclet number is a function of radial dispersion coefficient and is expressed as follow:

$$Pe_E = d_p u_z / E_{er} \quad (5-3)$$

In this context, it is interesting to consider the predicting accuracy of some alternative empirical correlations that have been proposed to represent the experimental data in liquid flow. These equations are dependent on molecular diffusion coefficient which is presented by dispersion Peclet number such as the equation of Gunn [Gunn, 1969]:

$$\frac{1}{Pe_E} = \frac{1}{Pe_D} + \frac{1}{\tau_p} \frac{\varepsilon}{Re_p Sc} \quad (5-4)$$

Where Reynolds, Schmidt, Peclet diffusion and Peclet thermal numbers are written as follow:

$$Re_p = \frac{u_z \rho_f d_p}{\mu_f}, Sc = \frac{\mu_f}{\rho_f D_m}, Pe_D = \frac{d_p u_z}{D_m} \quad (5-5a)$$

Where the Peclet diffusion number can be defined by Wen [Wen, 1975]:

$$Pe_D = 40 - 29e^{-7/Re_p} \quad \text{for spheres } \tau_p = 1.41 \quad (5-5b)$$

$$Pe_D = 11 - 4e^{-7/Re_p} \quad \text{for solid cylinders } \tau_p = 1.93 \quad (5-5c)$$

$$Pe_D = 9 - 3.3e^{-7/Re_p} \quad \text{for hollow cylinders } \tau_p = 1.8 \quad (5-5d)$$

There is another empirical equation proposed for all type of catalysts [Wen, 1975]:

$$Pe_E = \frac{17.5}{Re_p^{0.75}} + 11.4 \quad \text{for} \quad Pe_D = \frac{d_p u_z}{D_m} > 10^3 \quad (5-6)$$

After extensive review of the empirical values and from the experimental results, dispersion coefficient can be calculated according to the Schmidt and Peclet number [Delgado, 2006]:

For $Sc \leq 550$:

$$\frac{1}{Pe_E} = \frac{1}{\tau_p} \frac{1}{Pe_D} + \frac{1}{12} - \left(\frac{Sc}{1500}\right)^{4.8} * (\tau_p Pe_D)^{3.83 - 1.3 \log_{10}(Sc)} \frac{17.5}{Re_p^{0.75}} + 11.4 Pe_D \leq 1600$$

$$\frac{1}{Pe_E} = (0.058Sc + 14) - (0.58Sc + 2) \exp\left(-\frac{352Sc^{0.5}}{Pe_D}\right) \quad Pe_D > 1600 \quad (5-7)$$

For $Sc > 550$:

$$\frac{1}{Pe_E} = \frac{1}{\tau_p} \frac{1}{Pe_D} + \frac{1}{12} - 8.1 * 10^{-3} * (\tau_p Pe_D)^{0.268} \quad Pe_D \leq 1600$$

$$\frac{1}{Pe_E} = 49.5 - 33.9 * \exp\left(-\frac{15Sc}{Pe_D}\right)^{0.5} \quad Pe_D > 1600, \quad (5-8)$$

τ_p is the tortuosity factor for the packed beds and depends on the shape of the catalyst particles [Gunn, 1969]:

$\tau_p = 1.41$, spheres, $\tau_p = 1.93$, cylinders, $\tau_p = 1.8$, hollow cylinders

5.3 Radial Heat Transport Parameters

Absolute values of heat transfer parameters that can be used for scale up are difficult to determine due to very high gas velocities and heat fluxes in industrial units. The steam reforming reactions are strongly endothermic and limited by chemical equilibrium. This implies that for a new catalyst, the reaction will be close to chemical equilibrium in the major part of the reformer tube, so variation in catalyst activities will only have a small impact on the temperature profile. If, however, heat transfer is increased a corresponding amount of heat will be absorbed, resulting in a higher equilibrium conversion and a higher catalyst temperature. The heat transfer coefficient, as a good approximation, can be considered independent of kinetics, when evaluating heat transfer data from measurements including reaction, as long as the catalyst is highly active. The energy transport in axial direction is dominated by the transport from axial convection, and thus

axial conduction is neglected. With no radial convection, the only energy transport mechanism in radial direction is the effective conduction. Due to the resistance to heat and mass transfer in the radial direction the temperatures and conversions are not uniform in a cross section. There is a need for a model that predicts the detailed temperature and conversion pattern in the reactor. The heat transfer parameters in this model are the effective radial conductivity and the wall heat transfer coefficient [Dixon et al., 1979, 1984, 1988, 1998 and Kvamsdal, 2006] and are generally expressed in form of dimensionless groups and constants. Following is a review of the empirically developed correlations in the literature.

5.3.1 Radial Effective Thermal Conductivity

Effective thermal conductivity of the packed beds depends not only on the shape and size of the catalyst pellets but also on heat transfer mechanism and flow characteristics including stagnation point which are explained by Reynolds and Peclet numbers [Achenbach, 1995]. Due to dominant axial convection in steam reformers, axial term of thermal conductivity is usually neglected. This effective conductivity includes conduction in both the solid pellets and the gas phase and also some contribution from turbulence and between pellets. There are wide varieties of correlations for the effective radial conductivity in literature which are based on experimental results. Most of these correlations include the stagnant term which depends on particle and gas thermal conductivity and heat transfer [Wijngaarden, 1992, Peters et al., 1988, Borman et al., 1992 and Dixon et al., 1998]. There is no dependency of effective radial thermal conductivity on particle and tube diameter, (d_p and d_t) reported but tube to particle diameter ratio play an important role in these correlations and usually is larger than 5 to assure an appropriate packing at industrial conditions [Dixon et al., 1998]. Some of the most important variables are as follow [Kunii et al., 1960, Dixon et al., 1979, Peters et al., 1988, Borkling et al., 1992 and Wesenburg et al., 2006]:

$$\frac{\lambda_{er}}{\lambda_f} = 21 + 0.23 \text{Re}_p \quad \text{For cylinders} \quad 25 < \text{Re}_p < 350 \quad (5-9)$$

$$\lambda_{er} = 0.37 + 2.54 * 10^{-3} \text{Re}_p \quad \text{For rings} \quad 50 < \text{Re}_p < 1500 \quad (5-10)$$

$$\frac{\lambda_{er}}{\lambda_f} = \frac{\lambda^{stag}}{\lambda_f} + \frac{\text{Re}_p \text{Pr}_p}{\text{Pe}_D} \quad \text{All type} \quad 100 < \text{Re}_p < 900 \quad (5-11)$$

$$\text{Pe}_D = 3.2 + 49.4 \frac{d_p}{d_t}$$

$$\lambda_{er} = \lambda_f + \lambda_c \left(1 + \frac{8\lambda_f}{h_w d_t}\right) * \left[\frac{(1-\varepsilon) \left(\frac{d_p}{d_t}\right)^2}{1 + \frac{5.33\lambda_c}{h_w d_p} + \frac{0.1}{\lambda_c}} \right] \quad \text{For cylinders} \quad \text{Re}_p > 40 \quad (5-12)$$

$$\lambda_{er} = \lambda^{stag} + \frac{0.0026}{1 + 46\left(\frac{d_p}{d_t}\right)^2} \text{Re}_p \quad \dots \quad \text{For cylinders} \quad 100 < \text{Re}_p < 400 \quad (5-13)$$

λ^{stag} is measured in stagnation point:

$$\lambda^{stag} = \lambda_f \varepsilon_p + \lambda_f \frac{0.895(1-\varepsilon_p) \left(\ln \left[\frac{\lambda_c}{\lambda_f} - 0.5439 \left(\frac{\lambda_c}{\lambda_f} - 1 \right) \right] - 0.4561 \frac{\lambda_c - \lambda_f}{\lambda_c} \right)}{0.3521 \left(\frac{\lambda_c - \lambda_f}{\lambda_c} \right)^2} \quad (5-14)$$

In the above equations, Pe_p is Peclet thermal number and is calculated according to Reynolds and Prandtl numbers:

$$\text{Re}_p = \frac{u_z \rho_f d_p}{\mu_f}, \quad \text{Pr}_p = \frac{\mu_f C_p}{\lambda_f}, \quad \text{Pe}_p = \text{Re}_p \text{Pr}_p \quad (5-15)$$

It is proved that effective radial thermal conductivity decreases with increasing the length of the reactor. It is also observed that effective thermal conductivity decreases strongly in the vicinity of the wall which is probably due to the variations in the packing density and flow velocity. It is found that radial thermal conductivity is dependent on d_p/d_t but has no dependency on d_p and d_t [Achenbach, 1995]. The shape of the packing catalysts also effects thermal conductivity and can enhance heat transfer within the reactor.

5.3.2 Wall Heat Transfer Coefficient

The wall convection coefficient is more difficult to correlate due to the large variation in velocity profile close to the wall. Experimental and empirical correlations show that there is a relation between tube wall convection coefficient and radial convective coefficient which is expressed in form of Nusselt or Biot number and is a function of Reynolds, Peclet or Prandtl number [Dixon et al., 1998]. Different equations for wall heat transfer coefficient can be found in literature, depending on particle type, size and tube to particle diameter ratio [Dixon et al., 1988 and 1998 , Tsostas et al., 1990 and Pedernera et al., 2003]. The power of the Prandtl number is usually 0.33 but it should be noted that it may change significantly in the reactor from inlet to outlet. This is not only caused by temperature but also by changes in gas composition, since steam and hydrogen have different thermal conductivities. The power of the Reynolds number at high velocities has values between 0.5 and 1 in the literature and any references use 0.75. The most important correlations for the wall convection coefficient are [Peters et al., 1988, Tsostas et al., 1990, Derekx et al., 1997 and Pedernera et al., 2003]:

$$Nu_w = 0.17 Re_p^{0.8} \quad \text{spheres} \quad \begin{array}{l} 20 < Re_p < 7800 \\ 0.05 < \frac{d_p}{d_t} < 0.3 \end{array} \quad (5-16)$$

$$Bi_w \left(\frac{d_p}{d_t} \right) = 3 Pe_p^{-0.4} \quad \text{rings} \quad 20 < Pe_p < 350 \quad (5-17)$$

$$Nu_w = 0.16 Re_p^{0.93} \quad \text{cylinders} \quad \begin{array}{l} 20 < Re_p < 800 \\ 0.05 < \frac{d_p}{d_t} < 0.2 \end{array} \quad (5-18)$$

$$Nu_w = h_w + 0.13 \left(\frac{d_t}{d_p}\right) Re_p \quad \text{cylinders} \quad 100 < Re_p < 400 \quad (5-19)$$

$$Nu_w = 4.1 \left(\frac{d_t}{d_p}\right)^{0.39} Re_p^{0.5} Pr_p^{1/3} \quad \text{cylinders} \quad \begin{array}{l} 100 < Re_p < 8000 \\ 0.1 < \frac{d_p}{d_t} < 0.6 \end{array} \quad (5-20)$$

$$Nu_w = 5.1 \left(\frac{d_t}{d_p}\right)^{0.26} Re_p^{0.45} Pr_p^{1/3} \quad \text{spheres} \quad \begin{array}{l} 100 < Re_p < 8000 \\ 0.1 < \frac{d_p}{d_t} < 0.6 \end{array} \quad (5-21)$$

$$Nu_w = 17.94 + 18.4 * 10^{-3} \frac{Pe_E}{\varepsilon} \quad \text{rings} \quad \begin{array}{l} 150 < \frac{Pe}{\varepsilon} < 1000 \\ 6 < \frac{d_t}{d_p} < 16 \end{array} \quad (5-22)$$

$$Nu_w = 2.29 Re_p^{0.41} \quad \text{rings} \quad 100 < Re_p < 2000 \quad (5-23)$$

$$Bi_w \left(\frac{d_p}{d_t}\right) = 3 Re_p^{-0.25} \quad \text{rings} \quad Re_p > 50 \quad (5-24)$$

$$Nu_w = \left(1.3 + 5 \frac{d_p}{d_t}\right) \frac{\lambda_{er}}{\lambda_f} + 0.19 Re_p^{0.75} Pr_p^{0.33} \quad \text{All type} \quad \begin{array}{l} 1 < Pe_p < 2 * 10^4 \\ 1.17 < \frac{d_t}{d_p} < 51 \end{array} \quad (5-25)$$

Dimensionless groups are presented by following equations:

$$Nu_w = h_w \frac{d_P}{\lambda_f}, \quad Re_p = u_z \rho_f \frac{d_P}{\mu_f}, \quad Pr_p = \mu_f \frac{C_p}{\lambda_f}, \quad Pe_p = Re_p * Pr_p, \quad Bi_w = h_w \frac{Re_p}{\lambda_{er}}, \quad (5-26)$$

5.3.3 Component Diffusion Coefficient

Diffusion coefficient of each gas component in the gas mixture is estimated by correlation of Wilke [Wilke, 1950 and Perry et al., 1997]. The diffusivity of a component i in a gas mixture is expressed by the binary diffusion coefficients and the mole fractions of each component:

$$D_{m,i} = \frac{1}{\sum_{k \neq i} \frac{x_k}{D_{i,k}}} \quad (5-27a)$$

The binary diffusion coefficients are given as a function of diffusion volumes [Fuller et al., 1966 and Perry et al., 1997]:

$$D_{i,k} = \frac{0.01013T^{1.75} \left(\frac{1}{M_i} + \frac{1}{M_k} \right)^{1/2}}{p \left[\left(\sum_i V \right)^{1/3} + \left(\sum_k V \right)^{1/3} \right]^2} \quad (5-27b)$$

5.4 Catalyst Parameters

For very rapid reactions with an important heat effect it may be necessary to distinguish between conditions in the fluid and on the catalyst surface or even inside the catalyst. Heterogeneous models use parameters which present heat and mass transfer between catalyst and gas phase and reaction rates are calculated from the particle internal concentrations. These parameters are discussed briefly in this section.

5.4.1 Mass Transfer Coefficient of the Catalyst Particles

Mass transfer coefficient of the catalyst pellet is calculated from different correlations. Following correlations are suggested for k_g , [Wakao et al., 1978, Cussler, 1997 and Comiti et al., 2000]:

$$Sh_p = 2 + 1.1 Re_p^{0.6} Sc^{0.33} \quad 5 \leq Re \leq 10^4 \quad (5-28a)$$

$$Sh_p = 1.15 u_z Re_p^{-0.42} Sc^{-0.67} \quad Re \leq 10^4 \quad (5-28b)$$

$$Sh_p = 0.4548 \frac{u_z}{\varepsilon} Re_p^{-0.41} Sc^{-0.66} \quad 10 \leq Re \leq 1.5 * 10^4 \quad (5-28c)$$

Dimensionless Sherwood number is written as: $Sh_p = \frac{k_g d_p}{\rho_f D_m}$ (5-28d)

5.4.2 Convection Heat Transfer Coefficient of the Catalyst Particles

The convection coefficient between the gas and catalyst pellets is calculated, by following equations [Handley et al., 1968 and Wakao et al., 1979]:

$$Nu_p = \frac{0.255}{\varepsilon} Pr_p^{0.3} Re_p^{0.6} \quad Re \leq 10^3 \quad (5-29a)$$

$$Nu_p = 2 + 1.1 Pr_p^{0.3} Re_p^{0.6} \quad 10^3 \leq Re \leq 10^4 \quad (5-29b)$$

Dimensionless Nusslet number is calculated as: $Nu_p = \frac{h_f d_p}{\lambda_f}$ (5-29c)

5.4.3 Conductive Heat Transfer Coefficient of the Catalyst Particles

Conductive heat transfer of the catalyst pellet depends on the catalyst materials and is used according to catalyst materials and the data sheet of the manufacturer.

5.5 Thermodynamic of the Gas Mixture

The gas mixture in the packed bed reactors is considered as ideal gas and all its properties are function of temperature, pressure and composition of the mixture.

5.5.1 Density

The ideal gas law is used to calculate the gas density of the mixture which is the best approximation at high temperatures:

$$\rho_f = \frac{p}{R_g T} \sum_1^i x_i M_i \quad (5-30)$$

5.5.2 Thermal Conductivity

Polynomial equations are used to estimate the thermal conductivity of pure gases. The polynomial constants are shown in Table 5.1 [Reid et al., 1987 and Poling et al., 2001]:

$$\lambda_i = A_i + B_i T + C_i T^2 + D_i T^3 \quad (5-31a)$$

The gas mixture conductivity is calculated by [Reid et al., 1987 and Poling et al., 2001]:

$$\lambda_f = \sum_1^i \frac{x_i \lambda_i}{\sum_1^i x_j \phi_{ij}} \quad (5-31b)$$

$$\phi_{ij} = \frac{(1 + (\mu_i / \mu_j)^{1/2} (M_j / M_i)^{1/4})^2}{8(1 + (M_i / M_j))^{1/2}} \quad (5-31c)$$

	$i = 1$ (CH ₄)	$i = 2$ (H ₂ O)	$i = 3$ (CO)	$i = 4$ (H ₂)	$i = 5$ (CO ₂)	$i = 6$ (N ₂)
A_i	$-1.869 \cdot 10^{-3}$	$7.341 \cdot 10^{-3}$	$0.5067 \cdot 10^{-3}$	$8.099 \cdot 10^{-3}$	$-7.215 \cdot 10^{-3}$	$0.3919 \cdot 10^{-3}$
B_i	$8.727 \cdot 10^{-5}$	$-1.013 \cdot 10^{-5}$	$9.125 \cdot 10^{-5}$	$66.89 \cdot 10^{-5}$	$8.015 \cdot 10^{-5}$	$9.966 \cdot 10^{-5}$
C_i	$1.179 \cdot 10^{-7}$	$1.801 \cdot 10^{-7}$	$-0.3524 \cdot 10^{-7}$	$-4.158 \cdot 10^{-7}$	$0.05477 \cdot 10^{-7}$	$-0.5067 \cdot 10^{-7}$
D_i	$-3.614 \cdot 10^{-11}$	$-9.100 \cdot 10^{-11}$	$0.8199 \cdot 10^{-11}$	$15.62 \cdot 10^{-11}$	$-1.053 \cdot 10^{-11}$	$1.504 \cdot 10^{-11}$

Table 5.1 Constants for calculation of polynomials [Reid et al., 1987]

5.5.3 Specific Heat Capacity

Polynomial equations are used to estimate the specific heat capacity of pure gases. The polynomial constants are shown in Table 5.1 [Reid et al., 1987 and Poling et al., 2001]:

$$C_{p,i} = \frac{R}{M_i} (A_i + B_i T + C_i T^2 + D_i T^3 + E_i T^4) \quad (5-32a)$$

The gas mixture specific heat capacity is calculated by Poling [Reid et al., 1987 and Poling et al., 2001]:

$$C_p = \frac{\sum_{i=1}^5 x_i M_i C_{p,i}}{\sum_{i=1}^5 x_i M_i} \quad (5-32b)$$

	$i = 1$ (CH ₄)	$i = 2$ (H ₂ O)	$i = 3$ (CO)	$i = 4$ (H ₂)	$i = 5$ (CO ₂)	$i = 6$ (N ₂)
A_i	4.568	4.395	3.912	2.883	3.259	3.539
B_i	$-8.975 \cdot 10^{-3}$	$-4.186 \cdot 10^{-3}$	$-3.913 \cdot 10^{-3}$	$3.681 \cdot 10^{-3}$	$1.356 \cdot 10^{-3}$	$-2.610 \cdot 10^{-4}$
C_i	$3.631 \cdot 10^{-5}$	$1.405 \cdot 10^{-5}$	$1.182 \cdot 10^{-5}$	$-7.720 \cdot 10^{-6}$	$1.502 \cdot 10^{-5}$	$7.000 \cdot 10^{-8}$
D_i	$-3.407 \cdot 10^{-8}$	$-1.564 \cdot 10^{-8}$	$-1.302 \cdot 10^{-8}$	$6.920 \cdot 10^{-9}$	$-2.374 \cdot 10^{-8}$	$1.570 \cdot 10^{-9}$
E_i	$1.091 \cdot 10^{-11}$	$6.320 \cdot 10^{-12}$	$5.150 \cdot 10^{-12}$	$-2.130 \cdot 10^{-12}$	$1.056 \cdot 10^{-11}$	$-9.900 \cdot 10^{-13}$

Table 5.2 Constants for calculation of specific heat constant [Reid et al., 1987]

5.5.4 Viscosity

There are different methods to calculate the viscosity of a gas mixture. All these methods are essentially interpolative, and the viscosity values for the pure components, the molecular weight, dipole moment, critical temperature, and critical pressure must be available. The methods then lead to estimations showing how the mixture viscosity varies with composition, [Reid, 1987 and Poling, 2001]:

$$T_r = \frac{T}{T_C} \quad (5-33a)$$

$$\mu_r = 52.46 \frac{\mu_i P_C}{T_C^2} \quad (5-33b)$$

Based on the calculated μ_r , there are different criteria to calculate shape and polarity factor, which is related exclusively to the dipole moment [Poling et al., 2001]:

$$F_p^0 = 1 \quad 0 \leq \mu_r \leq 0.022 \quad (5-34a)$$

$$F_p^0 = 1 + 30.55(0.292 - Z_c)^{1.72} \quad 0.0022 \leq \mu_r \leq 0.075 \quad (5-34b)$$

$$F_p^0 = 1 + 30.55(0.292 - Z_c)^{1.72} |0.96 + 0.1(T_r - 0.7)| \quad 0.075 \leq \mu_r \leq 0.075 \quad (5-34c)$$

Z_c is compressibility factor and is given in Table 5.3 [Poling et al., 2001]. According to the Lucas method, the viscosity of each component is calculated:

$$\mu_i = \frac{F_{p,i}^0 F_{Q,i}^0}{\xi_i} \left[0.807 T_{r,i}^{0.618} - 0.357 e^{-0.449 T_{r,i}} + 0.340 e^{-4.058 T_{r,i}} + 0.018 \right] \quad (5-35a)$$

Where ξ_i is calculated by:

$$\xi_i = 0.176 \left(\frac{T_{C,i}}{M_i^3 p_{C,i}^4} \right) \quad (5-35b)$$

The correction factor, $F_{Q,i}^0$, for all components is equal to 1 but hydrogen:

$$F_{Q,H}^0 = 1.1708 \left(1 + 0.00385 \left[(T_{r,H_2} - 12)^2 \right]^{1/M_{H_2}} \text{SIGN}(T_{r,H_2} - 12) \right) \quad \dots (5-35c)$$

Where, the function SIGNS is equal to +1 or -1 for positive or negative arguments, respectively. The mixture viscosity is calculated by Wilke method [Poling et al., 2001]:

$$\mu_f = \frac{\sum_{i=1}^5 \frac{x_i \mu_i}{\sum_{j=1}^5 x_j \phi_{ij}}}{\sum_{j=1}^5 x_j \phi_{ij}} \quad (5-36a)$$

$$\phi_{ij} = \frac{(1 + (\mu_i / \mu_j)^{1/2} (M_j / M_i)^{1/4})^2}{8(1 + (M_i / M_j))^{1/2}} \quad (5-36b)$$

	$i = 1$ (CH ₄)	$i = 2$ (H ₂ O)	$i = 3$ (CO)	$i = 4$ (H ₂)	$i = 5$ (CO ₂)	$i = 6$ (N ₂)
T_c	190.56	647.14	132.85	32.98	304.12	126.20
P_c	45.99	220.64	34.94	12.93	73.74	33.98
Z_c	0.286	0.229	0.292	0.303	0.274	0.289
μ	0	1.8	0.1	0	0	0

Table 5.3 Critical factors for steam methane reforming components [Poling et al., 2001]

5.5.5 Porosity or Void Fraction

Porosity depends on shape and size of the catalyst particles and is considered constant in modeling. It is preferable to determine void fraction experimentally but whenever it is not possible it is correlated by Haughey and Beveridge equation [Froment et al., 2011]:

$$\varepsilon = 0.38 + 0.073 \left[1 + \frac{(d_t/d_p - 2)^2}{(d_t/d_p)^2} \right] \quad (5-37)$$

5.5.6 Partial Pressures

The reaction rates work with partial pressures. Partial pressures of the gas components are calculated by ideal gas law and the mixture is assumed as an ideal gas. The partial pressure is the molar fraction multiply by the total pressure. The partial pressure of a chemical species is calculated from the total pressure and the number of moles of that species:

$$p_i = p \frac{F_i}{F_{tot}} \quad (5-38)$$

6. Sulfur Poisoning and Carbon Formation

6.1 Introduction

The main constraints for optimum operation of steam reformer are related to poisoning by sulfur and formation of carbon. Carbon formation can not be tolerated as it may result in breakdown of the catalyst and increased pressure drop leading to overheating of the tubes. This will limit the plant capacity or the life of the catalyst tubes. Sulfur poisoning results in lower activity and hence higher tube wall temperature. This chapter investigates and formulates sulfur poisoning phenomena and reviews an introduction about carbon formation.

6.2 Sulfur Poisoning of Reforming Reactions

Steam reforming of light hydrocarbons is a major process for producing hydrogen, carbon monoxide, carbon dioxide and other chemicals. Hydrocarbons from gasified biomass which include hydrogen sulfide have to be steam-reformed over a special catalyst at temperatures up to 1000 °C [Rostrup-Nielsen, 2004]. Generally, reforming catalysts consist of a base (Ni, Co, etc.) or noble metal supported on stabilized supports (alumina, ceria, ceria promoted alumina, zeolite, etc.). Studies reveal that Ni based catalysts promoted with Rh supported on alumina are fairly active for reforming of light hydrocarbons [Rostrup-Nielsen, 1984 and Twigg, 1989]. Group VIII metals are susceptible to sulfur poisoning and hydrogen sulfide is known to deactivate nickel-based steam reforming catalysts by chemisorption on the metal surface. Numerous studies of

this phenomenon have revealed that the metal-sulfur bond is so strong that catalytic activity is substantially reduced, even at extremely low (ppm levels) gas-phase concentrations of hydrogen sulfide [Bartholomew et al., 1982 and Owens et al., 1994]. To fully exploit the activity of the catalyst, it would be necessary to remove the hydrogen sulfide before the steam reforming reactor. Using conventional sulfur cleaning and desulfurization methods, which are usually run at ambient temperatures, requires the product gas to be initially cooled down and then reheated after sulfur removal. To circumvent this procedure, which has a negative effect on process efficiency; steam reforming has to be run without cleaning the gas prior to the reactor. The early study of methane steam reforming [Rostrup-Nielsen, 1984], has suggested improvements in catalyst performance to protect against deactivation by sulfur. The process known as sulfur passivated reforming has been commercialized in natural gas steam reforming. It utilizes the fact that sulfur actually dilutes the active metal and reduces the effective ensemble size. Adsorbed sulfur will deactivate nickel surface but will also delineate ensembles of sites where sulfur is not adsorbed. The size of these ensembles was critical in allowing steam reforming with minimal formation of coke. Since most of the sulfur containing organic compounds present in the steam reforming feed is transformed to hydrogen sulfide under process conditions, it is chosen as the poisoning compound containing sulfur. The aim of this study has therefore been to investigate the steam reforming of hydrocarbons from gasified biomass, in the presence of variable amounts of hydrogen sulfide. These amounts were in the range of 0 - 200 ppm, which is typical for gasified biomass. In addition, this study investigates the possibility to describe sulfur deactivation and steam reforming in a combined kinetic equation. This can provide important data for reactor modeling and optimizing exercises.

6.2.1 Chemisorption of Hydrogen Sulfide

As shown in Figure 6.1, the catalysts which belong to the group five of metals are susceptible to sulfur poisoning and nickel is the most sensitive metal.

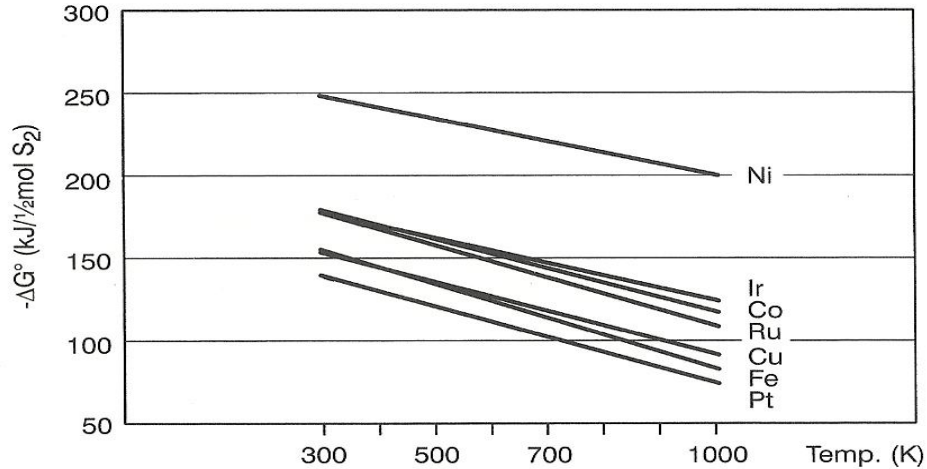


Figure 6.1 Chemisorption of hydrogen sulfide on metals [Rostrup-Nielsen, 2011]

Prior to steam reforming, sulfurous compounds must be removed from the feed stream because of their poisonous effects on the catalysts used. Sulfur poisoning occurs because sulfur adsorbs strongly on the active metal surface area of the catalyst, forming surface sulfides.

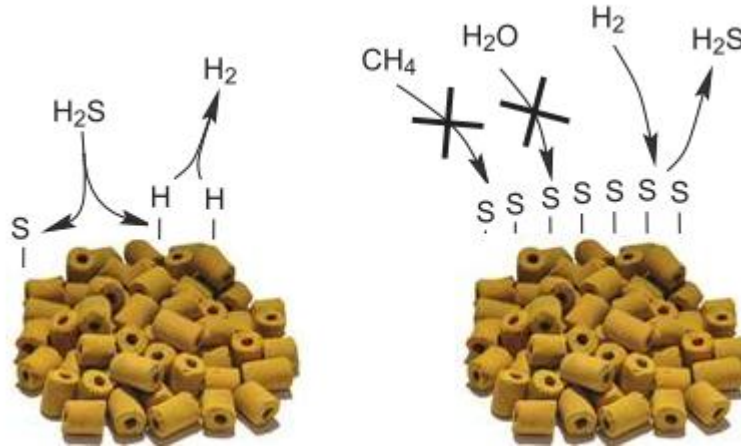


Figure 6.2 Sulfur poisoning scheme of the nickel catalysts

Sulfur is a selective poison and a partial surface coverage is sufficient for the catalyst to become essentially non-active which leads to the point that hydrocarbon conversion stops or is no longer at acceptable levels. This procedure is shown in Figure. 6.2. Due to the drop in steam reforming activity, tube wall temperatures can increase to non-optimal levels. In addition, the suppression of the reforming reaction can increase the possibility

to form carbon leading to pressure drop build-up. In industry, desulfurization accomplished either with an absorption process or via a two-step process, consisting of a hydrogenation of sulfur compounds to hydrogen sulfide and the corresponding hydrocarbons and a following chemisorption of the hydrogen sulfide, typically on zinc oxide. In Güssing plant in Austria, synthesis gas produced by steam reforming of hydrocarbons is used for synthesis of mixed alcohols. Due to the use of MoS catalysts, sulfur is necessary for the desired reactions to take place efficiently and should not be removed before the steam reforming process. The main challenge with the above described process scheme, however, is that typical steam reforming catalysts are poisoned by sulfur components. Poisoning effects are often correlated with the poison concentration in the feed stream which of course is the important parameter in practical operation and in a more detail analysis this approach can hardly be justified. The adsorption equilibrium depends on temperature and composition of the gas phase which varies through the reactor as well as within the single catalyst pellet. Therefore, it appears more rational to correlate the deactivation with the amount of poison present on the catalyst rather than with the poison concentration in the feed stream. However the correlation between sulfur in the feed and in the catalyst may be complex as illustrated below. Under reforming conditions, all sulfur compounds will be converted to hydrogen sulfide which is chemisorbed on the Ni surface:



This takes place at H_2S/H_2 ratios far below those required for formation of bulk sulfides [Rostrup-Nielsen, 1988]. Hydrogen sulfide chemisorbs on nickel and stable saturation of sulfur is observed at ratios of 10^{-5} up to close to 10^{-3} above which bulk sulfide is formed. The thermodynamic of nickel sulfide phases indicates that the formation of a bulk phase sulfide, Ni_3S_2 at temperatures around 500-700 °C requires a H_2S/H_2 concentration ratio in the order of 10^{-3} . This ratio is about 100-1000 times above what would normally cause poisoning at these temperatures [Rostrup-Nielsen, 2011].

6.2.2 Chemisorption Equilibrium

It is evident that the degree of deactivation likely depends on the sulfur adsorption equilibrium (Equation 6.1) as well as on the reaction of sulfur with the support. Both depend on the partial pressures of hydrogen sulfide and hydrogen in the gas-phase. Hydrogen addition, therefore, strongly enhances the attainable conversion when sulfur is present in the feed. As the amount of sulfur is fixed by the inlet conditions, the ratio is mainly governed by the hydrogen partial pressure, which in turn is determined by the conversion profile along the reactor length. It means the effective rate constant, (k_{CH_4}) is positively influenced by high hydrogen partial pressures and, as expected, negatively by sulfur in the feed. One approach to model the effect of sulfur poisoning is to relate the effective rate constant to the intrinsic rate constant under sulfur free operation multiplied by an activity factor, Φ , which depends on the nickel surface coverage with sulfur, θ_S [Rostrup-Nielsen, 2011]:

$$k_{sp} = \Phi * k_{sp}^0 \quad , \quad \Phi = f(\theta_S) \quad (6-2)$$

k_{sp}^0 is the reaction rate when there is no sulfur in the feed.

The experimental data, shown in Figure 6.3 are represented by linear isobars expressed as follow [Rostrup-Nielsen, 2011]:

$$\theta_S = 1.45 - 9.53 * 10^{-5} * T + 4.17 * 10^{-5} * T \ln\left(\frac{P_{H_2S}}{P_{H_2}}\right) \quad (6-3)$$

This reflects a Temkin isotherm as shown below:

A Langmuir isotherm satisfies the ideal adsorption conditions and can be written as:

$$\frac{\theta_S}{1 - \theta_S} = B * e^{-\frac{\Delta H_{ads}}{R_g T}} \left(\frac{P_{H_2S}}{P_{H_2}}\right) \quad (6-4)$$

If it is assumed that the adsorption heat is independent of the sulfur coverage, θ_S , a Temkin isotherm results :

$$-\Delta H_{ads} = -\Delta H^0_{ads} (1 - a\theta_S) \quad (6-5)$$

If these two equations are combined, the left hand side still reflects the Langmuir assumption that the rate of adsorption and desorption is proportional to the number of free and occupied sites, respectively. For dissociative adsorption as in equation (6-1) it is likely that the desorption rate of hydrogen sulfide is proportional to the non occupied sites available for hydrogen adsorption. If so it is more appropriate to represent the isotherm as a Temkin isotherm, where the heat of adsorption is independently calculated from equation (6-1) as:

$$\Delta G_{ads} = \Delta H_{ads} - T\Delta S_{ads} = -R_g T \ln\left(\frac{P_{H_2}}{P_{H_2S}}\right) \quad (6-6)$$

Insertion of equation (6-5) in equation (6-6) and rearrangement give:

$$\ln\left(\frac{P_{H_2S}}{P_{H_2}}\right) = \Delta H^0_{ads} (1 - \theta_S) - \frac{\Delta S_{ads}}{R_g} \quad (6-7)$$

Which after solving for θ_S can be written as:

$$\theta_S = \frac{1}{a} - \frac{T\Delta S}{a * \Delta H^0_{ads}} - \frac{R_g T}{a * \Delta H^0_{ads}} \ln\left(\frac{P_{H_2S}}{P_{H_2}}\right) \quad (6-8)$$

Equation (6-3) corresponds to the constants: $a=0.69$, $\Delta H^0_{ads} = -289 \text{ kJ/mol } H_2S$, and $\Delta S_{ads} = -0.019 \text{ kJ/mol } H_2S/K$ in equation (6-8).

Equation (6-1) implies an entropy of adsorption being independent of θ_S .

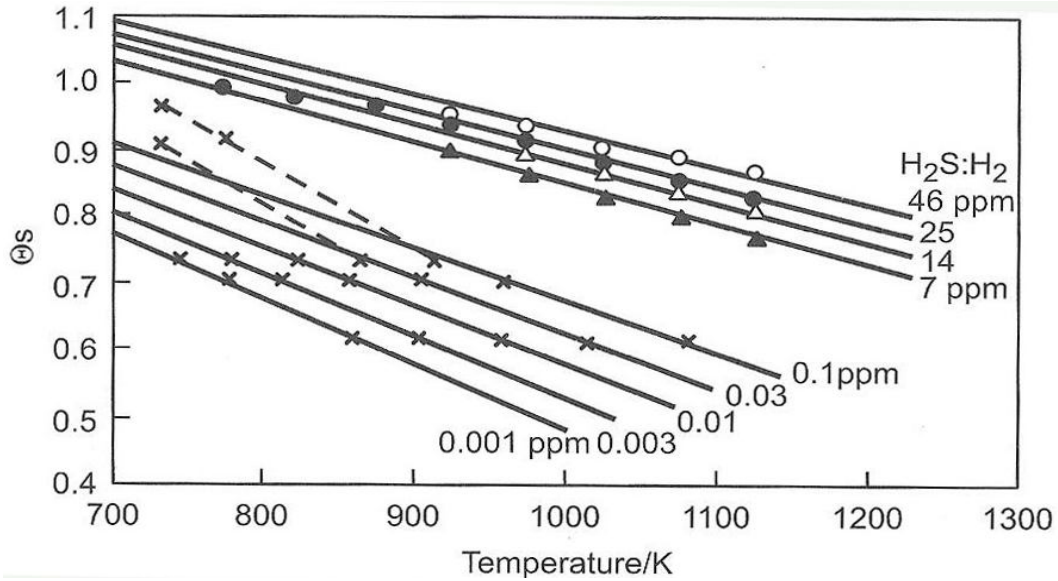


Figure. 6.3 Isobars for chemisorption of hydrogen sulfide on nickel catalysts [Rostrup-Nielsen, 2011]

The initial heat of chemisorption of $289 \text{ kJ/mol.H}_2\text{S}$ corresponds to $189 \text{ kJ/mol.H}_2\text{S}$ at $\theta_s=0.5$. These values are well above the heat of formation of bulk sulfur, Ni_3S_2 , $83 \text{ kJ/mol.H}_2\text{S}$. This demonstrates that the chemisorbed sulfur is strongly bond to the nickel surface.

6.2.3 Impact of Sulfur on Reforming Reactions

Sulfur has a strong impact on the reforming activity of nickel catalysts. The deactivation is strong at small coverage of sulfur and the catalyst is completely deactivated at full coverage, $\theta_s=1$. The nonlinear behavior is demonstrated in Figure 6.4. The intrinsic rate of the poisoned catalyst is around two sizes of orders less than that of the non poisoned catalyst. The rates are compared by referring to free nickel surface and using a simple Maxed model for poisoning [Rostrup-Nielsen, 2011]:

$$R_{sp} = R_{sp}^0 (1 - \theta_S)^n \quad (6-9a)$$

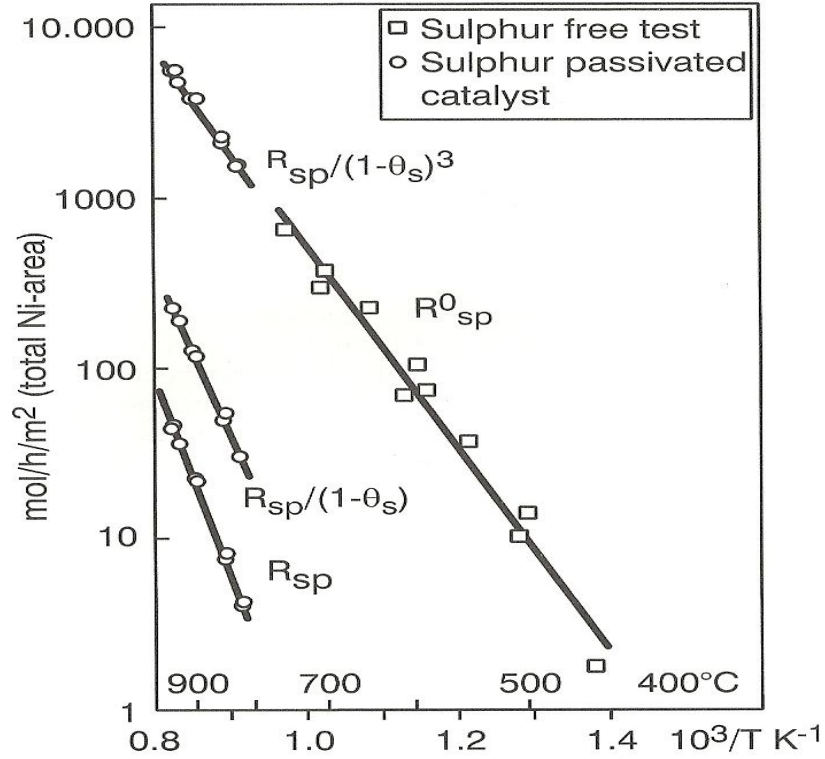


Figure. 6.4 Specific activity of sulfur poisoning on nickel catalyst [Rostrup-Nielsen, 2011]

As shown in Figure 6.4., $n=3$ leads to a reasonable agreement for R_{sp}^0 with the data for sulfur free catalyst extrapolated to higher temperature. The activation energy in the sulfur passivated reforming reaction in the presence of sulfur, in Figure 6.4 is estimated to 227 kJ/mol and the value of the sulfur free test is 110 kJ/mol .This can be explained by the heat of chemisorption of hydrogen sulfide by comparing the rate expressions for the sulfur poisoned and the sulfur free catalysts. The intrinsic rate of the poisoned catalyst could be fitted to the kinetic expression:

$$R_{sp} = k_{sp} * e^{\frac{-32100}{T}} * p_{CH_4}^{0.8} * p_{H_2}^{0.3} * p_{H_2S}^{-0.9} \quad (6-9b)$$

Rate expressions for sulfur free catalyst are discussed in section (3.2.1.3) and rate of reaction for all species are calculated. They are expressed in terms of partial pressures in combination to Arrhenius equation and activation energy .The rate of reaction of methane is expressed as :

$$r_1 = \frac{\frac{k_1}{p_{H_2}^{2.5}} \left[p_{CH_4} p_{H_2O} - \frac{p_{H_2}^3 p_{CO}}{K_1} \right]}{DEN^2} \quad (6-10a)$$

$$r_3 = \frac{\frac{k_3}{p_{H_2}^{3.5}} \left[p_{CH_4} p_{H_2O}^2 - \frac{p_{H_2}^4 p_{CO_2}}{K_3} \right]}{DEN^2} \quad (6-10b)$$

$$R_{CH_4,sp}^0 = -(r_1 + r_3) \quad (6-10c)$$

Where

$$DEN = 1 + K_{CH_4} P_{CH_4} + K_{CO} P_{CO} + K_{H_2} P_{H_2} + \frac{K_{H_2O} P_{H_2O}}{P_{H_2}} \quad (6-10d)$$

It was shown that equation (6-8) for sulfur coverage in the range of interest can be simplified to the following equation [Rostrup-Nielsen, 2011] :

$$1 - \theta_S = 0.293 e^{\frac{4300}{T}} \left(\frac{P_{H_2S}}{P_{H_2}} \right)^{-0.3} \quad (6-11)$$

Rate of reaction with sulfur poisoned catalysts could be achieved by following equation:

$$R_{CH_4,sp} = R_{CH_4,sp}^0 * (1 - \theta_S)^3 \quad (6-12)$$

6.3 Carbon Formation

At the operating temperatures some of the reactant may completely decompose and deposit a thick layer of inactive carbon on the catalyst surface (coke). Especially with nickel based catalysts, steam reforming involves the risk of carbon formation, which may cause serious operational problems and catalyst deactivation. Generally, higher

hydrocarbons are more prone to carbon formation than methane. This is related to the fact that for higher hydrocarbons the initial surface carbon intermediates are more readily formed. The concentration of these intermediates is an important factor, and is critical in influencing the delicate balance between carbon forming and carbon removing reactions.

Carbon type	Reactions involved	Phenomena	Critical parameters
Gum	$C_nH_m \rightarrow (CH_2)_n \rightarrow \text{gum}$	Blocking of surface by polymerisation of adsorbed C_nH_m radicals: progressive deactivation	Low S/C ratio, absence of H_2 , low temperature (below $\sim 500^\circ\text{C}$), presence of aromatics
Whisker carbon, amorphous carbon	$CH_4 \rightarrow C + 2H_2$ $2CO \rightarrow C + CO_2$ $CO + H_2 \rightarrow C + H_2O$ $C_nH_m \rightarrow nC + m/2H_2$	Break-up of catalyst pellet (whisker carbon: <i>no</i> deactivation of the surface)	Low S/C ratio, high temperature (above $\sim 450^\circ\text{C}$), presence of olefins, aromatics
Pyrolytic coke	$C_nH_m \rightarrow \text{olefins} \rightarrow \text{coke}$	Encapsulation of catalyst pellet (deactivation), deposits on tube wall	High temperature (above $\sim 600^\circ\text{C}$), high residence time, presence of olefins, sulfur poisoning

Table 6.1 Routes to carbon formation [Rostrup-Nielsen, 2002]

On nickel surfaces, carbon formation may take place mainly by three routes [Rostrup-Nielsen, 1984, Rostrup-Nielsen, 2002], as summarized in Table 6.1 and the equilibrium constants for the carbon formation reactions are written as follow:

$$k_w = \exp(-9573/T - 11.62) \quad \text{methane to carbon} \quad (6-13a)$$

$$k_w = \exp(13640/T - 14.84) \quad \text{carbon monoxide to carbon} \quad (6-13b)$$

$$k_w = \exp(18150/T - 19.08) \quad \text{carbon monoxide and hydrogen to carbon} \quad (6-13c)$$

Whisker carbon is formed as characteristic fibers (nano-tubes) from carbon monoxide, methane and higher hydrocarbons and is formed by dissociation of hydrocarbons or carbon monoxide on the surface of the catalyst. According to the classic model, adsorbed carbon atoms are dissolved in the metal particle. Carbon diffuses through the particle and

nucleates into the fiber at the rear interface, as shown in Figure 6.5. It may result in breakdown of the catalyst pellets [Wang et al., 1998, 2006 and Van der Lee et al., 2006].

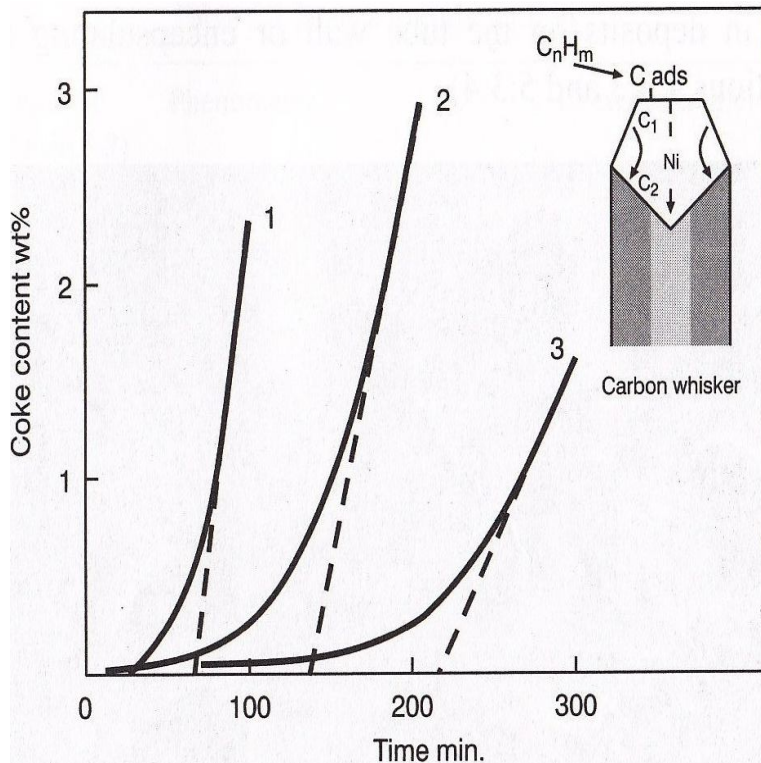


Figure 6.5 Rate of carbon formation, Nickel catalysts, 1 bar abs., 500 °C, n-heptane, 1:steam to carbon ratio=1.3, 2: Steam to carbon ratio=1.5, 3: steam to carbon ration=2 [Rostrup-Nielsen, 1984]

The low temperature phenomenon, gum formation, involves blockage of the metal surface by a film of polymerized carbonaceous material. Pyrolytic carbon is a result of thermal reactions as experienced in steam crackers and result in deposits on the tube wall or catalyst pellets. At lower temperatures (500°C and below), adsorbed hydrocarbons may accumulate on the surface and slowly be transformed into a non-reactive polymer film (gum) blocking and deactivating the surface. This phenomenon can be retarded by hydrogen. Note that because of the endothermic nature of the steam reforming reaction, high catalyst activity leads to a low temperature at the reaction site, resulting in a higher risk for carbon formation. At higher temperatures, whisker carbon is the principal product of carbon formation on nickel catalysts. The underlying mechanism is quite

comprehensive; it involves diffusion of carbon atoms through the metal particles [Rostrup-Nielsen, 1984]. The rate of carbon formation depends strongly on the type of hydrocarbons is illustrated in Figure 6.6 with alkenes being the most reactive [Rostrup-Nielsen, 1984]. After an introduction time; the carbon grows at a constant rate. The growth mechanism appears to be the same, irrespective of the type of hydrocarbon or whether it results from the endothermic dissociation of methane or the exothermic dissociation of carbon monoxide, Table 6.1 [Rostrup-Nielsen, 1984]. However, the carbon formation and degree of graphitization depends on parameters such as type of hydrocarbon, metal particle size and temperature. Hence, there might not be a unique growth mechanism for the formation of carbon fibers and nano-tubes. The catalyst particle size has an impact on the nucleation of carbon. The smaller the crystal, the more difficult is the initiation of carbon formation, [Rostrup-Nielsen, et al., 2002]. The rate of carbon formation was found to be far less on noble metals than on nickel [Rostrup-Nielsen, 1993]. This result may be explained by the fact that the noble metals do not dissolve carbon. The carbon formed on the noble metals was observed to be of a structure that was difficult to distinguish from the catalyst structure. The carbon formation mechanism is also blocked by sulfur poisoning of the catalyst surface. The carbon formation depends on the kinetic balance between the surface reaction of the adsorbed hydrocarbons with oxygen species and the further dissociation of the hydrocarbon into adsorbed carbon atoms. For a given hydrocarbon feed, carbon is formed below a critical steam to carbon ratio [Twigg, 1989, Rostrup-Nielsen, 2002]. This critical steam to carbon ratio increases with temperature and is dictated by thermodynamics. In practice however, carbon formation generally occurs before the thermodynamic limit is reached by poisons, temperature and concentration gradients, etc. By using noble metal catalysts, it is possible to push the carbon limit even beyond the thermodynamic limit. As already indicated in Table 6.1, not all carbon formation necessarily leads to catalyst deactivation. It is the nature of the deposited carbon that determines to what extent the catalytic activity will be effected. For instance, for dry reforming of methane it is shown that the relative ease with

which carbon is removed (oxidized) from the surface, affects the catalytic activity more than the actual amount of carbon that is present on the catalyst surface.

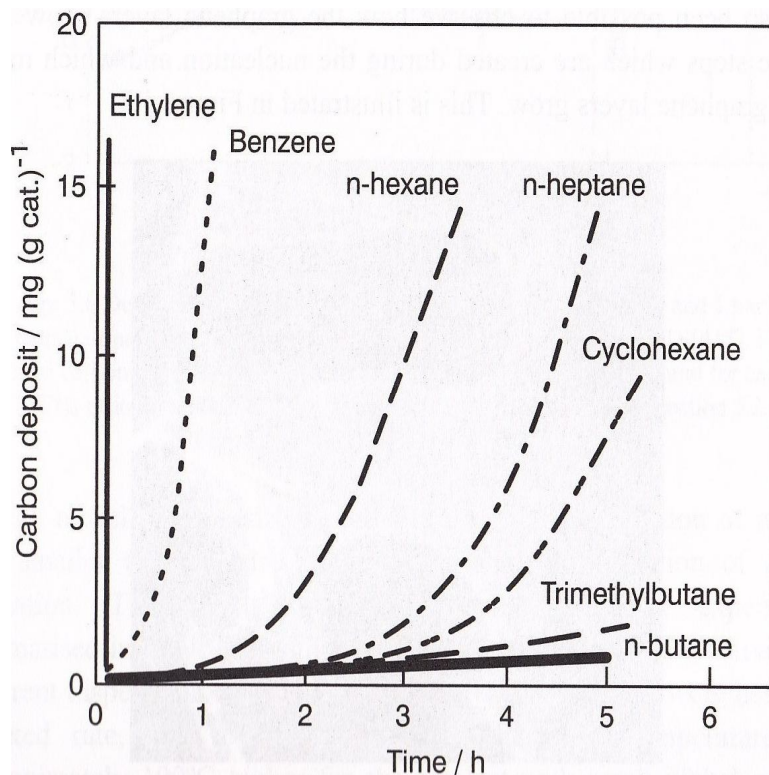


Figure 6.6 Rate of carbon formation from different hydrocarbons, steam to carbon ratio=2, 1 bar abs., 500 °C [Rostrup-Nielsen,1984]

It was concluded that graphitic carbon is more reactive than amorphous carbon, which in turn causes the varying catalytic activity and stability of the catalyst. This is consistent with Table 6.1: Whisker carbon, which does not necessarily lead to deactivation, is known to be graphitic [Rostrup-Nielsen, 1984].

7. Experiments and Modeling Results

7.1 Material and Reaction Kinetic Apparatus

The reaction mechanism of the steam-reforming process strongly depends on the catalyst pellets. The higher the active surface area of the catalyst, the greater the number of product molecules produced per unit time. Therefore, much of the art and science of catalyst preparation deals with high-surface-area materials. The catalyst used in these experiments is a commercial catalyst with noble metal as the active metal supported in alumina. It is a cylinder shape catalyst with center hole. It has a constant outside diameter of 7 mm and inside diameter of 4 mm. The gases used in this study were chemically completely pure. The schematic diagram of the experimental system is shown in Figure 7.1. The gas flow rate system consists of mass flow controllers which provide inlet gas in various blends of different gases, hydrogen, methane, carbon monoxide, carbon dioxide and Nitrogen as carrier gas. A bypass was inserted around the reactor allowing sampling of feed gas. Water is evaporated through heating tubes and a high performance liquid pump is used to control the liquid water flow rate. The liquid water was vaporized and mixed with the feed gas stream before entering the reactor. The reactor is made from a glass tube with 8 mm inside diameter. The height of the catalysts in the tube differs according to each experimental condition and the bulk density of the catalyst is $760 \text{ (kg/m}^3\text{)}$. The reactor tube is heated by an electric heater and the reactor is completely insulated. Thermocouples are placed on the surface of the reactor and are connected to a temperature indicator, computer monitoring system and temperature

controllers. Different height of catalyst beds was packed within the reactor, where reactions of hydrocarbons and steam occur to produce hydrogen, carbon monoxide and carbon dioxide. A conventional condenser was attached to the junction of the bypass and the reactor outlet. The gas leaving the reactor column was cooled in a condenser where liquid water is removed. Finally, the dry gas stream were routed into the online analyzer where their concentrations are analyzed, measured and presented in Lab view program which controls the online analyzer. The exiting gas goes to the venting system where the outlet flow rate can be measured. Using the outlet flow rate and cross sectional area of the reactor, outlet velocity can be calculated.

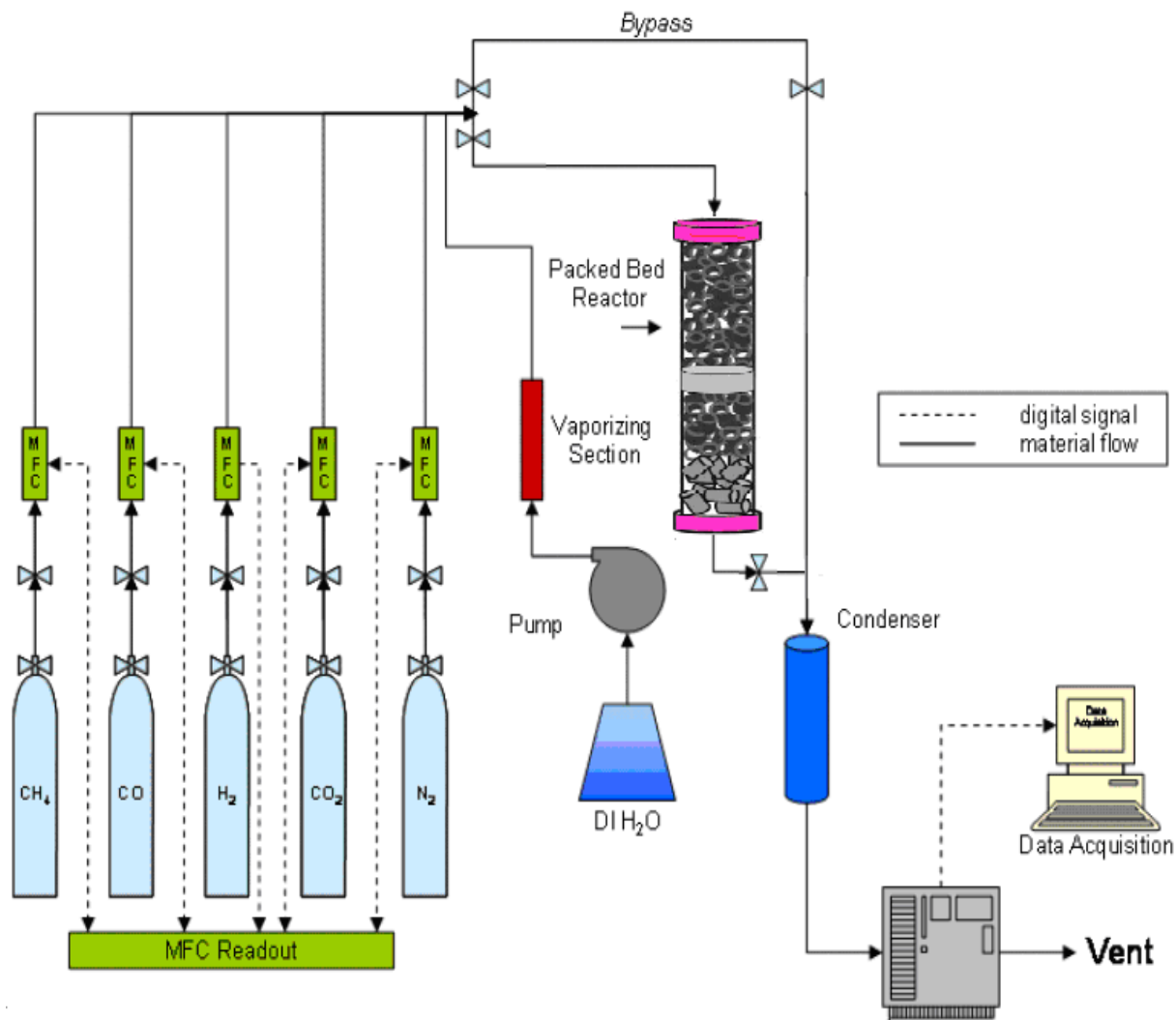


Figure.7.1 Schematic diagram of experimental setup.

7.2 Experimental Procedure

Inlet gas conditions at different steam to carbon ratios, space velocities, sulfur concentrations and temperatures (depending on each experiment) were conducted in the reactor. For the laboratory experiments typically 11 g of catalyst was loaded into the reactor and the height of the catalyst bed is about 11 cm. The reactor wall temperature is kept at 1123 (K) while line temperature was kept at a temperature above 130 °C to prevent condensation of the water vapor. The gases from the outlet of mass flow controllers are directed to come exactly above the packed bed and nitrogen is used as carrier gas. The feed conditions used are typical values for producer gas from the Güssing plant and are presented in Table 7-1.

Volume fraction (vol%)				
Hydrogen	Carbon monoxide	Carbon dioxide	Methane	Nitrogen
39	22	26	11	2

Table 7.1 The feed inlet dry mole concentration used for laboratory experiments

Different amount of water is fed into the reactor in order to adjust the desired steam to carbon ratio. In the system, gas temperatures and flow rates are fully controlled according to the set values. A thermocouple is sliding near the tube wall to measure and control reforming temperatures. Calibrations were done for the mass flow controllers in the range of flow necessary for the desired feed conditions. These calibrations were performed using a constant flow rate comprised of different concentrations of individual gas phase species balanced with inert nitrogen. To check that the flow rate that is flowing through the system is correct, the bypass section was left open, while the reactor sector was closed. The sample is then analyzed and checked if the results correspond to the calibration curve. After this, the bypass section was closed again and the reactor section opened. Different flow rates were employed covering temperatures 1000 (K) to 1150 (K) and steam to carbon ratios from 1.5 to 3. The reformer pressure is regulated at 1

atmosphere and space velocities are in the range of 6000 to 10000 1/hr. The simulations are done with the same parameters with COMSOL Multiphysics software and experimental and modeling results are compared and shown in the following sections. The following definitions are set to investigate the process and represent the reaction conditions:

$$X_{CH_4} \% = \frac{m_{CH_4,in} - m_{CH_4,out}}{m_{CH_4,in}} * 100 \quad (7-1a)$$

$$X_{C_2H_4} \% = \frac{m_{C_2H_4,in} - m_{C_2H_4,out}}{m_{C_2H_4,in}} * 100 \quad (7-1b)$$

X_{CH_4} and $X_{C_2H_4}$ are methane and ethylene conversion respectively.

$$CO_{sel} = \frac{m_{CO,out}}{m_{CO,out} + m_{CO_2,out}} * 100 \quad (7-2)$$

CO_{sel} is carbon monoxide selectivity.

$$H_{2,Yld} \% = 0.25 \frac{m_{H_2,in} - m_{H_2,out}}{m_{CH_4,in}} * 100 \quad (7-3)$$

$H_{2,Yld}$ is hydrogen yield.

$$X_{CO_2,methane} \% = \frac{m_{CO_2,in} - m_{CO_2,out}}{m_{CH_4,in}} * 100 \quad (7-4)$$

$X_{CO_2,methane}$ is carbon dioxide conversion to methane.

$$sv = \frac{V_{in}}{V_{catalyst}} \quad (7-5)$$

sv is space velocity, $\frac{1}{hr}$

7.3 Comparisons of Experimental and Modeling Results

In this section modeling and experimental results are compared. The input parameters to the reactor models are the inlet and initial conditions including different feed compositions, the physical properties and the geometry of the tube and of the catalyst pellets, and the heat flux profile located on the outer wall of the reactor tube which is kept constant for each experiment by electrical heating. The parameters that are varied are the temperature at the outer surface of the wall and therefore input heat flux into the reactor; steam to carbon ratio and space velocity. Sulfur concentration in the feed gas is changed from 0 to 160 ppm, which is typical for the feed gas produced from biomass gasification process. Pseudo-Heterogeneous model is used and appropriate correlations depending on catalyst type, dimension, and shape and process conditions are selected. The correlations for reactor model are listed in appendix 3.

7.3.1 Steam to Carbon Ratio Effects

The effect of steam to carbon ratio on methane conversion and hydrogen yield from simulation is shown in Figures 7.2-7.4. The reactor wall temperature is set at 1123 (K), the space velocity is 10000 1/hr. As it is shown by increasing steam to carbon ratio the methane conversion and hydrogen yield are increased. Sulfur has huge negative effect on conversion process and decreases the methane conversion and hydrogen yield drastically.

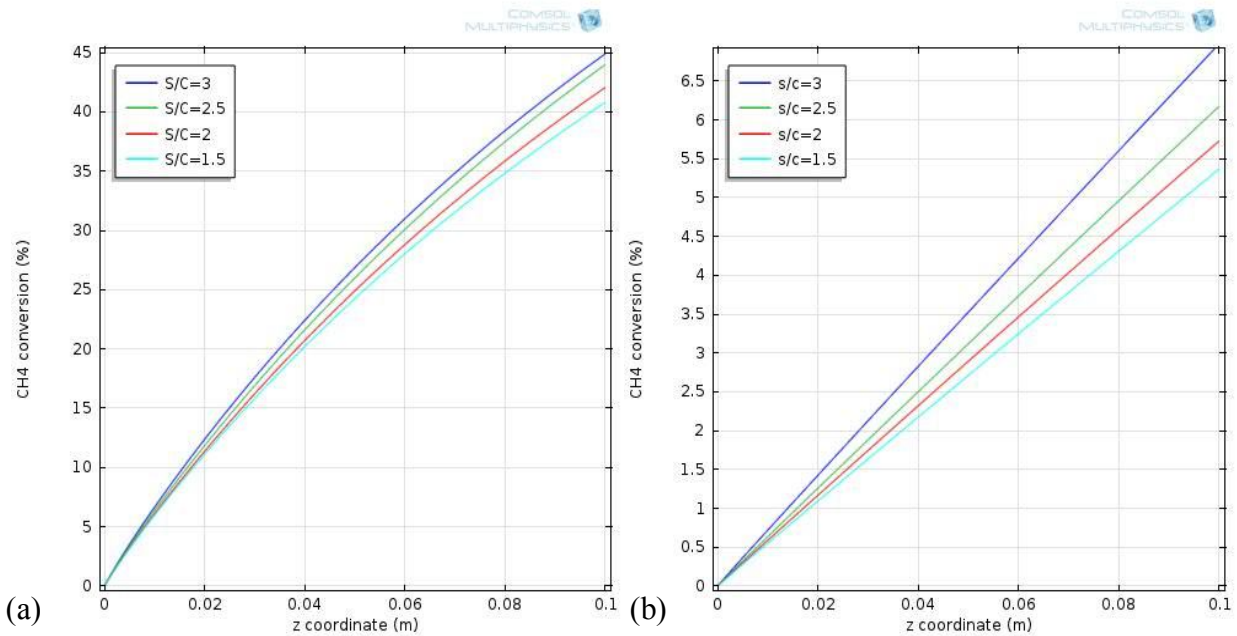


Figure 7.2(a,b) Comparison of methane conversion in the reactor, T=1123 (K), sv=10000 1/hr (a) without sulfur (b) sulfur amount=160 ppm

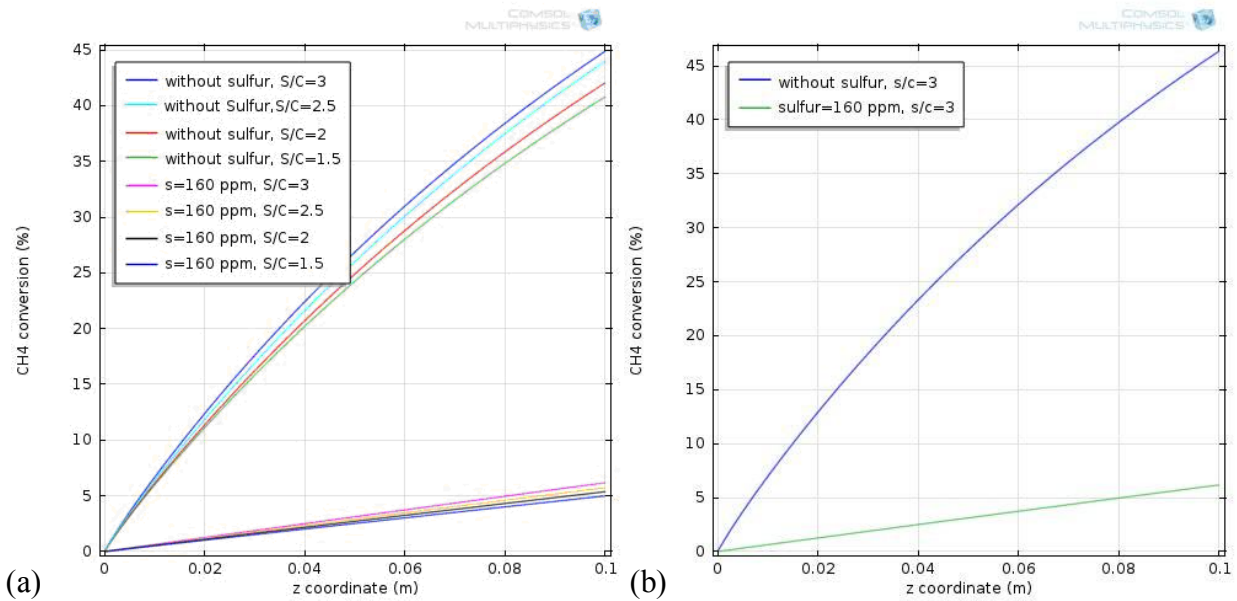


Figure 7.3 (a,b) Comparison of methane conversion in the reactor, T=1123 (K), sv=10000 1/hr (a) without sulfur (b) sulfur amount=160 ppm

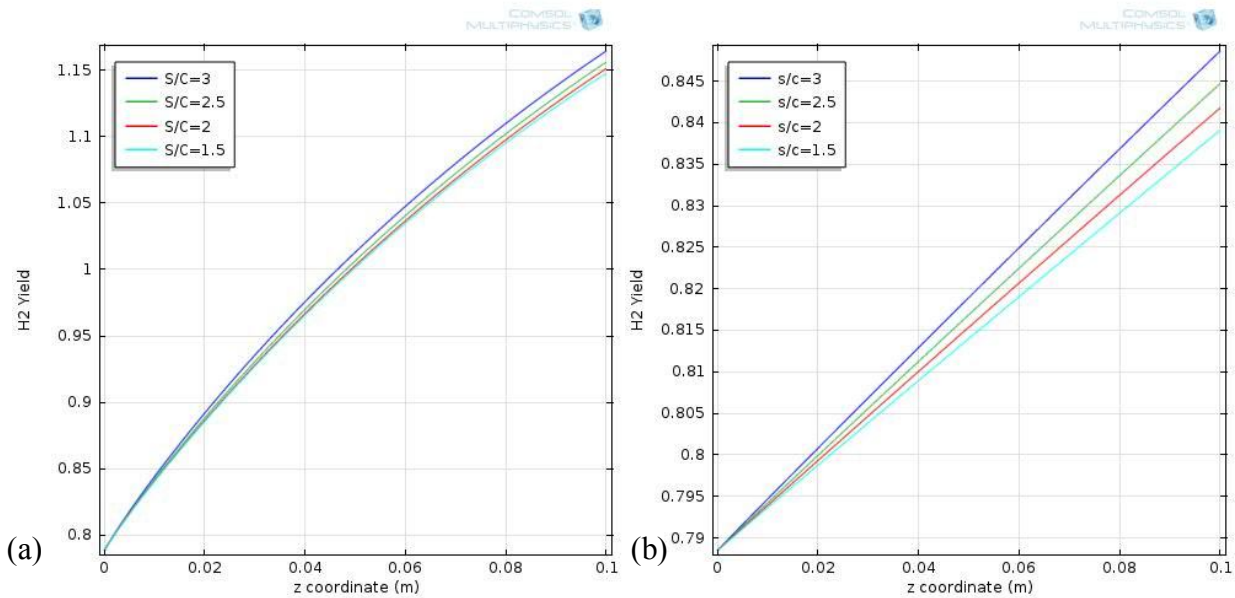


Figure 7.4 (a,b) Comparison of hydrogen yield in the reactor, T=1120 (K), sv=10000 1/hr (a) without sulfur, (b) sulfur amount=160 ppm

Steam to carbon ratio effects on temperature distribution in radial and axial direction in the reactor, are shown in Figures 7.5-7.7 while outer reactor wall temperature is fixed at 1123 (K).

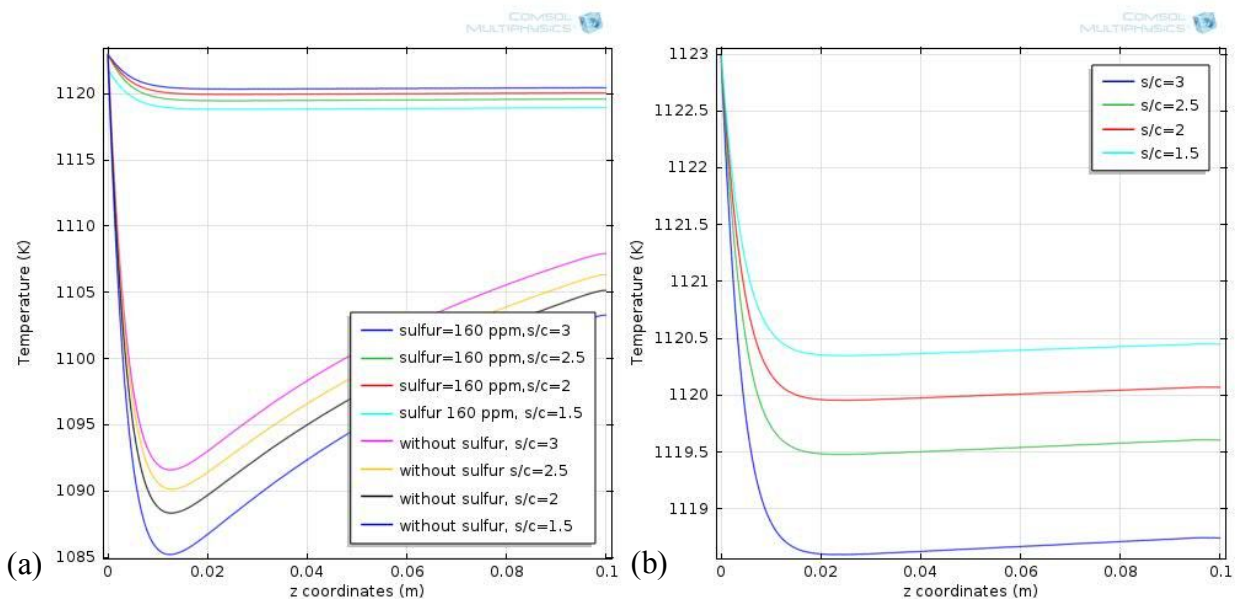


Figure 7.5 (a,b) Comparison of temperature distribution along the reactor, T=1123 (K), sv=10000 1/hr (a) without sulfur, (b) sulfur amount=160 ppm

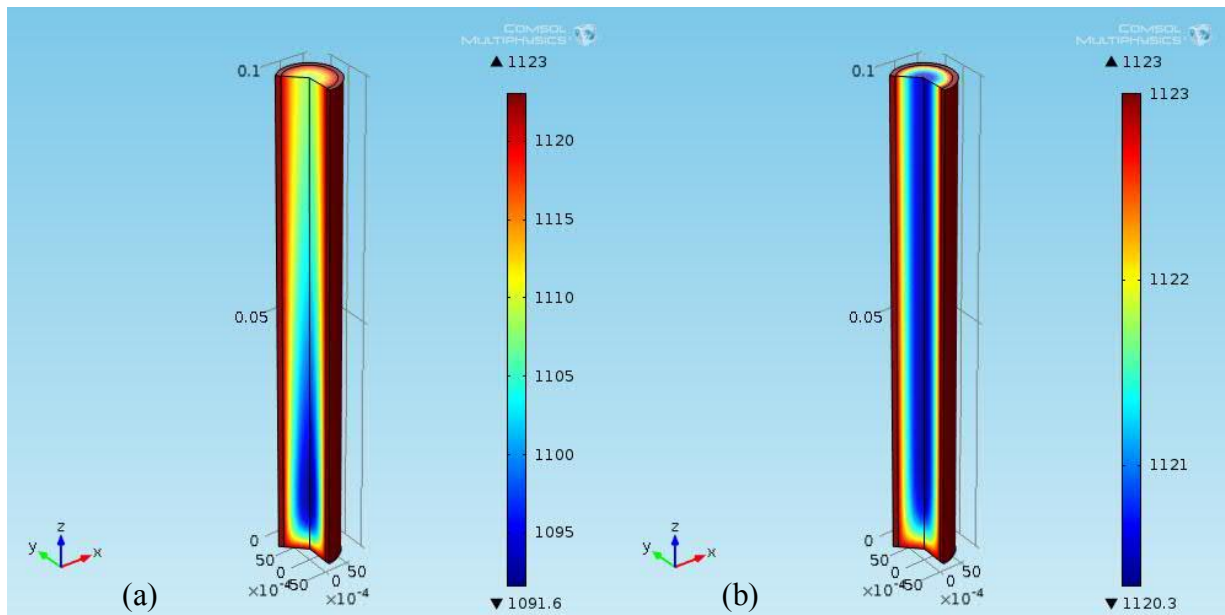


Figure 7.6 (a,b) Graphical view of temperature distribution along the reactor $S/C=3$, $T=1123$ (K), $sv=10000$ 1/hr (a) without sulfur, (b) sulfur amount=160 ppm

When sulfur is not included in the gas, temperature in radial direction decreases as soon as gas enters the reactor. It is because of high endothermic nature of the steam reforming reactions when gas enters the reactor, the reactions take place and decreases the temperature at very close distance to the entrance of the reactor. Later heat transfer from the wall into the reactor increases the temperature again. When sulfur is included in the gas, deactivates the catalyst and decreases the reaction rate, therefore decreasing temperature is not significant. Radial temperature distribution for $S/C=3$, are shown in Figure 7.7 at different distances from the inlet. When sulfur is not included in the gas, the radial changes in the gas temperatures at the reactor are high because of the high gradient of the effective radial thermal conductivity at the wall and high reaction rate of the reforming reactions. Both axial and radial temperature distributions are affected by change in steam to carbon ratio. Increasing steam to carbon ratio makes the temperature distribution more uniform within the reactor. Increasing too much steam to carbon ratio can be a bad option because it raises the flow and a higher flow needs a higher heat contribution and maybe the reaction does not have the necessary heat contribution to

reach the desired range of conversion. It should be taken into account that thermal effects could be higher than the chemicals.

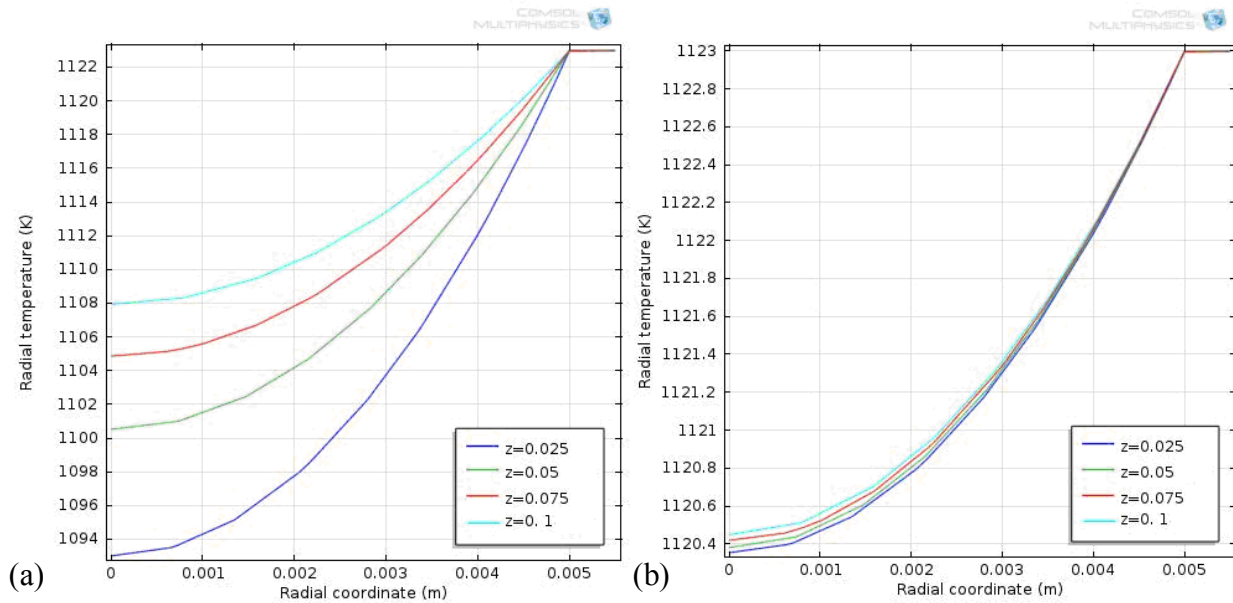


Figure 7.7 (a,b) Radial temperature distribution at different levels in the reactor, S/C=3, T=1123 (K), sv=10000 1/hr (a) without sulfur, (b) sulfur amount=160 ppm

Carbon monoxide selectivity and carbon dioxide conversion to methane are shown in Figure 7.8. It is shown that increasing steam to carbon ratio decreases carbon dioxide conversion and carbon monoxide selectivity in the reactor. The reason is that increasing the steam is not in the favor of water gas shift reaction and produces more carbon monoxide in the other direction and decreases also the carbon selectivity.

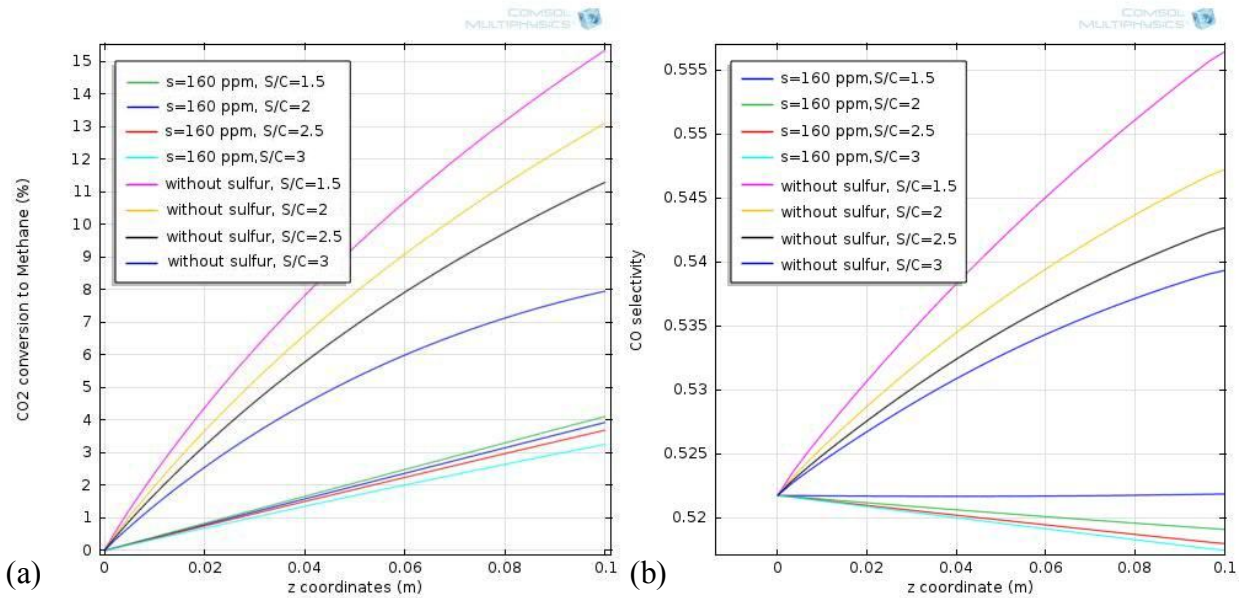


Figure 7.8 (a,b) Carbon dioxide conversion to methane and carbon monoxide selectivity in the reactor with and without sulfur, $T=11203$ (K), $sv=10000$ 1/hr (a) Carbon dioxide conversion, (b) Carbon monoxide selectivity

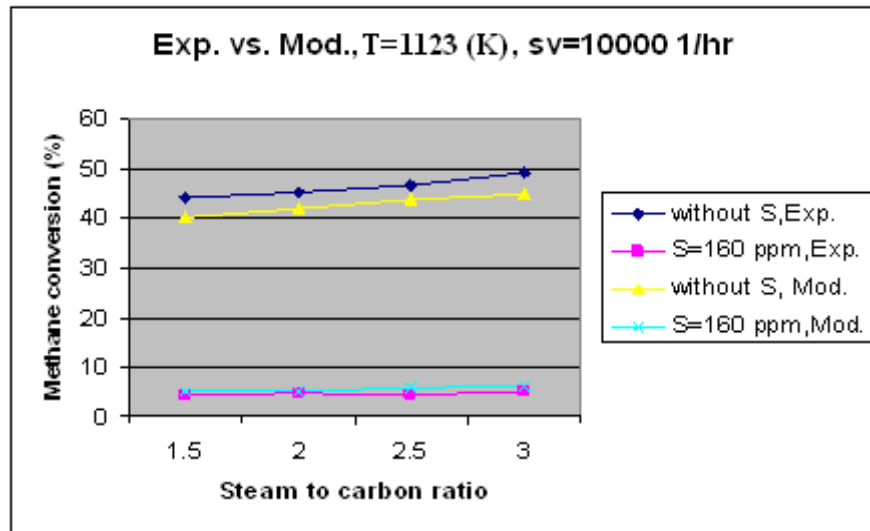
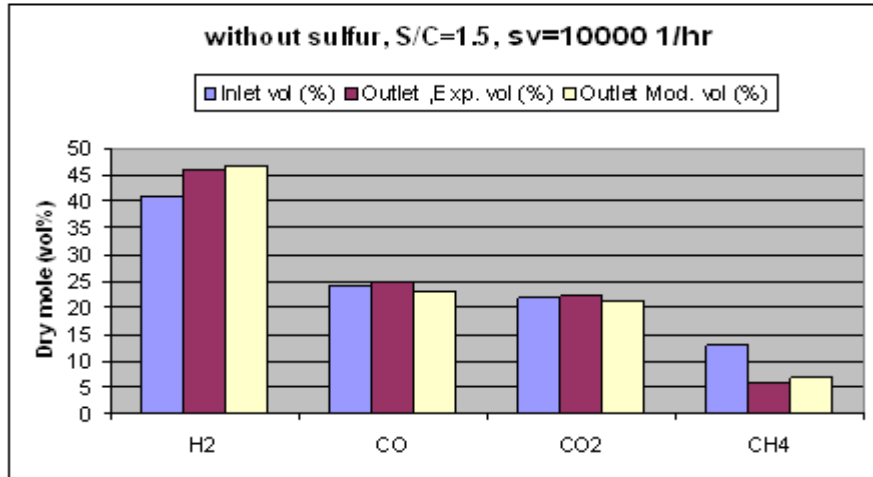
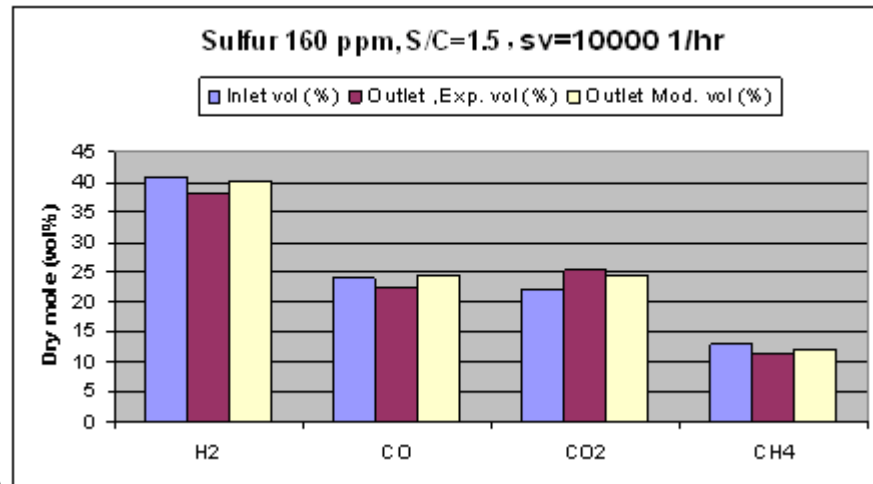


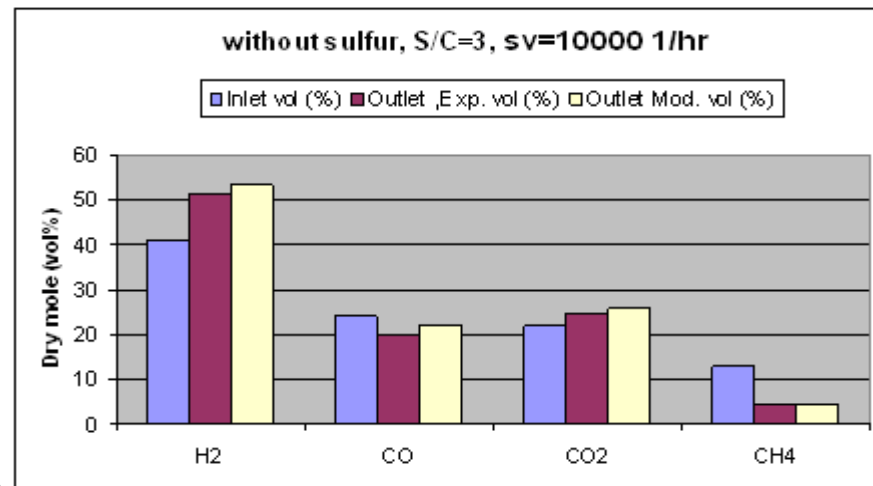
Figure 7.9 Comparison of modeling and experimental results of methane conversion in the reactor
 Experimental and modeling results are compared in following graphics and it is shown that modeling results fit well to the experimental results.



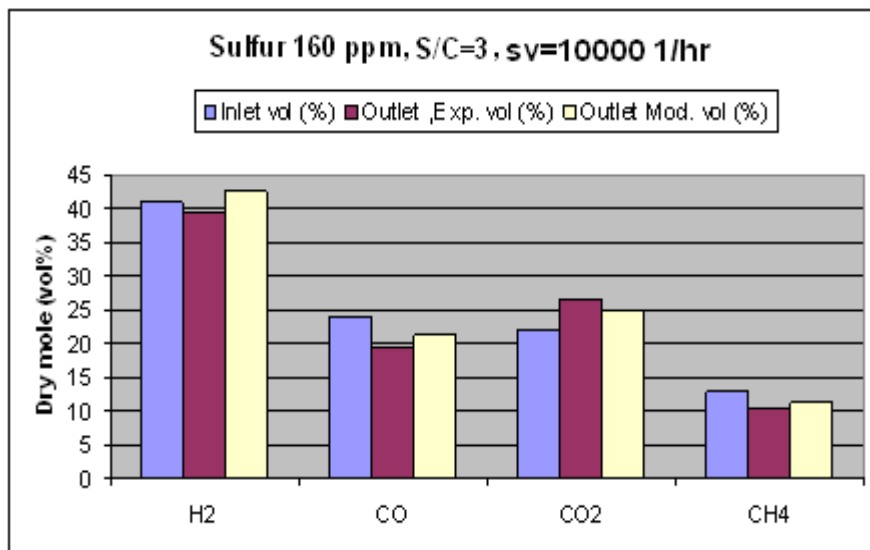
(a)



(b)



(c)



(d)

Figure 7.10 (a-d), Outlet mole concentration in the reactor, T=1123 (K) (a) S=0 ppm, S/C=1.5 (b) S=160 ppm, S/C=1.5 (c) S=0 ppm, S/C=3, (d) S=160 ppm, S/C=3

7.3.2 Sulfur Effects

The numerical model presented in this work provides the temperature and concentration profiles along the reactor radial and axial coordinates for both cases, with and without presence of sulfur in the gas. The effect of different amount of sulfur on methane conversion and reactor performance is investigated in following graphics. The reactor wall temperature is set at 1123 (K), the space velocity is 10000 1/hr and steam to carbon ratio is set at S/C=3.

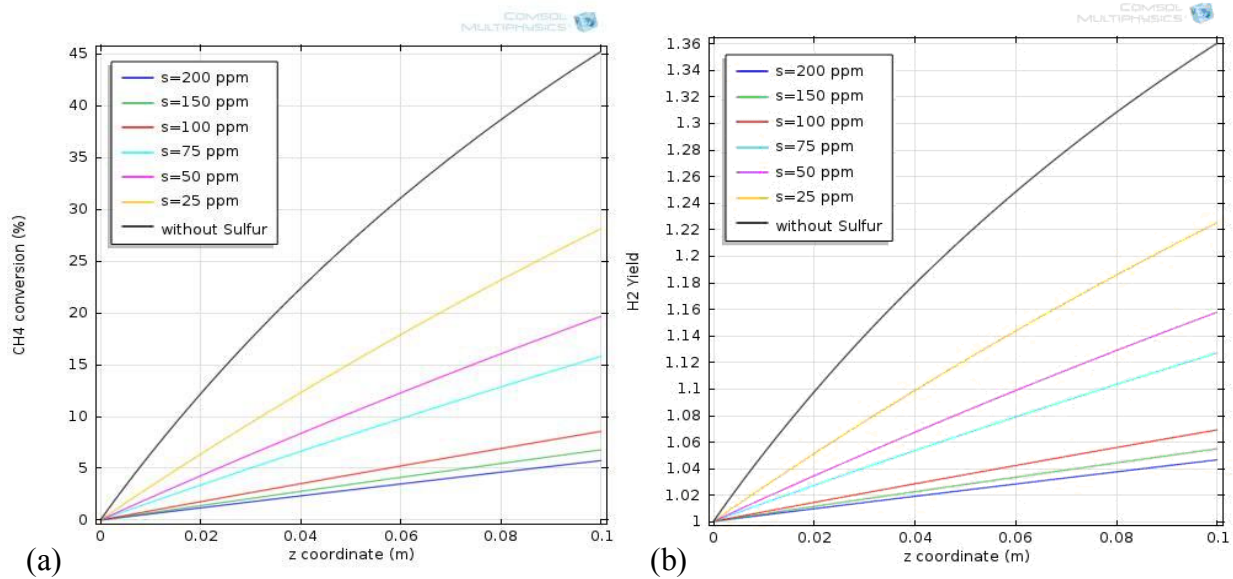


Figure 7.11 (a,b) Methane conversion and hydrogen yield, $T=1123$ (K), $sv=10000$ 1/hr, $S/C=3$ (a) methane conversion, (b) hydrogen yield

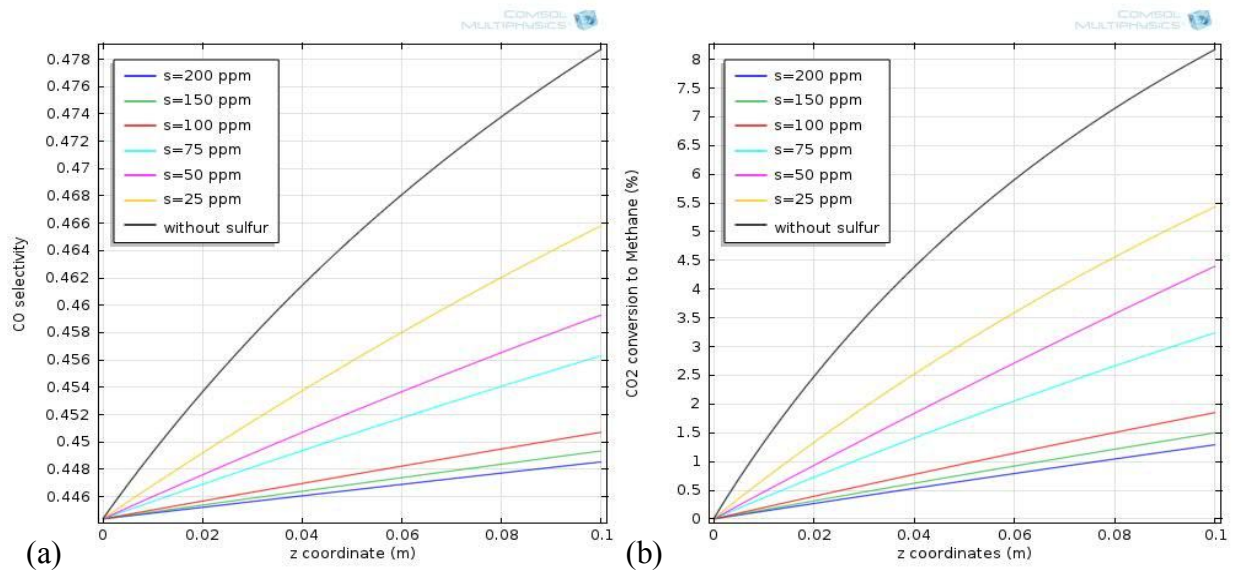


Figure 7.12 Carbon monoxide selectivity and carbon dioxide conversion to methane in the reactor, $T=1123$ (K), $sv=10000$ 1/hr, $S/C=3$ (a) carbon monoxide selectivity, (b) carbon dioxide conversion to methane

Figure 7.11(a,b) shows the effect of different amount of sulfur included in the hydrocarbon feedstock on methane conversion and hydrogen yield along the reactor catalytic bed. Sulfur can have a significant negative effect on reforming reactions, methane conversion and hydrogen yield. Even small amount of sulfur, (50 ppm), leads to around 50% reduction of methane conversion at the end of the reactor.

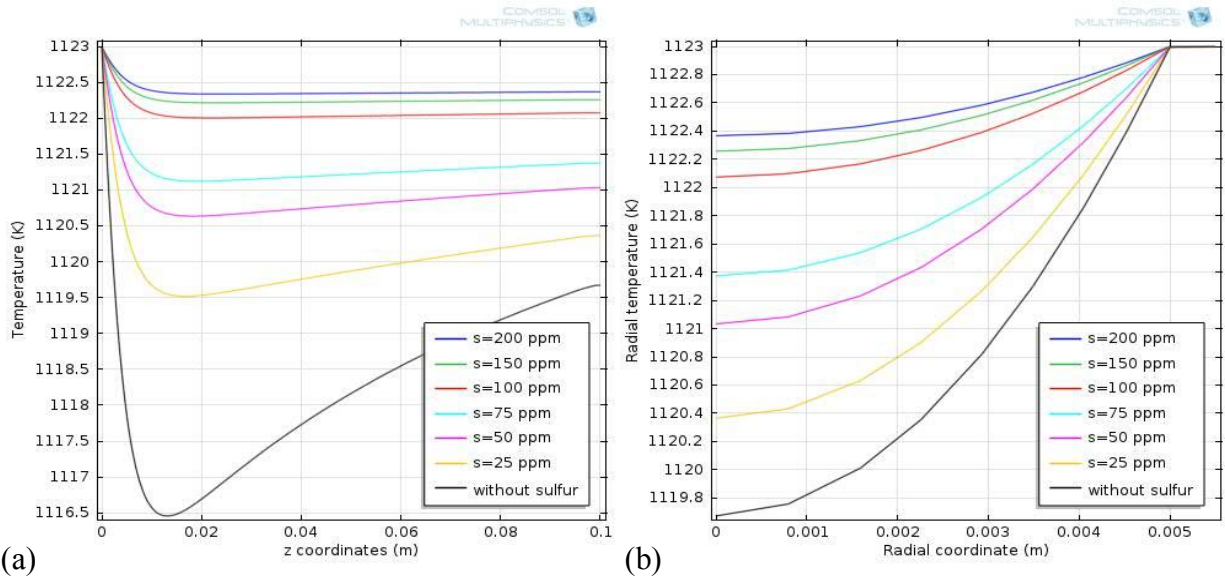


Figure 7.13 (a,b) Temperature distribution in the reactor, $T=1123$ (K), $sv=10000$ 1/hr, $S/C=3$ (a) axial temperature, (b) outlet radial temperature

In Figure 7.13(a) the temperature distribution along the reactor bed is displayed. The result shows that when sulfur is not present in the gas, the temperature dropped suddenly at the inlet of the reactor from the initial temperature of 1123 K to about 1115 K and then increased gradually to the outlet. This phenomenon is attributed to the large amount of heat required at the initial stage of the reactions due to the high endothermic nature of the reactions. The rising temperature after a sudden drop along the axial bed of the catalyst is due to the heat supplied by the outer surface of the reactor into the catalytic bed. Presence of sulfur in the gas leads to the catalyst deactivation and lower methane conversion rate. Therefore, small amounts of heat are consumed and temperature decreases gradually along the reactor bed.

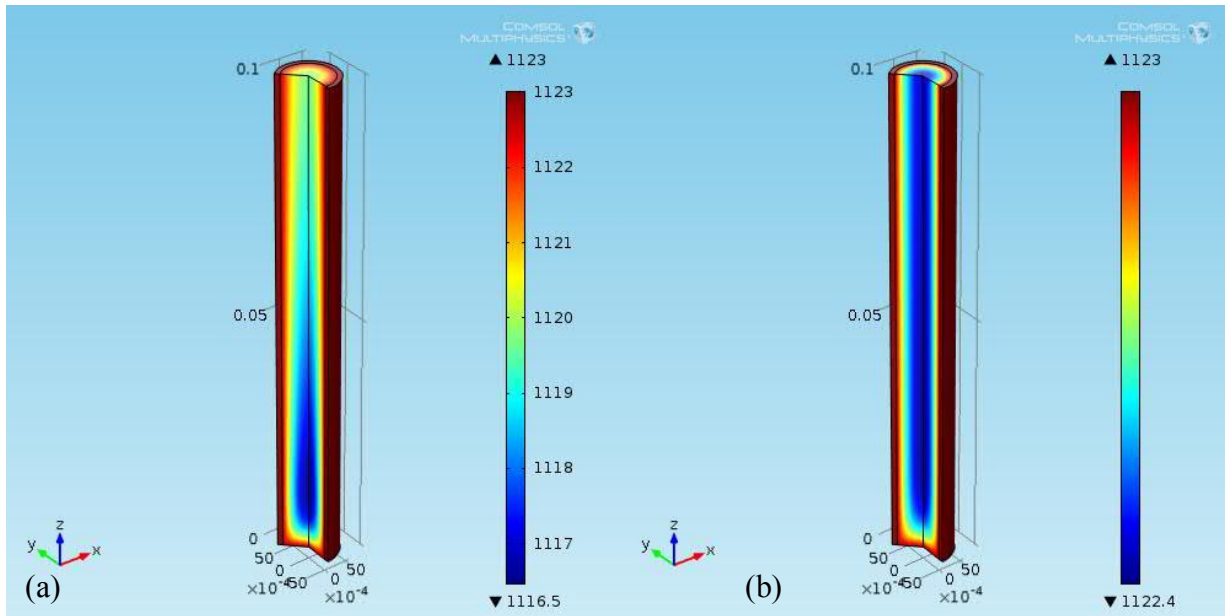


Figure 7.14 (a,b) Axial temperature distribution in the reactor, $T=1123$ (K), $sv=10000$ 1/hr, $S/C=3$ (a) without sulfur, (b) sulfur amount=200 ppm

Figure 7.13(b) shows radial temperature distribution at the outlet of the reactor for different amounts of sulfur included in the gas and compares it to the result when the gas is free of sulfur. It is shown that when sulfur is not included in the gas, the outlet temperature is lower compare to the cases when sulfur is included in the gas. Figure 7.14(a,b) shows the graphical view of the phenomena which is described in Figure 7.13 (a,b). Radial temperature distribution at different axial positions from the inlet are shown in Figure 7.15(a,b) The tube skin temperature is set at 1123 (K) and as shown significant radial temperature gradients close to the wall of the reactor are observed. When sulfur is not included in the gas, thermal radial gradients are more significant close to the wall due to the high endothermic nature of the process and distribution of the catalyst close to the wall. For all cases, the radial temperature gradients tend to decrease towards the outlet and center of the reactor and sulfur deactivation effects make temperature distribution more uniform at the outlet.

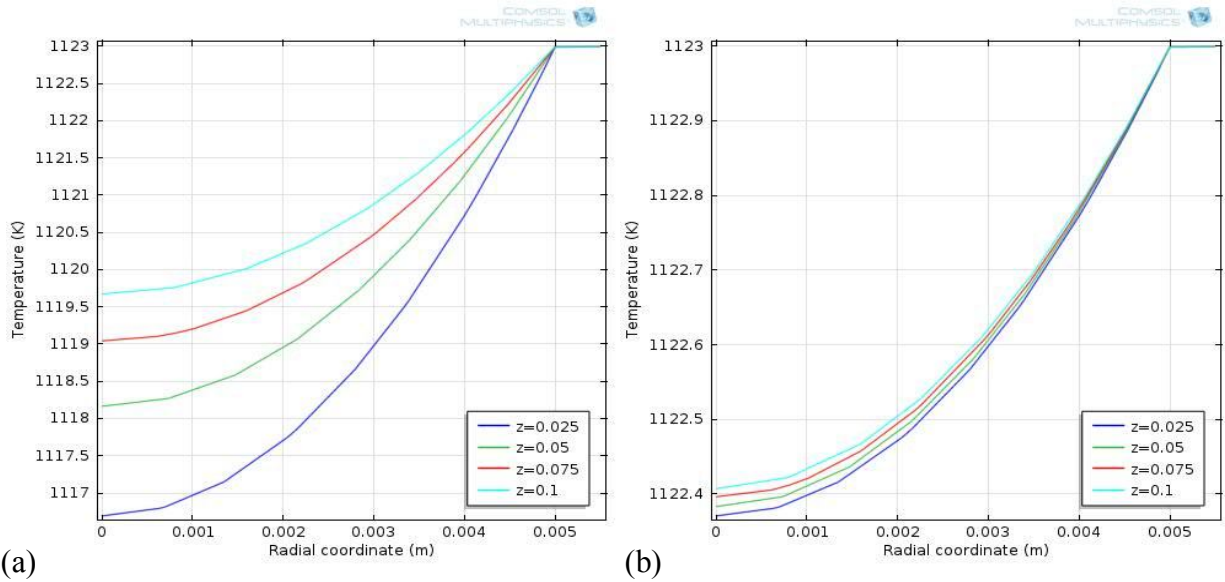


Figure 7.15 (a,b) Radial temperature distribution in the reactor at different distances from the inlet, $T=1123$ (K), $sv=10000$ 1/hr, $S/C=3$ (a) without sulfur, (b) sulfur amount=200 ppm

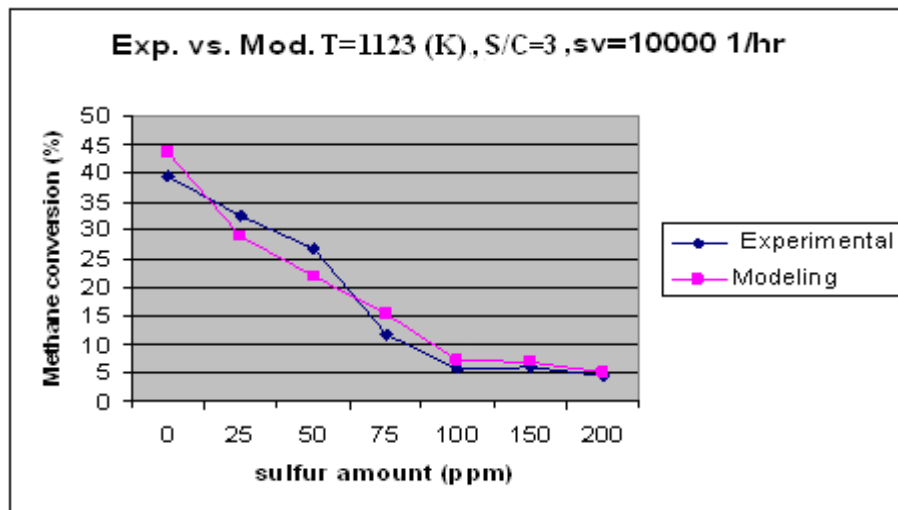


Figure 7.16 Comparison of modeling and experimental results of methane conversion in the reactor

Comparison of modeling and experimental results, are shown in the following graphics, Figures 7.16 and 7.17.

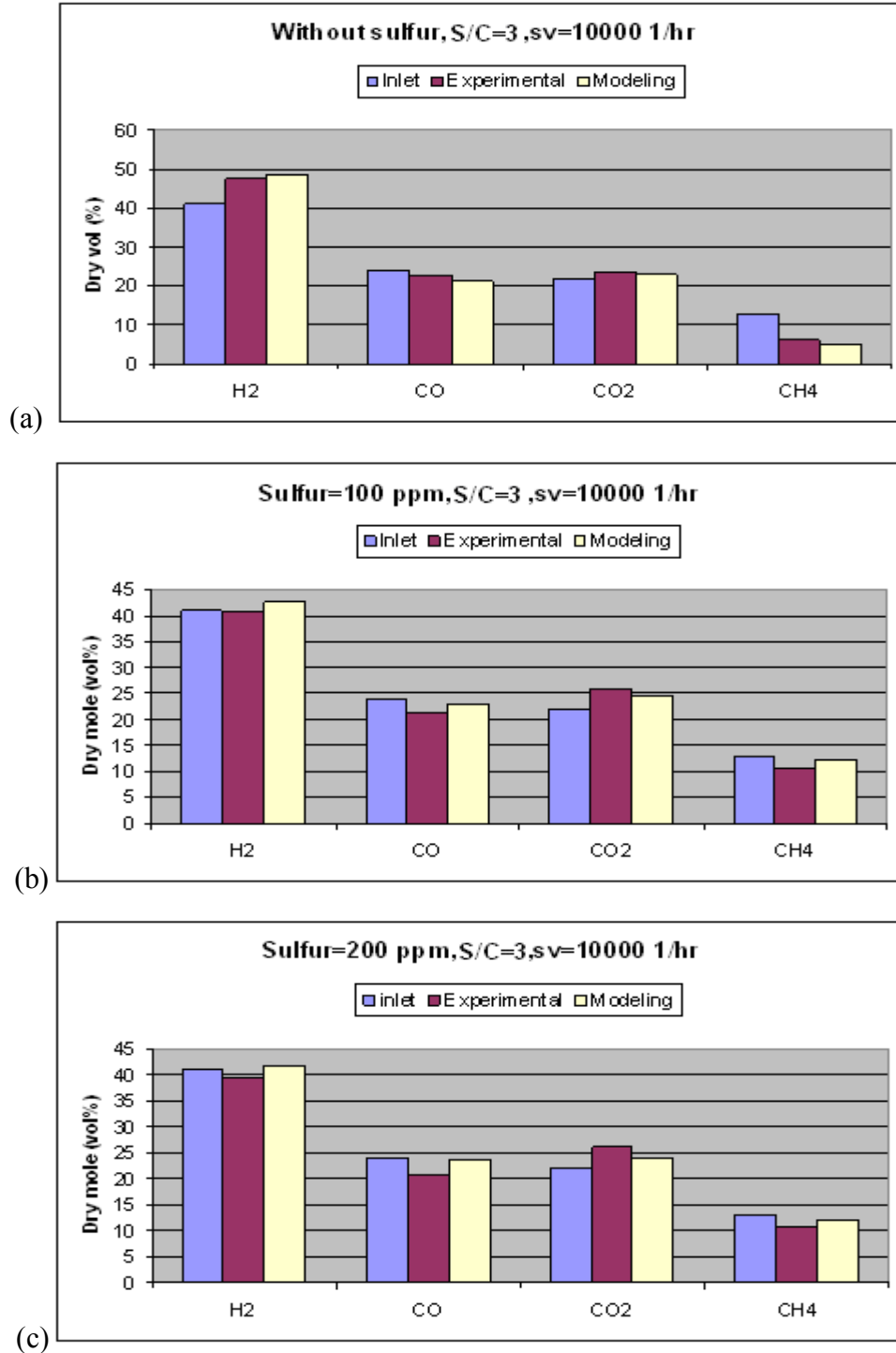


Figure 7.17 (a,b,c) Outlet mole concentration in the reactor, T=1123 (K) (a) S=0 ppm, (b) S=100ppm, (c) S=200 ppm

7.3.3 Temperature Effects

Increasing reactor wall temperature, heavily affects conversion of methane, hydrogen yield, carbon monoxide selectivity and carbon dioxide conversion to methane. In the following graphics, the space velocity is 10000 1/hr , steam to carbon ratio is 3 and sulfur amount is constant and is set to 160 ppm . The temperature varies from 1000 to 1150 (K).

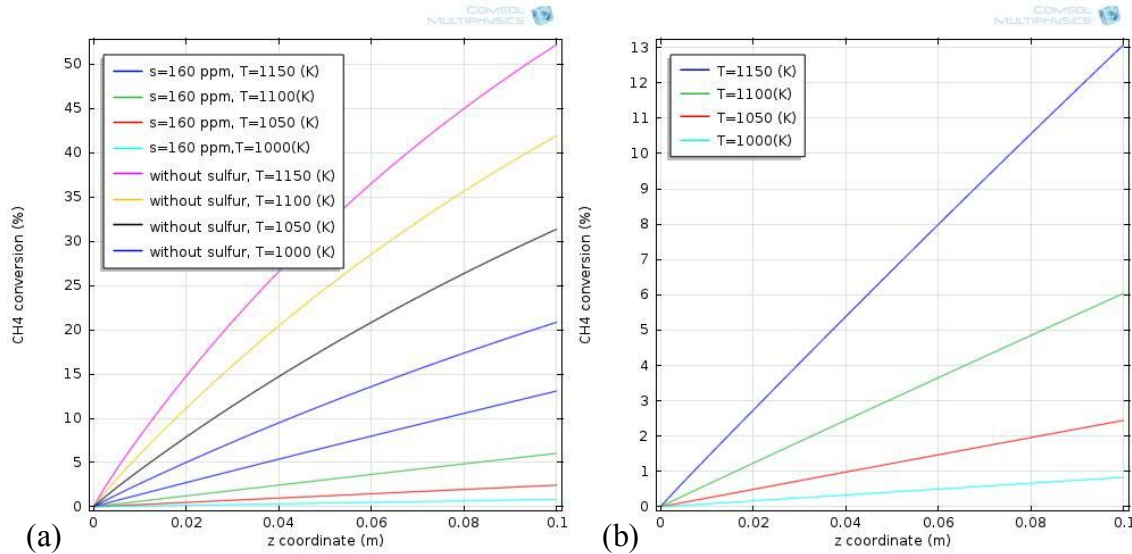


Figure 7.18 (a,b) Methane conversion in the reactor, S/C=3, sv=10000 1/hr, (a) with and without sulfur, (b) Sulfur=160 ppm

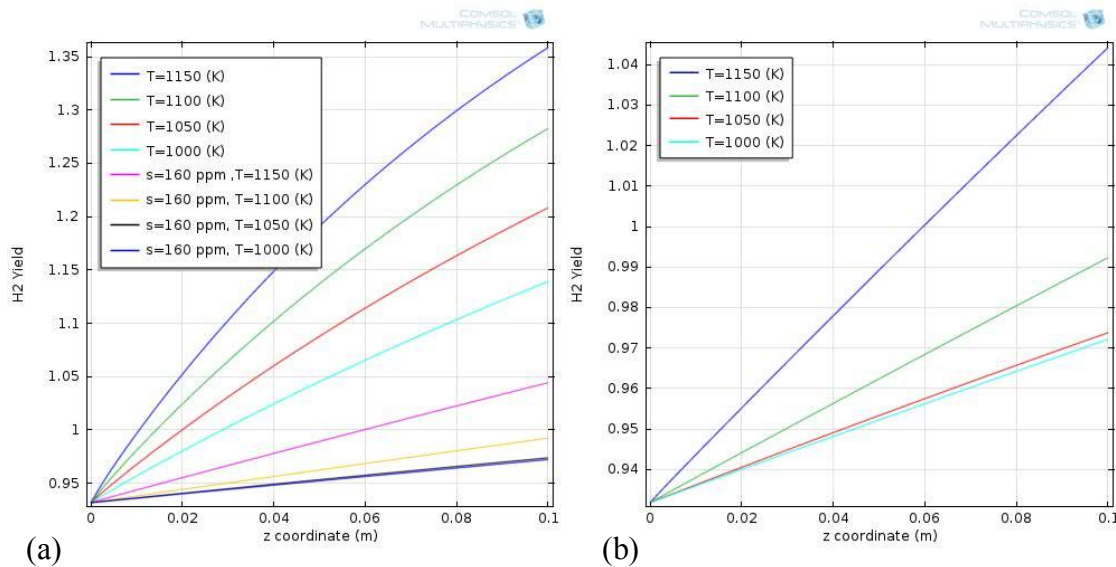


Figure 7.19 (a,b) Hydrogen yield in the reactor, S/C=3, sv=10000 1/hr, (a) with and without sulfur,(b) Sulfur=160 ppm

Figures 7.18 and 7.19 indicate the effect of the temperature variation on methane conversion and hydrogen yield in radial average position along the reactor length. As it is shown, increasing the wall temperature which leads to increasing the reaction temperature within the packed bed of the reactor increases the conversion of methane and hydrogen yield. At temperature of 1150 K the conversion of methane is at the highest level and corresponds to the highest level of hydrogen yield.

Carbon monoxide selectivity and carbon dioxide conversion to methane are shown in Figure 7.20 (a,b). It is shown that at low reaction temperatures, (1000 K) the carbon monoxide selectivity decreases. It is due to the fact that low temperatures are in favor of water gas shift reaction. At higher temperatures methane steam reforming reactions, (3-1,3-3) are dominant therefore, carbon monoxide selectivity increases along the axial bed of the catalyst. Higher temperatures are in favor of methane steam reforming reactions and by increasing the wall temperature conversion of carbon dioxide to methane also increases. In general higher temperatures lead to more uniform profile distributions. As mentioned earlier sulfur has negative effect on the process.

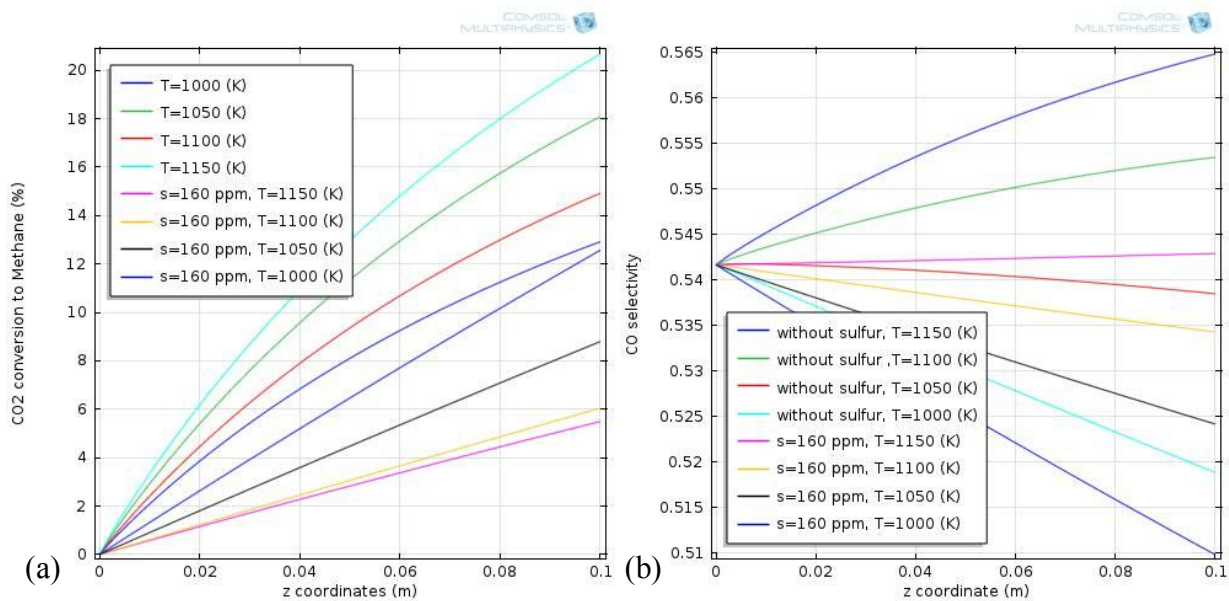


Figure 7.20 (a,b) Carbon monoxide selectivity and carbon dioxide conversion to methane in the reactor, S/C=3, sv=10000 1/hr, (a) carbon dioxide conversion to methane, (b) carbon monoxide selectivity

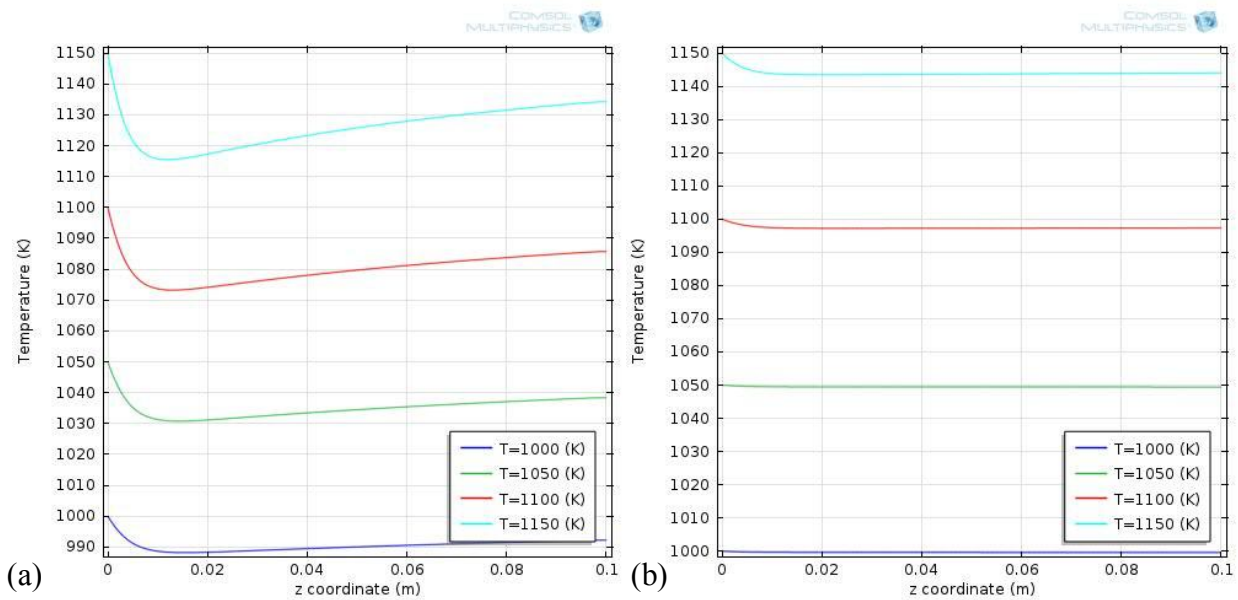


Figure 7.21 Axial temperature distribution within the reactor, $S/C=3$, $sv=10000$ 1/hr, (a) without sulfur, (b) sulfur amount=160 ppm

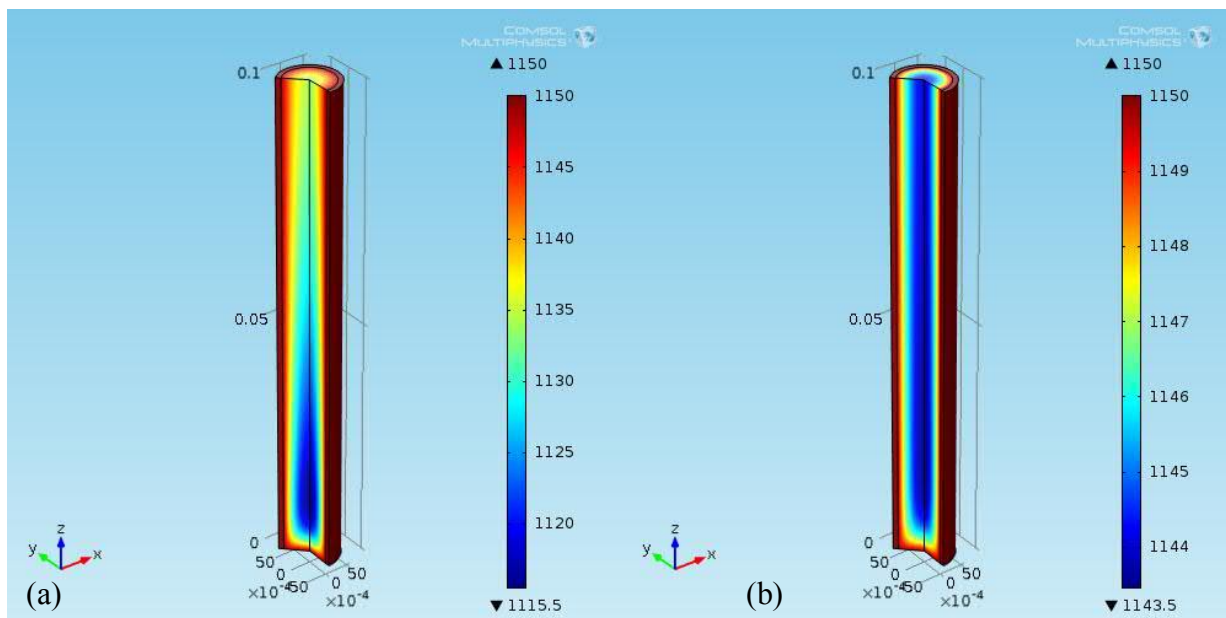


Figure 7.22 Axial graphical temperature distribution within the reactor, $S/C=3$, $sv=10000$ 1/hr, $T=1150$ (K) (a) without sulfur (b) sulfur amount=160 ppm

Axial and radial temperature profiles are shown in figures 7-21 to 7-24. Figure 7-21 shows the profile of the predicted reactor temperature along the bed length at various reaction temperatures. As soon as the gas enters the reactor due to the endothermic nature

of the reactions, the gas temperature is decreased. Then heat is conducted into the reactor via reactor wall and the temperature of the process gas increases from center of the reactor toward the wall.

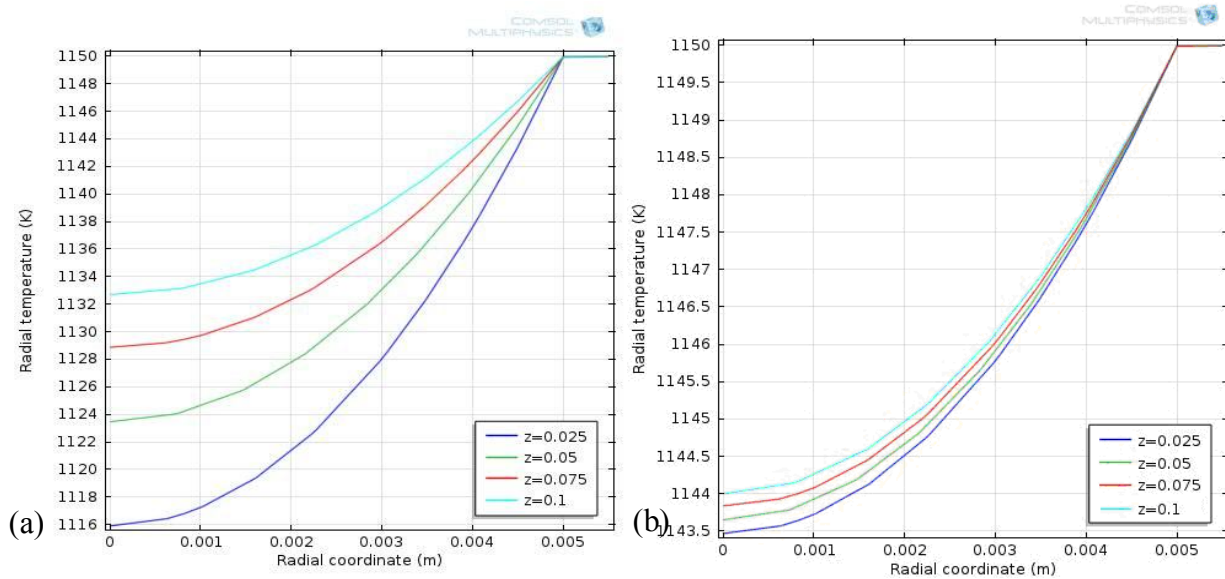


Figure 7.23 Radial temperature distribution within the reactor, $S/C=3$, $sv=10000$ 1/hr, $T=1150(K)$, (a) without sulfur, (b) Sulfur amount=160 ppm

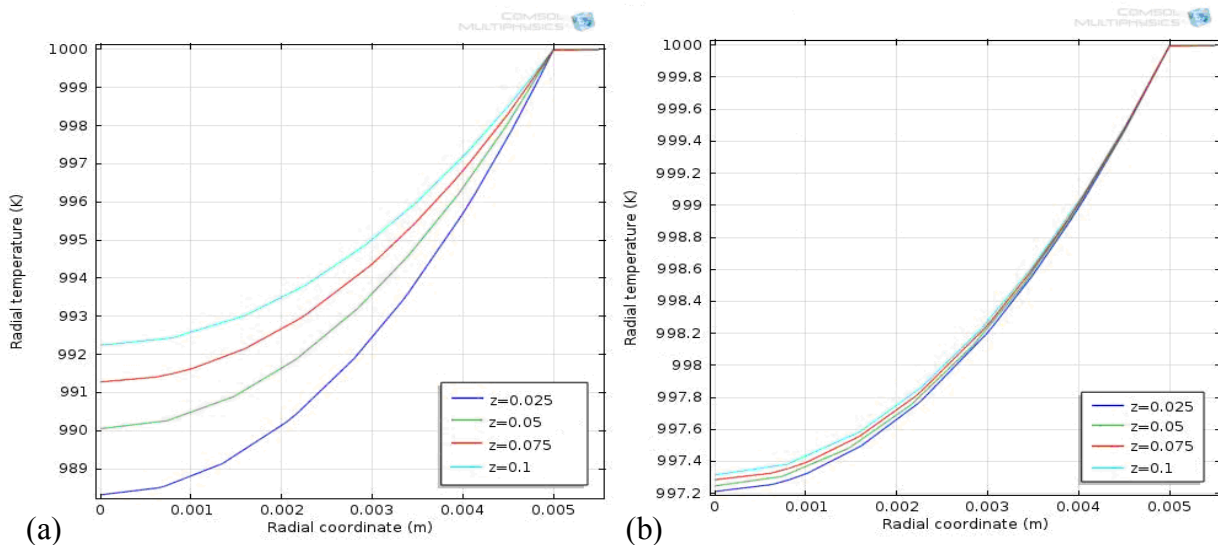


Figure 7.24 Radial temperature distribution within the reactor, $S/C=3$, $sv=10000$ 1/hr, $T=1000(K)$, (a) without sulfur, (b) sulfur amount=160 ppm

There is a temperature gradient between the centerline and wall of the reactor along the reactor length. It is shown that radial temperature gradients tend to decrease towards the reactor outlet because of the lower local heat fluxes and reforming reaction rates. The rate of reforming reactions is more rapid near the wall because the gas temperature is higher. It is shown that increasing reaction temperatures lead to the more uniform temperature profiles along the axial bed that finally results in a more efficient usage of the reactor. Comparison of modeling and experimental results is shown in the following graphics.

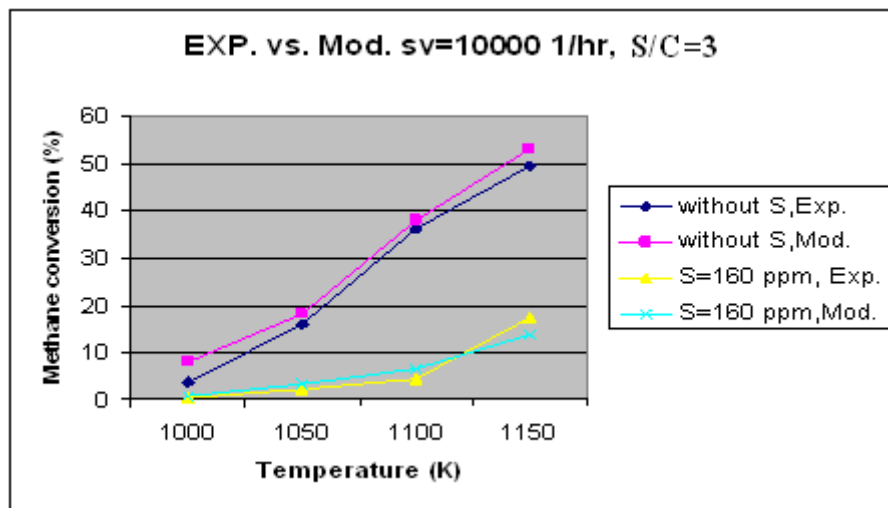
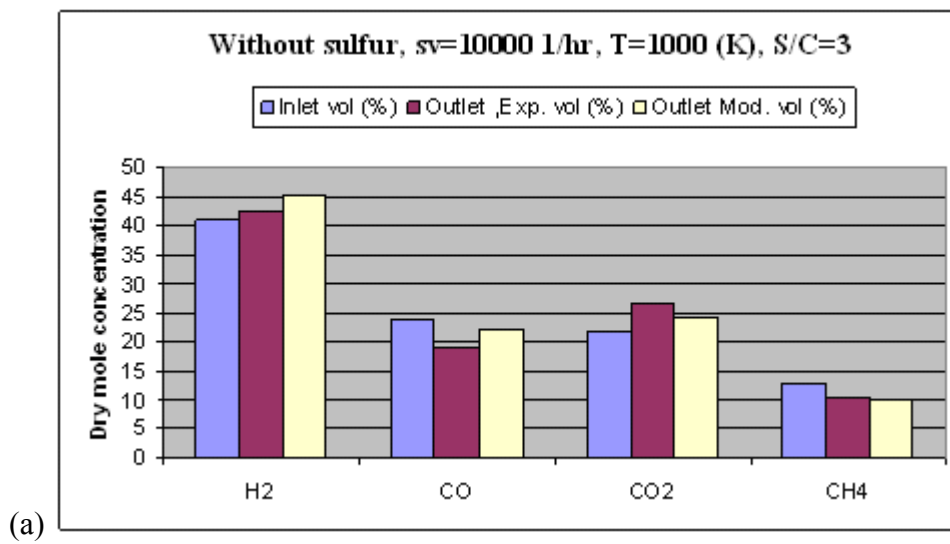


Figure 7.25 Comparison of modeling and experimental results of methane conversion in the reactor



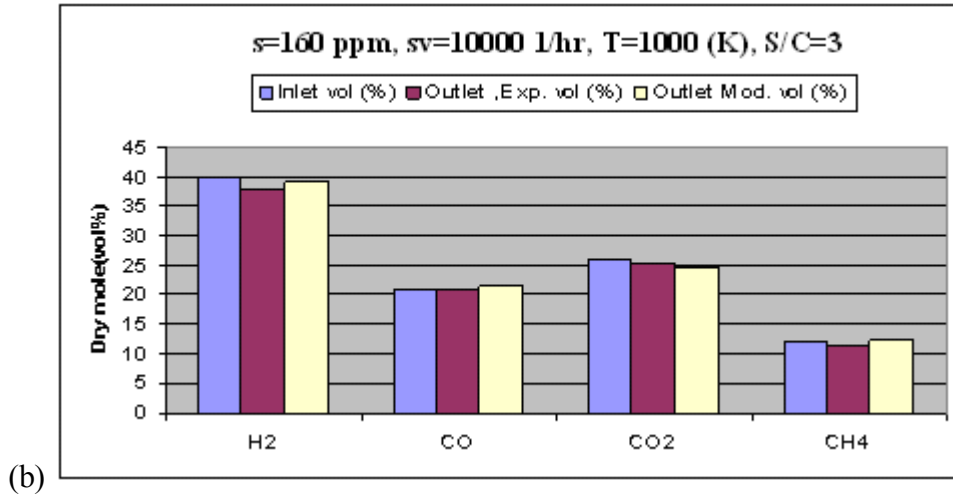


Figure 7.26 (a,b) Outlet mole concentration in the reactor, (a) sulfur=0 ppm (b) sulfur=160ppm

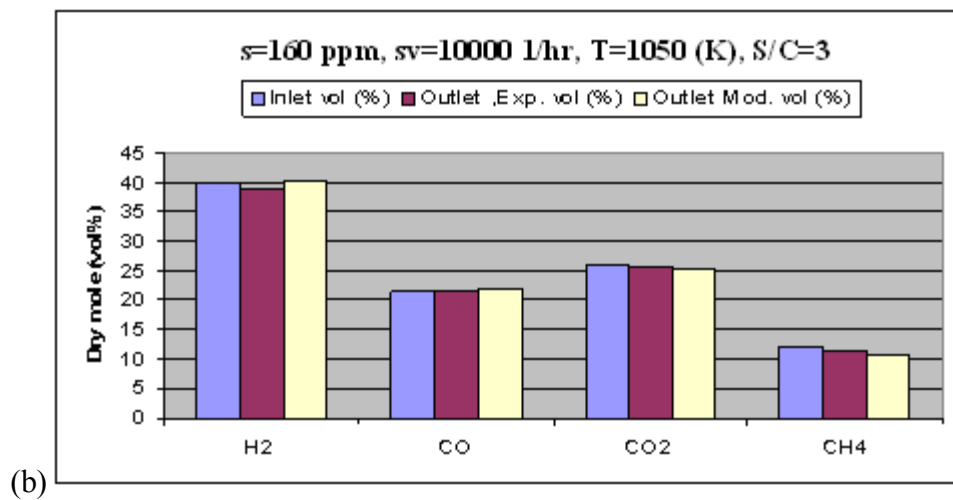
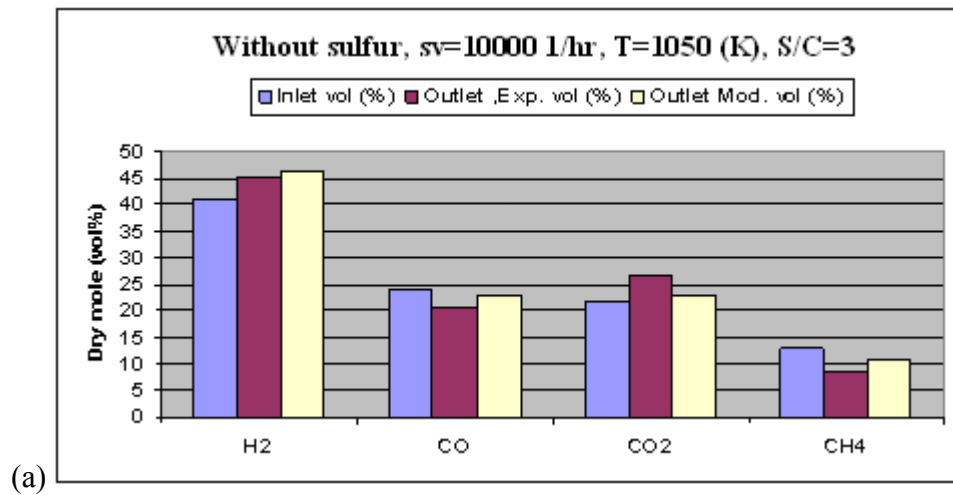


Figure 7.27 (a,b) Outlet mole concentration in the reactor, (a) sulfur=0 ppm, (b) sulfur=160ppm

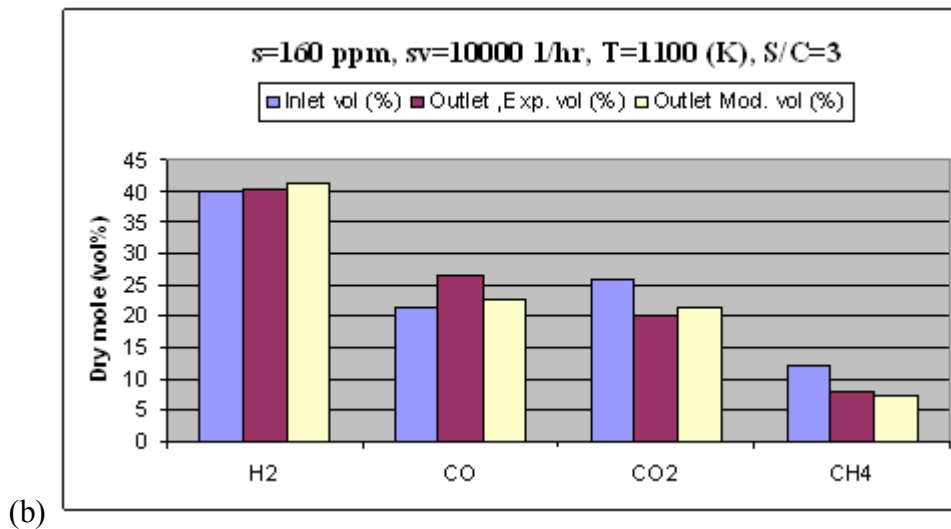
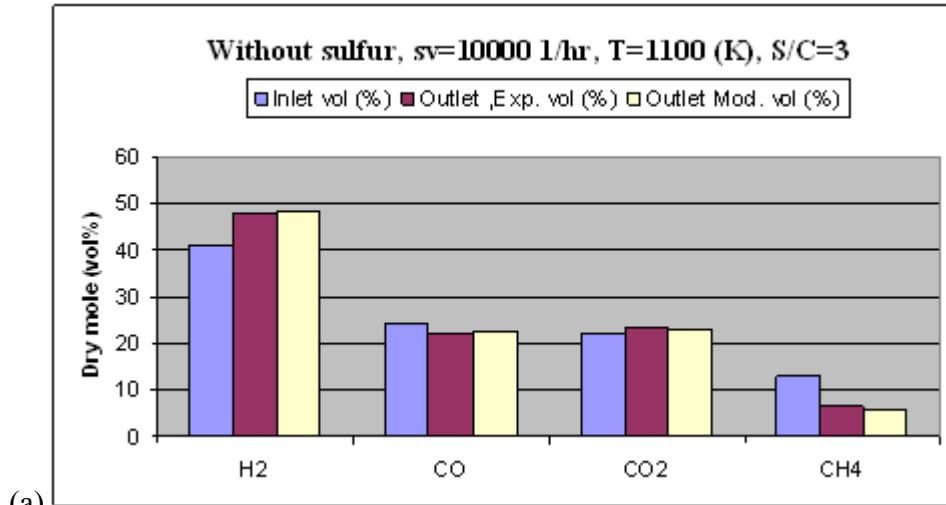
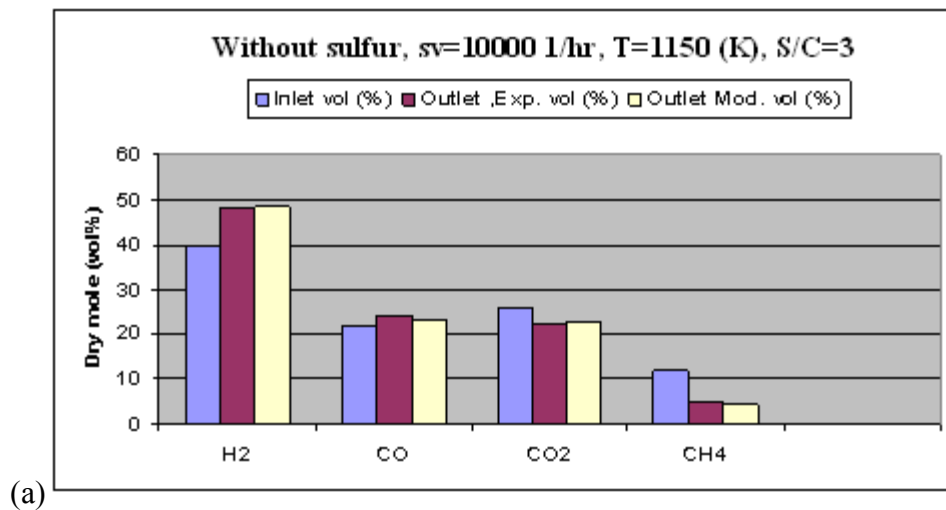


Figure 7.28 (a,b), Outlet mole concentration in the reactor, (a) sulfur=0 ppm, (b) sulfur=160ppm



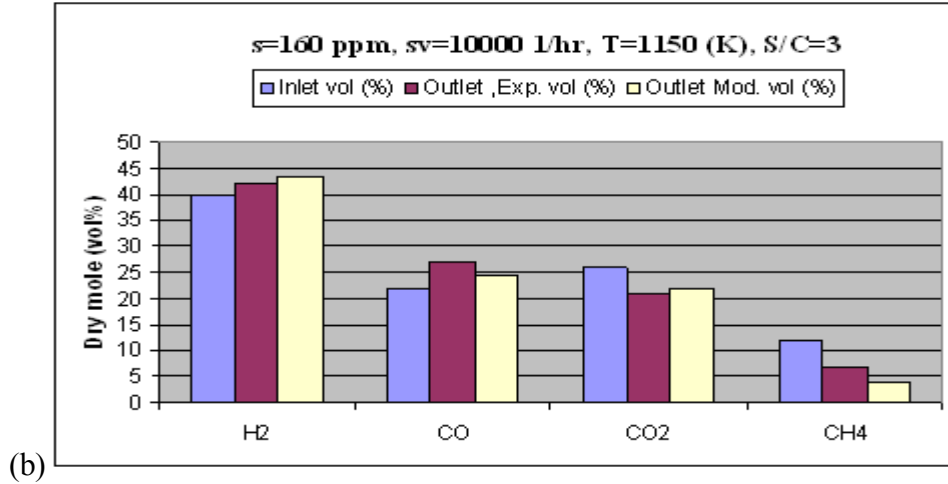


Figure 7.29(a,b) Outlet mole concentration in the reactor, (a) sulfur=0 ppm (b)sulfur=160ppm

7.3.4 Space Velocity

Space velocity is an important parameter for design and optimization of steam reformers and has a high impact on methane conversion and hydrogen yield. In the following graphics, it is shown how changing space velocities effect the reformer performance. Steam to carbon ratio is S/C=3 and sulfur amount is constant and is set to 160 ppm and outer reactor wall temperature is 1123 (K).

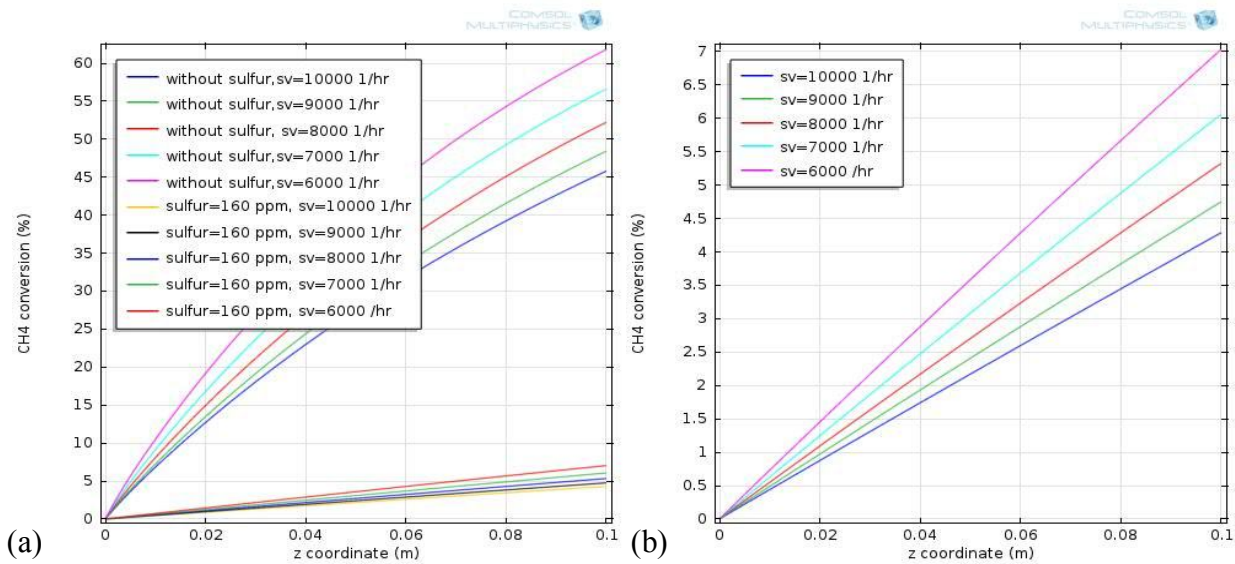


Figure 7.30.(a,b) Comparison of methane conversion at different space velocities within the reactor, S/C=3, T=1123 (K), (a) without sulfur, (b) sulfur=160 ppm

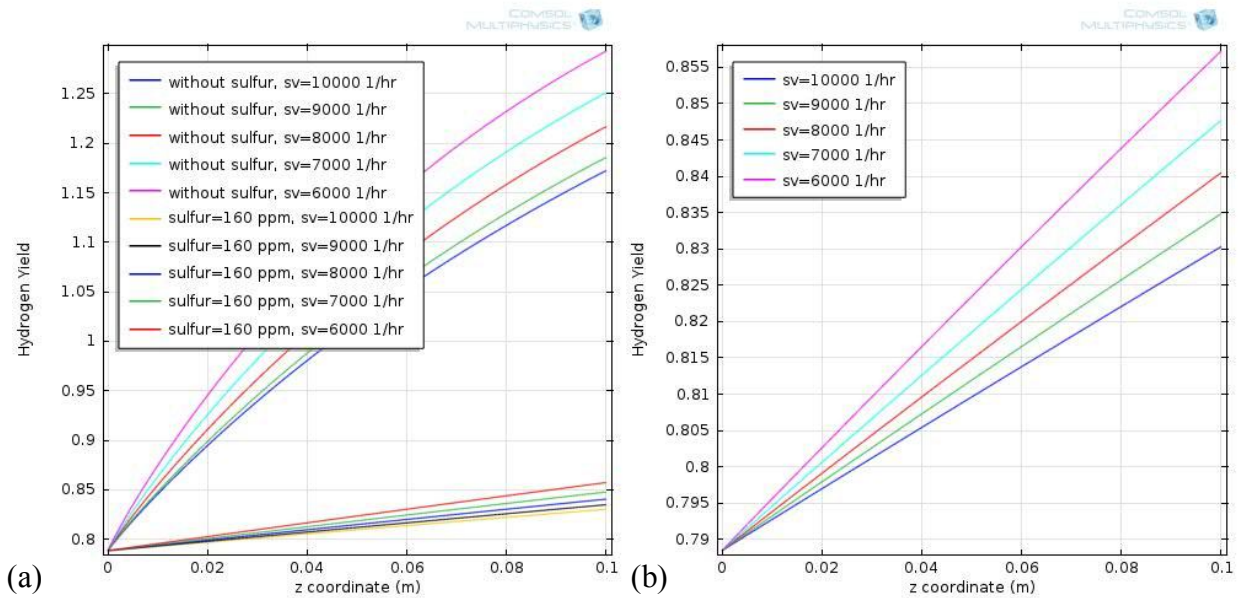


Figure 7.31(a,b) Comparison of hydrogen yield at different space velocities within the reactor, S/C=3, T=1123 (K), (a) without sulfur, (b) sulfur=160 ppm

Figures 7-30 and 7-31 show the effect of different space velocities on Methane conversion and hydrogen yield with and without presence of sulfur in the gas. It is evident that decreasing space velocity increases methane conversion. The reason is that at lower space velocities the contact time between gas and catalyst pellets increases and as a result methane conversion increases which corresponds to the highest level of hydrogen yield within the reactor. When sulfur is included in the gas, the same effect is seen but methane conversion and hydrogen yield are decreased due to negative effect of sulfur on reforming reactions.

Effect of changing space velocity on temperature distribution within the reactor is shown in Figures 7-32 to 7-34. As shown in Figure 7-32(a,b), the gas temperature decreases after entering the reactor due to reforming reactions. Heat transfer from the wall increases the temperature again along the reactor bed. Sulfur deactivates the catalysts and reforming reaction rates decreases. Therefore, temperature decreases slowly along the reactor. Decreasing space velocity increases the time for heat transfer into the reactor from the wall of the reactor. Therefore, the outlet temperature increases, Figure 7-33(a,b).

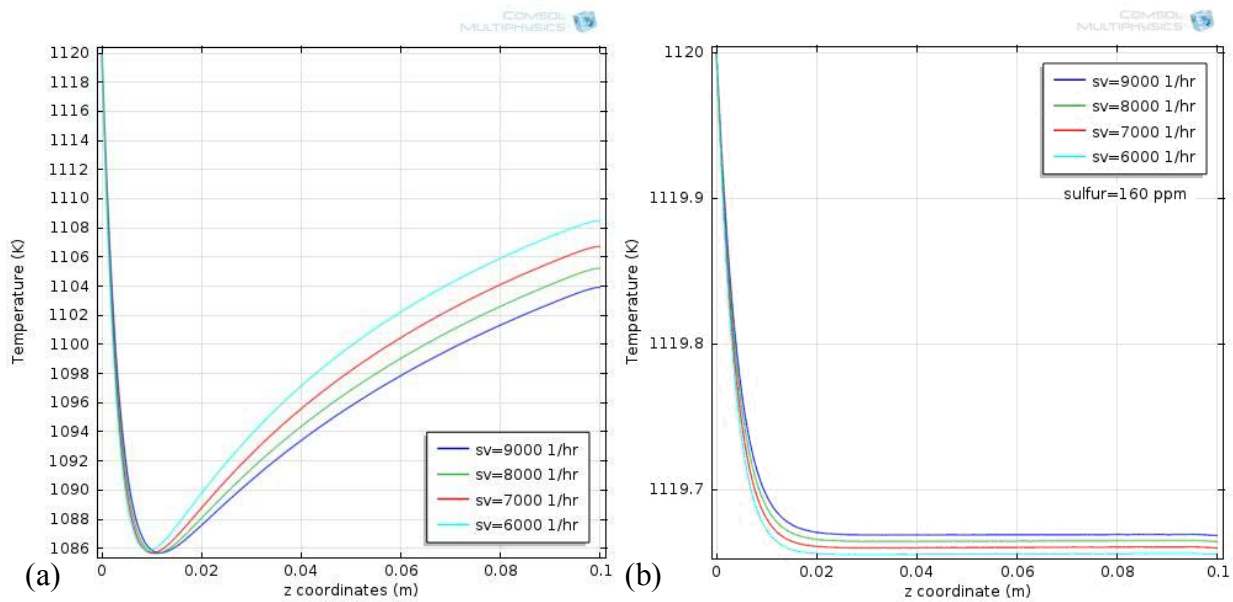


Figure 7.32(a,b) Axial temperature distribution at different space velocities within the reactor, S/C=3, T=1123 (K), (a) without sulfur, (b) sulfur=1160 ppm

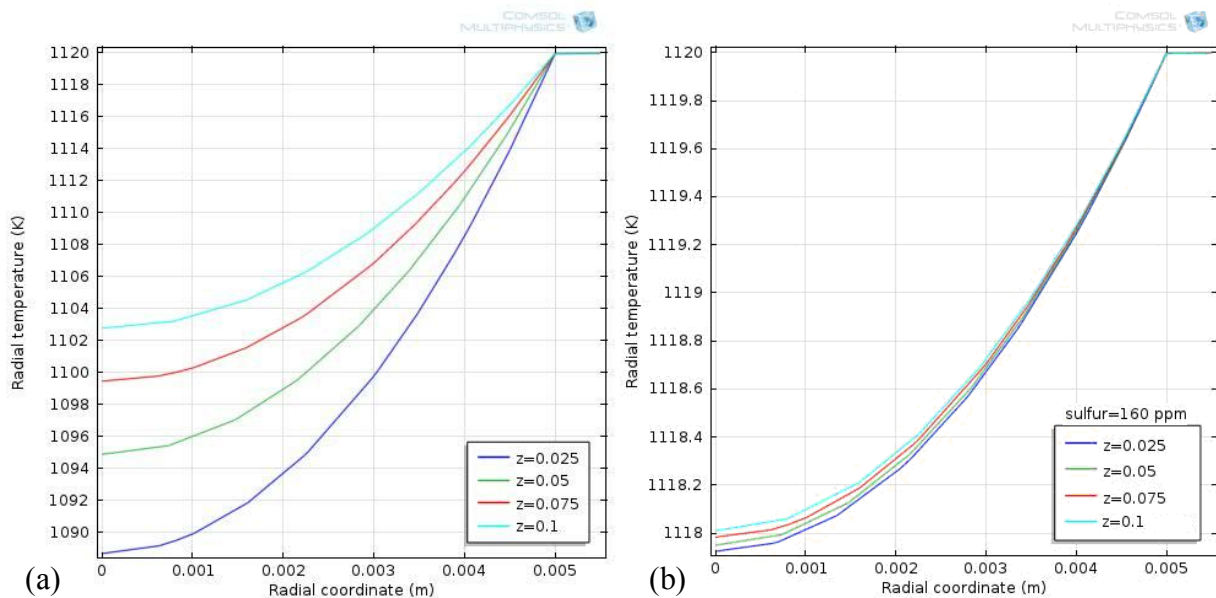


Figure 7.33(a,b) Radial temperature distribution at different levels within the reactor, sv=10000 1/hr, S/C=3, T=1123 (K), (a) without sulfur, (b) sulfur=160 ppm

Figure 7-34 shows the radial temperature distribution at different axial position within the reactor. Due to the void fraction of the catalyst close to the wall and heat fluxes, there are radial temperature gradients along the reactor close to the wall. As shown in Figures 7-33

and 7-34, decreasing space velocity increases the contact time between gas and the catalyst. The process increases the outlet temperature of the reactor and makes temperature distribution along the reactor more uniform.

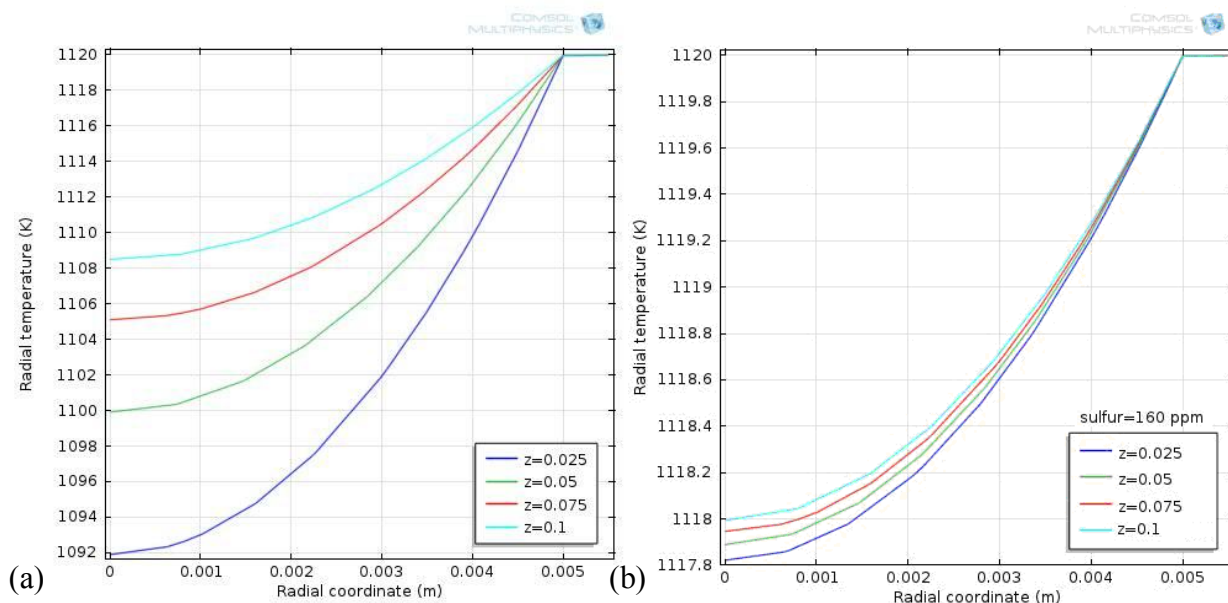


Figure 7.34(a,b) Radial temperature distribution at different levels within the reactor, sv=6000 1/hr, S/C=3, T=1123 (K), (a) without sulfur, (b) sulfur=160 ppm

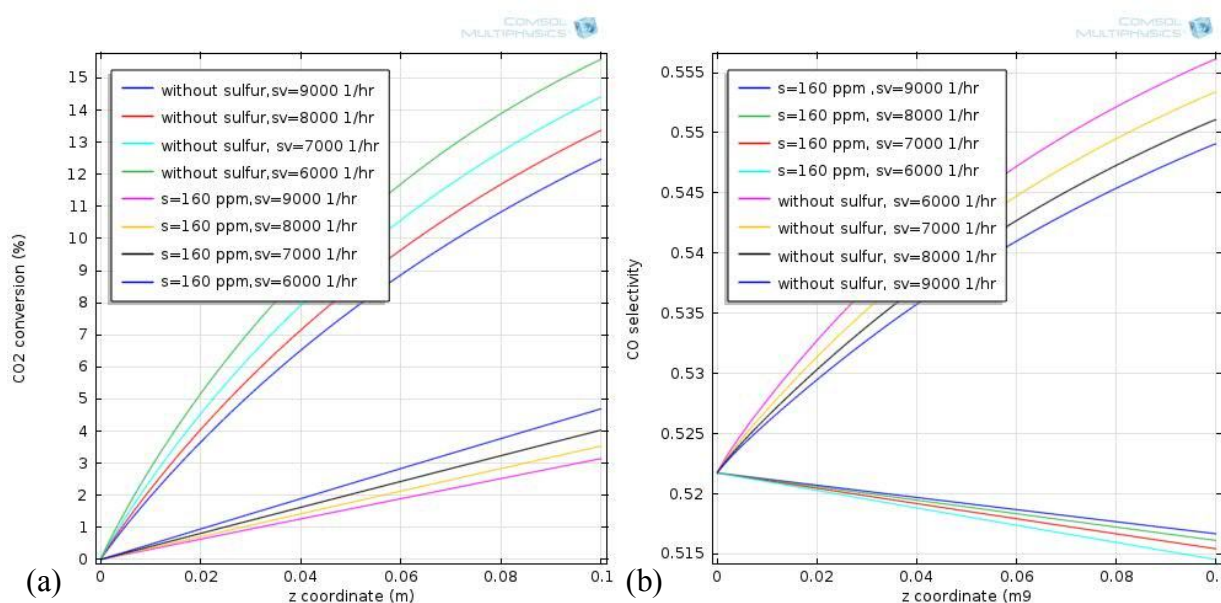


Figure 7.35(a,b) Carbon dioxide conversion to methane and carbon monoxide selectivity at different space velocities within the reactor, S/C=3, T=1123 (K), (a) carbon dioxide conversion, (b) carbon monoxide selectivity.

Comparison of modeling and experimental results, are shown in the following graphics:

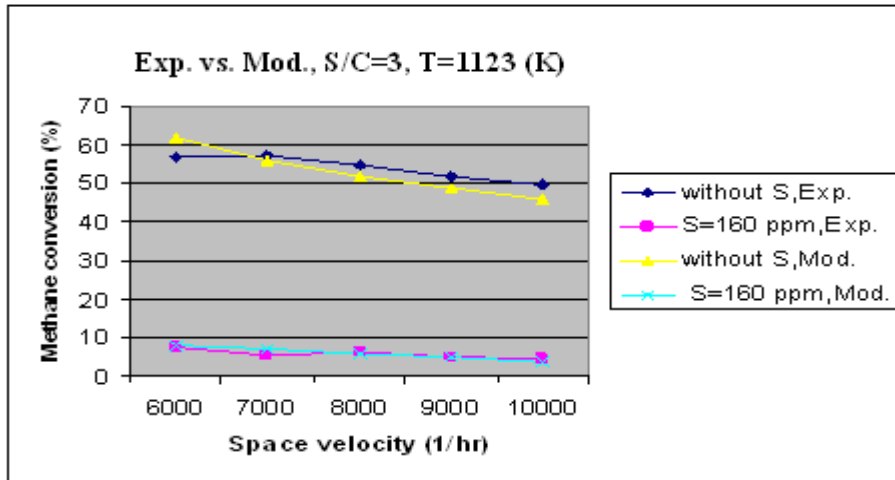


Figure 7.36 Comparison of modeling and experimental results of methane conversion in the reactor

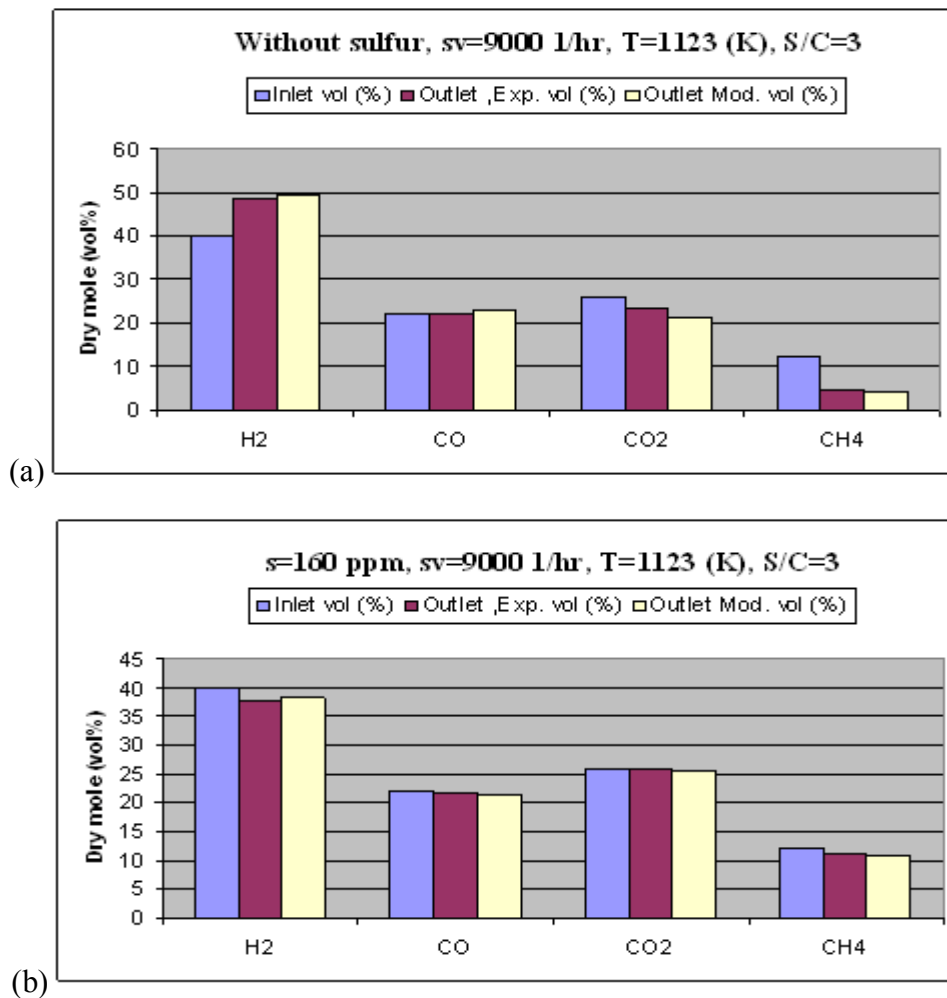


Figure 7.37 (a,b) Outlet mole concentration in the reactor,(a) sulfur=0 ppm (b) sulfur=160 ppm

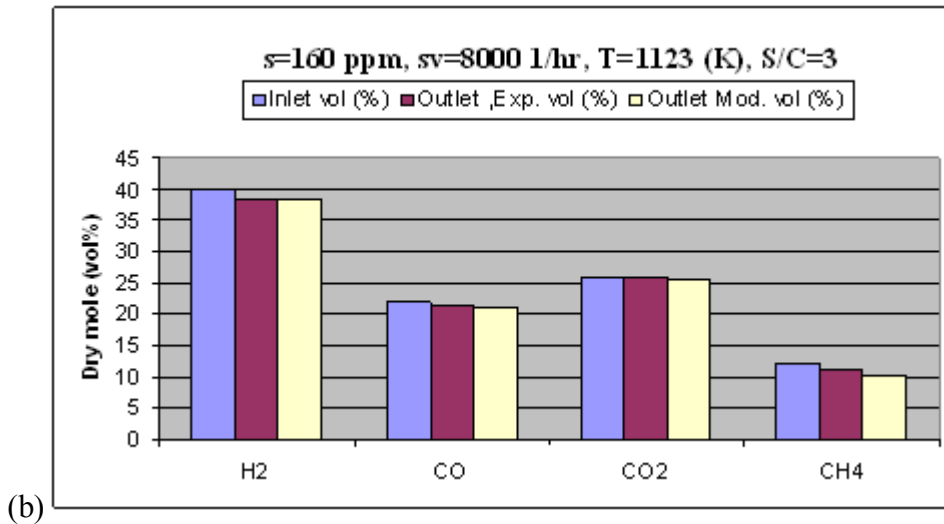
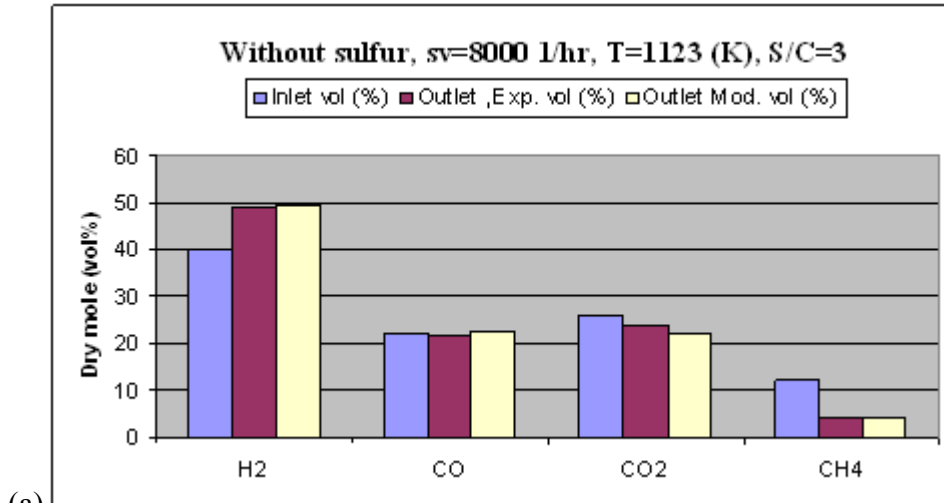
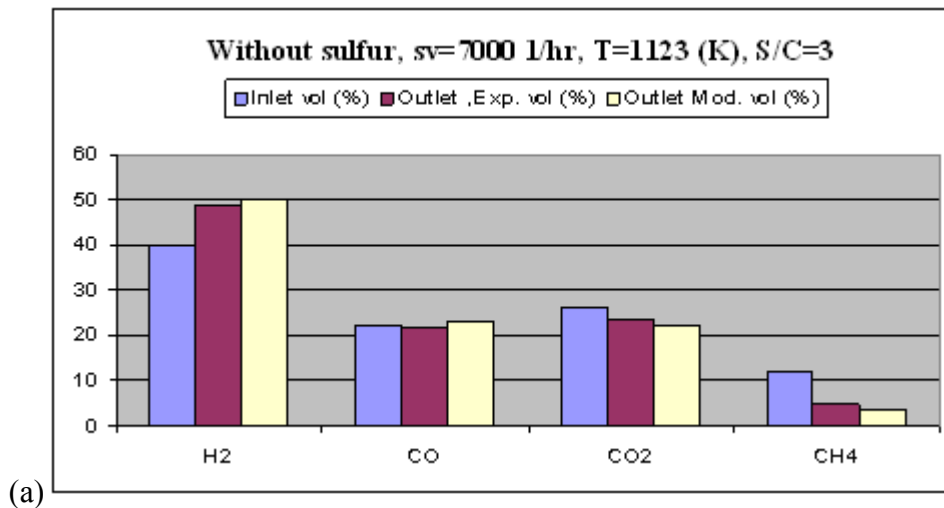


Figure 7.38 (a,b.) Outlet mole concentration in the reactor ,(a) sulfur=0 ppm (b) sulfur=160ppm



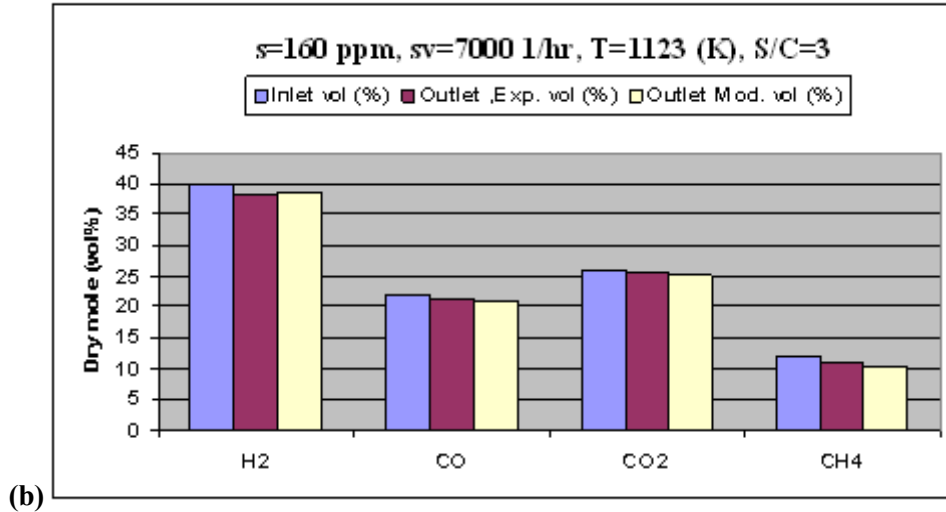


Figure 7.39 (a,b), Outlet mole concentration in the reactor ,(a) sulfur=0 ppm (b) sulfur=160ppm

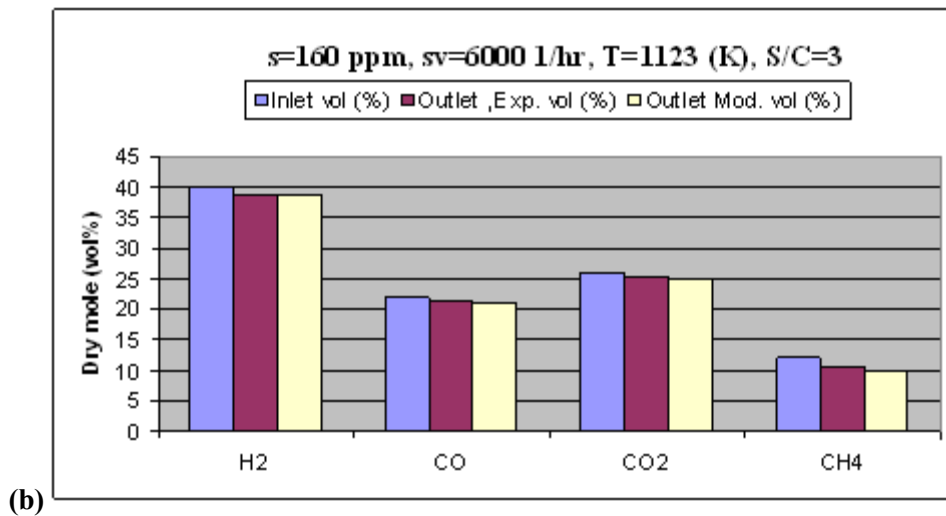
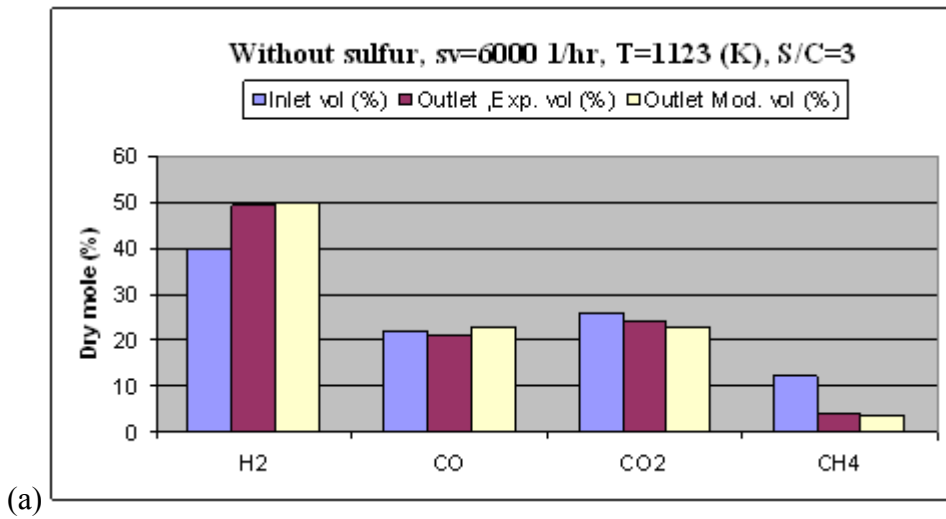


Figure 7.40 (a,b), Outlet mole concentration in the reactor ,(a) sulfur=0 ppm (b) sulfur=160 ppm

7.4 Experimental Results from Güssing Plant, Austria

In the following section the modeling results are compared to the actual experimental results with real producer gas from Güssing plant. Dimension of the tubular steam reformer in Güssing is 48.3x2.6 mm. The reformer is filled with reforming catalyst and according to each experiment, the height of the catalyst varies from 0.25 to 1.44 (m). Sulfur, which also is incorporated in the biomass structure, is released into the product gas during gasification as hydrogen sulfide, [Koningen et al., 1998]. Sulfur amount is measured as 150 ppm. Following gas composition is used in the experiments:

Volume fraction (vol%)					
CO	CO ₂	CH ₄	N ₂	C ₃ H ₆	H ₂
22	25	11	2	1	39

Table 7.1. Producer gas composition from Güssing plant

7.4.1 Experiment No. 1

250 gram of catalyst filled in the steam reformer and the height of the catalyst is 0.25 (m). Inlet temperature is 290°C and the flow rate is 1.3 Nm³ / hr . Outer temperature of the reformer is kept at 900°C and space velocity is 3650 1/hr . The experiments are conducted at atmospheric pressure and 3 liter of water per hour entered into the reactor. Following experimental and modeling results were obtained.

Figure 7.41 (a,b) shows methane and propylene conversion and hydrogen yield in the reactor. It is visible that when sulfur is not included in the gas, at very close distance from the inlet of the reactor propylene is almost 100 percent converted and methane is also completely converted at the end of the reactor. These are also corresponding to the highest level of hydrogen yield. When sulfur is included in the gas, deactivates the catalyst and conversion of the hydrocarbons is drastically decreases.

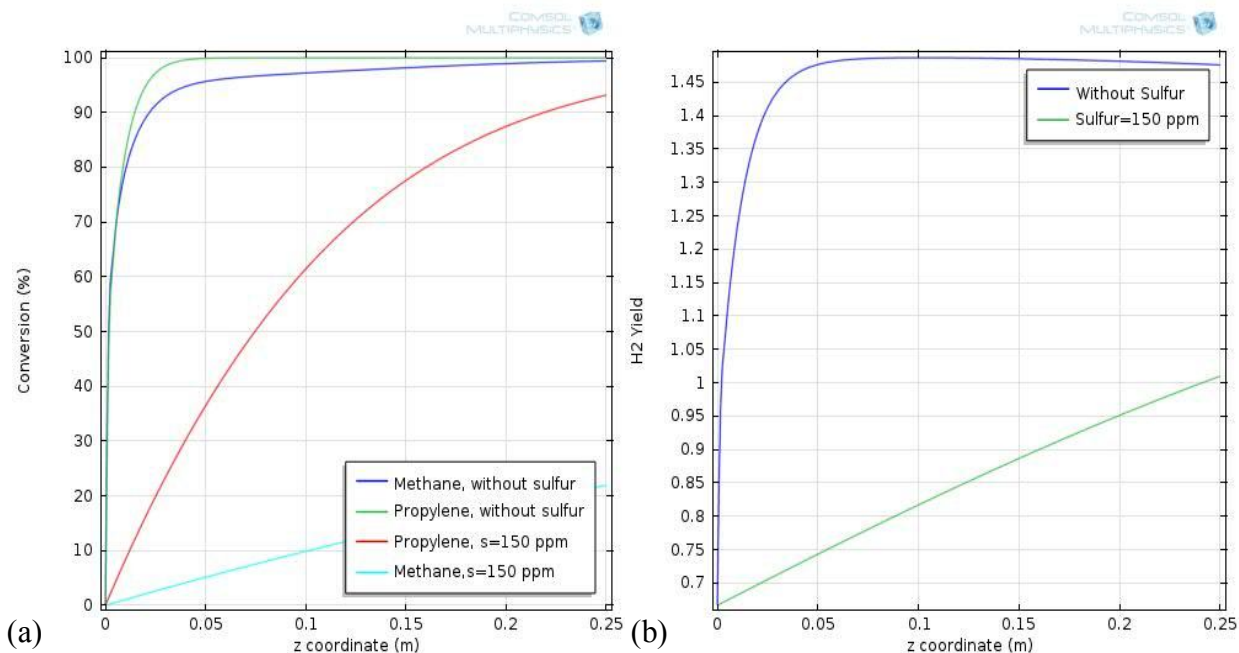


Figure 7.41(a,b) Methane and propylene conversion and hydrogen yield in the reactor, $S/C=3$, $T=1173$ (K), $sv=3650$ 1/hr, sulfur= 150 ppm, (a) methane and propylene conversion, (b) hydrogen yield

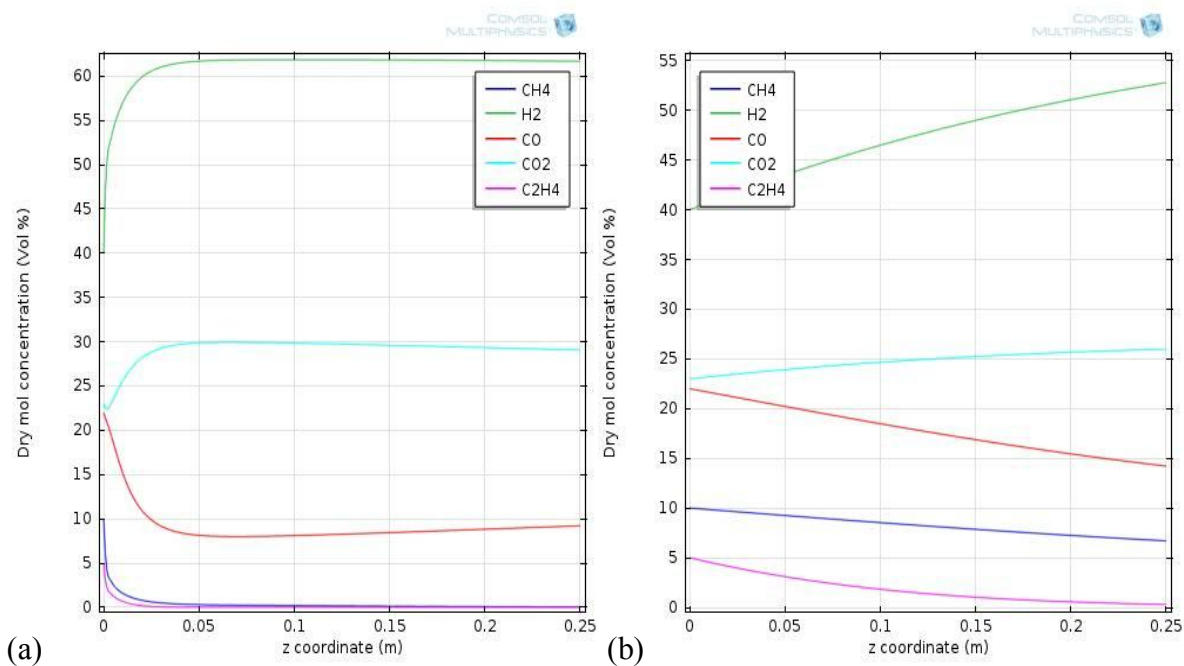


Figure 7.42 (a,b), Dry mole concentration of different species in the reactor, $S/C=3$, $T=1173$ (K), $sv=3650$ 1/hr, (a) without sulfur (b) sulfur=150 ppm.

Figure 7.42 (a,b) shows dry mole concentration of different species in the reactor. The modeling is also done when sulfur is included in the producer gas and the results are compared. For both cases, with and without sulfur in the gas, hydrogen concentration increases which is due to conversion of methane and propylene. When sulfur is not included in the producer gas, reforming reactions increases carbon dioxide concentration and decreases carbon monoxide concentration. Later, high concentration of hydrogen due to conversion of methane and propylene, cause water gas shift reaction to proceed in other direction. Therefore, carbon dioxide conversion decreases and carbon monoxide conversion increases along the reactor. Sulfur has negative effect on reforming reactions; therefore, hydrogen yield decreases. Lower reforming reaction rates due to sulfur deactivation effects, makes concentration profiles more uniform in the reactor.

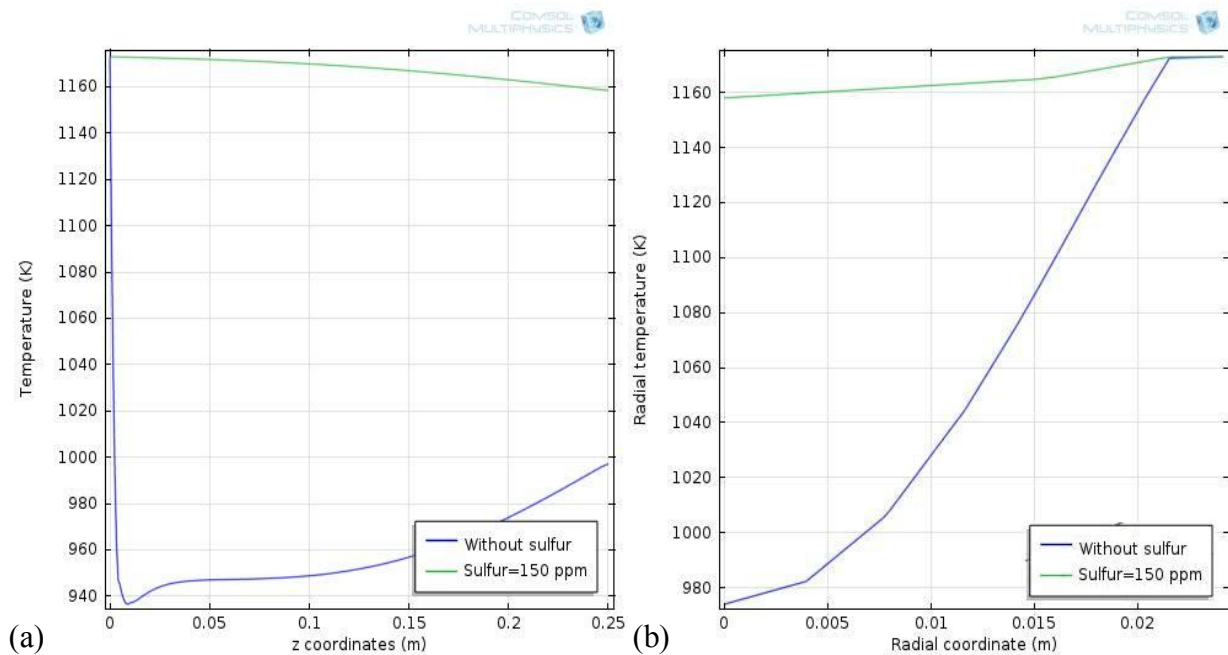


Figure 7.43 (a,b), Temperature distribution in the reactor with and without sulfur , S/C=3, T=1173 (K), sv=3650 1/hr, (a) axial temperature distribution, (b) Radial outlet temperature distribution

Temperature distribution in the reactor is shown in Figure 7.43 (a,b). Results show that as soon as gas enters into the reactor, due to high endothermic nature of the reforming reactions, temperature drops suddenly at the inlet of the reactor from the initial temperature of 1173 K to about 940 K and then increased gradually to the outlet. The

rising temperature after a sudden drop along the axial bed of the catalyst is due to the completion of methane and propylene conversion and heat supplied by the outer surface of the reactor into the catalytic bed. Presence of sulfur in the gas leads to the catalyst deactivation and lower methane and propylene conversion rate. Therefore, temperature decreases uniformly along the reactor bed. The graphical view of the phenomena, with and without sulfur included in the gas, can be seen in Figures 7.44 (a,b) and 7.45 (a,b).

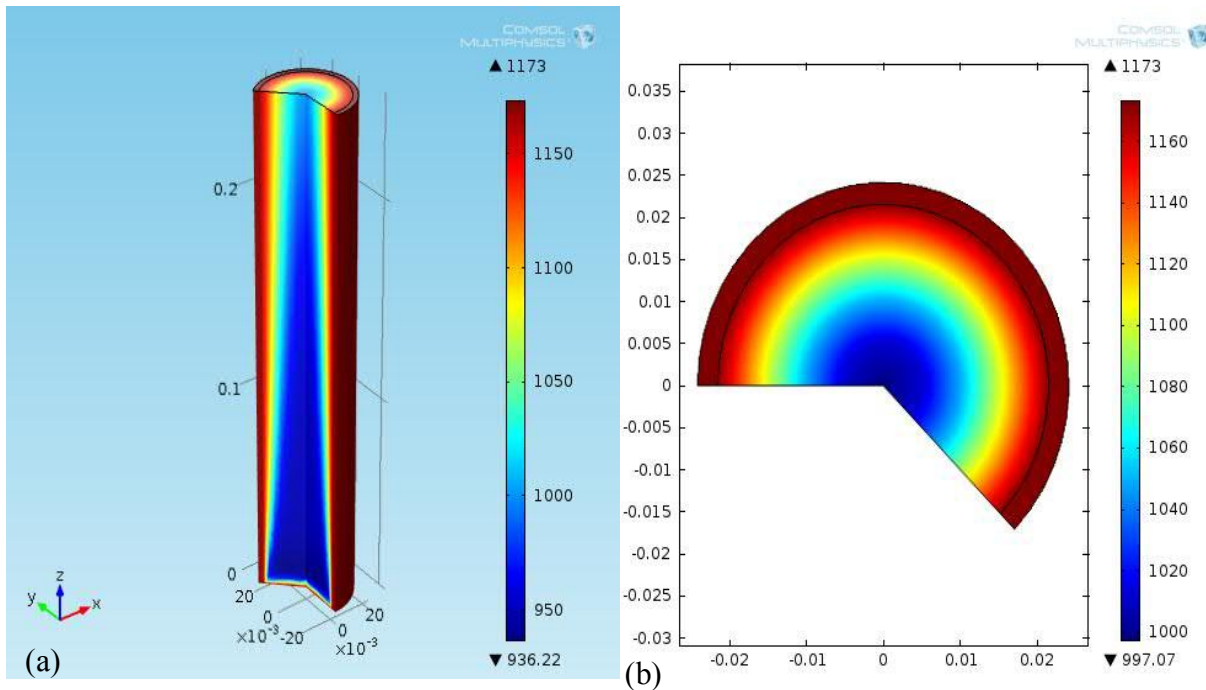


Figure 7.44 (a,b), Graphical view of modeling results of temperature distribution in the reactor without sulfur, $S/C=3$, $T=1173$ (K), $sv=3650$ 1/hr, (a) axial temperature distribution, (b) radial outlet temperature distribution

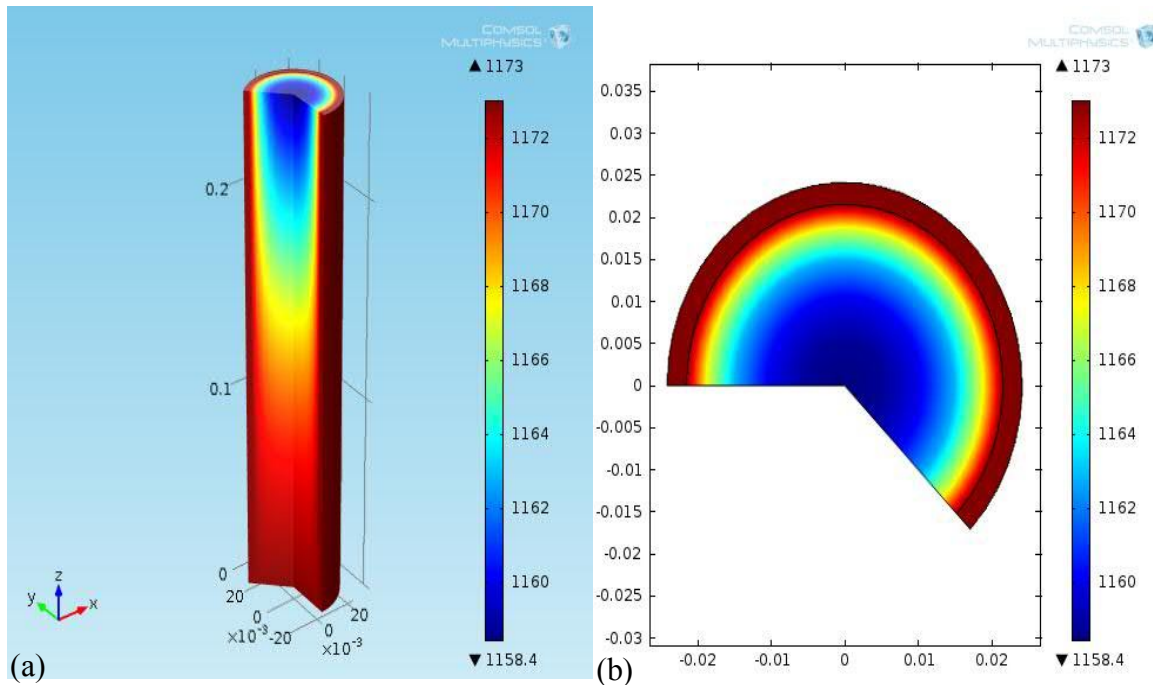


Figure 7.45 (a,b), Graphical view of modeling results of temperature distribution in the reactor S/C=3, T=1173 (K), sv=3650 1/hr, sulfur= 150 ppm, (a) axial temperature distribution, (b) radial outlet temperature distribution.

Conducting the modeling with the same experimental conditions allows to compare the modeling and experimental results in Figure 7.46.

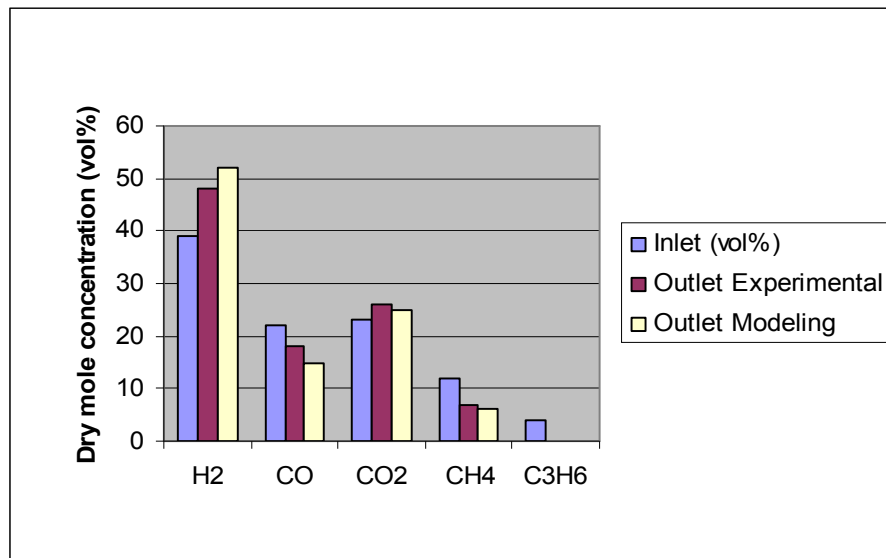


Figure 7.46 Comparison of experimental and modeling results of outlet dry mole concentration of different species in the reactor, S/C=3, T=1173 (K), sv=3650 1/hr, sulfur= 150 ppm

7.4.2 Experiment No.2

750 gram of catalyst filled in the steam reformer and the height of the catalyst is 0.7 (m). Inlet temperature is 290°C and the flow rate is $1.5 \text{ Nm}^3 / \text{hr}$. Outer temperature of the reformer is kept at 900°C and space velocity is $15001/\text{hr}$. The experiments are conducted at atmospheric pressure and 2.5 liter of water per hour entered the reactor. The gas composition is shown in Table 7.1.

Figure 7.47(a,b) shows modeling results of methane and propylene conversion and hydrogen yield in the reactor. Sulfur is also included in the gas and it is shown that in both cases propylene conversion is much more rapid than methane conversion. Even when small amount of sulfur are included in the producer gas, methane and propylene conversion and therefore, hydrogen yield decrease significantly.

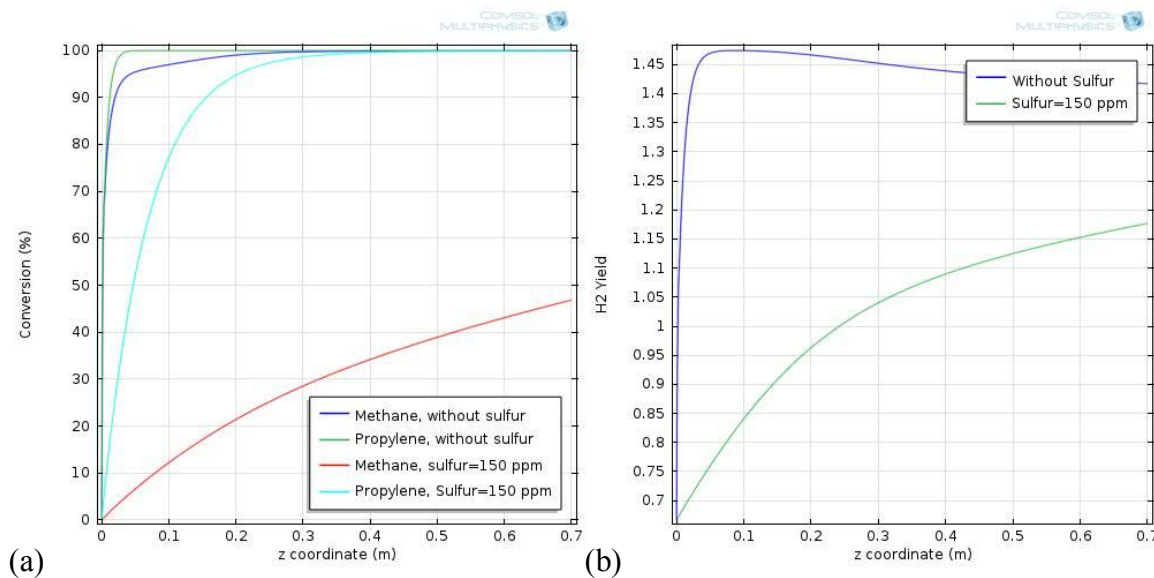


Figure 7.47(a,b) Methane and Propylene conversion and hydrogen yield in the reactor, $sv=1500$ 1/hr, $S/C=2$, sulfur= 150 ppm, $T=1173(\text{K})$, (a) Methane and propylene conversion, (b) Hydrogen yield

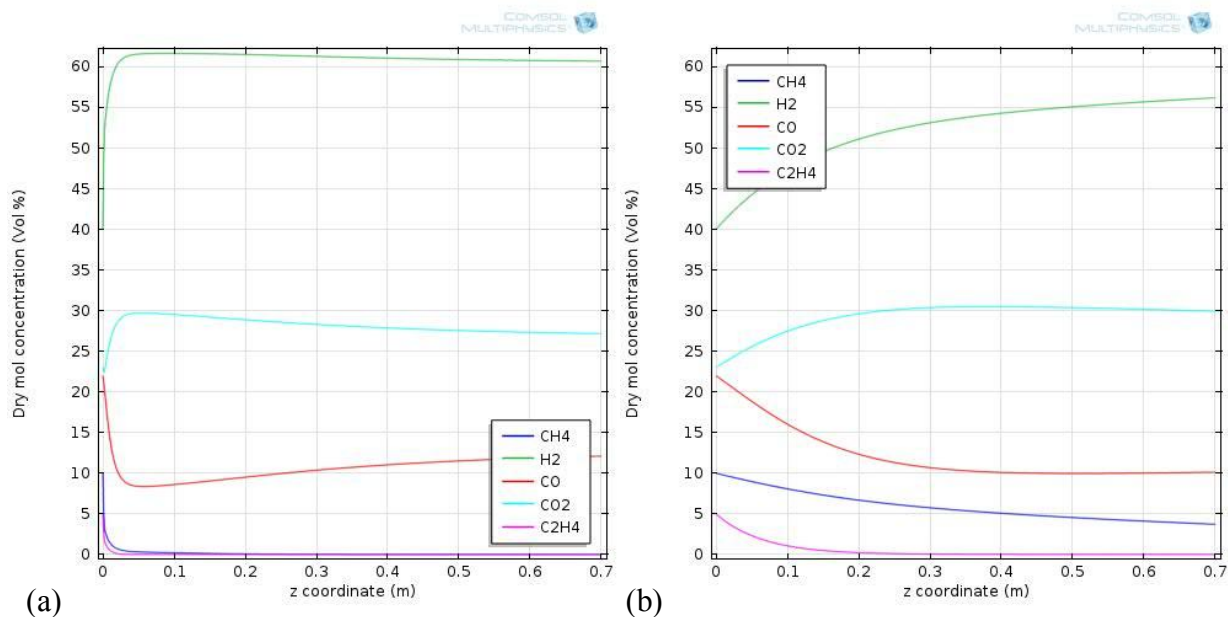


Figure 7.48 (a,b), Dry mole concentration of different species in the reactor, $sv=1500$ 1/hr, $S/C=2$, $T=1173(K)$, (a) without sulfur, (b) sulfur=150 ppm.

Figure 7.48(a,b) shows dry molar concentration of different species of the gas along the reactor length and compares the results to the case when sulfur is included in the gas. As it is shown in both cases, methane and propylene concentrations decrease along the reactor packed bed, therefore, hydrogen concentration increases. It is due to the consumption of methane and propylene in both reforming and water gas shift reactions. When sulfur is not included in the gas, it can be shown that the concentration of methane and propylene decrease sharply at very close distance to the entrance of the reactor which corresponds to the highest level of hydrogen yield. When sulfur is not present in the gas composition, it is shown that, the carbon monoxide concentration dropped and carbon dioxide concentration increases sharply at very close distance from the reactor entrance. Then, carbon monoxide gradually increases and carbon dioxide decreases along the axial bed of the catalyst. It is due to composition of the biogas and the fact that the rate of water gas shift reaction is higher than reforming reactions, therefore, carbon monoxide concentration decreases and carbon dioxide concentration increases. Later; hydrogen reaction with carbon dioxide is suppressed and cause the water gas shift reaction to proceed in other direction. Therefore, carbon monoxide concentration increases and

carbon dioxide concentration decreases along the reactor. Due to the sulfur presence in the gas and catalyst deactivation effects, carbon dioxide and carbon monoxide concentrations increase and decrease uniformly along the reactor length, respectively.

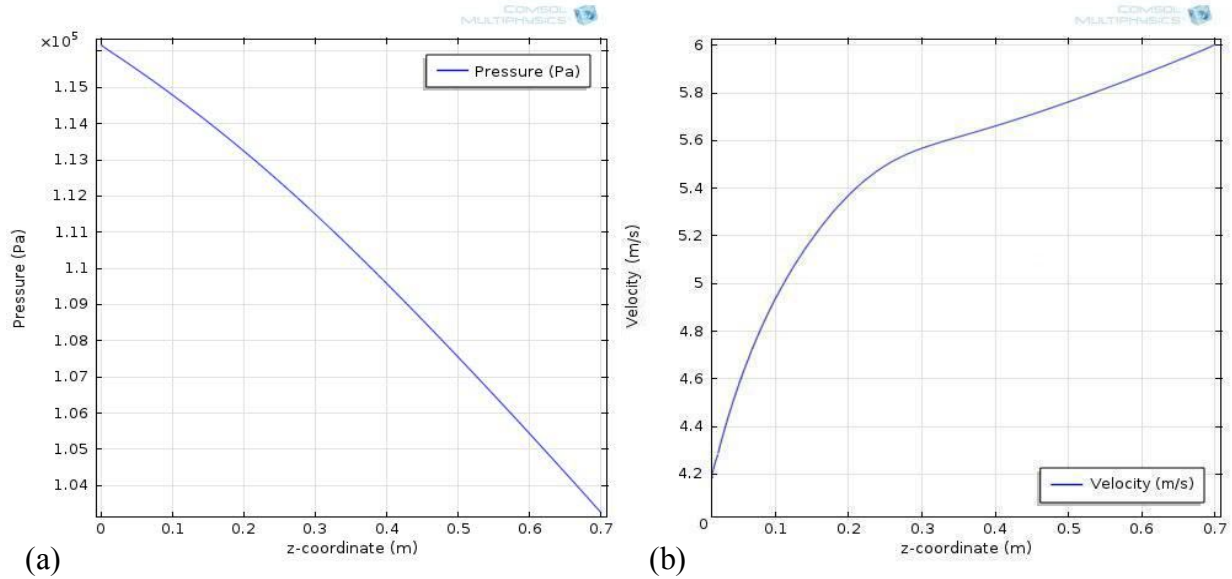


Figure 7.49 (a,b), Pressure drop and velocity change along the reactor, $sv=1500$ 1/hr, $S/C=2$, sulfur=150 ppm, $T=1173(K)$, (a) Pressure drop, (b) velocity

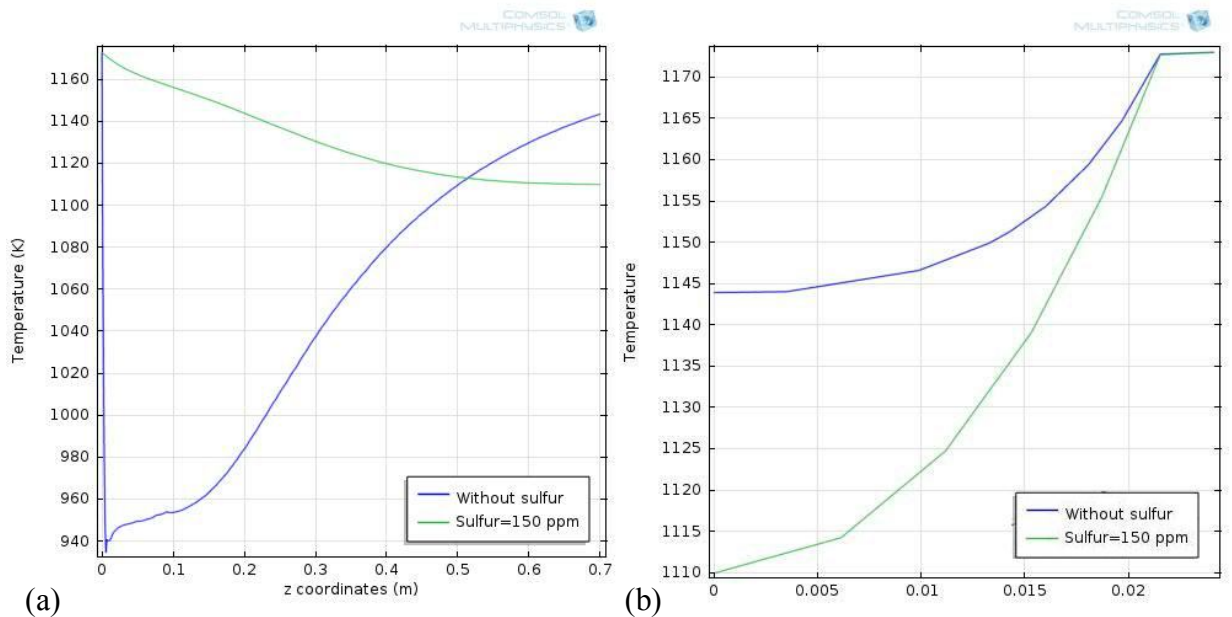


Figure 7.50 (a,b), Temperature distribution in the reactor with and without sulfur, $sv=1500$ 1/hr, $S/C=2$, sulfur=150 ppm, $T=1173(K)$, (a) axial temperature distribution, (b) radial outlet temperature distribution

Figure 7.49(a,b), shows pressure drop and velocity change along the reactor bed. Pressure drop is in good agreement with experimental results and according to the modeling results; the outlet velocity is about 6 m/s.

Axial temperature distribution and radial outlet temperature distribution are shown in Figure 7.50(a,b). As mentioned earlier, when sulfur is not included in the gas, due to high endothermic nature of reforming reactions, temperature sharply decreases as soon as gas enters the reactor. At this time, conversion of methane and propylene is almost completed and heat transfer from the outer surface of the reactor increases the temperature. Sulfur deactivates the catalysts and decreases the reaction rate of methane and propylene. Therefore, temperature decreases uniformly along the reactor bed. It is shown that when sulfur is not included in the gas, outlet temperature is higher than the case when sulfur is included. Graphical view of this phenomena and temperature distribution in axial and radial direction, is shown in Figures 7.51 and 7.52.

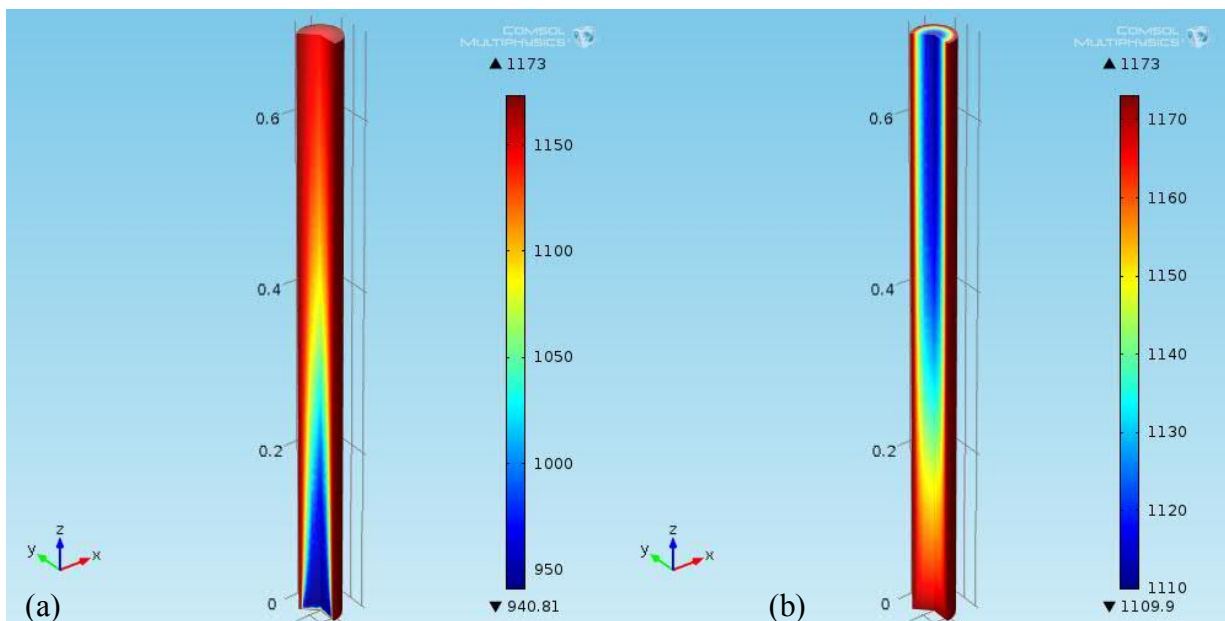


Figure 7.51 (a,b), Graphical view of axial temperature distribution in the reactor, $sv=1500$ 1/hr, $S/C=2$, sulfur= 150 ppm, $T=1173(K)$, (a) without sulfur (b) sulfur=150 ppm

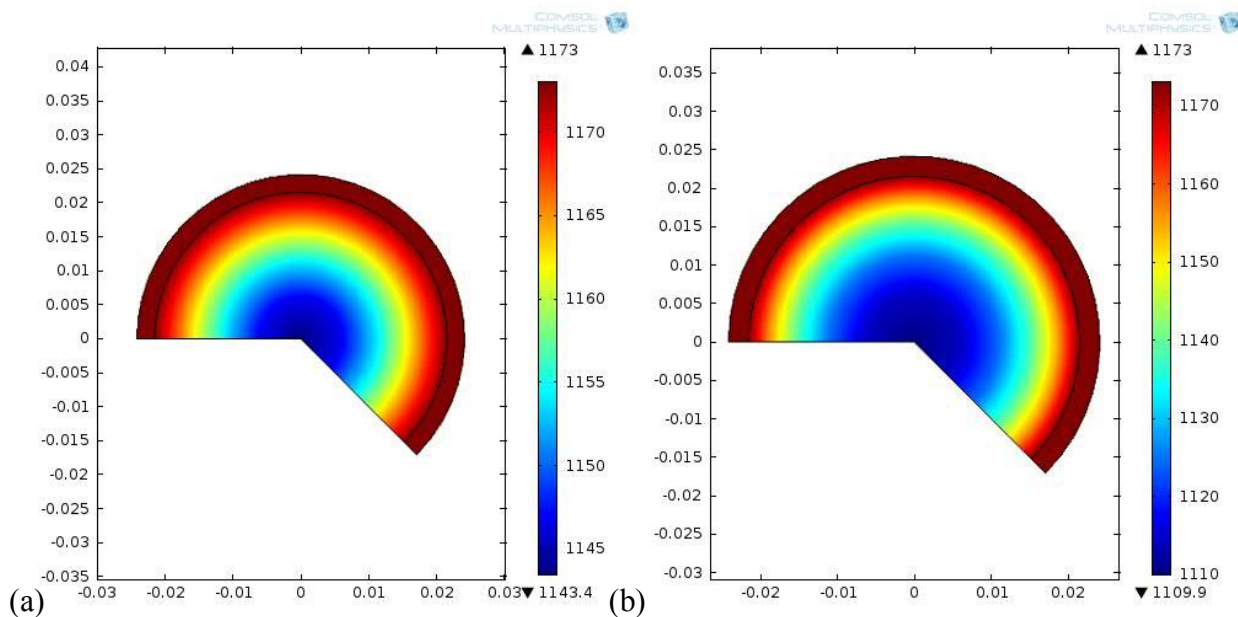


Figure 7.52 (a,b), Graphical view of radial outlet temperature distribution in the reactor, $sv=1500$ 1/hr, $S/C=2$, sulfur=150 ppm, $T=1173(K)$, (a) without sulfur (b) sulfur=150 ppm

Modeling and experimental results of outlet dry mole concentration of different species in the reactor are compared in Figure 7.53.

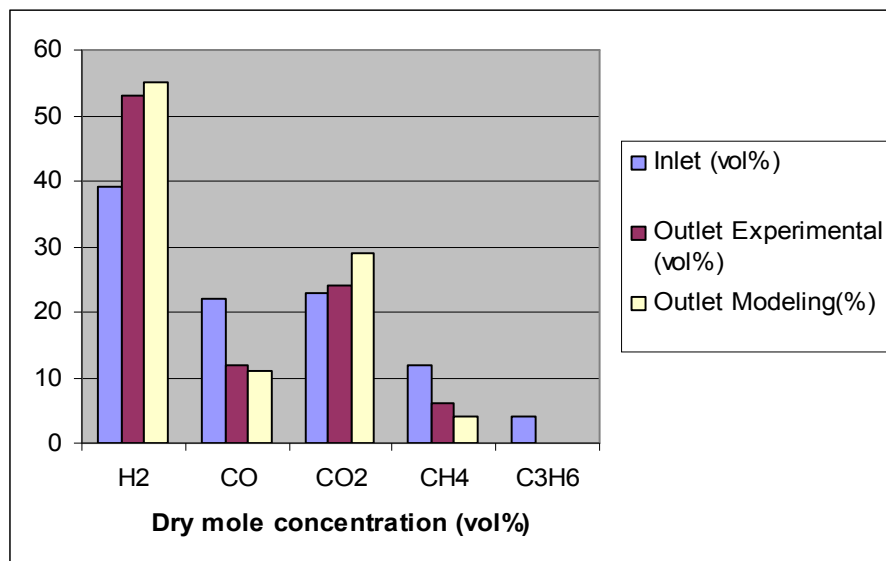


Figure 7.53 Comparison of experimental and modeling results of outlet dry mole concentration of different species in the reactor, $sv=1500$ 1/hr, $S/C=2$, sulfur=150 ppm, $T=1173$ (K)

7.3.3 Experiment No.3

1600 gram of catalyst filled in the steam reformer and the height of the catalyst is 1.44 (m). Inlet temperature is 290 °C and the flow rate is $2 \text{ Nm}^3 / \text{hr}$. Outer temperature of the reformer is kept at 900 °C and space velocity is $9501 / \text{hr}$. The experiments are conducted at atmospheric pressure and 2.5 liter of water per hour entered the reactor.

Figure 7.54(a,b) shows methane and propylene conversion and hydrogen yield along the reactor. It is shown that propylene conversion is very rapid and even when sulfur is included in the producer gas, at very short distance from the inlet of the reactor, propylene is completely converted. Sulfur has negative effect on methane conversion and therefore hydrogen yield and methane conversion decreases more than 50% at the outlet of the reactor. Figure 7.55(a,b) shows this phenomena by drawing dry mole distribution of different species along the reactor bed. Negative deactivation effects of sulfur on decreasing dry mole concentration of methane and hydrogen are more noticeable than propylene.

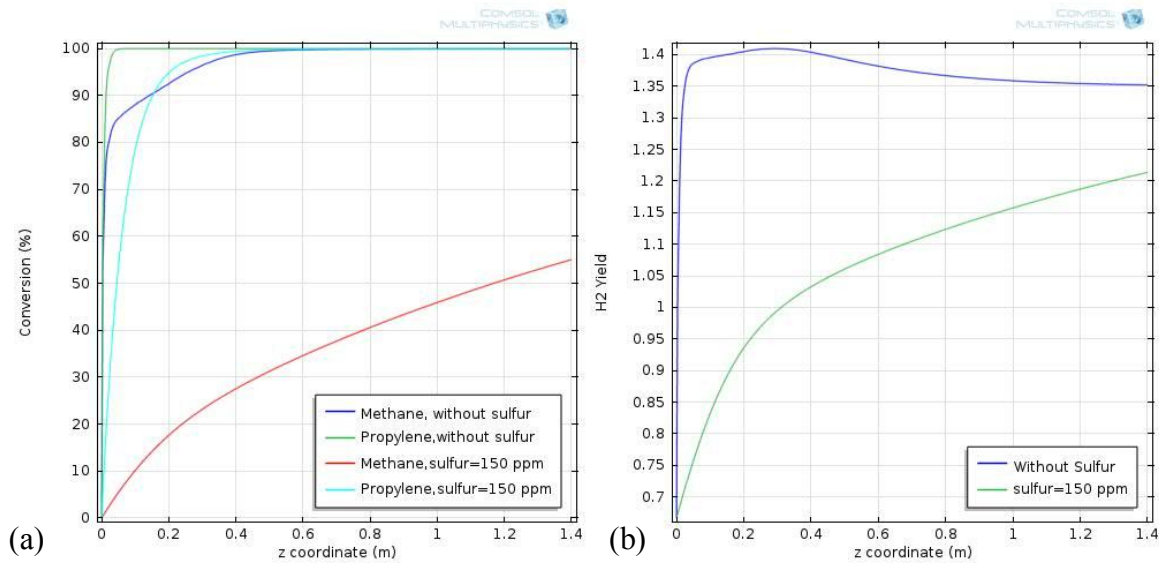


Figure 7.54 (a,b) methane and propylene conversion and hydrogen yield in the reactor, sv=950 1/hr, S/C=5, sulfur=150 ppm, T=1173 (K), (a) methane and propylene conversion, (b) hydrogen yield

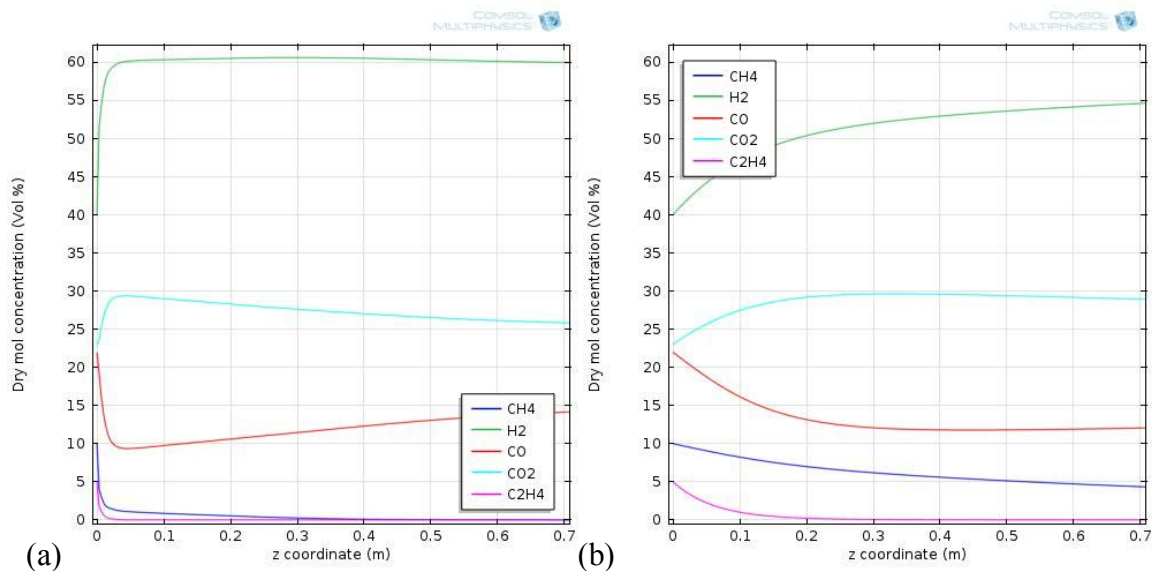


Figure 7.55 (a,b) Dry mole concentration of different species in the reactor, $sv=950$ 1/hr, $S/C=5$, sulfur=150 ppm, $T=1173$ (K) (a) without sulfur (b) sulfur=150 ppm.

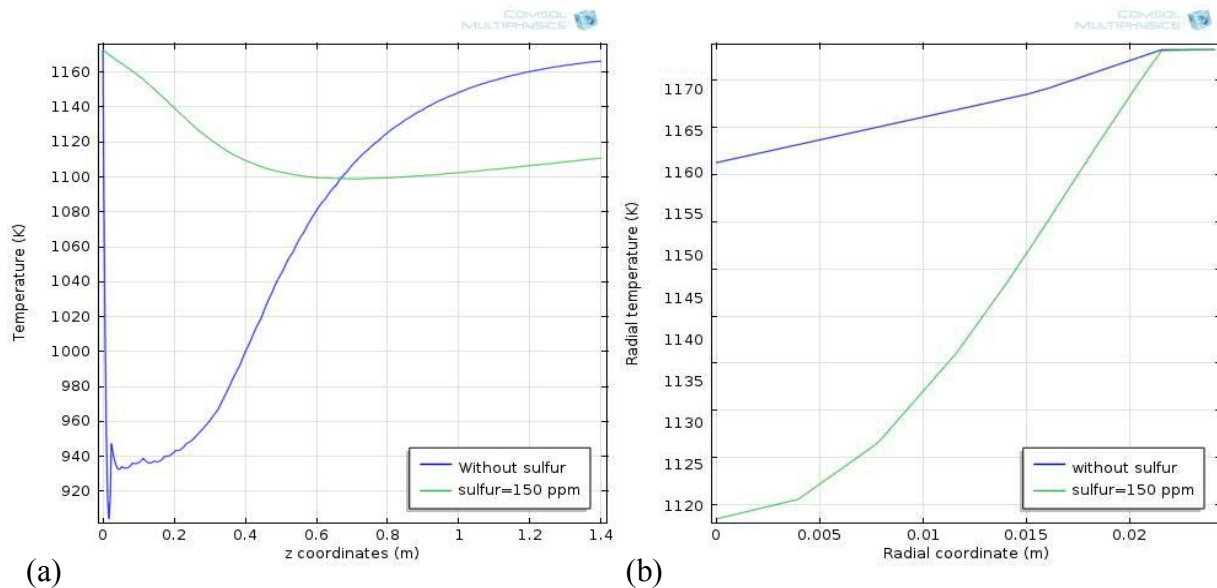


Figure 7.56 (a,b) Temperature distribution in the reactor with and without sulfur, $sv=950$ 1/hr, $S/C=5$, sulfur=150 ppm, $T=1173$ (K), (a) axial temperature (b) radial outlet temperature.

Axial and radial temperature distributions along the packed bed are shown in Figure 7.56(a,b). As shown in Figure 54(a,b), high steam to carbon ratio, ($S/C=5$) is in favor of reforming reactions and enhances decreasing the temperature, as soon as gas enters the reactor. Later, heat transfer from the outer surface of the reactor, increases the outlet

temperature distribution in both cases: without sulfur and when sulfur is included in the producer gas.

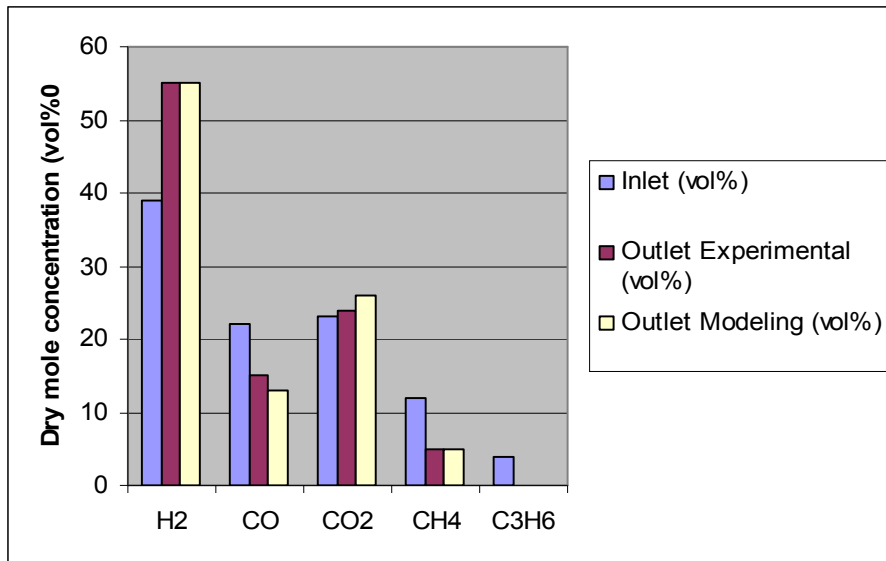


Figure 7.57 Comparison of experimental and modeling results of outlet dry mole concentration of different species in the reactor, $sv=950$ 1/hr, $S/C=5$, sulfur=150 ppm, $T=1173$ (K)

Comparisons of modeling and experimental results are also shown in Figure 7.54. It is shown that modeling results fit well with experimental results and modeling can be used as tool for design and optimizing of steam reformers.

Conclusion

A theoretical and experimental study of catalytic steam reforming of hydrocarbons produced by biomass gasification is presented. A steady state pseudo-homogeneous and heterogeneous model mathematically has been developed to address hydrogen and synthesis gas production. The catalytic conversion of all hydrocarbons present in the product gas such as methane and ethylene, to synthesis gas, a mixture of hydrogen and carbon monoxide are modeled and the results were compared to experimental results.

The aim of this study was a better knowledge of the reforming reactions and investigation of the influence and effect of different parameters on reforming process. The reforming unit is a fixed bed reactor packed with supported nickel or noble metal catalyst. The chosen geometry is a tubular reactor and due to the high endothermic nature of the process an electrical heating is used to keep the outer wall of the reactor at constant temperature in order to provide heat into the reactor. Therefore, reactor tube and catalyst particles are exposed to significant axial and radial temperature gradients.

A critical literature review is done to derive empirical correlations used in packed bed models in general, and to evaluate and find the suitable correlations for reactor models of steam reformers in special, including wall heat transfer coefficients, diffusion and dispersion coefficients and the reaction effectiveness factors. For this purpose, the reactor model comes in two versions: a heterogeneous model and a pseudo-homogeneous model. Temperature and heat flux profiles of the reactor tube wall are modeled carefully and the species transport is described by radial dispersion, axial convection and chemical reaction. The heat transport is modeled with terms for radial conduction, axial convection and the heat sink related to the net endothermic reactions. It is shown that due to the high heat input through the reformer tube wall and the endothermic nature of the reforming reactions, the catalyst tubes are exposed to high axial and radial temperature gradients. The chemistry of hydrocarbons steam reforming is addressed, including the thermodynamics and reaction kinetics. Simulation is done with Finite Element Method software, COMSOL Multiphysics, and an axial symmetrical model is created to

simultaneously solve mass and energy balance equations within the reactor and catalyst pellets. The kinetic model reported by Xu and Froment is adopted, and reaction rates and effectiveness factors are studied in detail. The partial differential equations included in the model were the mass transfer equations for all the components coupled with the energy balance equation. In order to evaluate the diffusional resistances the particle heat and mass balance equations are simultaneously solved in both axial and radial direction within the reactor and catalyst pellets.

The effect of varying operating parameters like steam to carbon molar ratio, temperature, gas composition, space velocity and different sulfur amount on the hydrogen yield and reforming efficiency are investigated. It is shown that increasing steam to carbon ratio, increases methane conversion and therefore hydrogen yield increases at the outlet of the reactor. Both axial and radial temperature distributions are affected by change of steam to carbon ratio. Increasing steam to carbon ratio makes the temperature distribution more uniform within the reactor. Increasing too much steam to carbon ratio can be a bad option because it raises the flow and a higher flow needs a higher heat contribution and maybe the reaction does not have the necessary heat contribution to reach the desired range of conversion.

The results show that reactor wall temperature plays a key role in reforming process and as a result the hydrocarbon conversion in the reactor. Increasing the wall temperature, which leads to increasing the reaction temperature within the packed bed of the reactor, increases the conversion of methane and hydrogen yield. There is a temperature gradient between the centerline and wall of the reactor along the reactor length. It is shown that radial temperature gradients tend to decrease towards the reactor outlet because of the lower local heat fluxes and reforming reaction rates. The rate of reforming reactions is more rapid near the wall because the gas temperature is higher. It is shown that increasing reaction temperatures lead to the more uniform temperature profiles along the axial bed that finally results in a more efficient usage of the reactor.

The results show that at decreasing the space velocity, increases the contact time between gas and catalyst pellets and as a result methane conversion increases which corresponds

to the highest level of hydrogen yield within the reactor. When space velocity decreases there is also more time for heat transfer from the wall into the reactor. This process increases the outlet temperature of the reactor and makes temperature distribution along the reactor more uniform.

Sulfur, which is also incorporated in the biomass structure, is released into the product gas during gasification as hydrogen sulfide and deactivates the steam reforming catalysts by chemisorptions on the metal surface. The steam reforming of hydrocarbons from gasified biomass, in the presence of variable amounts of hydrogen sulfide is investigated and it is shown that even at extremely low (ppm levels) gas-phase concentrations of hydrogen sulfide, the reforming efficiency is dramatically decreased. This modeling also describes sulfur deactivation and steam reforming in a combined kinetic equation which can provide important data for reactor modeling and design exercises. The obtained results show that when sulfur is not presented in the gas, the temperature dropped suddenly at the inlet of the reactor from the inlet temperature and then increased gradually to the outlet. This phenomenon is attributed to the large amount of heat required at the initial stage of the reactions due to the high endothermic nature of the reactions. The rising temperature after a sudden drop along the axial bed of the catalyst is due to the heat supplied by the outer surface of the reactor into the catalytic bed. Presence of sulfur in the gas leads to the catalyst deactivation and lower methane conversion rate. Therefore, small amount of heat is consumed and temperature decreases gradually along the reactor bed. These effects are carefully investigated and seem to fit well when compared with experimental results achieved by choosing similar operating conditions in terms of inlet composition and temperature. The obtained results play a key role in optimization and design of a commercial reactor.

Outlook and Future Work

The purpose and main focus of this thesis has been to develop a mathematical model to calculate and investigate the simulation of the steam reforming reactions of hydrocarbons produced from biomass gasification plant, which are further used in the synthesis to mixed alcohols or Fischer-Tropsch products. Production of liquid hydrocarbons fuel from biomass by Fischer-Tropsch synthesis is already among the ongoing projects in Güssing plant. The modeling in this thesis can be adjusted in a way to combine and simulate biomass gasification, steam reforming and Fischer-Tropsch synthesis in order to produce biofuels. Both of the reactor mathematical models investigated in this thesis, (Pseudo-Homogeneous and Pseudo-Heterogeneous models) can also be applied to any other types of reactors and be used to exactly model wide variety of chemical processes, such as methanation, partial oxidation, autothermal reforming, hydrogenation and membrane technologies. . In addition, the simulation results can be used for operating, developing and improving reactors when process conditions are changed. A parametric study may be done to investigate the critical and optimum operating conditions and use the simulation results for control and evaluating optimum geometry and configuration for a given requirement of a reactor. Simulation and modeling in this thesis has this potential to be adjusted into another mathematical model to describe and predict the operation and control of other chemical processes such as thermal cracking of higher hydrocarbons. Thermal cracking of higher hydrocarbons like naphtha is one of the most important aspects of a petrochemical plant and the cracking reactor is the heart of the process to produce lower hydrocarbons like olefins, aromatics, methane and hydrogen. Moreover, there is possibility to model coke formation which is one of the main problems in the thermal cracking process. The coking model may be combined with a kinetic model in order to exactly predict thermal cracking process, which leads to accurate optimization and design of the reactor.



Mathematical modeling of sulfur deactivation effects on steam reforming of producer gas produced by biomass gasification

Parham Sadooghi^{*}, Reinhard Rauch

Vienna University of Technology, Vienna, Austria

ARTICLE INFO

Article history:

Received 24 July 2012

Received in revised form 28 December 2012

Accepted 14 January 2013

Available online 14 February 2013

Keywords:

Steam reforming

Methane

Sulfur poisoning

Packed bed

Heat transfer

ABSTRACT

Product gas produced by biomass gasification contains small amounts of sulfur compounds (hydrogen sulfide) which can reduce catalyst activity during steam reforming process. Sulfur removal has a negative effect on process efficiency and steam reforming has to be run without cleaning the gas prior to the reactor. It is therefore of interest to investigate the effect of sulfur on the performance of steam reforming reactions. In this work a packed bed reactor filled with nickel based catalysts is mathematically modeled to simulate the steady state pseudo-heterogeneous equations representing heat and mass transfer in the reactor tube. Catalytic bed is subjected to hydrogen sulfide and an isotherm model for the sulfur coverage on the Ni surface is considered to exactly investigate sulfur poisoning effects on methane conversion, hydrogen yield, carbon dioxide and carbon monoxide concentration. It is shown that even when present in the hydrocarbon feedstock in small quantities, (ppm) levels, sulfur can have a significant effect in methane conversion and temperature distribution within the reactor.

© 2013 Elsevier B.V. All rights reserved.

1. Introduction

Energy prices and climate change are the most important challenges facing the world today and in the transition to sustainable energy, hydrogen plays a key role as energy carrier [1,2]. Among the renewable energies, one of the most important energy sources in near future is biomass. Potential of biomass has been widely recognized because of its widespread availability, renewable in nature and potential in relation to global warming [3–5]. Steam reforming of hydrocarbons from biomass gasification (product gas) is one of the most important and economic processes for production of hydrogen and synthesis gas (H₂ and CO), which can subsequently be converted to numerous valuable basic chemicals needed in many refinery and petrochemical processes [6–9]. Gaseous products of biomass gasification are mainly hydrogen, carbon monoxide, carbon dioxide and methane. Steam reforming process is highly endothermic which is carried out by passing a mixture of steam and product gas over a nickel based or noble metal catalyst in a tubular reactor operated at high temperature to increase methane conversion and hydrogen yield. Sulfur, which is also incorporated in the biomass structure, is released into the product gas during gasification process as hydrogen sulfide. Hydrogen sulfide is known to poison and deactivate nickel based steam reforming catalysts even at extremely low (ppb levels) gas-phase concentrations, by chemisorptions on the metal surface, therefore methane conversion is reduced [10,11]. Different methods are used to desulfurize the gas prior to the reforming process [12], which decreases the efficiency.

Different methods have been used to address and simulate the steady state and non steady state operation of catalytic steam reformers, and several reviews have been written about reforming of methane [13–19]. More recently comprehensive reviews are written by Rostrup-Nielsen and Christiansen [20] and K. Liu et al. [21]. Rostrup-Nielsen et al. provide a general overview of synthesis gas technologies as well as in depth analysis of steam reforming process, provide a comprehensive introduction to this complex field, complete review of the works done in last decades and give a detailed analysis of the catalyst and process problems. K. Liu et al. tackle crucial aspects in light of the new directions in the energy industry, in particular how to integrate fuel processing into contemporary systems. It comprehensively covers hydrogen and synthesis gas production and steam reforming process from its fundamentals to practical applications. However, published papers about the application of models for simulating industrial steam reformers including sulfur are very few in numbers [22–24]. More recently Wang et al. [25], also developed a novel highly active and sulfur-tolerant catalyst for steam reforming of liquid hydrocarbons. J.J. Strohm et al. [26] studied low temperature over Rh and Rh–Ni catalysts for fuel cells in the absence and presence of different amounts of organic sulfur. S. Lakhapatri et al. [27], studied deactivation due to sulfur poisoning and coke deposition on Rh–Ni based catalysts during steam reforming of sulfur-doped n-hexadecane. This work mathematically models the steam reforming of methane from gasified biomass, at high temperature (1173 K) in the presence of reasonable amount of hydrogen sulfide (80 ppm), which is typical for producer gas from biomass gasification. The choice for such a high temperature is driven by the reason that the poisoning effects of sulfurous contaminants in producer gas

^{*} Corresponding author. Tel.: +43 1 58801 0; fax: +43 1 58801 41099.

E-mail address: parham.sadooghi@tuwien.ac.at (P. Sadooghi).



Contents lists available at SciVerse ScienceDirect

Journal of Natural Gas Science and Engineering

journal homepage: www.elsevier.com/locate/jngse

Pseudo heterogeneous modeling of catalytic methane steam reforming process in a fixed bed reactor

Parham Sadooghi*, Reinhard Rauch

Vienna University of Technology, Vienna, Austria

ARTICLE INFO

Article history:

Received 16 August 2012
 Received in revised form
 6 December 2012
 Accepted 14 December 2012
 Available online

Keywords:

Steam reforming
 Catalyst
 Carbon monoxide
 Hydrogen
 Methane

ABSTRACT

A mathematical model is developed to simulate synthesis gas production by methane steam reforming process in a fixed bed reactor filled with catalyst particles. Due to the endothermic nature of the reforming reactions heat is supplied into the reactor by means of electrical heating, therefore, the reactor and catalyst particles are exposed to significant axial and radial temperature gradients. A pseudo heterogeneous model is used in order to exactly represent diffusion phenomena inside the reactor tube. Heat and mass transfer equations are coupled with detailed reaction mechanisms and solved for both the flow phase and within the catalyst pellets. The reaction has been investigated from a modeling view point considering the effect of different temperatures ranging from 873 to 1073 (K) on methane conversion and hydrogen yields. The result provides temperature and concentration distribution along the reactor axial and radial coordinates and strong radial temperature gradients particularly close to the entrance of the reactor have been found.

© 2013 Elsevier B.V. All rights reserved.

1. Introduction

In recent years, there are growing concerns worldwide over climate change and greenhouse gas emissions. Environmental problems derived from different energy generation sources and the increment of fossil fuels prices, have enhanced the development of new technologies for energy production (Liguras et al., 2004). In addition, significant reduction of carbon dioxide emissions in production of energy and fuels are essential to ensure sustainable developments, therefore, the energy supply system of the future features electricity and hydrogen as the dominant energy carriers. Although, steam reforming of natural gas has been the most suitable process for hydrogen production for years (Hoffmann and (FRW) Dorgan, 2012), hydrogen would be produced from a very diverse base of other primary energy feedstocks like biomass using the resources and processes that are economically or consciously preferred. Steam reforming of methane from biomass gasification (Yoshioka et al., 2005; Faaij, 2006) is one of the most important chemical processes for the production of hydrogen and synthesis gas which is one of the most important building blocks in chemical and refinery industry, for ammonia production or as feedstock to the Fischer–Tropsch process for liquid hydrocarbons production

(McKendry, 2002a; Rauch, 2011; Hofbauer et al., 1997; Adris et al., 1996; McKendry, 2002b). Methane is a very stable molecule and steam reforming takes place in packed bed reactors where methane reacts with excessive steam at high temperature over a Ni or noble metal based catalyst, because a reasonable conversion of methane is required (Rostrup-Nielsen et al., 2002; Rostrup-Nielsen and Bak Hansen, 1993).

Due to the strongly endothermic nature of the process, a large amount of heat is supplied into the reactor by means of electrical heating which keep the outer surface of the reactor at certain temperature, therefore reformer tube wall and the catalyst tubes are exposed to significant axial and radial temperature gradients (Rostrup-Nielsen et al., 1988). In developing of these kind of reactors the knowledge of the temperature profiles and gas compositions within the reactor play an important role and are important for designing and optimizing the catalysts structure and the reactor geometry to achieve the best performance. Although several models have been purposed to address mass transfer, operation conditions, kinetic modeling, gas composition of the methane steam reforming process (Kvamsdal et al., 1999; Quinta Ferreira et al., 1992; Rostrup-Nielsen, 1993; Adris et al., 1996; Elnashai and Elshishini, 1993), there are a few paper describing exactly heat transfer behavior in a fixed bed catalytic reactor. The present work investigates a heterogeneous model to exactly represent heat and mass transfer distribution in a catalytic steam methane reforming reactor. The reaction system was mathematically

* Corresponding author. Tel.: +43 1 58801 0; fax: +43 1 58801 41099.
 E-mail address: parham.sadooghi@tuwien.ac.at (P. Sadooghi).

Nomenclature

A	Cross sectional area of the reactor.....	m^2
a_v	External pellet surface area per unit reactor volume.....	m^2_p / m^3_r
Bi_w	Biot number.....	-
C_i	Concentration of reactant i.....	$kmol / m^3$
C_i^s	Concentration of reactant i at catalyst surface.....	$kmol / m^3$
C_p	Specific heat capacity.....	$J / (kg.K)$
$C_{p,i}$	Specific heat capacity of component i.....	$J / (kg.K)$
C_s	Solid concentration at catalyst surface.....	$kmol / m^3$
C_s^s	Solid concentration at catalyst surface.....	$kmol / m^3$
C_{tot}	Total concentration.....	$kmol / m^3$
C_0	Initial concentration.....	$kmol / m^3$
DEN	Denominator in the expressions of reaction rates.....	-
D_{er}	Effective radial diffusion coefficient	m^2 / s
$D_{er,i}$	Effective diffusion coefficient of component i.....	m^2 / s
$D_{i,k}$	Binary diffusion coefficient.....	m^2 / s
D_K	Knudsen diffusivity	m^2 / s
D_m	Diffusion coefficient of the gas mixture.....	m^2 / s
$D_{m,i}$	Diffusion coefficient of component i.....	m^2 / s
d_i	Particle inner diameter.....	m
d_o	Particle outer diameter.....	m
d_p	Equivalent particle diameter.....	m

d_t	Tube diameter	m
E	Activation energy	$kJ / kmol$
E_{er}	Effective radial dispersion coefficient	m^2 / s
F_i	Number of moles of component i	-
$F^0_{p,i}$	Polarity factor of component i	-
$F^0_{Q,i}$	Correction factor of component i	-
F_{tot}	Number of total moles in the mixture	-
f	Friction factor	-
f_j	Complex function of reaction j	variable
h_f	Heat transfer coefficient at catalyst surface	$W / (m^2 .K)$
h_w	Wall heat transfer coefficient	$W / (m^2 .K)$
K_i	Adsorption constant of component i	variable
K_j	Equilibrium constant of reaction j	variable
k_g	Mass transfer coefficient from fluid to solid interface	m^3_f / m^2
k_j	Rate coefficient of reaction j	variable
$k_{i,0}$	Pre-exponential Arrhenius factor for component i	-
$k_{j,0}$	Pre-exponential Arrhenius factor of reaction j	-
k_{sp}	Rate coefficient of reaction with sulfur, Chapter 7	$mol / (m^2 Ni.s)$
k^0_{sp}	Rate coefficient of reaction without sulfur, Chapter 7	$mol / (m^2 Ni.s)$
k_w	Reaction rate for carbon formation	$mol / (m^2 Ni.s)$
K_1	Equilibrium constant of reaction 1	bar^2
K_2	Equilibrium constant of reaction 2	-
K_3	Equilibrium constant of reaction 3	bar^2

k_1	Rate coefficient of reaction 1	$kmol.bar^{-0.5} (kg_{cat}.s)$
k_2	Rate coefficient of reaction 2	$kmol/(kg_{cat}.bar.s)$
k_3	Rate coefficient of reaction 3	$kmol.bar^{-0.5} (kg_{cat}.s)$
M	Molar weight	$kg / kmol$
M_i	Molar weight of component i	$kg / kmol$
M_k	Molar weight of component k	$kg / kmol$
m_i	Molar flow rate of component i	$kmol / s$
N_i	Total molar flux	$kmol / s$
Nu_p	Particle Nusslet number	-
Nu_w	Nusslet number	-
n	Molar flow rate	$kmol / s$
p	Pressure	bar
p_0	Initial Pressure	bar
p_c	Critical pressure	bar
$p_{c,i}$	Critical pressure of component i	bar
p_i	Partial pressure of component i	bar
p^s_i	Partial pressure of component i at catalyst surface	bar
Pe_D	Diffusion Peclet number	-
Pe_E	Dispersion Peclet number	-
Pe_p	Thermal Peclet number	-
Pr_p	Particle Prandtl number	-
R	Radius of the reactor	m
R_g	Gas constant	$kJ / (kmol.K)$

$R_{i,sp}$	Reaction rate of component i with sulfur, Chapter 7.....	$mol/(m^2 Ni.s)$
$R^0_{i,sp}$	Reaction rate of component i without sulfur, Chapter 7....	$mol/(m^2 Ni.s)$
R_p	Outer particle radius.....	m
R_{sp}	Reaction rate of reaction with sulfur, Chapter 7.....	$mol/(m^2 Ni.s)$
R^0_{sp}	Reaction rate without sulfur, Chapter 7.....	$mol/(m^2 Ni.s)$
Re_p	Particle Reynolds number.....	-
r	Radial coordinate.....	m
r_i	Reaction rate of component i	$mol/(kg_{cat}.s)$
r_j	Reaction rate of reaction j	$mol/(kg_{cat}.s)$
r^s_j	Reaction rate of reaction j at the catalyst surface.....	$mol/(kg_{cat}.s)$
r_p	Particle radius.....	m
r_1	Reaction rate of reaction 1.....	$mol/(kg_{cat}.s)$
r_2	Reaction rate of reaction 2.....	$mol/(kg_{cat}.s)$
r_3	Reaction rate of reaction 3.....	$mol/(kg_{cat}.s)$
S	External surface,.....	m^2
Sc	Schmidt number.....	-
Sh_p	Particle Sherwood number.....	-
T	Temperature	K
T_c	Critical temperature.....	K
$T_{c,i}$	Critical temperature of component i	K
T_f	Fluid temperature.....	K
T^s_f	Fluid temperature at catalyst surface.....	K
T_R	Outer radius temperature.....	K
T_r	Reduced temperature.....	K

$T_{r,i}$	Reduced temperature of component i	K
T_S	Solid temperature.....	K
T^s	Surface temperature	K
T^s_S	Solid temperature at Catalyst surface.....	K
T_W	Wall temperature	K
T_0	Initial Temperature	K
u	Fluid velocity	m/s
u_r	Fluid velocity in radial direction.....	m/s
u_z	Fluid velocity in axial direction	m/s
$u_{z,0}$	Initial Fluid velocity in axial direction	m/s
V	Volume.....	m^3
V_{in}	Total inlet volume flow rate.....	m^3/hr
V_p	Particle volume	m^3
W	Whisker carbon.....	-
X	Radius of the active part of the catalyst.....	m
X_i	Conversion of component i	-
$X_{i,j}$	Conversion of component i to component j	-
x_i	Molar fraction of component i	-
$x_{p,i}$	Molar fraction of component i at the catalyst surface.....	-
y	Depth coordinate for catalyst particle.....	m
Z	Function of partial pressures and adsorption constants...variable	
Z_c	Compressibility factor.....	-
z	Axial coordinate.....	m

Greek letters

ΔG	Gibbs energy	kJ
ΔG^0	Standard Gibbs energy	kJ
ΔG_{ads}	Gibbs energy of adsorption	kJ
ΔH_{ads}	Enthalpy of adsorption	kJ / mol
ΔH^0_{ads}	Standard enthalpy of adsorption	kJ / mol
ΔH^0_{298}	Standard enthalpy of formation	kJ / mol
ΔH_i	Enthalpy of adsorption of component..i	kJ / mol
ΔH_j	Enthalpy of reaction j	kJ / mol
ΔS_{ads}	Entropy of adsorption	$kJ / (mol.K)$
ε	Void fraction of packed bed	-
ε_p	Catalyst porosity	-
η_j	Effectiveness factor of reaction j	-
λ_c	Catalyst thermal conductivity	$W / (m.K)$
λ_{er}	Effective thermal conductivity	$W / (m.K)$
λ_f	Fluid thermal conductivity	$W / (m.K)$
λ_i	Thermal conductivity of component i	$W / (m.K)$
λ^{stag}	Fluid thermal conductivity at stagnation point	$W / (m.K)$
μ	Viscosity	$kg / (m.s)$
μ_f	Viscosity of the fluid	$kg / (m.s)$
μ_i	Viscosity of component i	$kg / (m.s)$
μ_r	Dipole moment	-
$\nu_{i,j}$	Stoichiometric coefficient of component i in reaction j ..-	
τ_p	Packed bed tortousity factor	-
ρ_f	Fluid density	kg / m^3

ρ_b	Catalyst bulk density.....	kg / m^3
ρ_c	Catalyst density	kg / m^3
ϕ	Ergun correlation.....	$kg / (m^3 .s)$
ϕ_{ij}	Factor for estimating mixture conductivity and viscosity....-	
ξ_i	Reduced inverse viscosity of component i	-
Φ	Catalyst activity factor.....-	
θ_s	Sulfur surface coverage.....-	

Subscripts

0	Initial condition.....-
b	Bulk.....-
C	Critical.....-
c	Catalyst.....-
er	Effective.....-
f	Fluid.....-
i	Reactant number
in	Inlet.....-
j	Reaction number
k	Reactant number
m	Number of moles in hydrocarbon compound.....-
n	Number of moles in hydrocarbon compound.....-
out	Outlet.....-
p	Particle.....-
R	Radius.....-
r	Radial direction.....-
S	Solid.....-

<i>sel</i>	Selectivity-
<i>sp</i>	With sulfur-
<i>sv</i>	Space velocity-
<i>t</i>	Tube-
<i>tot</i>	Total-
<i>V</i>	Volume-
<i>W</i>	Whisker-
<i>w</i>	Reactor wall-
<i>Yld</i>	Yield-
<i>z</i>	Axial direction-

Superscripts

0	Standard condition-
<i>a</i>	Order with respect to hydrocarbon-
<i>b</i>	Order with respect to hydrocarbon-
<i>c</i>	Order with respect to hydrocarbon-
<i>d</i>	Order with respect to hydrocarbon-
<i>s</i>	Condition at the catalyst surface-
<i>stag</i>	Stagnation point-

Abbreviations

<i>CSR</i>	Catalytic steam reforming-
<i>F - T</i>	Fischer - Tropsch-
<i>LPG</i>	Liquefied petroleum gas-
<i>RWGS</i>	Reverse water gas shift reaction-
<i>S / C</i>	Steam to carbon ratio-
<i>WGS</i>	Water gas shift reaction-

References:

Achenbach, E., **Heat and flow characteristics of packed beds**, Experimental Thermal Fluid Science, 10, 17-27, 1995

Adris, A.M., Pruden, B.B., Lim C.J. and Grace, J.R., **On the reported attempts to radically improve the performance of the steam reforming reactor**, Canadian Journal of Chemical Engineering, 74 , 177-185, 1996

Agar, D.W., **Multifunctional reactors: old preconceptions and new dimensions** Chemical Engineering Science, 54, 1299–1305, 1999

Ajanovic, A., **Bio-fuels versus food production**, Energy Journal, 36, 4, 2070-2076, 2011

Akande, A.J., **Production of hydrogen by reforming of crude ethanol**, Thesis, university of Saskatchewan, Canada, 2005

Alzarmora, L.E., Ross, J.R.H., Krossinik, E.C. and Van Reijen, L.L., **Heterogeneous catalysis**, Chemical Society Faraday Transactions, 77, 665-671, 1981

American Association of Petroleum Geologists Report, **History of the world energy consumption and world energy demand in 2050, 2011**

Aparicio, L., **Transient isotopic studies and micro-kinetic modeling of methane reforming over nickel catalysts**, Journal of Catalysis, 165, 2, 262-274, 1997

Aparicio, F., Benito, M.J., and Santz, J.L., **New trends in reforming technologies**, Catalysis Reviews, 2005, 47, 491-502, 2005

Aris, R., **Elementary chemical reactor analysis**, prentice hall, Englewood cliffs, NJ., 1969

Armor, J.N., **The multiple roles for catalysis in the production of hydrogen**, Applied Catalysis, 176, 2, 159-165, 1999

Basu, P., **Biomass gasification and pyrolysis: practical design and theory**, academic press, 2010

Bartholomew C.H., **Carbon deposition in steam reforming and methanation**, Catalysis Review Science and Engineering, 24, 67-112, 1982

Borkling, J.G.H. and Westerterp, K.R., **Influence of tube and particle diameter on heat transport in packed beds**, AIChE Journal, 38, 5, 703-715, 1992

Bridger, G.W., **Catalysis and steam reforming**, Chemical Engineering Progress, 53, 39-44, 1972

Bridger, G.W., **The steam reforming of hydrocarbons**, Catalysis, 3, 39-69, 1980

Briggs, M.S., **Energy strategies and efficiency**, Science, 325, 812-820, 2009

Borman, P.C., Borkink, J.G.H. and Westerterp, K.R., **Heat transfer in a wall heated tubular packed bed reactor at elevated pressures and temperatures**, Chemical Engineering Communications, 114, 17-47, 1992

Brwon, C.R., **Thermo-chemical processing of biomass conversion into fuels and power**, Wiley; 1st Edition, 2011

Cao, C., Wang, Y. and Rozmiarek, R.T., **Heterogeneous reactor model for steam reforming of methane in a micro-channel reactor with micro-structured catalysts**, Catalysis Today, 110, 92-97, 2005

Choudhary, V.R., Rane, V. H., and Rajput, A. M., **High temperature catalytic oxidative conversion of propane to propylene and ethylene involving coupling of exothermic and endothermic reactions**, Industrial and Engineering Chemistry Research, 39, 904-908, 2000

Comiti, J., Mauret, E. and Renaud, M., **Mass transfer in fixed Beds: proposition of a generalized correlation based on an energetic criterion**, Chemical Engineering Science, 55, 5545-5554, 2000

Craciun, R., Shereck, B. and Goorte, R.J., **Kinetic studies of methane steam reforming on ceria-supported Pd**. Catalysis Letters, 51, 3-4, 149-153, 1998

Crocker, M., **Thermo-chemical conversion of biomass to liquid fuels and chemicals**, Royal Society of Chemistry, 1st Edition, 2010

Cussler, E.L., **Diffusion: mass transfer in fluid systems**, 2nd Edition, Cambridge University Press: Cambridge, 1997

De Groote, A.M. and Froment, G.F., **Reactor modeling and simulations in synthesis gas production**, Review Chemical Engineering Journal, 11, 2, 145-183, 1995

Delmas, H. and Froment G.F., **A simulation model accounting for structural radial non-uniformities in fixed bed reactors**, Chemical Engineering Science, 43, 8, 2281-2287, 1988

Delgado, J.M., **A critical review of dispersion in packed beds**, Heat and Mass Transfer, 42, 279-310, 2006

Deluga, G.A. Salge, J.R. and Schmidt L.D. **Renewable hydrogen from ethanol by auto-thermal reforming**, Science, 303, 993-1001, 2004

Derekx, O.R. and Dixon, A.G., **Effect of the wall Nusselt number on the simulation of catalytic fixed bed reactors**, Catalysis Today, 35, 435-442, 1997

De Wasch, A.P. and Froment, G.F., **Heat Transfer in Packed Beds**, Chemical Engineering Science, 27, 557-576, 1972

Dixon, A.G. and Cresswell, D.L., **Theoretical Prediction of effective heat transfer parameters in packed beds**, AIChE Journal, 25 , 4, 663-676, 1979

Dixon, A.G., Di Costanzo, M.A. and Soucy, B.A., **Fluid phase radial transport in packed beds of low tube to particle diameter ratio**, International Journal of Heat and Mass Transfer, 27, 10, 1701-1713, 1984

Dixon, A.G., **Wall and particle shape effects on heat transfer in packed beds**, Chemical Engineering Communications, 71, 217-237, 1988

Dixon, A.G. and van Dongeren, J.H., **The influence of the tube and particle diameters at constant ratio on heat transfer in packed beds**, Chemical Engineering Processing, 37, 23-32, 1998

Dybkjaer, I., **Tubular reforming and auto-thermal reforming of natural gas: an overview of available processes**, Fuel Processing Technology, 42, 85-107, 1995

Dybkjaer, I., **Ammonia**, Springer-Verlag, Berlin, 1995

Energy information agency, **Energy in the United States**, 2003

Ergun, S., **Fluid flow through packed columns**, Chemical Engineering Progress, 48, 2, 89-94, 1952

Elnashaie, S., Adris, A.M., Soliman, M.A. and Alubaid, A.S., **Digital simulation of industrial steam reformers for natural gas using heterogeneous models**, Canadian Journal of Chemical Engineering, 70 , 786-794, 1992

Ferreira, R.M.Q., Marques, M.M., Babo, M.F. and Rodrigues, A.E., **Modeling of the methane steam reforming reactor with large pore catalyst**, Chemical Engineering Science, 47, 9-11, 2909-2914, 1992

Ferreira, R.M.Q., Aparicio, P., Benito M.J. and Sanz J., **New trends in reforming technologies**, Catalysis Review, 47, 491-502, 2005

Figueiredo, J.L. and Trimm, D.L., **Carbon formation on unsupported and supported nickel catalysts**, Journal of Chemical Technology and Biotechnology, 28, 9, 611-616, 1978

Finlayson, B., **Nonlinear analysis in chemical engineering**, New York: McGraw-Hill., 1981

Fogler, H.S., **Essentials of chemical reaction engineering**, 2nd Edition, Prentice-Hall: Englewood Cliffs, N.J., 2011

Fonseca, A. and Assaf, E.F., **Production of hydrogen by methane steam reforming over nickel catalysts**, Journal of power sources, 142, 154-159, 2005

Froment, G.F., **Chemical reaction engineering**, Advances in chemistry series, 109, A.C.S., Washington D.C., 1972

Froment, G. F., **Fixed bed catalytic reactors technological and fundamental design aspects**, Chemical Engineering Technology, 46, 374-386, 1974

Froment, G.F. and Hofmann, P.K., **Design of fixed bed gas solid catalytic reactor**, chemical Reaction and Reactor Engineering, Marcel Dekker: New York, 1987

Froment, G.F., **Production of synthesis gas by steam and Carbon dioxide reforming of natural gas**, Journal of Molecular Catalysis A, 163, 147-156, 2000

Froment, G.F., **Modeling of Catalyst Deactivation**, Applied Catalysis A, 212, 117–128, 2001

Froment, G.F., Bischoff, K.B. and De Wilde, J., **Chemical reactor analysis and design**, 3rd Edition, Wiley, New York, 2011

Fuller, E.N., Schettler, P.D. and Giddings, J.C., **A new method for prediction of binary gas-phase diffusion coefficients**, Industrial Chemical Engineering, 58, 5, 19-27, 1966

Gencieu, A.F., **Review of fuel processing catalysts for hydrogen production**, Current opinion in solid state and material science, 1, 389-394, 2002

Gokon, N., Osawa, Y., Nakazawa, D. and Kodama, T., **Kinetics of Carbon dioxide reforming of methane by catalytically activated metallic foam absorber for solar receiver reactors**, International Journal of Hydrogen Energy, 34, 2, 1787-1792, 2009

Gunn, D.J., **Theory of axial and radial dispersion in packed beds**, Transactions of Chemical Engineering, 47, 351–359, 1969

Handley, D. and Heggs, P.J., **Momentum and heat transfer mechanisms in regular shaped packings**, Transactions of International Chemical Engineering, 46, 9, 251-264 1968

Hansen, J.B. and Rostrup Nielsen, J.R., **Sulfur poisoning on Ni catalysts and anodes**, Hand book of fuel cells, Haldor Topsøe, A/S, Lyngby, Denmark, Wiley, 2010

Higman, C. and Van der burgt, M., **Gasification**, New York, Elsevier Science, 2003

Hodge, B.K., **Biomass alternative energy systems and applications**, Wiley, 2010

Huber, G.W., Iborra, S. and Corma, A., **Synthesis of transportation fuels**, Chemical Review, 106, 4044-4098, 2006

Hou, K. and Hughes, R., **The kinetics of methane steam reforming over a Nickel catalyst**, Chemical Engineering Journal, 82, 1-3, 311-328 , 2001

Jorgensen, K. and Djik, A.V., **Overview of biomass for power generation in Europe**, ECN publications, 2003

Khanal, S. and Surampalli, Y., **Energy and biofuel from biowastes and biomass**, American Society of Civil Engineers, 2011

Kolios, G., Gritsch, A., Glo1ckler, B. and Sorescu G., **Novel Reactor concepts for thermally efficient methane steam reforming: modeling and simulation**, Industrial Engineering Chemical Research, 43, 74-85, 2004

Koningen, J. and Sjostrom, K., **Sulfur deactivated steam reforming of biomass**, Industrial Engineering Chemistry Research, 37, 341-346, 1998

Kunii, D. and Smith, J.M. **Heat transfer characteristics of porous rocks**, AIChE Journal, 6, 71-78, 1960

Kvamsdal, H.M., Svendsen, H.F., Hertzberg, T. and Olsvik, O., **Dynamic simulation and optimization of a catalytic steam reformer**, Chemical Engineering Science, 54, 2697-2706, 2006

Lakshapatri, S. and Abraham, M.A., **Deactivation due to sulfur poisoning and carbon deposition on Nickel catalyst during steam reforming of sulfur doped n-hexadecane**, Applied Catalysis A: General, 364, 113–121, 2009

Licht, F.O and Berg, C., 8th Annual world Biofuel conference, Seville, Spain, 2009

Liu, K., Takahashi K., Fuchikami, K. and Uematsu, K., **Hydrogen production by catalytic methanol reforming**, Applied Catalysis A, 299, 58-64, 2005

Liu, K., Song, C. and Subramani, V., **Hydrogen and synthesis gas production and purification technologies**, AICHE, Wiley Inc., 2010

Luna, C. and Becerra, A.M., **Kinetics of methane steam reforming on a Ni on alumina-titania catalyst**, Reaction Kinetics Catalysis Letters, 2, 369-374, 1997

Machac, A., Henda, R. and Nilsson, B., **Modeling of heat and mass transport in a nonlinear catalytic bed reactor**, Proceeding of the Nordic COMSOL Conference, 2006

Matsumara, Y. and Nakamori T., **Steam reforming of methane over nickel catalysts at low reaction temperatures**, Applied Catalysis A: General, 258, 107-113, 2004

Mcintosh, S. and Gorte, R.J. **Direct hydrocarbon solid oxide fuel cells**, Chemical Reviews, 104, 10, 4845-4852, 2004

Mench, M.M., **Fuel cell engines**, Wiley, Hoboken, New Jersey, 2008

Momirlan, M. and Veziroglo, T.N., **The properties of hydrogen as fuel in sustainable energy system for a cleaner planet**, International Journal of Hydrogen Energy, 30,795-808, 2005

Nelson, V.N., **Introduction to renewable energy, energy and environment**, CRC Press, 2011

Nurunnabi, M., Mukainakano, Y., Kado, S., Kunimori, K. and Tomishige, K., **Additive effect of noble metals on Nickel solid catalyst in oxidative steam reforming of methane under atmospheric and pressurized conditions**, Catalysis Communications, 7, 7, 488-492, 2006

Olaf, G.A., Geoppert, A., and Prakash, G.K.S., **Beyond oil and gas: The methanol economy**, John Wiley, 2006

Ogden, J.M., Steinbugler, M.M. and Krutz T.G., **A comparison of methanol and gasoline as fuel for fuel cell vehicles**, Journal of Power Sources, 79, 143-150, 1999

Owens, W.T, Rodriguez, N.M. and Baker, R.T.K, **Effect of sulfur on the interaction of nickel with ethylene**, Catalysis Today 21, 3-22, 1994

Papageorgiou, J.N. and Froment, G.F., **Simulation models accounting for radial voidage profiles in fixed-bed reactors**, Chemical Engineering Science, 50, 19, 3043-3056, 1995

Pedernera, M.N., Pina, J., Borio, D.O. and Bucala, V., **Use of a heterogeneous two-dimensional model to improve the primary steam reformer performance**, Chemical Engineering Journal, 94, 29-40, 2003

Perry, R.H. and Green, D.W., **Perry's Chemical Engineers' Handbook**, 7th, Edition McGraw-Hill: New York, 1997

Peters, P.E., Schiffino, R.S. and Harriott, P., **Heat Transfer in Packed tube Reactors**, Industrial Engineering Chemical Research, 27, 226-233, 1988

Pichler, H. and Hector F.W., **Synthesis gas**, 2nd Edition, Munchen-Berlin, 1965

Piña, J., Schbib, N.S., Bucalá, V. and Borio, D.O., **Influence of the Heat Flux Profiles on the Operation of Primary Steam Reformers**, Industrial Engineering Chemical Research, 40, 5215-5221, 2001

Poling, B.E., Prausnitz, J.M. and O'Connell, J.P., **The properties of gases and liquids**, 5th Edition, McGraw-Hill: New York, 2001

Pryor, R.W., **Multiphysics Modeling Using COMSOL, A First Principle Approach**, Jones & Bartlett Publishers, 2009

Quinta M.R., Ferreira, Marques, M.M., Babo M.F. and Rodrigues, A.E., **Modeling of the methane steam reforming reactor with large pore catalyst**, Chemical Engineering Science, 47, 2909-2918, 2009

Rase, H.F., **Fixed-bed reactor design and diagnostics**, Stoneham, MA, Butterworths publishers, 1990

Reid, R.C., Prausnitz, J.M. and Poling, B.E., **The properties of gases and liquids**, 4th Edition, McGraw-Hill: New York, 1987

Renewable Global Status Report, 2012

Richardson, J.T. and Parytadiader, S.A, **Carbon dioxide reforming of methane with supported rhodium**, Applied Catalysis, 61, 1, 293-301, 1999

Ridler, D. E. and Twigg, M. V., **Steam Reforming**, Catalyst Handbook, London: Wolfe Publishing Ltd., 1989

Robbins, F., Zhu, A. and Jackson, G.S., **Transient modeling of combined catalytic combustion and methane steam reforming**, Catalysis Today, 83, 1-4, 141–156, 2003

Ross, J.R.H., **Natural gas reforming and Carbon dioxide mitigation**, Catalysis Today, 100, 151-158, 2005

Rostrup-Nielsen, J. R., **Steam reforming catalysts: an investigation of catalysts for tubular steam reforming of hydrocarbons**, Teknisk Forlag A/S, Copenhagen, 1975

Rostrup-Nielsen, J.R., **Catalytic steam reforming**, Catalysis Science and Technology, Anderson, J.R. and Boudart, M. Editors, Springer-Verlag: Berlin, 1984

Rostrup-Nielsen, J.R., **Sulfur passivated nickel catalysts for carbon-free steam reforming of methane**, Journal of Catalysis 85 ,31–43, 1984

Rostrup-Nielsen, J.R., Christiansen, L.J. and Bak Hansen, J.H., **Activity of steam reforming catalysts: Role and assessment**, Applied Catalysis, 43, 287-303, 1988

Rostrup-Nielsen, J.R., **Production of synthesis gas**, Catalysis Today, 18, 305-312, 1991

Rostrup-Nielsen, J.R. and Bak Hansen, J.H., **CO₂ reforming of methane over transition metals**; Journal of Catalysis 144, 38-49, 1993

Rostrup-Nielsen, J.R., **Innovation and the catalytic process industry: the science and challenge**, Chemical Engineering Science, 50, 24, 4061-4071, 1995

Rostrup-Nielsen, J.R., **Hydrogen and synthesis gas by steam and Carbon dioxide reforming**, Advances in Catalysis, 47, 6572-6582, 2002

Rostrup-Nielsen, J.R. and Rostrup-Nielsen, T., **Large scale hydrogen production**, Catalysis Technology, 6,150-159, 2002

Rostrup-Nielsen, J.R., **Fuels and energy for the future: the role of catalysis**, Catalysis Review Science and Engineering, 46, 247-270, 2004

Rostrup-Nielsen, J.R., **Manufacture of hydrogen**, Catalysis Today, 106, 293-301, 2005

Rostrup Nielsen, J.R., **Handbook of heterogeneous catalysis**, Weinheim, Wiley-VCH Verlag, 6, 2008

Rostrup-Nielsen, J. R and Christiansen, L.J., **Concept in syngas manufacture**, Imperial College Press, 2011

Ruan, L., Besenbacher, F., Steensgard, I. and Laegsgaard, E., **Experimental observations of sulfur poisoning effects on nickel catalysts**, Physics Review Letters, 69, 3523-3528, 1992

Salmi T. and Warna J., **Modeling of catalytic packed bed reactors, comparison of different diffusion models**, Computer Chemical Engineering, 15, 715-727, 1991

Schijndel, J.V., **Integrated modeling using Matlab, Simulink and Comsol**, VDM-Verlag, 2008

Sehested, J., **Four challenges for steam reforming catalysts**, Catalysis Today, 111, 1-2, 103-110, 2001

Sehested, J., **Four challenges for nickel steam reforming catalysts**, Catalysis Today, 111, 1-2, 36-48, 2006

Smith, T.F., Shen, Z.F. and Friedman, J.N., **Evaluation of coefficients for the weighted sum of grey gases model**, Journal of Heat Transfer, 104, 602-608, 1982

Snoeck, J.W., Froment, G.F. and Fowles, M., **Filamentous carbon formation and gasification thermodynamics, driving force, nucleation and steady state growth**, Journal of Catalysis, 169, 240-249 , 1997a

Snoeck J.W., Froment G.F. and Fowles, M., **Kinetic study of the carbon filament formation by methane cracking on a nickel catalyst**, Journal of Catalysis, 169, 250-262 1997b

Song, C.S., **Global challenges and strategies for control, conversion and utilization of Carbon dioxide for sustainable developments involving energy, catalysis, adsorption and chemical processing**, Catalysis Today, 115, 2-18, 2006

Strohm, J.J., Zehng, J. and Song, C., **Low temperature steam reforming of jet fuel in the absence and presence of sulfur over Rh and Rh-Ni catalysts for fuel cells**, Journal of Catalysis, 238, 2, 309-320, 2006

Tabatabaian, M., **COMSOL for Engineers**, Mercury Learning & Information, 2014

Tallmadge, J.A., **Packed bed pressure drop: an extension to higher Reynolds Numbers**, AIChE Journal, 19, 1092-1093, 1970

Therdthianwong, A., Sakulkoakiet, T. and Therdthianwong, S., **Hydrogen production by catalytic ethanol steam reforming**, Science Asia, 27, 193-199, 2001

Tsotsas, E. and Schlünder, E.U., **Heat transfer in packed beds with fluid flow: remarks on the meaning and the calculation of a heat transfer coefficient at the wall**, Chemical Engineering Science, 45, 4, 819-837, 1990

Trimm, D.L., **The formation and removal of coke from nickel catalysts**, Catalysis Review Science and Engineering, 16, 1, 155-161, 1977

Trimm, D.L., **The formation and removal of coke from nickel catalysts**, Catalysis Today, 37, 233-238, 1997

Trimm D.L. and Onsan, Z.I, **Onboard fuel conversion for hydrogen fuel cell driven vehicles**, Catalysis Review: Science and Engineering, 43, 31-40, 2001

Twigg, M.V., **Catalyst handbook**, London: Wolfe Publishing, 1989

Van der Lee, M.K., Van Dillen, A.N. Geus, J.W., Dejong, K.P. and Bitter, J.H., **Deposition precipitation for the preparation of carbon nano-fiber supported nickel catalysts**, Carbon, 44, 629-637, 2006

Velu, S. and Song, C., **Advances in catalysis and processes for hydrogen production from ethanol reforming**, Catalysis, 20, 65-73, 2007

Wakao, N. and Funazkri, T., **Effect of fluid dispersion coefficients on particle to fluid mass transfer coefficients in packed beds, correlation of Sherwood numbers**, Chemical Engineering Science, 33, 1375-1384, 1978

Wakao, N., Kaguei, S. and Funazkri, T., **Effect of fluid dispersion coefficients on particle to fluid heat transfer coefficients in packed beds, correlation of Nusselt numbers**, Chemical Engineering Science, 34, 325-336, 1979

Wang, S. and Lu, G.Q., **Catalytic activities and coking characteristics of oxides supported Ni catalysts for CH₄ reforming with carbon dioxide**, Energy and Fuels, 12, 248-256, 1998

Wang, L., Murata, K. and Inaba, M., **Development of novel highly active and sulphur tolerant catalysts for steam reforming of liquid hydrocarbons to produce hydrogen**, Applied Catalysis A: General 257, 43-47, 2006

Wei, J. and Iglesia E., **Rate expressions for methane steam reforming reactions**, Journal of Catalysis, 370-383, 2004

Wen, C.Y. and Fan, L.T., **Models for systems and chemical reactors**, Marcel Dekker, 1975

Wesenberg, M.H., Grislingas, A. and Grevsokott, S., **Modeling of steam reformer tubes**, 6th World Congress of Chemical Engineering, Melbourne, 2001

Wesenberg, M.H., Ströhle, J. and Svendsen, H.F., **A study of the heating section of a gas heated reformer**, International Journal of Chemical Reactor Engineering, 33, 46-53, 2006

Wijngaarden, R.J. and Westerterp, K.R., **Effective heat conductivity and the heat transfer coefficient at the wall inside a packed bed depend on chemical reaction weaknesses and applicability of current models**, Chemical Engineering Science, 44, 8, 1663-1663 , 1989

Wijngaarden, R.J. and Westerterp, K.R., **Radial heat transport in packed beds at elevated pressures**, Chemical Engineering Processing, 31, 157-160, 1992

Wilke, C.R., **Diffusional properties of multi-component gases**, Chemical Engineering Progress, 46, 2, 95-104, 1950

World Energy Outlook, International world energy agency, 2012

World Energy Outlook, International world energy agency, 2013

Xu, J. and Froment, G.F., **Methane steam reforming I. methanation and water gas shift reaction , intrinsic kinetics**, AIChE Journal, 35, 1, 88-96, 1989a

Xu, J. and Froment G.F., **Methane steam reforming: II. Diffusional limitations and reactor simulation**, AIChE Journal, 35, 1, 97-103, 1989b

Yu, Y.H. and Sosna, M.H., **Modeling for industrial heat exchanger type steam reformer**, Korean Journal of Chemical Engineering, 18, 1, 127-132, 2001

Zanfir, M. and Gavriilidis, A., **Catalytic combustion assisted methane steam reforming**, Chemical Engineering Science, 58, 3947– 3960, 2003

Zittel, W. and Wurster, R., **Hydrogen in the energy sector**, Ottobrunn: Ludwig –Bolkow System Technik GmbH, 1996

Appendix 1

Enthalpy of formation

Enthalpy coefficients in H (kJ/mol) $H_i = \sum_{k=1}^5 E_k \cdot T^{k-1}$

	E_1	E_2	E_3	E_4	E_5
O_2	$-7.962663 \cdot 10^0$	$2.427982 \cdot 10^{-2}$	$9.023752 \cdot 10^{-6}$	$-3.098198 \cdot 10^{-9}$	$4.552447 \cdot 10^{-13}$
H_2	$-8.838190 \cdot 10^0$	$3.016572 \cdot 10^{-2}$	$-2.325840 \cdot 10^{-6}$	$2.027647 \cdot 10^{-9}$	$-3.426771 \cdot 10^{-13}$
H_2O	$-2.513828 \cdot 10^2$	$3.106223 \cdot 10^{-2}$	$2.641890 \cdot 10^{-6}$	$2.466168 \cdot 10^{-9}$	$-6.372514 \cdot 10^{-13}$
N_2	$-8.270338 \cdot 10^0$	$2.702524 \cdot 10^{-2}$	$2.168403 \cdot 10^{-6}$	$8.503154 \cdot 10^{-10}$	$-3.202777 \cdot 10^{-13}$
CO	$-1.186737 \cdot 10^2$	$2.621832 \cdot 10^{-2}$	$3.759823 \cdot 10^{-6}$	$2.129007 \cdot 10^{-11}$	$-1.733685 \cdot 10^{-13}$
CO_2	$-4.029275 \cdot 10^2$	$2.448608 \cdot 10^{-2}$	$2.651733 \cdot 10^{-5}$	$-9.591309 \cdot 10^{-9}$	$1.423390 \cdot 10^{-12}$
CH_4	$-8.211111 \cdot 10^1$	$1.405654 \cdot 10^{-2}$	$3.554687 \cdot 10^{-5}$	$-2.975929 \cdot 10^{-9}$	$-1.066366 \cdot 10^{-12}$
C_2H_6	$-9.266902 \cdot 10^1$	$-4.343278 \cdot 10^{-4}$	$1.007521 \cdot 10^{-4}$	$-3.255931 \cdot 10^{-8}$	$4.787174 \cdot 10^{-12}$
C_4H_{10}	$-1.407352 \cdot 10^2$	$-2.401684 \cdot 10^{-3}$	$1.952472 \cdot 10^{-4}$	$-6.701212 \cdot 10^{-8}$	$1.002040 \cdot 10^{-11}$
C_7H_{16}	$-2.131201 \cdot 10^2$	$-4.456496 \cdot 10^{-3}$	$3.353877 \cdot 10^{-4}$	$-1.191684 \cdot 10^{-7}$	$1.837205 \cdot 10^{-11}$
CH_3OH	$-2.109931 \cdot 10^2$	$2.014756 \cdot 10^{-2}$	$4.225563 \cdot 10^{-5}$	$4.233056 \cdot 10^{-10}$	$-4.017644 \cdot 10^{-12}$
$(CH_3)_2O$	$-1.966958 \cdot 10^2$	$1.646284 \cdot 10^{-2}$	$9.291303 \cdot 10^{-5}$	$-2.199279 \cdot 10^{-8}$	$1.358183 \cdot 10^{-12}$

Table values with enthalpies of formation at selected temperatures, kJ/mol
 O_2 , H_2 , H_2O , N_2 , CO , CO_2 , CH_4 , C_2H_6 , C_4H_{10} , C_7H_{16} Methanol and DME.

Temp. °C	O_2	H_2	H_2O	N_2	CO	CO_2
0	-0.72	-0.73	-242.65	-0.71	-111.23	-394.45
25	0.00	0.00	-241.83	0.00	-110.52	-393.51
50	0.73	0.73	-240.99	0.71	-109.81	-392.55
75	1.46	1.46	-240.15	1.43	-109.09	-391.57
100	2.20	2.19	-239.31	2.15	-108.37	-390.57
125	2.95	2.92	-238.46	2.88	-107.64	-389.54
150	3.71	3.65	-237.60	3.61	-106.91	-388.50
175	4.47	4.38	-236.74	4.34	-106.17	-387.43
200	5.24	5.11	-235.86	5.08	-105.43	-386.35
225	6.02	5.84	-234.99	5.82	-104.69	-385.25
250	6.80	6.57	-234.10	6.56	-103.94	-384.13
275	7.59	7.30	-233.21	7.31	-103.18	-382.99
300	8.38	8.03	-232.32	8.06	-102.43	-381.83
325	9.18	8.76	-231.41	8.81	-101.66	-380.66
350	9.99	9.50	-230.50	9.57	-100.90	-379.48
375	10.80	10.23	-229.58	10.33	-100.13	-378.28
400	11.62	10.96	-228.65	11.10	-99.35	-377.06
425	12.44	11.70	-227.72	11.87	-98.57	-375.83
450	13.27	12.43	-226.78	12.64	-97.79	-374.59
475	14.10	13.17	-225.83	13.42	-97.00	-373.34
500	14.93	13.91	-224.88	14.20	-96.21	-372.07
525	15.77	14.65	-223.91	14.98	-95.41	-370.79
550	16.62	15.39	-222.94	15.77	-94.61	-369.50
575	17.47	16.13	-221.96	16.56	-93.81	-368.20
600	18.32	16.88	-220.98	17.36	-93.00	-366.89
625	19.17	17.63	-219.98	18.16	-92.19	-365.57
650	20.03	18.37	-218.98	18.96	-91.38	-364.24
675	20.90	19.12	-217.97	19.77	-90.56	-362.90
700	21.76	19.88	-216.95	20.58	-89.73	-361.55
725	22.63	20.63	-215.93	21.39	-88.91	-360.19
750	23.51	21.39	-214.89	22.21	-88.08	-358.83
775	24.38	22.15	-213.85	23.03	-87.25	-357.46
800	25.26	22.91	-212.80	23.86	-86.41	-356.08
825	26.14	23.67	-211.75	24.68	-85.57	-354.69
850	27.02	24.44	-210.68	25.51	-84.73	-353.30
875	27.91	25.20	-209.61	26.35	-83.88	-351.90
900	28.80	25.97	-208.53	27.18	-83.04	-350.50
925	29.69	26.75	-207.44	28.03	-82.18	-349.09
950	30.58	27.52	-206.35	28.87	-81.33	-347.67
975	31.48	28.30	-205.25	29.72	-80.47	-346.25
1000	32.38	29.08	-204.14	30.56	-79.61	-344.82

Temp. °C	CH ₄	C ₂ H ₆	C ₄ H ₁₀	C ₇ H ₁₆	CH ₃ OH	(CH ₃) ₂ O
0	-75.69	-85.91	-128.13	-191.64	-202.35	-185.71
25	-74.85	-84.67	-125.79	-187.65	-201.25	-184.10
50	-73.97	-83.33	-123.27	-183.36	-200.10	-182.40
75	-73.05	-81.91	-120.59	-178.78	-198.90	-180.61
100	-72.09	-80.40	-117.73	-173.92	-197.65	-178.73
125	-71.09	-78.81	-114.72	-168.79	-196.35	-176.77
150	-70.06	-77.13	-111.55	-163.39	-195.00	-174.72
175	-68.98	-75.37	-108.23	-157.74	-193.60	-172.58
200	-67.87	-73.53	-104.76	-151.85	-192.16	-170.37
225	-66.72	-71.61	-101.15	-145.71	-190.67	-168.07
250	-65.53	-69.63	-97.40	-139.35	-189.13	-165.70
275	-64.31	-67.56	-93.52	-132.76	-187.55	-163.25
300	-63.05	-65.43	-89.51	-125.95	-185.92	-160.73
325	-61.76	-63.24	-85.37	-118.94	-184.25	-158.14
350	-60.43	-60.97	-81.12	-111.73	-182.53	-155.47
375	-59.07	-58.65	-76.75	-104.32	-180.78	-152.74
400	-57.67	-56.26	-72.26	-96.72	-178.98	-149.94
425	-56.24	-53.81	-67.67	-88.95	-177.14	-147.08
450	-54.77	-51.30	-62.97	-80.99	-175.26	-144.15
475	-53.28	-48.73	-58.17	-72.88	-173.35	-141.16
500	-51.75	-46.12	-53.27	-64.59	-171.40	-138.11
525	-50.19	-43.44	-48.28	-56.16	-169.41	-135.00
550	-48.60	-40.72	-43.19	-47.57	-167.39	-131.83
575	-46.99	-37.95	-38.02	-38.84	-165.33	-128.61
600	-45.34	-35.13	-32.76	-29.96	-163.24	-125.34
625	-43.66	-32.26	-27.42	-20.96	-161.12	-122.01
650	-41.96	-29.35	-22.00	-11.82	-158.97	-118.63
675	-40.23	-26.39	-16.51	-2.56	-156.79	-115.21
700	-38.47	-23.39	-10.94	6.81	-154.58	-111.73
725	-36.68	-20.35	-5.30	16.31	-152.35	-108.22
750	-34.87	-17.27	0.41	25.91	-142.19	-104.65
775	-33.04	-14.15	6.18	35.62	-147.81	-101.05
800	-31.18	-10.99	12.01	45.43	-145.51	-97.40
825	-29.30	-7.80	17.91	55.35	-143.19	-93.72
850	-27.40	-4.57	23.87	65.35	-140.85	-90.00
875	-25.47	-1.31	29.88	75.45	-138.50	-86.24
900	-23.52	1.98	35.95	85.63	-136.13	-82.44
925	-21.56	5.31	42.07	95.90	-133.74	-78.62
950	-19.57	8.67	48.24	106.25	-131.35	-74.76
975	-17.56	12.06	54.46	116.68	-128.94	-70.87
1000	-15.54	15.47	60.72	127.19	-126.53	-66.95

Appendix 2

Chemical equilibrium constants

Coefficients in equilibrium function:

$$\ln(K_{eq,j}) = C_{1,j} \cdot \ln(T) + \frac{C_{2,j}}{T} + C_{3,j} + C_{4,j} \cdot T + C_{5,j} \cdot T^2 + C_{6,j} \cdot T^3$$

	<chem>CH4+H2O=CO+3H2</chem>	<chem>CO+3H2=CH4+H2O</chem>	<chem>CO+H2O=CO2+H2</chem>
C ₁	8.611124 10 ⁰	-8.611124 10 ⁰	-3.161652 10 ⁻¹
C ₂	-2.264801 10 ⁴	2.264801 10 ⁴	5.016474 10 ³
C ₃	-2.898252 10 ¹	2.898252 10 ¹	-4.104367 10 ⁰
C ₃ P (bar)	-2.895619 10 ¹	2.895619 10 ¹	-4.104367 10 ⁰
C ₄	-4.980062 10 ⁻³	4.980062 10 ⁻³	2.139623 10 ⁻³
C ₅	3.977411 10 ⁻⁷	-3.977411 10 ⁻⁷	-6.044372 10 ⁻⁷
C ₆	2.013436 10 ⁻¹¹	-2.013436 10 ⁻¹¹	7.582519 10 ⁻¹¹
	<chem>CO2+H2=CO+H2O</chem>	<chem>CH4+CO2=2CO+2H2</chem>	<chem>C2H6+2H2O=2CO+5H2</chem>
C ₁	3.161652 10 ⁻¹	8.927289 10 ⁰	1.702761 10 ¹
C ₂	-5.016474 10 ³	-2.766448 10 ⁴	-3.775312 10 ⁴
C ₃	4.104367 10 ⁰	-2.487816 10 ¹	-5.358552 10 ¹
C ₃ P (bar)	4.104367 10 ⁰	-2.485183 10 ¹	-5.353287 10 ¹
C ₄	-2.139623 10 ⁻³	-7.119686 10 ⁻³	-1.324748 10 ⁻²
C ₅	6.044372 10 ⁻⁷	1.002178 10 ⁻⁶	2.273621 10 ⁻⁶
C ₆	-7.582519 10 ⁻¹¹	-5.569083 10 ⁻¹¹	-2.234181 10 ⁻¹⁰

Note:

The constant C₃ (bar) is calculated by inserting the reference pressure so that the pressure unit of measurement must be in bar abs.

Equilibrium constants in reforming reactions at selected temperatures.
Pressure unit is bar.

Temp. °C	CH ₄ +H ₂ O= CO+3H ₂	CO+3H ₂ = CH ₄ +H ₂ O	CO+H ₂ O= CO ₂ +H ₂	CO ₂ +H ₂ = CO+H ₂ O	CH ₄ +CO ₂ = 2CO+2H ₂	C ₂ H ₆ +2H ₂ O =2CO+5H ₂
100	2.6892 10 ⁻¹⁸	3.7186 10 ¹⁷	3.5870 10 ³	2.7878 10 ⁻⁴	7.4971 10 ⁻²²	3.8926 10 ⁻²⁶
150	8.1934 10 ⁻¹⁵	1.2205 10 ¹⁴	7.6626 10 ²	1.3050 10 ⁻³	1.0693 10 ⁻¹⁷	2.8934 10 ⁻²⁰
200	4.8681 10 ⁻¹²	2.0542 10 ¹¹	2.2943 10 ²	4.3586 10 ⁻³	2.1218 10 ⁻¹⁴	1.3665 10 ⁻¹⁵
225	7.4724 10 ⁻¹¹	1.3383 10 ¹⁰	1.3802 10 ²	7.2453 10 ⁻³	5.4140 10 ⁻¹³	1.3610 10 ⁻¹³
250	8.9260 10 ⁻¹⁰	1.1203 10 ⁹	8.7377 10 ¹	1.1445 10 ⁻²	1.0215 10 ⁻¹¹	8.8782 10 ⁻¹²
275	8.5795 10 ⁻⁹	1.1656 10 ⁸	5.7805 10 ¹	1.7300 10 ⁻²	1.4842 10 ⁻¹⁰	4.0128 10 ⁻¹⁰
300	6.8220 10 ⁻⁸	1.4658 10 ⁷	3.9731 10 ¹	2.5169 10 ⁻²	1.7171 10 ⁻⁹	1.3168 10 ⁻⁸
325	4.5925 10 ⁻⁷	2.1775 10 ⁶	2.8235 10 ¹	3.5417 10 ⁻²	1.6265 10 ⁻⁸	3.2617 10 ⁻⁷
350	2.6689 10 ⁻⁶	3.7468 10 ⁵	2.0662 10 ¹	4.8398 10 ⁻²	1.2917 10 ⁻⁷	6.3030 10 ⁻⁶
375	1.3613 10 ⁻⁵	7.3462 10 ⁴	1.5517 10 ¹	6.4445 10 ⁻²	8.7726 10 ⁻⁷	9.7702 10 ⁻⁵
400	6.1800 10 ⁻⁵	1.6181 10 ⁴	1.1924 10 ¹	8.3866 10 ⁻²	5.1829 10 ⁻⁶	1.2441 10 ⁻³
425	2.5279 10 ⁻⁴	3.9559 10 ³	9.3521 10 ⁰	1.0693 10 ⁻¹	2.7030 10 ⁻⁵	1.3284 10 ⁻²
450	9.4142 10 ⁻⁴	1.0622 10 ³	7.4704 10 ⁰	1.3386 10 ⁻¹	1.2602 10 ⁻⁴	1.2105 10 ⁻¹
475	3.2213 10 ⁻³	3.1044 10 ²	6.0662 10 ⁰	1.6485 10 ⁻¹	5.3101 10 ⁻⁴	9.5608 10 ⁻¹
500	1.0208 10 ⁻²	9.7962 10 ¹	4.9994 10 ⁰	2.0002 10 ⁻¹	2.0418 10 ⁻³	6.6330 10 ⁰
525	3.0168 10 ⁻²	3.3147 10 ¹	4.1757 10 ⁰	2.3948 10 ⁻¹	7.2247 10 ⁻³	4.0903 10 ¹
550	8.3663 10 ⁻²	1.1953 10 ¹	3.5303 10 ⁰	2.8326 10 ⁻¹	2.3698 10 ⁻²	2.2654 10 ²
575	2.1890 10 ⁻¹	4.5684 10 ⁰	3.0177 10 ⁰	3.3138 10 ⁻¹	7.2537 10 ⁻²	1.1372 10 ³
600	5.4296 10 ⁻¹	1.8418 10 ⁰	2.6056 10 ⁰	3.8379 10 ⁻¹	2.0838 10 ⁻¹	5.2172 10 ³
625	1.2823 10 ⁰	7.7985 10 ⁻¹	2.2705 10 ⁰	4.4043 10 ⁻¹	5.6477 10 ⁻¹	2.2033 10 ⁴
650	2.8945 10 ⁰	3.4548 10 ⁻¹	1.9952 10 ⁰	5.0120 10 ⁻¹	1.4507 10 ⁰	8.6210 10 ⁴
675	6.2665 10 ⁰	1.5958 10 ⁻¹	1.7669 10 ⁰	5.6597 10 ⁻¹	3.5467 10 ⁰	3.1438 10 ⁵
700	1.3052 10 ¹	7.6615 10 ⁻²	1.5758 10 ⁰	6.3459 10 ⁻¹	8.2829 10 ⁰	1.0741 10 ⁶
725	2.6229 10 ¹	3.8126 10 ⁻²	1.4146 10 ⁰	7.0690 10 ⁻¹	1.8541 10 ¹	3.4543 10 ⁶
750	5.0980 10 ¹	1.9615 10 ⁻²	1.2776 10 ⁰	7.8271 10 ⁻¹	3.9902 10 ¹	1.0503 10 ⁷
775	9.6062 10 ¹	1.0410 10 ⁻²	1.1603 10 ⁰	8.6182 10 ⁻¹	8.2787 10 ¹	3.0306 10 ⁷
800	1.7585 10 ²	5.6867 10 ⁻³	1.0593 10 ⁰	9.4403 10 ⁻¹	1.6601 10 ²	8.3291 10 ⁷
825	3.1333 10 ²	3.1915 10 ⁻³	9.7169 10 ⁻¹	1.0291 10 ⁰	3.2245 10 ²	2.1873 10 ⁸
850	5.4436 10 ²	1.8370 10 ⁻³	8.9532 10 ⁻¹	1.1169 10 ⁰	6.0800 10 ²	5.5046 10 ⁸
875	9.2360 10 ²	1.0827 10 ⁻³	8.2838 10 ⁻¹	1.2072 10 ⁰	1.1149 10 ³	1.3312 10 ⁹
900	1.5326 10 ³	6.5248 10 ⁻⁴	7.6941 10 ⁻¹	1.2997 10 ⁰	1.9919 10 ³	3.1011 10 ⁹
925	2.4907 10 ³	4.0149 10 ⁻⁴	7.1723 10 ⁻¹	1.3943 10 ⁰	3.4727 10 ³	6.9749 10 ⁹
950	3.9691 10 ³	2.5195 10 ⁻⁴	6.7084 10 ⁻¹	1.4907 10 ⁰	5.9166 10 ³	1.5178 10 ¹⁰
975	6.2091 10 ³	1.6105 10 ⁻⁴	6.2943 10 ⁻¹	1.5887 10 ⁰	9.8645 10 ³	3.2018 10 ¹⁰
1000	9.5454 10 ³	1.0476 10 ⁻⁴	5.9232 10 ⁻¹	1.6883 10 ⁰	1.6115 10 ⁴	6.5590 10 ¹⁰

Coefficients in equilibrium function:

$$\ln(K_{eq,j}) = C_{1,j} \cdot \ln(T) + \frac{C_{2,j}}{T} + C_{3,j} + C_{4,j} \cdot T + C_{5,j} \cdot T^2 + C_{6,j} \cdot T^3$$

	<chem>CO+2H2=CH3OH</chem>	<chem>2CH3OH=(CH3)2O+H2O</chem>	<chem>N2+3H2=2NH3</chem>
C ₁	-7.986366 10 ⁰	8.695637 10 ⁻¹	1.372121 10 ¹
C ₂	8.977513 10 ³	3.138192 10 ³	1.548699 10 ⁴
C ₃	2.381310 10 ¹	-9.077292 10 ⁰	-1.178399 10 ²
C ₃ P (bar)	2.378677 10 ¹	-9.077292 10 ⁰	-1.177873 10 ²
C ₄	5.189461 10 ⁻³	1.328249 10 ⁻³	3.052080 10 ⁻³
C ₅	-2.196947 10 ⁻⁷	-1.225171 10 ⁻⁶	2.960918 10 ⁻⁷
C ₆	-1.266439 10 ⁻¹⁰	3.510445 10 ⁻¹⁰	-8.885442 10 ⁻¹¹
	<chem>COS+H2O=H2S+CO2</chem>	<chem>H2S+2H2O=SO2+3H2</chem>	
C ₁	-1.198941 10 ⁰	3.450676 10 ⁰	
C ₂	3.199162 10 ³	-2.388664 10 ⁴	
C ₃	7.283090 10 ⁰	-1.638488 10 ¹	
C ₃ P (bar)	7.283090 10 ⁰	-1.637172 10 ¹	
C ₄	1.207978 10 ⁻³	3.945482 10 ⁻⁴	
C ₅	-1.912639 10 ⁻⁷	-5.425752 10 ⁻⁷	
C ₆	1.258838 10 ⁻¹¹	9.033646 10 ⁻¹¹	

Note:

The constant C₃ (bar) is calculated by inserting the reference pressure so that the pressure unit of measurement must be in bar abs.

Equilibrium constants in syngas reactions at selected temperatures.

Pressure unit is bar.

Temp. °C	CO+3H ₂ = CH ₃ OH	CH ₃ OH= (CH ₃) ₂ O+H ₂ O	N ₂ +H ₂ = 2NH ₃	COS+H ₂ O= H ₂ S+CO ₂	H ₂ S+2H ₂ O= SO ₂ +3H ₂
100	1.1584 10 ¹	1.2465 10 ²	4.6793 10 ²	9.7124 10 ³	9.9322 10 ⁻²⁷
150	3.1673 10 ⁻¹	5.2833 10 ¹	2.2917 10 ¹	3.1985 10 ³	2.9551 10 ⁻²³
200	1.7636 10 ⁻²	2.7184 10 ¹	2.6115 10 ⁰	1.3258 10 ³	1.6898 10 ⁻²⁰
225	5.0970 10 ⁻³	2.0578 10 ¹	1.1115 10 ⁰	9.1098 10 ²	2.5385 10 ⁻¹⁹
250	1.6455 10 ⁻³	1.6031 10 ¹	5.3474 10 ⁻¹	6.4838 10 ²	2.9659 10 ⁻¹⁸
275	5.8490 10 ⁻⁴	1.2801 10 ¹	2.8556 10 ⁻¹	4.7578 10 ²	2.7881 10 ⁻¹⁷
300	2.2621 10 ⁻⁴	1.0440 10 ¹	1.6676 10 ⁻¹	3.5854 10 ²	2.1689 10 ⁻¹⁶
325	9.4244 10 ⁻⁵	8.6740 10 ⁰	1.0518 10 ⁻¹	2.7658 10 ²	1.4292 10 ⁻¹⁵
350	4.1940 10 ⁻⁵	7.3234 10 ⁰	7.0927 10 ⁻²	2.1779 10 ²	8.1366 10 ⁻¹⁵
375	1.9793 10 ⁻⁵	6.2710 10 ⁰	5.0693 10 ⁻²	1.7466 10 ²	4.0690 10 ⁻¹⁴
400	9.8453 10 ⁻⁶	5.4371 10 ⁰	3.8124 10 ⁻²	1.4238 10 ²	1.8130 10 ⁻¹³
425	5.1343 10 ⁻⁶	4.7665 10 ⁰	2.9985 10 ⁻²	1.1776 10 ²	7.2860 10 ⁻¹³
450	2.7942 10 ⁻⁶	4.2197 10 ⁰	2.4533 10 ⁻²	9.8685 10 ¹	2.6687 10 ⁻¹²
475	1.5806 10 ⁻⁶	3.7686 10 ⁰	2.0786 10 ⁻²	8.3683 10 ¹	8.9909 10 ⁻¹²
500	9.2603 10 ⁻⁷	3.3923 10 ⁰	1.8168 10 ⁻²	7.1724 10 ¹	2.8083 10 ⁻¹¹
525	5.6020 10 ⁻⁷	3.0752 10 ⁰	1.6325 10 ⁻²	6.2075 10 ¹	8.1894 10 ⁻¹¹
550	3.4896 10 ⁻⁷	2.8056 10 ⁰	1.5037 10 ⁻²	5.4201 10 ¹	2.2433 10 ⁻¹⁰
575	2.2329 10 ⁻⁷	2.5745 10 ⁰	1.4161 10 ⁻²	4.7710 10 ¹	5.8035 10 ⁻¹⁰
600	1.4644 10 ⁻⁷	2.3749 10 ⁰	1.3604 10 ⁻²	4.2308 10 ¹	1.4248 10 ⁻⁹
625	9.8254 10 ⁻⁸	2.2014 10 ⁰	1.3306 10 ⁻²	3.7774 10 ¹	3.3336 10 ⁻⁹
650	6.7320 10 ⁻⁸	2.0495 10 ⁰	1.3226 10 ⁻²	3.3937 10 ¹	7.4619 10 ⁻⁹
675	4.7030 10 ⁻⁸	1.9158 10 ⁰	1.3341 10 ⁻²	3.0667 10 ¹	1.6033 10 ⁻⁸
700	3.3452 10 ⁻⁸	1.7975 10 ⁰	1.3636 10 ⁻²	2.7860 10 ¹	3.3173 10 ⁻⁸
725	2.4195 10 ⁻⁸	1.6923 10 ⁰	1.4106 10 ⁻²	2.5435 10 ¹	6.6271 10 ⁻⁸
750	1.7774 10 ⁻⁸	1.5983 10 ⁰	1.4752 10 ⁻²	2.3328 10 ¹	1.2815 10 ⁻⁷
775	1.3248 10 ⁻⁸	1.5141 10 ⁰	1.5581 10 ⁻²	2.1487 10 ¹	2.4042 10 ⁻⁷
800	1.0009 10 ⁻⁸	1.4382 10 ⁰	1.6606 10 ⁻²	1.9869 10 ¹	4.3849 10 ⁻⁷
825	7.6577 10 ⁻⁹	1.3697 10 ⁰	1.7845 10 ⁻²	1.8442 10 ¹	7.7894 10 ⁻⁷
850	5.9286 10 ⁻⁹	1.3076 10 ⁰	1.9321 10 ⁻²	1.7177 10 ¹	1.3500 10 ⁻⁶
875	4.6410 10 ⁻⁹	1.2512 10 ⁰	2.1064 10 ⁻²	1.6050 10 ¹	2.2863 10 ⁻⁶
900	3.6710 10 ⁻⁹	1.1998 10 ⁰	2.3108 10 ⁻²	1.5042 10 ¹	3.7891 10 ⁻⁶
925	2.9322 10 ⁻⁹	1.1529 10 ⁰	2.5497 10 ⁻²	1.4138 10 ¹	6.1531 10 ⁻⁶
950	2.3636 10 ⁻⁹	1.1100 10 ⁰	2.8280 10 ⁻²	1.3324 10 ¹	9.8026 10 ⁻⁶
975	1.9218 10 ⁻⁹	1.0706 10 ⁰	3.1519 10 ⁻²	1.2588 10 ¹	1.5338 10 ⁻⁵
1000	1.5753 10 ⁻⁹	1.0345 10 ⁰	3.5285 10 ⁻²	1.1920 10 ¹	2.3593 10 ⁻⁵

Coefficients in equilibrium function:

$$\ln(K_{eq,j}) = C_{1,j} \cdot \ln(T) + \frac{C_{2,j}}{T} + C_{3,j} + C_{4,j} \cdot T + C_{5,j} \cdot T^2 + C_{6,j} \cdot T^3$$

	CH ₄ = C+2H ₂	CH ₄ = C(whisker)+2H ₂	2CO= C+CO ₂	CO+H ₂ = C+H ₂ O
C ₁	5.291666 10 ⁰	0	-3.635623 10 ⁰	-3.319458 10 ⁰
C ₂	-7.610846 10 ³	-1.0779 10 ⁴	2.005364 10 ⁴	1.503716 10 ⁴
C ₃	-2.449759 10 ¹	1.268 10 ¹	3.805679 10 ⁻¹	4.484935 10 ⁰
C ₃	-2.448443 10 ¹	1.269 10 ¹	3.674049 10 ⁻¹	4.471772 10 ⁰
P (bar)				
C ₄	-2.023153 10 ⁻³	0	5.096533 10 ⁻³	2.956910 10 ⁻³
C ₅	-1.593520 10 ⁻⁷	0	-1.161530 10 ⁻⁶	-5.570931 10 ⁻⁷
C ₆	7.797205 10 ⁻¹¹	0	1.336629 10 ⁻¹⁰	5.783769 10 ⁻¹¹

Note:

The constant C₃ (bar) is calculated by inserting the reference pressure so that the pressure unit of measurement must be in bar abs.

Equilibrium constants in syngas reactions at selected temperatures.

Pressure unit is bar.

Temp. °C	CO+3H ₂ = CH ₃ OH	CH ₃ OH= (CH ₃) ₂ O+H ₂ O	N ₂ +H ₂ = 2NH ₃	COS+H ₂ O= H ₂ S+CO ₂	H ₂ S+2H ₂ O= SO ₂ +3H ₂
100	1.1584 10 ¹	1.2465 10 ²	4.6793 10 ²	9.7124 10 ³	9.9322 10 ⁻²⁷
150	3.1673 10 ⁻¹	5.2833 10 ¹	2.2917 10 ¹	3.1985 10 ³	2.9551 10 ⁻²³
200	1.7636 10 ⁻²	2.7184 10 ¹	2.6115 10 ⁰	1.3258 10 ³	1.6898 10 ⁻²⁰
225	5.0970 10 ⁻³	2.0578 10 ¹	1.1115 10 ⁰	9.1098 10 ²	2.5385 10 ⁻¹⁹
250	1.6455 10 ⁻³	1.6031 10 ¹	5.3474 10 ⁻¹	6.4838 10 ²	2.9659 10 ⁻¹⁸
275	5.8490 10 ⁻⁴	1.2801 10 ¹	2.8556 10 ⁻¹	4.7578 10 ²	2.7881 10 ⁻¹⁷
300	2.2621 10 ⁻⁴	1.0440 10 ¹	1.6676 10 ⁻¹	3.5854 10 ²	2.1689 10 ⁻¹⁶
325	9.4244 10 ⁻⁵	8.6740 10 ⁰	1.0518 10 ⁻¹	2.7658 10 ²	1.4292 10 ⁻¹⁵
350	4.1940 10 ⁻⁵	7.3234 10 ⁰	7.0927 10 ⁻²	2.1779 10 ²	8.1366 10 ⁻¹⁵
375	1.9793 10 ⁻⁵	6.2710 10 ⁰	5.0693 10 ⁻²	1.7466 10 ²	4.0690 10 ⁻¹⁴
400	9.8453 10 ⁻⁶	5.4371 10 ⁰	3.8124 10 ⁻²	1.4238 10 ²	1.8130 10 ⁻¹³
425	5.1343 10 ⁻⁶	4.7665 10 ⁰	2.9985 10 ⁻²	1.1776 10 ²	7.2860 10 ⁻¹³
450	2.7942 10 ⁻⁶	4.2197 10 ⁰	2.4533 10 ⁻²	9.8685 10 ¹	2.6687 10 ⁻¹²
475	1.5806 10 ⁻⁶	3.7686 10 ⁰	2.0786 10 ⁻²	8.3683 10 ¹	8.9909 10 ⁻¹²
500	9.2603 10 ⁻⁷	3.3923 10 ⁰	1.8168 10 ⁻²	7.1724 10 ¹	2.8083 10 ⁻¹¹
525	5.6020 10 ⁻⁷	3.0752 10 ⁰	1.6325 10 ⁻²	6.2075 10 ¹	8.1894 10 ⁻¹¹
550	3.4896 10 ⁻⁷	2.8056 10 ⁰	1.5037 10 ⁻²	5.4201 10 ¹	2.2433 10 ⁻¹⁰
575	2.2329 10 ⁻⁷	2.5745 10 ⁰	1.4161 10 ⁻²	4.7710 10 ¹	5.8035 10 ⁻¹⁰
600	1.4644 10 ⁻⁷	2.3749 10 ⁰	1.3604 10 ⁻²	4.2308 10 ¹	1.4248 10 ⁻⁹
625	9.8254 10 ⁻⁸	2.2014 10 ⁰	1.3306 10 ⁻²	3.7774 10 ¹	3.3336 10 ⁻⁹
650	6.7320 10 ⁻⁸	2.0495 10 ⁰	1.3226 10 ⁻²	3.3937 10 ¹	7.4619 10 ⁻⁹
675	4.7030 10 ⁻⁸	1.9158 10 ⁰	1.3341 10 ⁻²	3.0667 10 ¹	1.6033 10 ⁻⁸
700	3.3452 10 ⁻⁸	1.7975 10 ⁰	1.3636 10 ⁻²	2.7860 10 ¹	3.3173 10 ⁻⁸
725	2.4195 10 ⁻⁸	1.6923 10 ⁰	1.4106 10 ⁻²	2.5435 10 ¹	6.6271 10 ⁻⁸
750	1.7774 10 ⁻⁸	1.5983 10 ⁰	1.4752 10 ⁻²	2.3328 10 ¹	1.2815 10 ⁻⁷
775	1.3248 10 ⁻⁸	1.5141 10 ⁰	1.5581 10 ⁻²	2.1487 10 ¹	2.4042 10 ⁻⁷
800	1.0009 10 ⁻⁸	1.4382 10 ⁰	1.6606 10 ⁻²	1.9869 10 ¹	4.3849 10 ⁻⁷
825	7.6577 10 ⁻⁹	1.3697 10 ⁰	1.7845 10 ⁻²	1.8442 10 ¹	7.7894 10 ⁻⁷
850	5.9286 10 ⁻⁹	1.3076 10 ⁰	1.9321 10 ⁻²	1.7177 10 ¹	1.3500 10 ⁻⁶
875	4.6410 10 ⁻⁹	1.2512 10 ⁰	2.1064 10 ⁻²	1.6050 10 ¹	2.2863 10 ⁻⁶
900	3.6710 10 ⁻⁹	1.1998 10 ⁰	2.3108 10 ⁻²	1.5042 10 ¹	3.7891 10 ⁻⁶
925	2.9322 10 ⁻⁹	1.1529 10 ⁰	2.5497 10 ⁻²	1.4138 10 ¹	6.1531 10 ⁻⁶
950	2.3636 10 ⁻⁹	1.1100 10 ⁰	2.8280 10 ⁻²	1.3324 10 ¹	9.8026 10 ⁻⁶
975	1.9218 10 ⁻⁹	1.0706 10 ⁰	3.1519 10 ⁻²	1.2588 10 ¹	1.5338 10 ⁻⁵
1000	1.5753 10 ⁻⁹	1.0345 10 ⁰	3.5285 10 ⁻²	1.1920 10 ¹	2.3593 10 ⁻⁵

Appendix 3

Empirical correlations used in reactor model

Radial dispersion coefficient:

$$Pe_E = \frac{10}{\varepsilon} \left(1 + 19.4 \left(\frac{d_p}{d_t}\right)^2\right) \quad 10 < Re_p < 1000 \quad \text{Froment et al., 1987} \quad (5-2)$$

Effective radial thermal conductivity:

$$\frac{\lambda_{er}}{\lambda_f} = \frac{\lambda^{stag}}{\lambda_f} + \frac{Re_p Pr_p}{Pe_D} \quad \text{All type } 100 < Re_p < 900 \quad \text{Peters et al., 1988} \quad (5-11)$$

$$Pe_D = 3.2 + 49.4 \frac{d_p}{d_t}$$

$$\lambda^{stag} = \lambda_f \varepsilon_p + \lambda_f \frac{0.895(1 - \varepsilon_p) \left(\ln \left[\frac{\lambda_c}{\lambda_f} - 0.5439 \left(\frac{\lambda_c}{\lambda_f} - 1 \right) \right] - 0.4561 \frac{\lambda_c - \lambda_f}{\lambda_c} \right)}{0.3521 \left(\frac{\lambda_c - \lambda_f}{\lambda_c} \right)^2}$$

Kunii et al., 1960 (5-14)

Wall heat transfer coefficient:

$$Nu_w = 4.1 \left(\frac{d_p}{d_t}\right)^{0.39} Re_p^{0.5} Pr_p^{1/3} \quad \text{cylinders} \quad \begin{array}{l} 100 < Re_p < 8000 \\ 0.1 < \frac{d_p}{d_t} < 0.6 \end{array} \quad \text{Peters et al., 1988} \quad (5-20)$$

Diffusion coefficient in gas mixture:

$$D_{m,i} = \frac{1}{\sum_{k \neq i} \frac{x_k}{D_{i,k}}} \quad \text{Wilke 1950} \quad (5-27a)$$

Binary diffusion coefficients:

$$D_{i,k} = \frac{0.01013T^{1.75} \left(\frac{1}{M_i} + \frac{1}{M_k} \right)^{1/2}}{p \left[(\sum_i V)^{1/3} + (\sum_k V)^{1/3} \right]^2} \quad \text{Fuller et al., 1966} \quad (5-27b)$$

Mass transfer coefficients:

$$Sh_p = 2 + 1.1 Re_p^{0.6} Sc^{0.33} \quad 5 \leq Re_p \leq 10^4 \quad \text{Wakao et al., 1978} \quad (5-28a)$$

Interphase heat transfer coefficient:

$$Nu_p = \frac{0.255}{\varepsilon} Pr_p^{0.3} Re_p^{0.6} \quad Re_p \leq 10^3 \quad \text{Handley et al., 1968} \quad (5-29a)$$